Structure Property Relationship and Therapeutic Potential of Poly(2-oxazoline)s and Poly(2-oxazine)s based Amphiphiles

Thesis to obtain “Doktor der Naturwissenschaften”
(Dr. rer. nat.)
awarded by the
Julius-Maximilians-Universität Würzburg, Germany

Submitted by
Malik Salman Haider

From
Dera Ismail Khan, Pakistan

Würzburg, Germany, 2022

Submitted to the Faculty of Chemistry and Pharmacy

on date (DD MM YYYY)_____

Evaluators of the written Dissertation (Thesis)

Supervisor - 1. Evaluator:_____

2. Evaluator:_____

Examiners of the Public Defense

1. Examiner:_____

2. Examiner:_____

3. Examiner:_____

Date of the Public Defense_____

Doctoral Certificate awarded on_____

Acknowledgement

I would like to express my sincere gratitude to my supervisor, Prof. Dr. Robert Luxenhofer for his encouragement and tremendous support throughout my PhD journey. I appreciate his patience and confidence in me from the very first day. His positive impact in my research is incalculable. I always had the opportunity to discuss with him my scientific ideas and issues at first call. I was always inspired by his insights and creativity into science. With his overwhelming attitude to help his students and his timely and scholarly advice have helped me to a great extent to accomplish this task.

I would also pay special thanks to all the colleagues at the department. I really enjoyed working with you and during the outdoor activities like ChemCup, boßeln and barbecues. In this regard, I would like to quote few names i.e. Jochen Löblein, Mengshi Yang, Sebastian Halupczok, Chen Hu, Lukas Hahn, Solomiia Borova, Anita Luxenhofer, Christine Schlutt, Stefan Forster, Daniel Nahm and Robin Bissert, you really made my stay memorable. Special thanks to Michael Lübtow, with whom I worked closely in the lab, supporting each other with respect to various scientific problems and discussing the further plans.

I thank profusely all the staff at chair including Ulrike Midtboe, Diana Stürmer for their excellent administrative support, Dr. Guntram Schwarz for occasional scientific discussions, Christian May, Anna Kucharski, Sandra Stockmann and Stephanie Maß for their technical support and support during everyday laboratory life.

Furthermore, I would like to thank Higher education commission of Pakistan in collaboration with German academic exchange services Germany (HEC-DAAD-Pakistan/Germany) for the award of PhD scholarship. Apart from that, I would like to thank Deutsche Forschungsgemeinschaft (DFG) for the financial support for research.

I want to thank all my collaborators, specifically, PD. Dr. Mathias Kroiss, Jun-Prof Oliver Scherf-Clavel, Jun-Prof. Ann-Christin Pöppler, Dr. Yulia Sidorova, Prof. Dr. Jürgen Groll and Dr. Taufiq Ahmed, who enabled to study the polymers and polymer formulations and also for their valuable discussions.

Last but not the least, and the most important, **I thank my entire family** and friends for their ongoing support.

List of Publication

13. Malik Salman Haider, and Robert Luxenhofer. "Development of Poly(2-oxazoline)s and poly(2-oxazine)s based formulation library and estimation of polymer/drug compatibility." (2022). Available as preprint DOI: 10.26434/chemrxiv-2022-s8xc3

12. Malik Salman Haider, Arun Kumar Mahato, Anastasiia Kotliarova, Stefan Forster, Bettina Böttcher, Philipp Stahlhut, Yulia Sidorova, Robert Luxenhofer **"**Unlocking the therapeutic potential of RET agonist: Nanoformulations of BT-44, In vitro and In vivo evaluation for the treatment of neurodegenerative disorders" 2022. **Accepted by "Biomacromolecules".** Available as preprint DOI: 10.26434/chemrxiv-2021-ffsvz.

11. Malik Salman Haider, Taufiq Ahmad, Mengshi Yang, Chen Hu, Lukas Hahn, Philipp Stahlhut, Jürgen Groll, and Robert Luxenhofer. "Tuning the Thermogelation and Rheology of Poly(2-Oxazoline)/Poly(2-Oxazine)s Based Thermosensitive Hydrogels for 3D Bioprinting." **Gels** 7, no. 3 (2021): 78.

10. Malik Salman Haider, Taufiq Ahmad, Jürgen Groll, Oliver Scherf-Clavel, Matthias Kroiss, and Robert Luxenhofer. "The challenging pharmacokinetics of mitotane: an old drug in need of new packaging." **European Journal of Drug Metabolism and Pharmacokinetics** 46, no. 5 (2021): 575-593.

9. Malik Salman Haider, Michael M. Lübtow, Sebastian Endres, Stefan Forster, Vanessa J. Flegler, Bettina Böttcher, Vladimir Aseyev, Ann-Christin Pöppler, and Robert Luxenhofer. "Think beyond the core: impact of the hydrophilic corona on drug solubilization using polymer micelles." **ACS applied materials & interfaces** 12, no. 22 (2020): 24531-24543.

8. Malik Salman Haider, Jochen Schreiner, Sabine Kendl, Matthias Kroiss, and Robert Luxenhofer. "A Micellar Mitotane Formulation with High Drug-Loading and Solubility: Physico-Chemical Characterization and Cytotoxicity Studies in 2D and 3D In Vitro Tumor Models." **Macromolecular Bioscience** 20, no. 1 (2020): 1900178.

7. Mengshi Yang, **Malik Salman Haider,** Stefan Forster, Chen Hu, and Robert Luxenhofer." Synthesis and investigation of chiral poly(2,4-distributed-2-oxazoline) based triblock copolymer for chiral drug delivery applications". **Macromolecules** 55, no. 14 (2022) 6176–6190

6. Chen Hu, **Malik Salman Haider**, Lukas Hahn, Mengshi Yang, and Robert Luxenhofer. "Development of a 3D printable and highly stretchable ternary organic–inorganic nanocomposite hydrogel." **Journal of Materials Chemistry B** 9, no. 22 (2021): 4535-4545.

5. Chen Hu, Taufiq Ahmad, **Malik Salman Haider**, Lukas Hahn, Philipp Stahlhut, Jürgen Groll, and Robert Luxenhofer. "A thermogelling organic-inorganic hybrid hydrogel with excellent printability, shape fidelity and cytocompatibility for 3D bioprinting." **Biofabrication** 14, no. 2 (2022): 025005.

4. Michael M. Lübtow, , Sabrina Oerter, Sabina Quader, Elisabeth Jeanclos, Alevtina Cubukova, Marion Krafft, **Malik Salman Haider,** Clemens Schulte, Laura Meier, Maximilian Rist, Oltea Sampetrean, Hiroaki Kinoh, Antje Gohla, Kazunori Kataoka, Antje Appelt-Menzel, and Robert Luxenhofer "In Vitro Blood–Brain Barrier Permeability and Cytotoxicity of an Atorvastatin-Loaded Nanoformulation Against Glioblastoma in 2D and 3D Models." **Molecular Pharmaceutics** 17, no. 6 (2020): 1835-1847.

3. Michael M. Lübtow, **Malik Salman Haider**, Marius Kirsch, Stefanie Klisch, and Robert Luxenhofer. "Like dissolves like? A comprehensive evaluation of partial solubility parameters to predict polymer–drug compatibility in ultrahigh drug-loaded polymer micelles." **Biomacromolecules** 20, no. 8 (2019): 3041-3056

2. Thomas Lorson, Michael M. Lübtow, Erik Wegener, **Malik Salman Haider**, Solomiia Borova, Daniel Nahm, Rainer Jordan, Marina Sokolski-Papkov, Alexander V. Kabanov, and Robert Luxenhofer. "Poly (2-oxazoline) s based biomaterials: A comprehensive and critical update." **Biomaterials** 178 (2018): 204-280.

1. Michael M. Lübtow, Lukas Hahn, **Malik Salman Haider**, and Robert Luxenhofer. "Drug specificity, synergy and antagonism in ultrahigh capacity poly (2-oxazoline)/poly (2-oxazine) based formulations." **Journal of the American Chemical Society** 139, no. 32 (2017): 10980-10983.

Table of Contents

List of Abbreviations

17-AAG	17-allylamino-17-demethoxygeldanamycin
API	active pharmaceutical ingredient
approx.	approximately
ATV	atorvastatin
AUC	area under the curve
BSA	bovine serum albumin
CED	cohesive energy density
CMC	critical micelle concentration
CsA	cyclosporin A
CUR	curcumin
D_2O	deuterated water
DDS	drug delivery system
D_h	hydrodynamic diameter (investigated by DLS)
Đ	Dispersity
DLS	dynamic light scattering
DMF	dimethylformamide
DOX	doxorubicin
DSC	differential scanning calorimetry
etc.	et cetera (and so on)
e.g.	exempli gratia (for example)
ELP	ellipticine
et al.	et aliae (and others)
FDA	U.S. Food and Drug Administration
FT-IR	Fourier-transform infrared spectroscopy
GCM	group contribution method
GF	griseofulvin
HETCOR	heteronuclear correlation (in 2D NMR spectroscopy)
HPMAm-Bz	poly(*N*-(2-benzoyloxypropyl) methacrylamide)
HPMAm-Nt	poly(*N*-(2-napthoyloxypropyl) methacrylamide)
HPMCAS	hydroxypropylmethyl cellulose
HSP	Hansen solubility parameter
i.e.	id est (that is)
IMC	indomethacin
KETO	ketoconazole
LC	loading capacity; ($m_{drug}/(m_{drug} + m_{excipient})$)
LE	loading efficiency; ($m_{drug,\ solubilized}/m_{drug,\ added}$)
log *P*	partition coefficient (ratio of concentrations of a compound in a mixture of two immiscible phases, usually between octanol and water)
m-THPC	*meta*-tetra(hydroxyphenyl)chlorin
MD	molecular dynamics
nab	nanoparticle albumin-bound

NCE	new chemical entity
NMR	nuclear magnetic resonance
NP	nanoparticle
NCL	Nanotechnology Characterization Laboratory
IM	intramuscular
IV	intravenous
Ox	2-oxazoline; unspecified substituent at 2-position (according to the Hantzsch-Widmann-Patterson nomenclature for heterocyclic systems) systematic IUPAC name: 4,5-dihydrooxazole
Ozi	2-oxazine; unspecified substituent at 2-position (according to the Hantzsch-Widmann-Patterson nomenclature for heterocyclic systems) systematic IUPAC name: 5,6-dihydro-4*H*-1,3-oxazine
PAA	polyacrylic acid
PBS	phosphate buffered saline
PLA	polylactic acid
PDI	polydispersity index
PD	pharmacodynamics
PEG	polyethylene glycol
PEG-hexPLA	polyethylene glycol-*b*-poly(hexyl-substituted lactic acid)
PEG-PLA	polyethylene glycol-*b*-polylactic acid
pH	$-\log_{10}[H^+]$
Phe	phenylalanine
PHEA	poly[(*N*-2-hydroxyethyl)-aspartamide]
PLA	polylactic acid
PLGA	poly(*D*,*L*,-lactic-*co*-glycolic acid)
PMMA	poly(methacrylic acid)
PMs	polymeric micelles
PK	pharmacokinetics
POx	poly(2-oxazoline)
POzi	poly(2-oxazine)
ppm	parts per million
PTX	paclitaxel
PVP	polyvinylpyrrolidine
PVA	polyvinyl acetate
quer	quercetin
QSPR	quantitative structure-property relationship
R_h	hydrodynamic radius (investigated by DLS)
RNA	ribonucleic acid
SPR	Structure property relationship
SC	subcutaneous
SiRMS	simplex representation of a molecular structure
SPs	solubility parameters
SITUA	stable isotope tracer ultrafiltration assay
T2A	tanshinone IIA
TEM	transmission electron microscopy

List of symbols

°C	degree Celsius
δ	solubility parameter
	δ_T total solubility parameter (Hildebrand solubility parameter)
	δ_D, δ_P, δ_H contributions from intermolecular van-der-Waals forces, dipole-dipole interactions and hydrogen bonding, respectively
E_{total}	total energy of a system derived by COMPASS force field
ΔG_{mix}	Gibbs' free energy of mixing
g/L	grams/Liter
ΔH_M	enthalpy of mixing
h	hour
m	milli, 10^{-3}
ms	milliseconds
M	molar concentration, [mol/L]
M_w	weight average molar mass
M_n	Number average molar mass
mg/ml	milligram/milliliter
wt.%	weight percent ($w_{substance}/w_{mixture} \cdot 100\%$)
	e.g. 25 wt.% solution = 250 mg (substance)/0.75 mL (H_2O)
	= 250 mg (substance)/1000 mg (total)
mol	amount of substance: Avogadro number (N_A = 6.022…x10^{23}) x substance
χ_{FH}	Flory Huggins interaction parameter

1 Introduction

Humankind has always remained under the assault of various diseases, infections, and physical/ psychological trauma and the extent of suffering is continuously increasing with the increasing population and age. In spite of significant advancements in healthcare facilities, the medical experts and the scientists have to deal with variety of new cases everyday, which demands new materials (active pharmaceutical ingredients, excipients or biomaterials) capable to fulfill the medical needs. Additionally, because of rapidly growing interest in precision medicine, gene and immune therapies [1], advancements in tissue engineering [2] and three-dimensional (3D) bio printing [3, 4], there is further substantial push for this demand.

The technological innovations in drug discovery has led to development of larger, more complex hydrophobic compounds. According to an estimate, 40% of the drugs in market and 90% of the new chemical entities (NCEs) are mainly hydrophobic [5]. These molecules require specialized processing and safe vehicles for solubilisation to overcome these issues [6]. From the drug design and screening to drug delivery, the poor aqueous solubility is a key problem in the pharmaceutical industry.

Polymeric micelles (PMs) have emerged as a promising drug delivery platform. They are nanoscopic architectures formed by the self-assembly of amphiphilic polymers [7, 8]. During the self-assembly process, PMs are capable to encapsulate/solubilize the accompanied hydrophobic molecules. Owing to their unique characteristics, several PMs formulations are already in clinical trails like, NK105 and Genexol-PM [9-12]. However, PMs in general, suffer from intrinsic issues like low drug loading, instability [13] and poor permeability across cell membrane [14].

When the nature of a medical condition not necessarily demands the use of xenobiotics and the goal of treatment is to restore, maintain or improve damaged tissue or whole organ then the health care professionals seek help from the tissue-engineering experts. Currently, tissue engineering plays a relatively small role in patients treatment e.g. small arteries, cartilage, skin grafts, supplemental bladders and even full trachea have been implanted in patients, but the procedures are still experimental and costly. The highly complex organ-tissues like heart, liver, and lungs have been successfully created in the laboratories, but there is a long way from being fully reproducible and ready to implant organ into a patient. These tissues, however, can be quite useful in research, especially in drug development or ex-vivo experiments. Over the past two decades, hydrogels have been used as one of the most common tissue engineering scaffolds. They are capable to maintain a distinct 3-dimensional (3D) structure, provide mechanical support for the cells in the engineered tissues, and simulate the native extracellular matrix. Like native

tissues, hydrogels provide the high water content, which is ideal environment for cell survival. Hydrogels can also serve as a supportive matrix for cell immobilization and growth factor/small molecule delivery.

Thus, for the delivery of either hydrophobic drugs or for development of scaffolds for tissue engineering applications, there is clear need to find alternative formulations/vehicles and biomaterials, respectively, which can successfully assure their dispensing for the better outcomes of the patients. The successful utilization and future of these materials is not limited only to the development but more importantly, understanding of structural information with respect to their properties or simply structure property relationship (SPR). The development of SPR is very important to understand the complex nature of various process for the development of optimized materials.

In the past decades, poly(2-oxazoline)s (POx) and poly(2-oxazine)s (POzi) have gained significant attention for pharmaceutical and biomedical applications [15-17]. Unlike other systems, the POx/POzi based ABA triblock copolymer (A and B, standard for the hydrophilic and hydrophobic blocks, respectively) have shown great potential for development of ultra-high drug loaded micellar formulations [15]. At the same time, POx/POzi based hydrogel forming amphiphiles have also shown great potential for tissue engineering applications.

In the literature, sometimes, the terms “pharmaceutical” and “biomedical” are used interchangeably. However, in this thesis, for the ease of understanding, they are clearly segregated i.e. pharmaceutical for drug delivery applications and biomedical, for tissue engineering applications. The major aim of this project was to explore the pharmaceutical and biomedical applications of POx/POzi based ABA triblock and AB diblock copolymers, respectively with the special emphasis on SPR. To address the issue of poor aqueous solubility, initially I have developed a formulation library comprising 21 highly diverse, hydrophobic drugs with POx/POzi based ABA triblock copolymers library. Theoretically, the extent of compatibility between polymers and drug was determined by calculating solubility parameters (SPs). The SPs were thoroughly investigated to check their applicability in present systems. The selected formulations were further characterized by various physico-chemical techniques. For the biomedical applications, a novel thermoresposive diblock copolymer was synthesized which has shown promising properties to be used as hydrogel bioink or can potentially be used as fugitive support material. The most important aspect i.e. SPR, was studied with respect to hydrophilic block in either tri or diblock copolymers. In the following sections we will learn that how this hydrophilic block affected the drug loading in case of micelles or the physico-chemical properties of hydrogel bioink. Apart from the basic research, the therapeutic applications of two formulations i.e. mitotane (commercially available as tablet dosage form) and BT-44 (lead compound for nerve regeneration) were studied in more detail.

2 State of the Art

Depending upon overall aim of the project (as mentioned in the introduction part), in the following sections, insights into the various aspects are given which are directly or indirectly related to the goals of project. The most important aspect is structure property relationship, which has remain a central point for both pharmaceutical (micelles), and biomedical applications (hydrogels) of POx based amphiphiles.

2.1 Smart Materials for Drug Delivery and Tissue Engineering

Advances in high throughput screening, polymer synthesis, molecular self-assembly, microfabrication technology, peptide and protein engineering have collectively introduced next generation smart materials [18, 19]. These are capable to adopt their physico-chemical properties in response to change in external stimuli (Figure 1). Some smart materials also display unique mechanical properties like self-healing or shape memory behavior [20, 21].

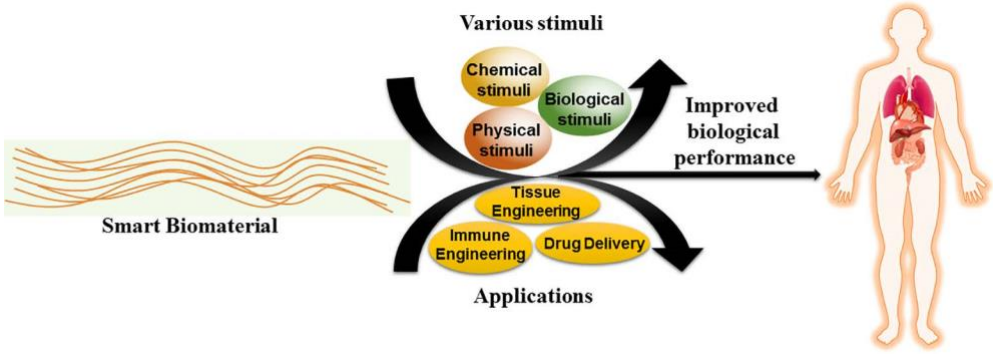

Figure 1: Schematic representation of importance and application of smart biomaterials. Reprinted with permission from [19]. Copyrights 2018, American Chemical Society.

Besides many other types of polymers used for tissue engineering and drug delivery applications [22, 23], the demand for amphiphilic block copolymers is on surge [24]. They are highly popular because of their great potential in terms of stimuli responsiveness, drug loading capabilities, and reversible thermal gelation properties. These features make amphiphilic block copolymers an excellent candidate for small molecule delivery, gene therapy and for designing injectable hydrogels for tissue engineering or 3D bioprinting applications (Figure 2).

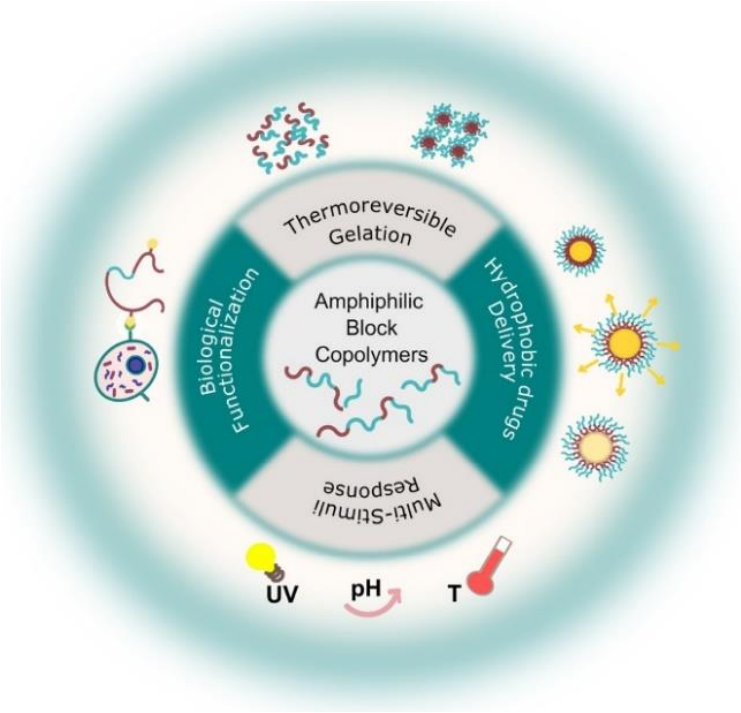

Figure 2: Schematic representation of properties and applications of amphiphilic block copolymers. Reprinted with permission from [24]. Copyrights 2021, Elsevier.

Despite their tremendous potential, such materials need extensive research before they can used for clinical applications. It is worth mentioning here, this thesis is mainly focusing on the design, development and applications of POx/POzi based di and triblock copolymers. In the later sections, we will learn how they are segregated in the main aims of the thesis and how their structure property relationship appeared as controlling tool for tuning their physico-chemical properties and ultimate performance.

Drug delivery is the method or process of administering a pharmaceutical compound to achieve a therapeutic effect in humans or animals [25]. Therefore, drug delivery systems (DDS) can be interpreted as an interface between patient and drug [26]. To obtain an optimal therapeutic response, the appropriate amount of drug must be absorbed and transported to general circulation (in case of oral administration) and with the safe amount of biocompatible carriers in case of intravenous (IV) administration.

Many existing and new therapeutic entities are characterized as Biopharmaceutical classification system (BCS) class II (low solubility and high permeability) or BCS class IV (low solubility and low permeability) (Figure 3a). According to an estimate, 80 out of 200 commercially available drugs for oral administration are practically insoluble in water (Figure 3b) [27]. The pharmacodynamic (PD) and pharmacokinetic (PK) properties of any drug molecule are critically affected by its physico-chemical properties.

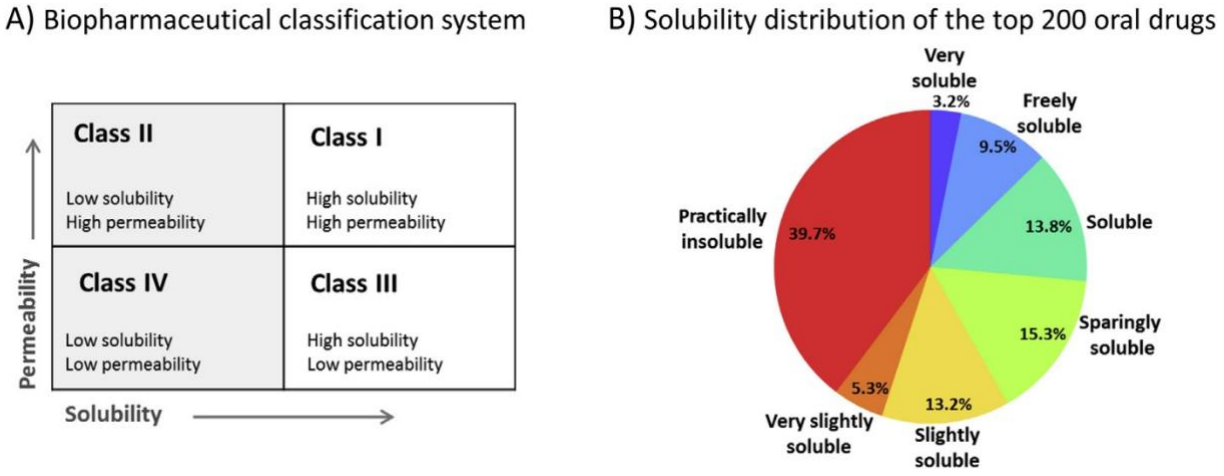

Figure 3: A) The biopharmaceutical classification system (BCS) and B) the solubility of the top 200 marketed oral drugs in the United States and Europe. Reprinted with permission from [27]. Copyrights 2015, Elsevier.

Extensive research is on going to overcome the problems of poor drug solubility and poor permeability. Various techniques e.g use of salt form, precipitation inhibitors, pH modifier, surfactants, drug nanocrystals, micellar solubilization, solid dispersion, microemulsion and nanonisation are being applied to address these issues [27, 28]. The potential benefits of insoluble drug delivery technologies are shown in Figure 4.

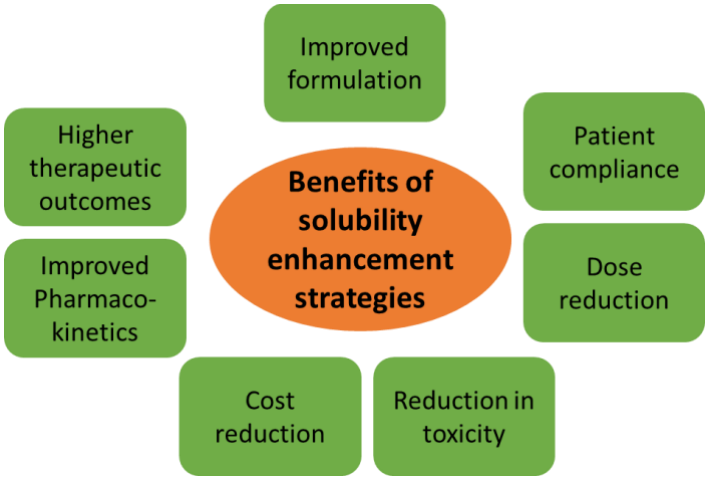

Figure 4: Schematic representation of benefits of solubility enhancement strategies.

To overcome these issues, the clinical practice still involves the use of excipients that can cause life threatening side effects, such as Cremophor EL (now re-branded as Kolliphor EL) and ethanol in Taxol (paclitaxel, PTX), or polysorbate 80 and ethanol in Taxotere (docetaxel, DTX) and Jevtana (cabazitaxel, CBZ). These excipients can cause severe hypersensitivity reactions in patients [29].

Additionally, one of the biggest clinical issue related to accidental injuries is the repair/regeneration of soft and hard tissue defects or damages. Initially, the patients are treated with surgical reconstruction, artificial implants or organ transplantation. The most commonly used method is allograft or autograft

transplantation and associated donor shortage and donor morbidity are big hurdles. Because of these limitations, the number of patients waiting for transplants grows annually, and clinicians and scientists require alternative treatment methods to avoid such a long wait. To repair the tissue defect or initiate tissue regeneration, the tissue engineers have provided the material based therapeutic solutions to enhance the rate and quality of patient's lives. The prevailing paradigm is associated with design and development of appropriate (bio) materials and simultaneously, delivery of seeded cells and/or signaling molecules. Tissue engineering application also involve nearly all the drug delivery applications. The delivery strategies have ranged from simple matrix embedding, development of microparticles for sustained drug release, or covalent attachment of drugs to the scaffolds for tissue engineering applications.

2.2 Demand for New Excipients and (Bio) Materials

Ali and Kolter having long-term industrial formulation experience, give a somewhat drastic assessment of the situation writing "The continued trend of increased number of poorly soluble and permeable molecules is alarming and has brought the industry nearly to a standstill" [5]. Obviously, the demand for excipients, which increase the aqueous solubility and thus, the bioavailability of hydrophobic drugs is enormous. For example, there are few excipients, which are specially developed for hot melt extrusion (e.g. Soluplus). It is estimated that the existing monographed excipients will not be sufficient to support newly discovered active pharmaceutical ingredients in future. In short, the constant shift of trends in the pharmaceutical sectors, especially new drug development, continuous manufacturing, and novel drug technologies, lead to a surge in demand for excipients with smart functions. Besides the pharmaceutical sectors, the demand for smart biomaterials for tissue engineering applications is also on surge.

2.3 Nanomedicine

Nanomedicine utilizes the properties by a material at its nanometric scale 10^{-9} m that often differ in terms of physics, chemistry or biology from the same material at a larger scale [30]. It applies nanotechnology to achieve innovation in healthcare. The nano-sized carrier systems, i.e. drug delivery systems with sizes below 100 nm have emerged in various pharmaceutical areas including drug delivery, diagnosis and imaging, synthetic vaccine development and miniature medical devices. However, in various scientific contributions the systems with size < 500 nm also described as "nano". In majority cases, for drug delivery applications, nanomedicine is mainly concerned with liposomes, organic/inorganic nanoparticles and micelles (Figure 5).

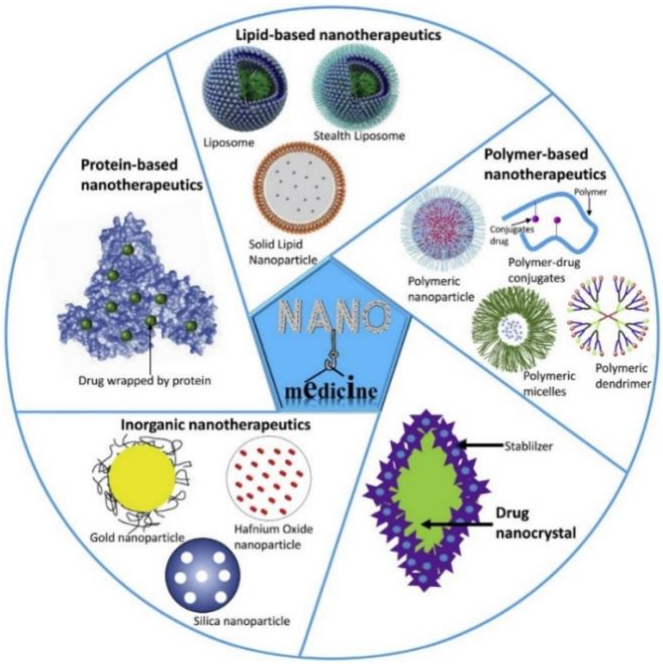

Figure 5: Nano-therapeutic platforms in clinical use i.e. lipid based, polymer based, drug nanocrystals, inorganic and protein based nano-theraputics. Reprinted with permission from [31]. Copyrights 2020, Elsevier.

A recent review published by European technology platform on nanomedicine (ETPN) explain the importance and progress of nanomedicine field in the last decade [32]. This review came out particularly in response to the an editorial by Prof. Park, Purdue University, USA published in Journal of Controlled Release mentioning that in the last 15 years, nanomedicine has failed to deliver the promised innovative clinical solutions to the patients [33]. However, the ETPN team respectfully disagreed and presented a review which is based on facts and figures [32] explain breakthroughs in the field of nanomedicine and over all success rate (Figure 6)

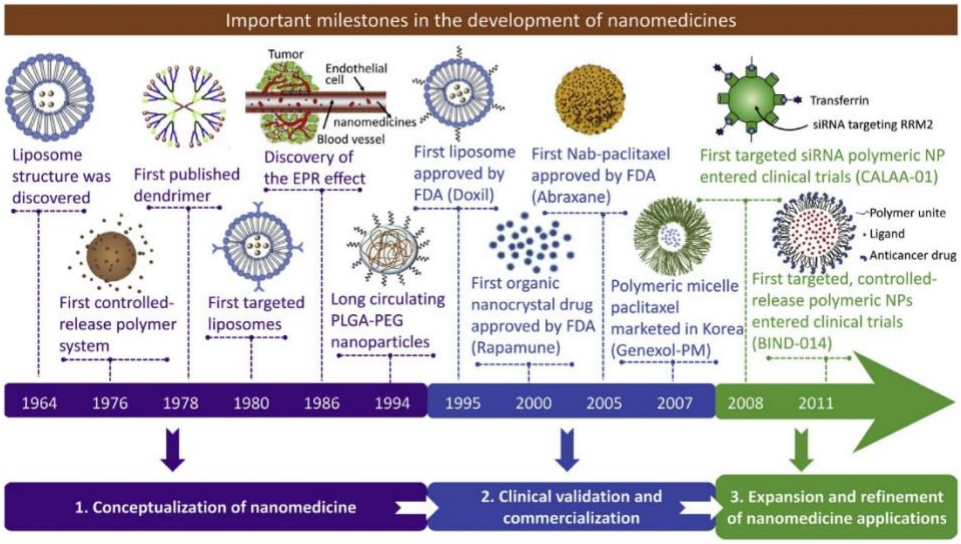

Figure 6: Schematic representation of the progress of nanomedicine development (purple to green, lower panel). Some important milestones throughout the history of the development of nanomedicine. Reprinted with permission from [31]. Copyrights 2020, Elsevier.

On the other hand, the level of expectations related to nanosystems have not always been met, because of e.g. potential toxicity of nanomaterials, lower level of in vitro/in vivo correlation, and scale up/production. Nevertheless, a growing number of nanocarriers are presently approved and many are in clinical trails and in the market. The progress in nanomedicine can be divided into 3 stages (Figure 6), the first 30 years (royal blue) mainly involved the discovery, basic understanding and development of the nanomedicine which finally resulted in first nanomedicine product i.e. liposomal doxorubicin. The second stage (blue) majorly involved the clinical validation commercialization while in the third stage (green) until now; we have observed an exponential progress in smart nanotherapeutics.

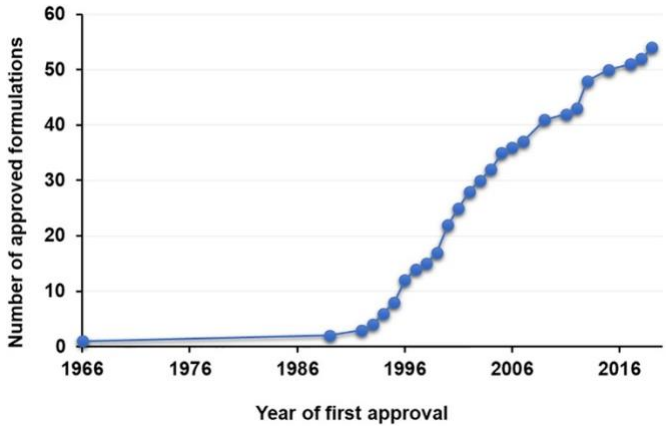

Figure 7: Evolution of the approved nanomedicine formulations (cumulative number/year). First year of approval reported for formulations approved by multiple agencies (e.g. EMA and FDA). Reprinted with permission from [32]. Copyrights Elsevier 2020.

The published data shows, there are more than 50 formulation (Figure 7), currently in the market and > 400 nanomedicine formulations are in the clinical trials. The approval of three new formulations (Vyxeos, Onpattro and Hensify) are clearly demonstrating that new generations of nanomedicine has already reached to the market and opened new gateways for future development with innovation. The data from the clinical trials obtained from the year 2008 to 2020 shows that the 65% of nanomedicine based formulations are focusing on the cancer treatment while 35% are for other ailments (Figure 8).

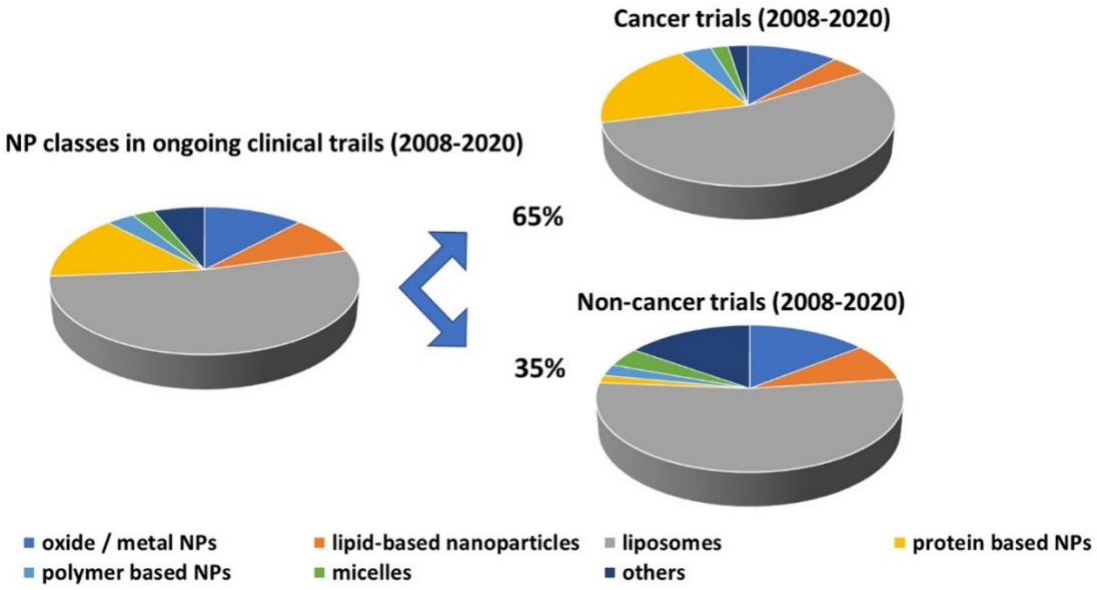

Figure 8: Nanoparticle classes investigated in ongoing clinical trials. The analysis was performed on 409 clinical trials from 2008 to 2020 (active, ongoing or recruiting), identified in the clinicaltrials.gov database in May 2020. Search limited to trials identified with the following keywords: nanoparticle, liposome, liposomal, lipid, vaccine, micelle, nanocrystal, virus like particle, silica particle, iron oxide, extracellular vesicle, dendrimer, nanobubble, lipoplex, gold nanoparticle. These keywords were used alone or in association with other diseases or technologies specific keywords: COVID-19, mRNA, nucleic acid, cancer. Only trials using nanoparticles were selected. Repartition of nanoparticle types is presented for all ongoing clinical trials, for cancer related applications (65% of the total) and for all applications outside oncology (35% of the total). Reprinted with permission from [32]. Copyrights 2020, Elsevier.

2.4 Polymeric Micelles

Polymeric micelles (PMs) have emerged as a promising drug delivery platform. They are nanoscopic architectures formed by the self-assembly of amphiphilic polymers (Figure) [7, 8]. During the self-assembly process, PMs are capable to encapsulate/solubilize the accompanied hydrophobic molecules and can potentially overcome several issue related to drug administration from poor aqueous solubility to poor membrane permeability across biological barriers [11, 34].

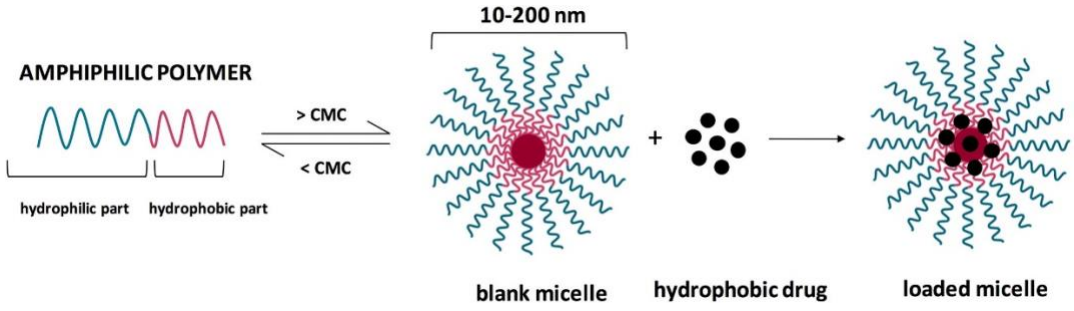

Figure 9: Schematic representation of polymeric micelles. Reprinted with permission from [34]. Copyrights 2021, Elsevier.

The standard model of drug loaded micelles is that of a core-shell structure, where core is responsible for drug encapsulation and shell provide the colloidal stability and some level of protection for the drug. In the following sections, we will learn that simple core-shell architecture is the oversimplification of micellar structure particularly in case of POx based micelles. Owing to their unique characteristics, several PMs formulations are already in clinical trials and available in the market (Figure 10) [9-12].

Product	Incorporated drug	Status	Company
Genexol PM	Paclitaxel	Marketed	Samyang
Estrasorb	Estrogen	Marketed	Novavax
Medicelle	DACH-platin-PEG-polyglutamic acid	phase I/II	NanoCarrier
Flucide	Anti-influenza	phase I/II	Nano Viricides
Basulin	Insulin	phase II/III	Flamel Technologies
DO/NDR/02	Paclitaxel	phase I/II	Dabur Research Foundation
NK-911	Doxorubicin	phase II	Nippon Kayaku Co.
NK-105	Paclitaxel	phase II/III	Nippon Kayaku Co.
NK-012	SN-38	phase II	Nippon Kayaku Co.
NC-6004	Cisplatin	phase III	Nanocarrier Co.
NC-4016	Oxaliplatin	phase I/II	Nanocarrier Co.
SP-1049C	Doxorubicin	phase II/III	SupratekPharma Inc.
NC-6300	Epirubicin	phase I/II	Nanocarrier Co.

Figure 10: Representative list of drug-loaded polymeric micelles based products. Reprinted with permission from [35]. Copyrights 2015, Chinese Pharmaceutical Association and Institute of Materia Medica, Chinese Academy of Medical Sciences. Production and hosting by Elsevier B.V.

Hydrophilic and hydrophobic polymers have been used for the design and development of amphiphilies to harness their potential for drug delivery applications e.g. polyethylene glycol (PEG), POx, poly(sarcosine), polysaccharides as hydrophilic and polyethers, polyesters, poly(aminoacid)s, POx, POzi etc. as hydrophobic polymers [11]. However, PMs in general, suffer from intrinsic issues like low drug loading, instability [13] and poor permeability across cell membrane [14].

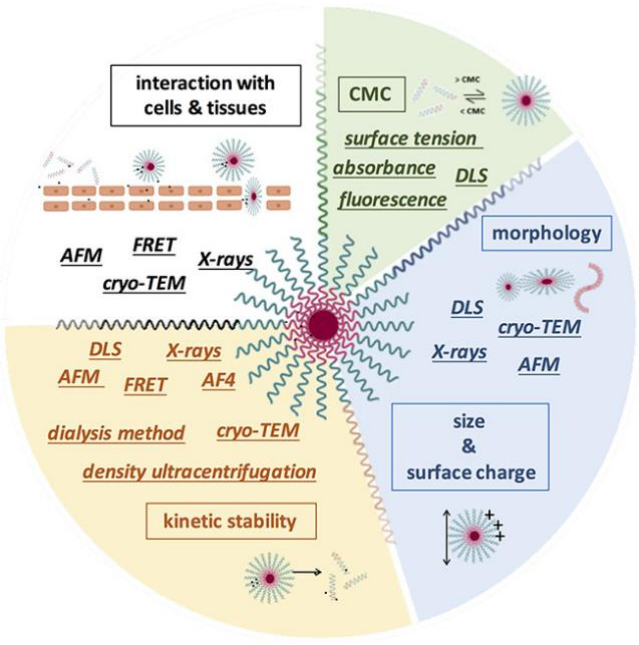

Figure 11: Schematic representation of polymeric micelles with various characterization techniques. Reprinted with permission from [34]. Copyrights 2021, Elsevier.

The development and clinical success of the micellar formulation demands their thorough characterization including their basic characteristics (critical micelle concentration, size, surface charge, morphology), interaction of cargo with carrier, kinetic stability, drug release, behaviour in the presence of biological media/substrate and in vivo fate (Figure 11) [34]. Variety of different techniques with their own advantages and limitations are available to achieve a deeper understanding of polymeric micelles.

2.5 Hydrogels

The Van and Bemmelen first introduced the term hydrogel in 1894, however the first report on biomedical applications of hydrogels was published by Wichterle and Lim in 1960 followed by further developments (Figure 12) [36, 37]. Since then a lot of research is going on about hydrogels in the field of agriculture, food industry, drug delivery, tissue engineering and regenerative medicine [38]. Hydrogels are 3D network structure; these are capable to hold large volume of water, due to presence of hydrophilic moieties. Besides high water content, the other properties of hydrogels like porosity, flexibility, stimuli-responsive, soft structure and its resemblance to living tissue pose them the ideal candidate for biomedical applications. Hydrogels can be presented as solid or semi-solid formulations by tuning their physicochemical properties and crosslinking reactions. Hydrogels are classified based on its source, preparation, physical properties, ionic charge, crosslinking and response. For few decades, hydrogel has been a field of research, so there have been hydrogel commercial products finding most applications in the medical field [38, 39].

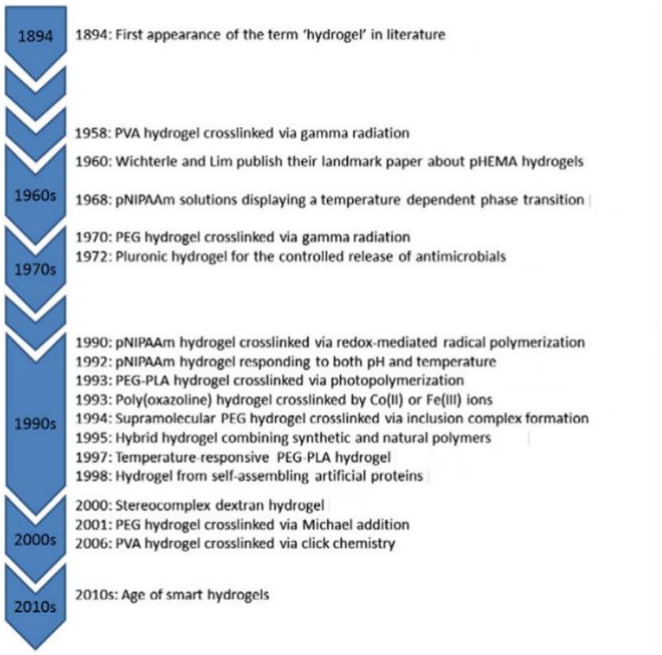

Figure 12: Timeline presenting the most important events in the history of hydrogel research. Reprinted with permission from [37]. Copyrights 2014, Elsevier.

With in smart hydrogels, a thermogel is a stimuli-responsive "smart" material, which responds to change in temperature, above or below the critical temperature by a (typically reversible) sol-gel transition. The gelation process is mainly due to the development of supramolecular structures yielding 3D, physically cross-linked networks because of hydrogen-bonding, coulomb/hydrophobic interactions or simple physical entanglement [40]. In the majority of cases, the transition takes place upon increase in temperature [41] but inverse gelation has also been observed [42-44]. So the thermoresponsive hydrogels as an injectable hydrogels have specially become popular in the field of tissue engineering and drug delivery (Figure 13 a) because of low invasive surgical procedure and shape adoptability in real time [45, 46].

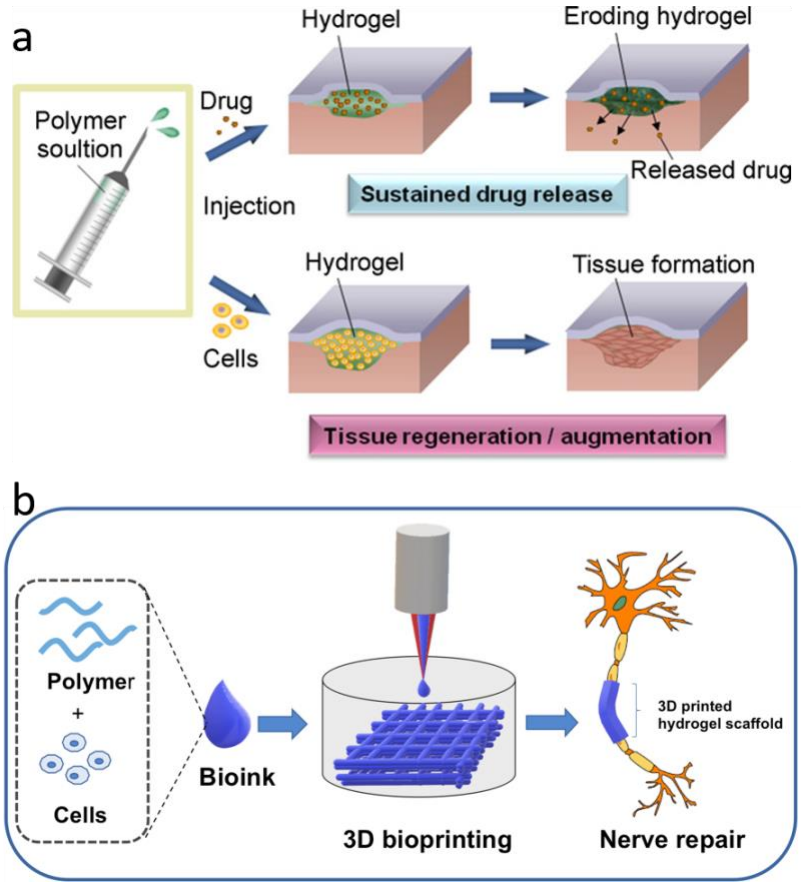

Figure 13: a) Applications of *in situ*-forming hydrogels for biomedical purposes. As injectable depots for sustained delivery of therapeutic molecules, the drug is co-dissolved with the polymer, injected into the body, and forms a gel, which releases the encapsulated drug in a sustained manner controlled by mass erosion of the hydrogel matrix. As an injectable, tissue supporting matrix, the hydrogel can be mixed with therapeutic cells and injected into a defective tissue site to promote the regeneration of tissue. Reprinted with permission from reference [47]. Copyrights 2009, Elsevier. b) schematic representation of bioink, 3D bioprinting and its application for tissue engineering applications [48]. Published by MDPI, Distributed under the Creative Commons Attribution License (CC B-Y 4.0).

Injectable hydrogels are actively used for 3D bioprinting. To develop complex tissues and organ constructs, 3D bioprinting by additive manufacturing is most promising technology for the scientist. The 3D bioprinting generally involve the addition of live cells to the hydrogels and printed in well arranged fashion to obtain 3D construct (Figure 13 b) [48]. These constructs offer a suitable environment to the cells by a nutrient support, gases exchange, waste removal and, depending upon chemistry of scaffold, the cell attachments sites. The researchers are now capable of creating the tissues structures similar to native tissues or organ with biomimetic functionalities.

The importance of hydrogels can be evidently observed from the growing number of publication each year (Figure 14). To show the publication trend (from 1950 to 2020), Janarthan et al. collected data by using specific search string like, “hydrogels”, injectable gel”, injectable hydrogels”, and 3D print hydrogels on the PubMed website [49].

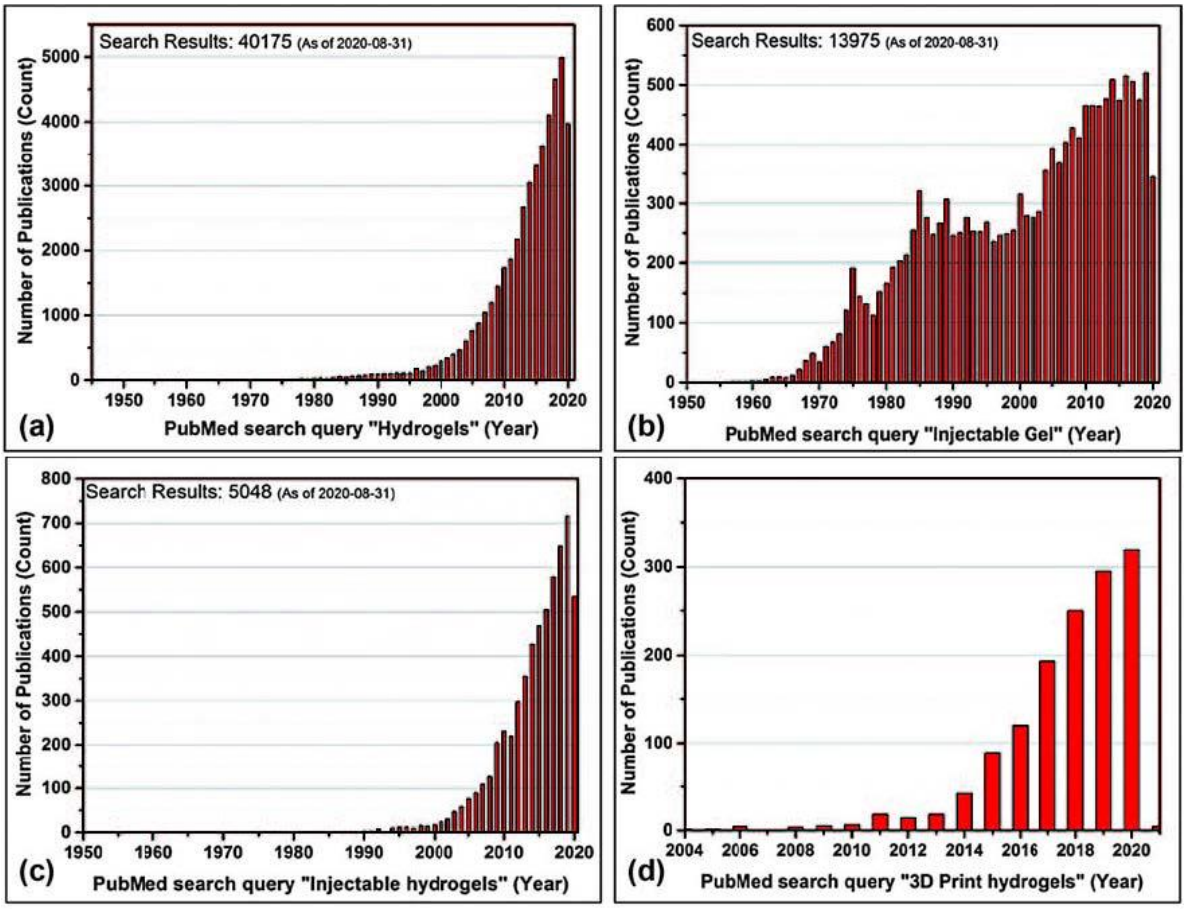

Figure 14: Number of search results (papers) obtained from PubMed search engine with different keywords: (a) Hydrogel, (b) injectable gel, (c) injectable hydrogels and (d) 3D print hydrogels. Reprinted with permission from [49]. Copyrights 2021, Royal Society of Chemistry.

Injectable hydrogels for biomedical applications should fulfill the certain criteria e.g. the sol-gel transition should be possible under mild conditions, the gelation should be relatively fast to prevent the outflow of

materials to the surrounding tissues and it should be (bio) degradable. When it comes to 3D printing, the rheology of the hydrogel plays a very important role for further translation. All the hydrogels should be thoroughly tested for rheological profile (Figure 15) [50].

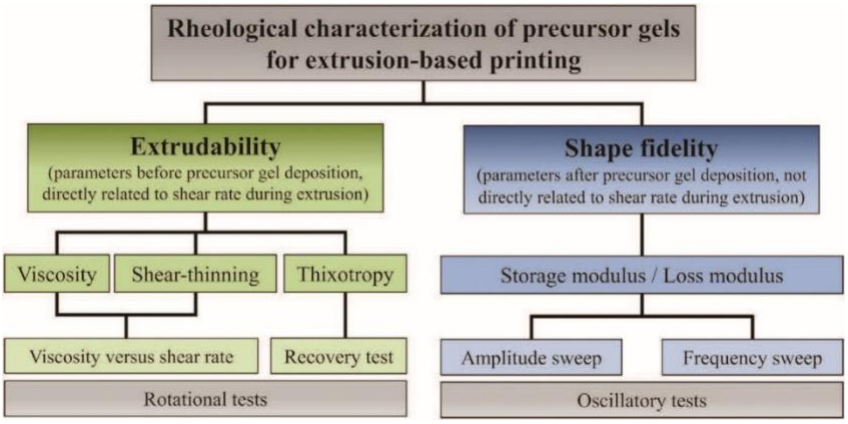

Figure 15: Summary of tests for rheological characterization of precursor gels based on key variables for extrusion-based printing. Reprinted with permission from [50]. Copyrights 2020, Wiley-VCH Verlag GmbH & Co. KGaA, Weinheim.

2.6 Prediction of Polymer Drug Compatibility

In 1950s, Hildebrand reported that the physical and the chemical bonds in any material (e.g. covalent bonds, hydrogen bonds, ionic bonds, and Van der Waals interaction) are calculable values. In this regard, the energy needed to overcome these forces and pull a molecule or an atom from the whole assembly is called cohesive energy [51]. If we divide this energy with the molar volume of the compound, we get cohesive energy density (CED) or solubility parameters (δ). When two substances have same or close CED or δ values, it means they are miscible or considered as compatible [52]. However, the predictive power of the Hildebrand solubility parameters is limited to nonpolar and slightly polar systems such as hydrocarbons without hydrogen bonding. In 1967, the Charles M. Hansen divided the CED into 3 individual components, i.e. dispersion (δ_d), polar (δ_p) and hydrogen bonding contributions (δ_h) and this became the core idea of Hansen solubility parameters (HSPs) [53]. This division had broadened the possible applications of HSPs in not only chemical but oil, paint and most importantly pharmaceutical industries. The predetermination of solubility parameters between solute and solvent (or drug and polymer) and subsequent compatibility estimation can save both time and cost in industrial processes. Many researchers are using the SPs for variety of applications [54-56]. The use of SPs has shown some success in paint and oil industries. Additionally, the SPs are also frequently used in other sectors to find the best solvents for drugs [57], cosmetics [58], oligomers [59] etc. However, in this regard the systematic determination of SPs and its application in wide variety of drug/polymer formulation (or complexes) remained limited without any solid outcome. There can be two main reasons for this; the first one is that drugs and cosmetics have

typically more varied functional groups (which in turn effect the physicochemical properties) and the second reason is the SPs do not include the thermodynamics consideration.

In this regard, while considering the thermodymics, Allen and coworkers tried to predict physico-chemical properties of polymer based formulations of the hydrophobic, anticancer drug, ellipticine (ELP; water solubility = 0.153 mg/L) by determining partial and total solubility parameters [60]. The enthalpy of mixing (ΔH_M) was calculated by considering the volume fractions of drug and polymer. The lower ΔH_M values obtained by HSPs indicated higher compatibility between ELP/PCL (polycaprolactone) than ELP/PLA (poly(D, L-lactide)) (Figure 16 a). In the FTIR spectra of the physical mixtures of the respective polymers and ELP, no obvious shifts occured in any peaks corresponding to functional groups capable of hydrogen bonding. In contrast, in the spectra of formulated ELP/polymer films, slight shifts in characteristic peaks occurred, suggesting specific drug/polymer interactions (spectra not shown). The ELP micellar formulations with block copolymers comprising PCL (PEG_{113}-*b*-PCL_{35}) or PLA (PEG_{113}-*b*-PLA_{60}) as hydrophobic core were prepared by dry down and dialysis method. For both methods, the PCL based formulations exhibited much higher loading efficiencies (LE) at all investigated ELP/polymer feed concentrations (Figure 16 b). It can be concluded that the compatibility between ELP and polymers predicted with ΔH_M correlated well with the obtained LEs. Overall, a good correlation was observed between theoretical compatibility profile and experimental results of the formulation.

a)

polymer	$\Delta\delta_D$	$\Delta\delta_P$	$\Delta\delta_H$	$\Delta\delta_T$	ΔH_M
PCL	6.5	1.1	-0.7	5.9	**10.8**
PLA	6.6	-3.6	-4.1	2.8	**14.3**

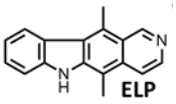

ELP

b)

ELP/polymer [w/w]	dialysis method *LE* [%]		dry-down-method *LE* [%]	
	PEG-PCL	PEG-PLA	PEG-PCL	PEG-PLA
1/20	72	1.9		
1/10	76	1.2	65	6.2
1/5	76	0.6		
1/2	65	--		

Figure 16: a) Difference between total δ_T and partial solubility parameters δ_D, δ_P, δ_H and enthalpy of mixing ΔH_M of ELP and PCL or PLA; b) LE of PEG-PCL and PEG-PLA based ELP formulations prepared by dialysis or dry-down-method at polymer concentration of 10 g/L. Modified and reprinted with permission from [60]. Copyrights 2004, Elsevier.

In addition, Louwerse et al. revisited the SPs by implementing further details of the thermodynamics of dissolution and mixing. By going into the detail of enthalpy and entropy, the authors have suggested certain corrections, which include accounting for the solvent molecule size, the destruction of solid crystal structure, and the specificity of hydrogen bonding interactions as well as the opportunities to predict the

SPs at extrapolated temperatures. The improved methods were tested on large industrial dataset and the percentage of correct predictions rose from 54 to 78%.

In the work presented by Möller and coworkers [61], the extent of compatibility (by Flory-Huggins interaction parameter χ_{FH}) between the polymer and drugs were determined by molecular dynamics (MD) simulations instead of using conventional group contribution methods. The tested polymer was an amphiphilic diblock copolymer with PEG as hydrophilic block and poly(hexyl-substituted PLA as hydrophobic block (hexPLA-PEG)) and the four different model drugs were employed i.e. cyclosporine; CsA, aqueous solubility ≈ 12 mg/L , griseofulvin; GF ≈ 21 mg/L, ketoconazole; keto ≈ 17 mg/L, quercetin dihydrate; quer ≈ 60 mg/L (Figure 17 a). More importantly, in this case the whole diblock copolymer (hydrophobic as well as hydrophilic block) was brought into considerations for estimating the compatibility profile. The solubilizing capacity of hexPLA-PEG diblock copolymer was tested for all of the listed drugs by cosolvent evaporation method (Figure 17 b). The solubility of CsA, GF and Keto was increased significantly by hexPLA-PEG formulation, however, the solubility of quer dihydrate remained nearly the same. After the formulation results, MD simulations were run using AMBER 10 software. The block copolymer as well as the drugs were parametrized using the "general AMBER force field (GAFF)". For MD simulations, 16 polymer chains were disposed randomly and uniformly in space. From the formulation results, the stoichiometric ratio between polymer/drugs was calculated (per micelle) and the same respective number of drug molecules were chosen for MD simulations. To guarantee, almost equal spacing, the drug molecules were added randomly and uniformly in the empty cavities between the polymer chains (Figure 17 c). After equilibrating the hexPLA-PEG/drug micelles in vacuum to account for compaction that is present in the bulk of the micelles, water molecules were added (Figure 17 d). The χ_{FH} values were obtained for every polymer/drug combination after reaching equilibrium with stability. The negative χ_{FH} values in all systems suggested that hexPLA-PEG diblock copolymer should be capable to solubilize all four drugs, which, according to the authors, nicely reflected in experimental formulation results. However, it is obvious from the formulation experiments, that the increase in solubility of quer dihydrate is rather negligible. Nevertheless, the trend in χ_{FH} was in accordance with experimental solubilities with CsA having the highest and quer dihydrate having the lowest molar solubility with polymer formulation (Figure 17 e). Unfortunately, the impact of different polymer/drug ratios deviating from the experimentally determined, "optimal" ratios has not been further investigated. At the same time, the formulation results were extrapolated in a way to check the applicability and validity of MD simulations, which ideally should be other way round.

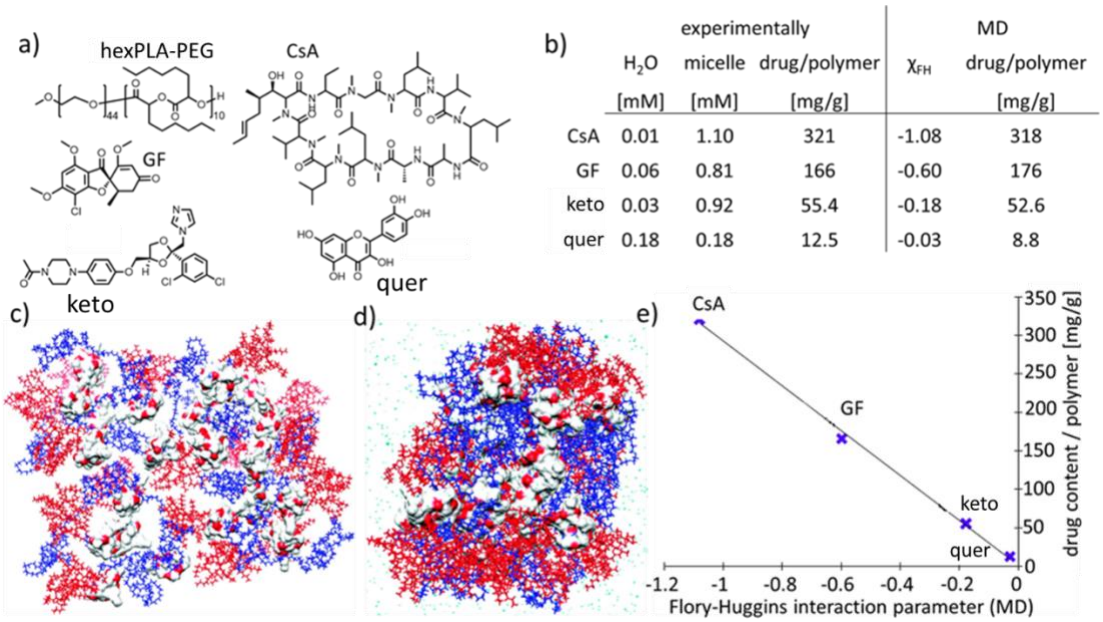

Figure 17: a) Chemical structure of polymeric drug carrier hexPLA-PLA as well as hydrophobic drugs; b) experimentally as well as MD determined solubilities of the different drugs in water as well as hexPLA-PEG/drug formulations; c) snapshot of the initial „open configuration" of the CsA loaded PEG-hexPLA system (blue: PEG; red: hexPLA). The 21 drug molecules are presented as van-der-Waals surface; d) snapshot from the production-phase MD simulation of CsA loaded hexPLA-PEG micelles. (c); water molecules are represented in cyan); e) relationship between χ_{FH} (derived from MD simulations) and the experimentally determined maximum drug loading. Modified and reprinted with permission from [61]. Copyrights 2012, American Chemical Society.

Despite the predictive power, the MD simulations are expensive and still limited by two principal factors i.e. the force fields (which require further refinements) and high computational demands e.g. one microsecond simulation (of a small system approximately 25,000 atoms) running on 24 processers may take several months to complete. So collectively, their routine application, particularly in pharmaceutics and drug delivery is hampered. In contrast, as discussed previously, the routinely used, fast screening of polymer/drug interactions based on group contribution methods such as Hildebrand or Hansen solubility parameters is many times unreliable and non-systematic.

In the year 2019, Kabanov and coworkers presented a cheminformatics driven discovery of a suitable drug carriers [62]. It required less computational power than MD simulation, additionally, the predictive power was found to be much higher than conventional group contribution methods based compatibility evaluation. The novel descriptors of POx/drug complexes were used to predict LC and LE of POx based formulation. The work-flow included the following steps; a. the selection of 21 chemically diverse, hydrophobic drugs (based on previously collected data on 20 drugs); b. compilation and integration of experimentally determined LC and LE of 41 drugs, which collectively comprised 408 experimental data points (including different drug feed concentrations, structural diversity of POx polymers and experimental

conditions); c. identification of novel chemical descriptors for polymers and polymer/drug complexes; d. development and interpretation of quantitative structure property relationship (QSPR) models; e. the virtual screening of poorly soluble drugs with high or low LC and LE and f. validation of model predictions with experimentally determined LC and LE values of virtually selected hits (Figure 18 a).

The HiT QSAR software was used to generate the 2D SiRMS (simplex representation of molecular structure) descriptors of tetratomic fragments (consisting of four atoms) with fixed composition and topological structures. At the 2D level, the connectivity of atoms in a simplex includes atom type and bond nature (single, double, triple or aromatic). The SiRMS, additionally accounts for atomic characteristics such as partial charge, lipophilicity, or ability to form hydrogen bonds. At the same time, each block of the POx polymer was described by the number of its repeating units (Figure 18 b). Generally, the SiRMS descriptors were calculated for simplified polymer representations as pseudo small molecules. In the case of formulation, i.e. polymer/drug complexes, each complex was represented as a binary mixture composed of drug molecule, and the simplified representation of the polymer. The random forest algorithm was used to develop the QSPR models, which were further used for virtual screening of DrugBank database to identify the drugs predicted to have both, high and low LC and LE.

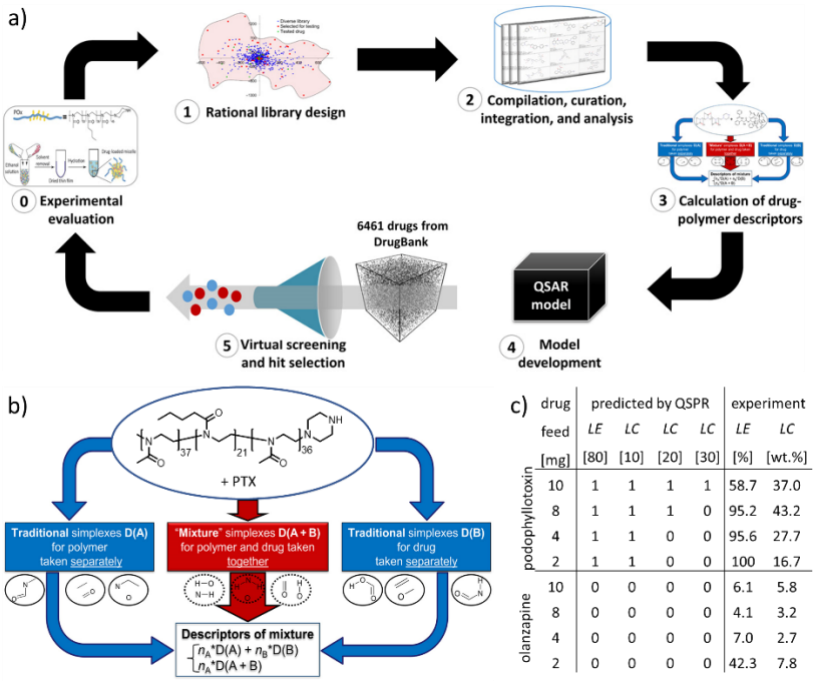

c)

	drug feed [mg]	predicted by QSPR LE [%]	predicted by QSPR LC [80]	predicted by QSPR LC [10]	predicted by QSPR LC [20]	predicted by QSPR LC [30]	experiment LE [%]	experiment LC [wt.%]
podophyllotoxin	10	1	1	1	1	58.7	37.0
	8	1	1	1	0	95.2	43.2
	4	1	1	0	0	95.6	27.7
	2	1	1	0	0	100	16.7
olanzapine	10	0	0	0	0	6.1	5.8
	8	0	0	0	0	4.1	3.2
	4	0	0	0	0	7.0	2.7
	2	0	0	0	0	42.3	7.8

Figure 18: a) Study design to identify suitable POx based drug-carriers for the solubilization of poorly-soluble drugs. The process (step 3) to obtain descriptors of polymer, drug, or polymer/drug complexes is shown in b). The n_A and n_B are molar fractions of components A and B; c) LC and LE of POx based formulations of podophyllotoxin (positive hit) or olanzapine (negative hit) either predicted by QSPR or experimentally determined. Predicted values are based on

a binary code (0 = false; 1 = true) and the respective units (brackets) correspond to a predicted LC < 10, 10-20, 20-30 or >30 wt.% and LE > 80 %. Distributed under the Creative Commons Attribution License, CC BY-NC 4.0 [62].

Overall, a 75% experimental hit rate was achieved between predicted and experimentally verified polymer/drug compatibility. In the predicted positive hits (high LC and LE), the three out of four drugs displayed moderate to excellent solubilization in POx micelles e.g. LC ≈ 43 wt.% for podophyllotoxin (Figure 18 c). In contrast, the diosmin to be the best solubilized, was a false positive, i.e. insoluble in POx micelles. Besides correctly predicting low LC and LE for olanzapine, the false negative simvastatin was found to be highly soluble in POx micelles (LC ≈ 41 wt.%). Besides, the predicted LC < 10 wt.% of spironolactone and tamibarotene was also not in good agreement with the experimentally determined LCs ≈ 17 wt.% and 25 wt.%, respectively. Therefore, the prediction of negative hits generally seemed to be less reliable than of positive hits. Nevertheless, it is quite remarkable that the variation between predicted and experimental LC and LE of 6 out of 8 drugs was small. Furthermore, to the best of my knowledge, this is the first study about the prediction of polymer/drug compatibility that considers the impact of experimental formulation conditions such as drug-feed concentration, solvent used for hydration, hydration temperature or total solvent volume before evaporation. Indeed, it was proven multiple times that these conditions have a large impact on formulation properties [63], wherefore a reliable prediction of polymer/drug compatibility is only possible under consideration of the latter. In summary, the philosophy of SPs is correct and applicable but at the same time it carries certain limitation which scientist are trying to overcome with certain methodologies [54-56, 58, 62].

2.7 Poly(2-Oxazoline)s and Poly(2-Oxazine)s based Amphiphiles

Poly(2-oxazoline)s (POx) have recently attracted considerable attention for biomedical applications [15, 64]. However, they have been discussed to have significant potential as biomaterials for decades [16, 65, 66]. POx also have close relative i.e. their higher and much less investigated homologue named poly(2-oxazine)s (POzi) [67]. The renaissance of the POx family dates back to the early 2000s, when their potential use as biomaterials in medical applications, namely as an alternative to poly(ethylene glycol) (PEG), has been recognized. This spike culminated most recently first-in-human studies were initiated using a POx-based therapeutic for the treatment of Parkinson´s disease [68, 69]. The recent couple of years have additionally seen a particular increase in the use of POx-based systems for drug delivery and tissue engineering applications [15, 64, 70-74].

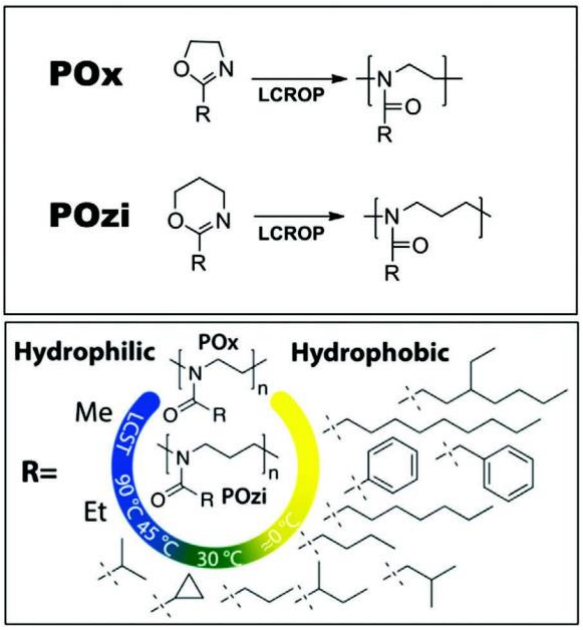

Figure 19: Polymerization of POx and POzi, variability of solubility profile depending upon side chain of POx/POzi. Published by John Wiley and Sons, distributed under the Creative Commons Attribution License, CC. B-Y. 4.0 [15].

POx and POzi can easily be synthesized via living cationic ring-opening polymerization (LCROP) (Figure 19) [75]. They are highly tunable with respect to their amphiphilic character, particularly the side chain substituent of 2-oxazoline or 2-oxazine monomer can be varied providing access to large library of amphiphilic copolymers with unique properties (the longer the side chain, the more hydrophobic the polymer is, as shown in Figure 19 lower panel). In this series, the polymers with shortest side chain are poly(2-methyl-2-oxazoline) (pMeOx) and poly(2-ethyl-2-oxazoline) (pEtOx). Regardless of temperature, pMeOx is soluble in water while pEtOx exhibit lower critical solution temperature (LCST) type behaviour and temperature dependent aqueous solubility [76, 77]. Both of these, i.e. pMeOx and pEtOx have been studied thoroughly as highly hydrophilic polymers which are discussed as one potential alternative to PEG, because of non-toxic and non-immunogenic nature, low unspecific organ uptake and rapid clearance (at right size) [17, 78-80]. Both of these polymers have shown distinct physico-chemical solution properties. Grube et al. explained the solution properties of POx in comparison to PEG, both pMeOx and pEtOx with same molar mass (as PEG) were less solvated and physically more compact [81]. Without significant accumulation in organs and tissues, the homopolymers of pMeOx and pEtOx have shown rapid clearance from the blood stream in mice [82, 83]. The POxylation of various molecules (i.e. covalent attachment of hydrophilic pMeOx or pEtOx) for drug delivery applications (such as in case of liposomes) have shown longer circulation time and provide protection from reticuloendothelial system (RES) similar to their PEGylated counter parts [84, 85]. The cytocompatiblity of various POx/POzi has been established several times in variety of cell lines in vitro and in vivo models [15, 71, 86-93]. In various attempts to control the

protein adsorption and cell adhesion on biomaterials, the POx particularly pMeOx, pEtOx and pMeOzi (poly(2-methyl-2-oxazine)) showed better performance than PEG [94-96].

POx and POzi based ABA triblock copolymers have shown tremendous potential to deal with difficult to solubilize drugs. In majority cases, the hydrophilic block A is pMeOx while hydrophobic block B can be from a series of linear [97, 98], branched (aliphatic POx with varying side chain lengths; C4-C9) [87, 99] or an aromatic ring side chains [90, 100]. Amongst many POx based triblock copolymers [87], the most commonly explored amphiphile is A-pBuOx-A [15, 70, 90] allowing, *inter alia*, ultra high drug loading for PTX (≈ 50 wt.%) (A= pMeOx, B= pBuOx; poly(2-n-butyl-2-oxazoline)).

The clinically approved formulations of paclitaxel (Taxol® and Abraxane®) and other Paclitaxel formulation in advanced clinical stages (Genexol-PM and NK105) are diverse in nature. While the two polymer based nanoformulations Genexol-PM and NK105 have high relative drug loading of approximately 20 wt.% (Figure 20) their solubility is low and the final injectable formulation has a very low PTX concentration (< 1 mg/mL), requiring large injection volumes and long perfusion times.

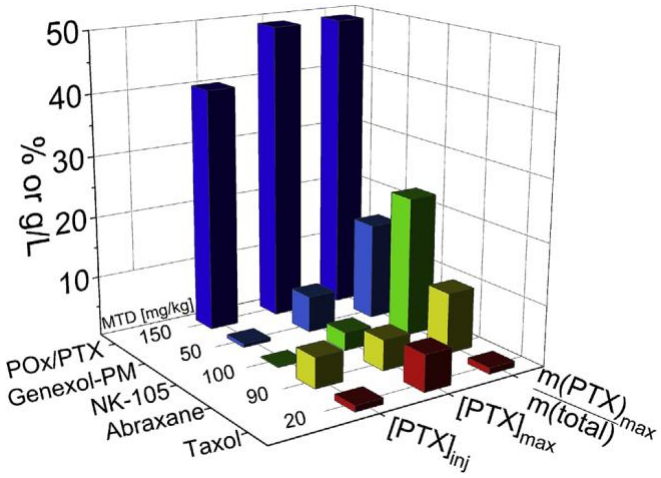

Figure 20: Comparison of drug loading and paclitaxel concentrations (maximal and *ad injectbilia*) of various clinically approved paclitaxel formulation with A-pBuOx-A based formulation with the reported MTD (maximum tolerated dose). Reprinted with permission from [101]. Copyrights 2016, Elsevier.

In the case of A-pBuOx-A/PTX formulation, the final PTX concentration was found 4 times higher (up to 40 mg/mL) as compared to Abraxane (Figure 20) [102]. Because of the ultra-high drug loading, the total amount of polymeric excipient was significantly reduced to administer the therapeutic doses of PTX. As a result, the potential excipient related toxicity was reduced and the maximum tolerated dose was increased as compared to Taxol and Abraxane (commercially available) in mouse models.

Utilizing the same formulation, very recently, Hwang et al. reported on the comprehensive preclinical assessment of A-pBuOx-A/PTX formulation including its detailed PK/PD profile and bioequivalence to the Abraxane in rats and non-human primate models (rhesus macaques) [103]. The physico-chemical

characterization and toxicity analysis were conducted by using standardized protocols by the Nanotechnology Characterization Laboratory (NCL). The bioequivalence studies were performed by NCL's established stable isotope tracer ultrafilteration assay (SITUA) to delineate the plasma PK of each PTX fraction (i.e. encapsulated in micelles, protein bound and free PTX in plasma). As compared to previously reported study [101] (where MTD was found to be 150 mg/kg) (Figure 20), the maximum tolerated dose (MTD) was found to be 125 mg/Kg in the same strain of mice (Figure 21 a). The author claim that this slight difference can be attributed to the slightly different hydrophilic-lipophilic balance (the hydrophilic block length in triblock copolymer used in present study differed from the one used in previous study. This had potentially lead to the varied drug disposition and subsequent drug toxicity profile. The tumor inhibition study revealed the comparable anti-tumor efficacy in xenograft tumor model (in mice). The Abraxane and the POx based formulation displayed similar tumor inhibition in MDA-MB-231 human breast xenograft model in mice at dose of 90 mg/kg (Figure 21 b). The well documented PTX related neurotoxicity was also studied by investigating the demyelination of sciatic nerve in mice. The luxol fast blue stain was used for staining the myelinated region (as blue) and demyelinated region (as pink) (Figure 21 c). Both A-pBuOx-A/PTX and abraxane showed comparable severity of neuropathy i.e. 2.0 and 2.2, respectively (Figure 21 d).

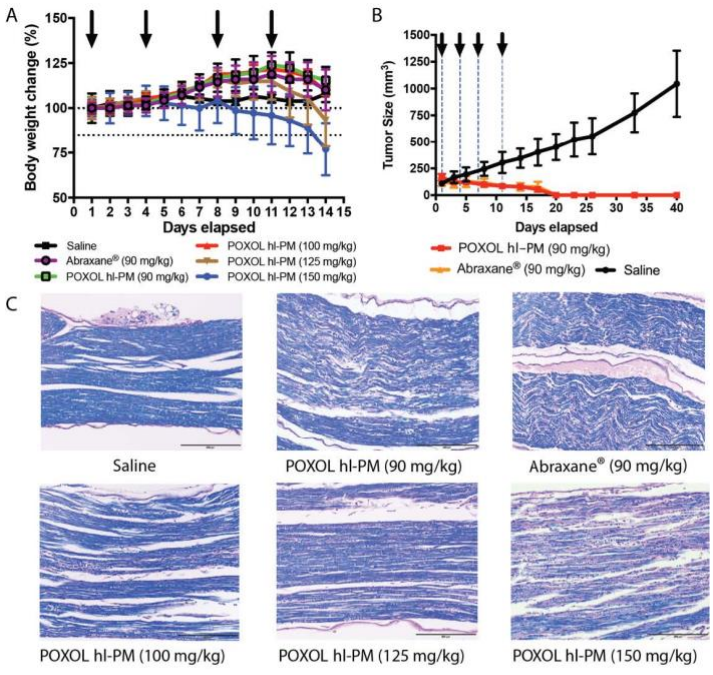

D

Treatment	n	0	1+	2+	3+
Saline	2	1		1	
Abraxane® (90 mg/kg PTX equivalent)	3			2	1
POXOL hl-PM (90 mg/kg PTX equivalent)	3			3	
POXOL hl-PM (100 mg/kg PTX equivalent)	3	1	1	1	
POXOL hl-PM (125 mg/kg PTX equivalent)	3			1	2
POXOL hl-PM (150 mg/kg PTX equivalent)	3				3

Figure 21: Toxicity and efficacy assessment of POXOL *hl*-PM and Abraxane® in mouse**.** (A) MTD of PTX equivalent (batch 2) (B) Tumor inhibition in MDA-MB-231 human breast xenograft model. (C) LFB-PAS-stained sciatic nerve sections for the histological assessment of neurotoxicity following treatments with saline, Abraxane® (90 mg/kg PTX equivalent) and POXOL hl-PM (90 mg/kg, 125 mg/kg, and 150 mg/kg PTX equivalent). (D) Scoring of neuropathy in a 4-point scale (POXOL hl-PM = A-pBuOx-A/PTX micellar formulation). Reprinted with permission from [103]. Copyrights Elsevier 2021.

To investigate the PK profile, both animal models i.e. rats and rhesus macaque were employed. The SITUA method (Figure 22 a) was used to quantify the various drug fractions in the blood. In rats, the A-pBuOx-A/PTX formulation exhibited tri-phasic concentration time curves. The encapsulated drug was found in low quantities for both formulation i.e. A-pBuOx-A/PTX and Abraxane. The free drug represented approximately 10 % of the total drug, while the protein bound drug was dominated and found identical in both formulations. In addition to the total PTX PK, subset drug fractions such as encapsulated, protein-bound, and unbound drug PK were bioequivalent in rats (Figure 22 b). Similar results were also obtained in rhesus macaque (Figure 22 c).

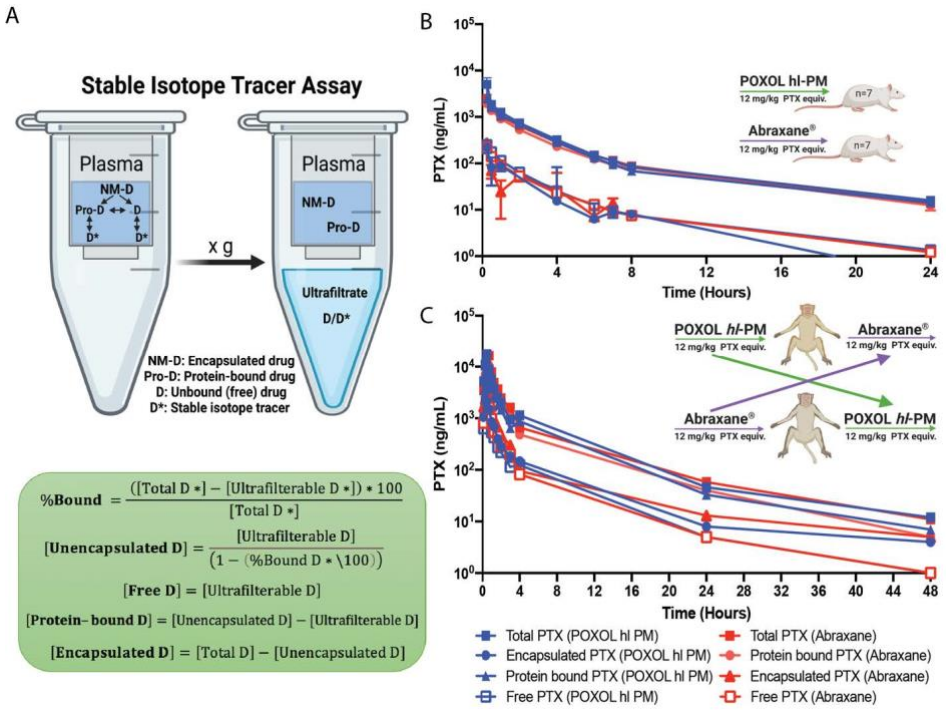

Figure 22: Pharmacokinetics of POXOL and Abraxane® in rats and rhesus macaques. (A) Schematic illustration of stable isotope ultrafiltration assay (SITUA) (created with BioRender.com). Equations for free, encapsulated and protein-bound PTX time concentration comparison for POXOL (batch 3) and Abraxane® in (B) utilized rats and (C) rhesus macaques. A two-arm parallel study design was in rats (n=7-8) and a crossover design was used in rhesus macaques (n=2) (POXOL hl-PM = A-pBuOx-A/PTX micellar formulation). Reprinted with permission from [103]. Copyrights Elsevier 2021.

Besides taxanes, several structurally very distinct drugs have also been successfully formulated by same amphiphile, including, mitotane, atorvastatin, curcumin, vismodegib, etoposide, 17-AAG, bortezomib,

cyclosporine A etc. [62, 70, 71, 88-91]. This novel platform combines a number of advantages, which summarily makes this material uniquely suited for the formulation of water-insoluble drugs [104]. At the same time, the POzi based structural isomers i.e. poly(2-n-butyl-2-oxazine) (pBuOzi) or poly(2-n-propyl-2-oxazoline/oxazine) (pPrOx/pPrOzi) have also shown very interesting properties such as ultra-high drug loading, excellent cytocompatibility and are very well tolerated upon in vivo administration [16, 29, 92]. More importantly, they also allow a significant therapeutic improvements as demonstrated for several drugs and drug combinations [71, 89, 101, 105]. For POx based amphiphiles, it has been established repeatedly, that a minimal contrast in hydrophilic/lipophilic domains is beneficial [99], to achieve high drug loading [63, 88, 90, 100, 105, 106]. Therefore, in this thesis, ABA triblock copolymers with minor amphiphilic contrast were selected and further explored.

The POx based polymers have also shown great potential in tissue engineering, bio-fabrication and design of synthetic bio-interfaces. In 2013, Farrugia and the coworkers reported the first example of pMeOx based hydrogels as a support for 3D cell culture [107]. The statistical copolymer including hydrophilic pMeOx and 2-(dec-9-enyl)-2-oxazoline (DecEnOx) (hydrophobic) were synthesized by LCROP with the terminal alkene groups (Figure 23 a). RGD peptides featuring thiol group were subsequently coupled to the alkene group of p(MeOx-ran-DecEnOx) precursors by UV-mediated thiol-ene reaction. The formation of p(MeOx-ran-DecEnOx-RGD) hydrogels (5, 10 and 25% RGD) were further enabled by second thiol-ene reaction using dithiothreitol (DTT) as crosslinking agent and Irgacure 2959 as photo initiator.

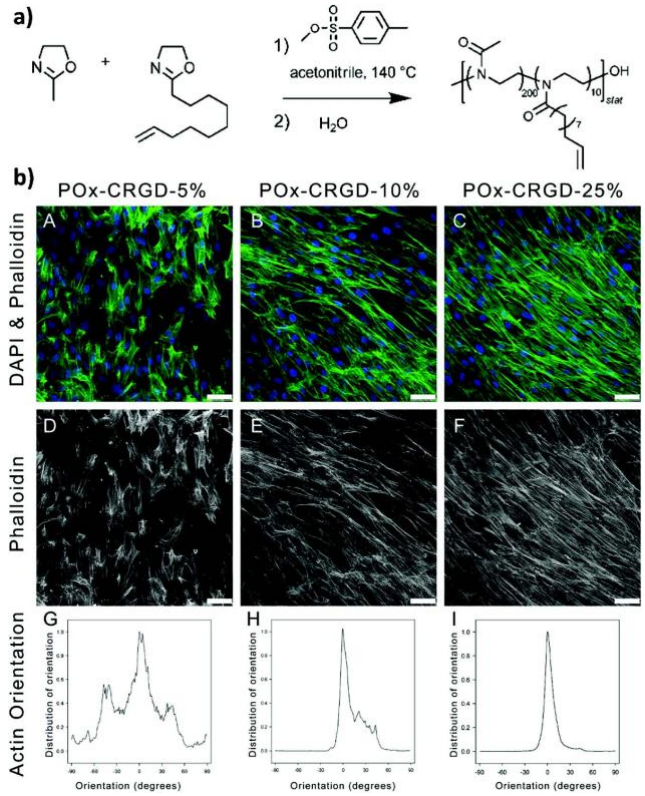

Figure 23: (a) CROP of pMeOx and DecEnOXA, using methyl para-toluenesulfonate as the initiator and water as the terminating agent to yield (pMeOx-ran-DecEnOXA). (b) Effect of an increasing amount of the incorporated RGD peptide into pMeOx hydrogels on fibroblast attachment and morphology; (A, D) 5% RGD, (B, E) 10% RGD, and (C, F) 25% RGD. (A–C) Immunofluorescence micrographs showing the cells seeded onto the pMeOx hydrogels, following staining with phalloidin and DAPI to visualize actin cytoskeleton fibres and cell nuclei, respectively. (D–F) Immunofluorescence micrographs showing the actin fibres. Scale bar = 50 µm. (G–I) Quantification of the actin orientation of fibroblasts adhered to the surface of pMeOx hydrogels with an increasing amount of RGD. Reprinted with permission from [107] Copyrights 2013, American Chemical Society.

The moduli of RGD functionalized hydrogels were in close range i.e. 3.5, 4.3 and 4.5 kPa for 5, 10 and 25%, respectively. In order to investigate the effect of RGD concentration on the fibroblast attachment and morphology, the cells were cultured on the surface of hydrogels for 3 days (Figure 23 b). The increase in RGD loading did not significantly change the number of cells on the hydrogel surface but the cell morphological changes were apparent. The cells attached to the 5% RGD hydrogel had wide variability in actin orientation (Figure 23 c). With the increasing RGD loading, the actin fibres become more aligned and cells on 25% RGD hydrogels exhibited spindle like fibroblast morphology. From the chemical structure, it is apparent that the hydrogel lack the degradation sites and are too tightly crosslinked to enable the cells to fully form the spread morphology and migrate through the hydrogel. At the same time, no morphological features of the hydrogels itself were presented or discussed.

In a very recent study, You et al. presented the first in vivo data on POx based hydrogels [73]. The authors fabricated the p(EtOx-ran-pButenOx) (poly(2-butenyl-2-oxazoline)) based hydrogels for epicardial placement of mesenchymal stromal cells (MSCs) for cardiac repair post-myocardial infarction. The hydrogels were crosslinked by thiol-ene chemistry and made cell-degradable by incorporating the di-cysteine cell-degradable peptides. Initially, the morphology of MSCs was regulated by tuning mechanical and cell-degradable properties, which can directly influence the expression and secretion of proangiogenic cytokines and growth factors. In the rat myocardial infarction models, the pre-hydrogel mixture (with excellent tissue adhesiveness) was directly applied onto the epicardium, followed by photocrosslinking yielding cell-laden hydrogels at area of interest. After the application of MSC-loaded hydrogels, the neovascularization in the infarcted cardiac tissue at the epicardium-hydrogel interface was confirmed by the immunostaining of the epicardium for isolectin B4 (the microcapillary specific marker) (Figure 24 a, b, c). In comparison to an untreated infarcted cardiac tissue, a significant upregulation of cardiac reparative factors i.e. VCAM-1 and VEGF in the infarcted epicardium treated with the MSC-loaded hydrogels was observed (Figure 24 d). The echocardiographic imaging of the rat heart, 28 days post myocardial infarction induction demonstrated the enhanced cardiac function after epicardial placement of MSC-loaded

hydrogels. The histological analysis exhibited the reduction in collagen deposition and interstitial fibrosis (which are directly related to scar formation).

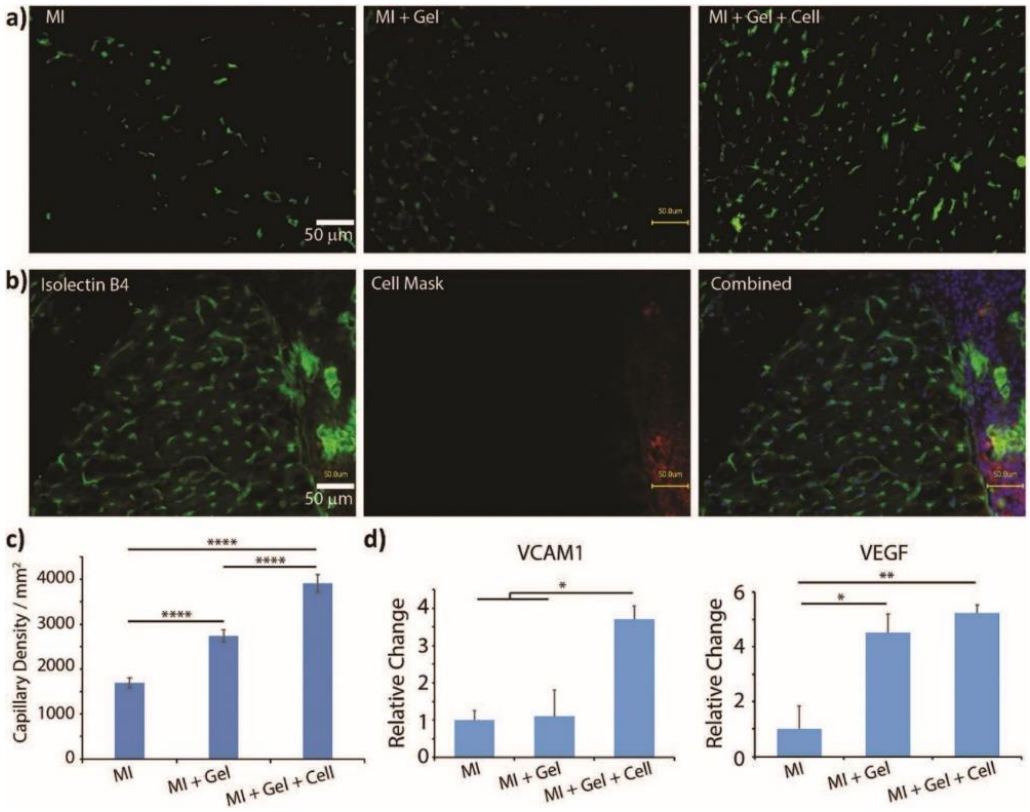

Figure 24: (a) Isolectin B4 staining demonstrated increased capillary density in the border area of myocardial infarction (MI) induction followed by hydrogel placement (MI + Gel) and MI induction followed by MSC-loaded hydrogel (MI + Gel + cell) treatment groups compared to the MI only group; scale bar = 50 µm. (b) Capillaries formed inside the hydrogel layer. Red, CM Dil labelled MSCs; blue, DAPI; green, isolectin B4; scale bar = 50 µm. (c) Corresponding quantification of capillary densities. MI group (n = 3), MI + Gel group (n = 4) and MI + Gel + cell group (n = 4). (d) Quantification of VCAM-1 and VEGF gene expression in different MI groups (n = 3 for each group). *p < 0.05; **P < 0.01; ****p < 0.0001. Reprinted with permission from [73]. Copyright 2021, Elsevier.

As mentioned previously, a substantial increase in the applicability of POx/POzi based polymers have been observed in the past two decades for pharmaceutical and biomedical applications. However, the use of these polymers in hydrogel formulations and carrier materials for biomedical applications is still limited. The pioneering examples (Table shown below, Published by Royal Society of Chemistry, distributed under the Creative Commons Attribution License, CC BY-NC 3.0) of such materials are summarized in a latest review by Benetti and the coworkers. For further details on each hydrogel presented in the table, the readers are referred to the original review [64].

Summary of the different hydrogels formulations and biofabrication techniques that included POx/POzi based amphiphiles

Polymer composition	Type of crosslinking	Fabrication/ processing	Application	Ref.
P(MOXA-*ran*-DecEnOXA) 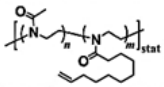	Thiol–ene reaction using DTT and CRGDSCG for cross-linking	UV irradiation	Human dermal fibroblasts 3D culture	33
P(MOXA-*ran*-DecEnOXA) 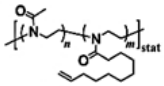	Thiol–ene reaction using DTT for cross-linking and to couple CRGDSG peptide	UV irradiation	Human primary stromal cell 3D culture	38
P(MOXA-*ran*-ButenOXA) and P(EOXA-*ran*-ButenOXA) 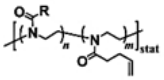 R = Me or Et functionalized with catechol groups	$NaIO_4$-mediated oxidation of catechols to quinones that react with each other forming crosslinks	—	Injectable tissue adhesive hydrogel for articular cartilage defect treatment	39
P(EOXA-*ran*-BocABuOXA), subsequently deprotected to P(EOXA-*ran*-ABuOXA) 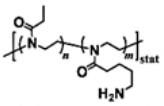	The addition of epichlorohydrin that reacts with the amines on the polymer resulting in crosslinking	—	Cationic hydrogels for reversible DNA complexing	49
P(EOXA-*ran*-BocABuOXA), subsequently deprotected to P(EOXA-*ran*-ABuOXA) 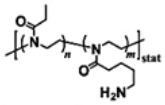	Supported structures were generated by soaking porous PE or PP filter materials in a copolymer/epichlorhydrin solution that cross-linked upon heating	Thermal treatment	Matrix supported hydrogels for DNA binding and release upon change in the temperature or pH	50
P(ButenOXA-*ran*-EI) 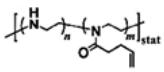	Hydrogels formed by thiol–ene cross-linking using dithiols	UV irradiation	DNA binding and release	51
P(EOXA-*ran*-ButenOXA) 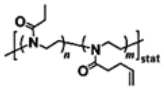 functionalized with di-cysteine cell-degradable and -adhesive peptides	Hydrogels formed by thiol–ene cross-linking	UV irradiation	Epicardial placement of mesenchymal stem cells for myocardial repair	40
P(MOXA-*ran*-MCEOXA) and P(EOXA-*ran*-MCEOXA) 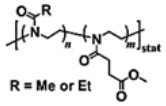 R = Me or Et functionalized with SA-substrate peptides	Hydrogels formed by enzyme (SA)-mediated cross-linking	—	Injectable hydrogel for 3D cell culture of human articular chondrocytes	46
P*n*PrOZI-*b*-PMOXA 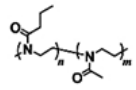	Thermogelation after extrusion yields hydrogels	Extrusion-based 3D printing	3D bioprinting of fibroblast-loaded hydrogel grids	56

continued

Polymer composition	Type of crosslinking	Fabrication/ processing	Application	Ref.
P*n*PrOZI-*b*-PMOXA 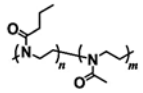	Thermogelation after extrusion yields hydrogels	Extrusion-based 3D printing	Improving the printability of the thermoresponsive ink by the addition of clay minerals (LAPONITE® XLG)	60
PMOXA-*b*-PPhOZI-*b*-PMOXA 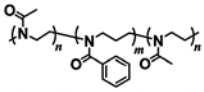	Inverse thermogelation of the amphiphilic triblock copolymers	Extrusion-based 3D printing	Sacrificial support material by 3D printing of alginate	54
P(EOXA-*ran*-MCEOXA) functionalized with SA-substrate peptides 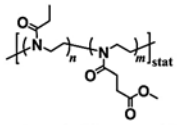	SA-mediated and ionic cross-linking of PEOXA and alginate, respectively, post extrusion forming hydrogels	Extrusion-based 3D printing	3D bioprinting of human auricular chondrocytes-loaded constructs	61
P(EOZI-*ran*-PI) functionalized with furan and maleimide moieties 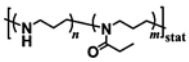	Spontaneous cross-linking *via* dynamic DA reaction post processing	MEW	Fabrication of micro-periodic fibrous scaffolds for human embryonic kidney cells	66
P(EOXA-*ran*-ButenOXA) 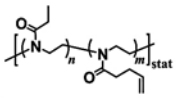	MEW of PCL fibres acting as a sacrificial template within photo-cross-linked PEOXA hydrogels	UV irradiation	Fabrication of hydrogel supports with interconnected channels that mimic organized vasculature	67
P(EOXA-*ran*-ButenOXA) 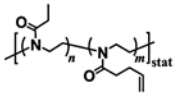	Thiol–ene cross-linking during electrospinning	Solution electrospinning and UV irradiation	Hydrogels from cross-linked fibrous structures	68
P(EOXA-*ran*-EI) functionalized with selenol groups 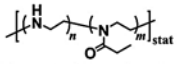	Formation of diselenide bonds between selenol-modified P(EOXA-*ran*-EI)	Solution electrospinning	Degradable diselenide-cross-linked nanofibres	70
P(EOXA-*ran*-EI) functionalized with benzophenone groups 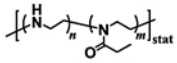	Radical addition of benzophenone to neighboring polymer chains forming cross-links	Solution electrospinning UV irradiation	Fabrication of water-stable nanofibres using temporally controlled UV crosslinking	71
PEOXA-DA telechelic macromonomers 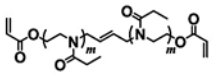	2PP	Near-infrared laser irradiation	3D micro-structured PEOXA hydrogels	73

Abbreviations: MOXA: 2-methyl-2-oxazoline, DecEnOXA: 2-(dec-9-enyl)-2-oxazoline, DTT: dithiothreitol, ButenOXA: 2-butenyl-2-oxazoline, BocABuOXA: 2-(4-((*tert*-butoxycarbonyl)amino)butyl)-2-oxazoline, ABuOXA: 2-aminobutyl-2-oxazoline, PE: polyethylene, PP: polypropylene, EI: ethylene imine, MCEOXA: 2-methylcarboxyethyl-2-oxazoline, SA: sortase A, P*n*PrOZI: poly(2-*n*-propyl-2-oxazine), PPhOZI: poly(2-phenyl-2-oxazine), EOZI: 2-ethyl-2-oxazine, PI: propylene imine, MEW: melt electrowriting, DA: Diels–Alder, and PCL: poly(ε-caprolactone).

2.8 Structure Property Relationship

Structure property relationship (SPR) have long been considered very important explanatory concepts in many disciplines like chemistry, pharmacology and biology [108]. The functioning of natural as well as synthetic materials depends on the composition, shapes and relationships of certain key parts as well as on the characteristics of the materials from which they are made of (Figure 25). The most common

example can be solubility of polymer in water, which increases when it has short branches and can be reduced by increasing the branch length or crosslinking. The relationship between the structure and function of a molecule is very important to not only understand their applications but also for the design of optimized systems for further applications in future.

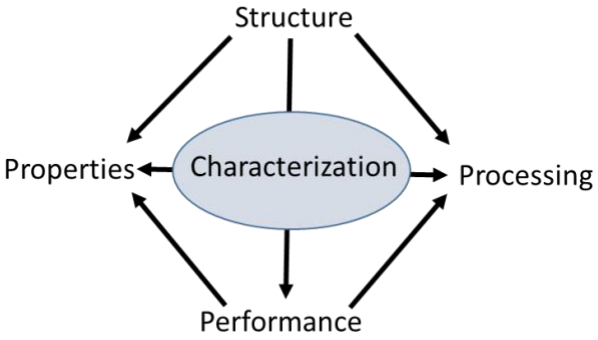

Figure 25: Schematic representation of structure property relationship and its interdependence on performance.

The SPR plays a very important role in drug delivery/tissue engineering applications of an amphiphile, as the performance of any materials is directly influenced by it characteristic. Naturally, all these characteristics strongly depend on the colloidal properties (size, charge, stability) of the respective formulation. Unfortunately, colloidal properties cannot be simply derived from the initial properties of the neat polymers, but are strongly affected by the kind and amount of incorporated drug (micelles) or the overall composition/concentration of polymer itself (hydrogels). The former case became more evident by the drug induced morphology switch of poly(2-oxazoline)s (POx) based micelles from worm-like, to spherical and raspberry-like structures with increasing loading (0-50 wt.%) of the chemotherapeutic agent paclitaxel (PTX) [109].

Despite the significant impact, the self-assembly process and the drug-polymer interaction are little understood. In majority cases in the literature, the out dated perception of like dissolve like or micellar core-shell architecture, where hydrophobic core is responsible for drug encapsulation and hydrophilic shell interacts with solvent molecules providing colloidal stability [110, 111], are repetitively discussed. Depending upon the nature of hydrophilic domain, cargo and employed (cargo) load, it is becoming more evident that at certain threshold concentration, the hydrophilic domain also start to interact [112-117] with cargo, indicative of much complex morphologies [118, 119]. Therefore, besides SPR, the interaction of molecules, their concentration and the process parameters collectively define the final performance of the product. In the context of colloidal stability, polymer-drug interactions also play a critical role in the drug loading capacity (LC), i.e. the amount (%) of drug solubilized within a formulation. Currently the gold standard for polymer therapeutics is PEGylation [120] but in majority cases a high drug loading is difficult

to achieve using conventional PEGylation procedure [121] and in most of micellar formulation the upper limit for LC is 20-30 wt.%. For in vitro biological activity (or cytotoxicity), only lower drug concentrations are required (typically nano- to micromolar range) but when it comes to in vivo studies, typically a high dose is required due to the (often)-large volume of distribution. In addition, ultra-high drug loaded formulations are favorable, particularly for injectable administration, because of limitation of injectable volume, in particular in mouse models. Therefore, various strategies have been employed in recent years to increase LC and stability of drug-loaded micelles.

The scope of such efforts is systematically displayed by the work of Börner and coworkers. To formulate a non-water soluble, anti-Alzheimer compound B4A1, a combinatorial approach was used to identify suitable peptide sequences out of 7^7 possible heptamers [122]. To select B4A1-binding peptides from large one-bead-one-compound peptide libraries (Figure 26 a) Raman microscopy was used. By split-and-mix procedures on ChemMatrix resin, the sequential space of 7^7 different heptamer peptides were synthesized. It was speculated that coulomb interactions and π-π stacking would dominate B4A1-peptide binding as the high affinity peptide sequences were rich in phenylalanine (Phe) and basic residues (Figure 26 b). LC was strongly dependent on the peptide sequence, as Pep_1-PEG, Pep_2-PEG and Pep_3-PEG exhibited payloads of 0.83 mol, 0.94 mol and 0.65 mol B4A1 per mol carrier, respectively. It is worth mentioning that such low drug loading are indicative of colloidal aggregate formation, rather than drug loaded micelles. However, the payloads were five to seven times higher than those achieved with the common solubilizer Chremophor EL. The dynamic light scattering (DLS) further confirmed the formation of aggregates (hydrodynamic radii (R_h) = 105-175 nm). The idealized 1:1 complexes of B4A1 and the peptide domains were simulated showing considerable binding of all three peptide sequences to B4A1 (Figure 26 c, d). Furthermore, the proposed π-π interactions between the Phe residues and the central pyrimidine ring of B4A1 were clearly visible, despite the dynamic nature of the model complexes (interaction energies between -150 and -200 kJ/mol).

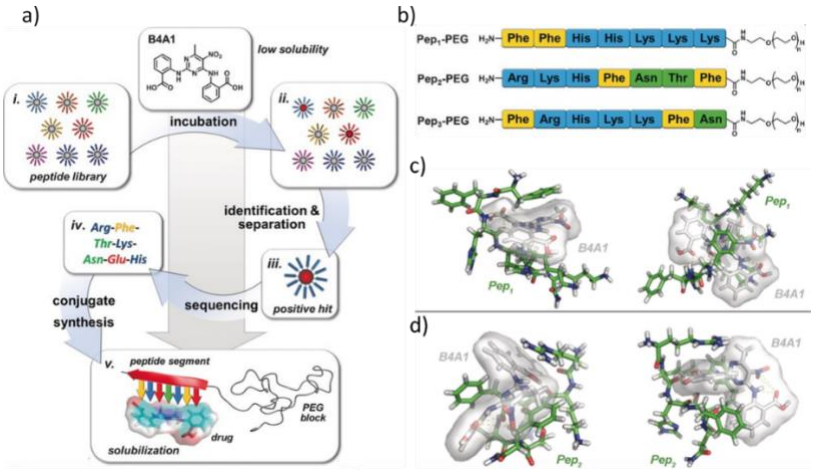

Figure 26: a) Selection of suitable peptide sequences for the solubilization of B4A1: (i) incubation of a one-bead-one-compound peptide library with B4A1 followed by (ii) Raman microscopy to identify (iii) compound-enriched beads; (iv) single-bead sequencing revealed b) peptides with high B4A1 binding capacities; c,d) representative snapshots from molecular dynamics simulations of B4A1 (shown as van-der-Waals surface) bound to tailored peptide sequences (sticks) shown in b). Reprinted with permission from [123]. Copyrights 2016, WILEY-VCH Verlag GmbH & Co. KGaA, Weinheim.

Peptide-drug specificities were also observed, when the structurally similar photosensitizers were formulated i.e. Chlorin E6 (Ce6), meta-tetra(hydroxyphenyl)chlorin (*m*-THPC) and Pheophorbide A (Pba) (Figure 27 a). The peptide sequence most suitable for Ce6 loaded, 18 and 5 times more Ce6 than m-THPC and Pba, respectively (Figure 27 b) [124]. On the other hand, the peptide sequence selected for m-THPC exhibited higher compatibility with Ce6 and Pba than with m-THPC.

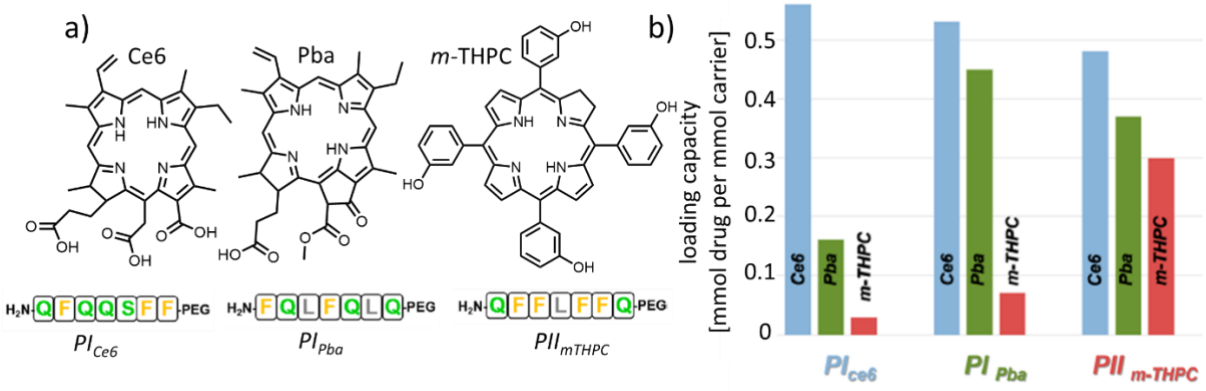

Figure 27: a) Chemical structure of photosensitizers Ce6, Pba, *m*-THPC as well as of peptide based drug carriers with the highest affinity for the latter (Q = glutamine; F = phenylalanine; S = serine; L = leucine); b) maximum *LC*s of the three different solubilizers. Modified and reprinted with permission from [124]. Copyrights 2017, American Chemical Society.

To evaluate the impact of amino acid residues (at specific sequence positions) towards overall LC, systematic residue point mutations alanine (Ala) scans were performed [124]. Again, the major driving forces for solubilization were found to be π-π stacking and hydrophobic interactions. The replacement of a Phe residue with Ala lead to decrease in LC (almost 100% decrease) for m-THPC, bearing easily accessible phenyl-rings, while replacing glutamine (Gln) or serine (Ser) residues with Ala caused a similar dramatic reduction in LC. The authors argued that this highlights the importance of hydrogen bonding for solubilization. However, taking into account the impact of the various point mutations gives a rather random picture and casts doubt on conclusive structure property relationships.

Another very good example of structure property relationship is displayed by the work of Press and coworkers [72]. They synthesized an amphiphilic graft copolymer based on poly(methyl methacrylate)-graft-oligo(2-ethyl-2-oxazoline)($EtOx_{15}$-MA or represented as P5). The backbone end group of P5 was further modified to obtain P5-SH (thiol), P5-DY654 (hydrophilic dye) and P5-MAA_4 (four repeating units of

methacrylic acid) (Figure 28, left panel). Besides using end group modified P5, the plain P5 and physical mixture of P5/P5-MAA_4 was also used to understand the influence on in vivo fate of the resultant nanocarriers. The DLS and cry-TEM showed the presence of spherical micelles around 10 nm in either blank or neutral lipid orange dye loaded micelles. No differences were observed in size or morphology of the micelles in any case (Figure 28, right panel).

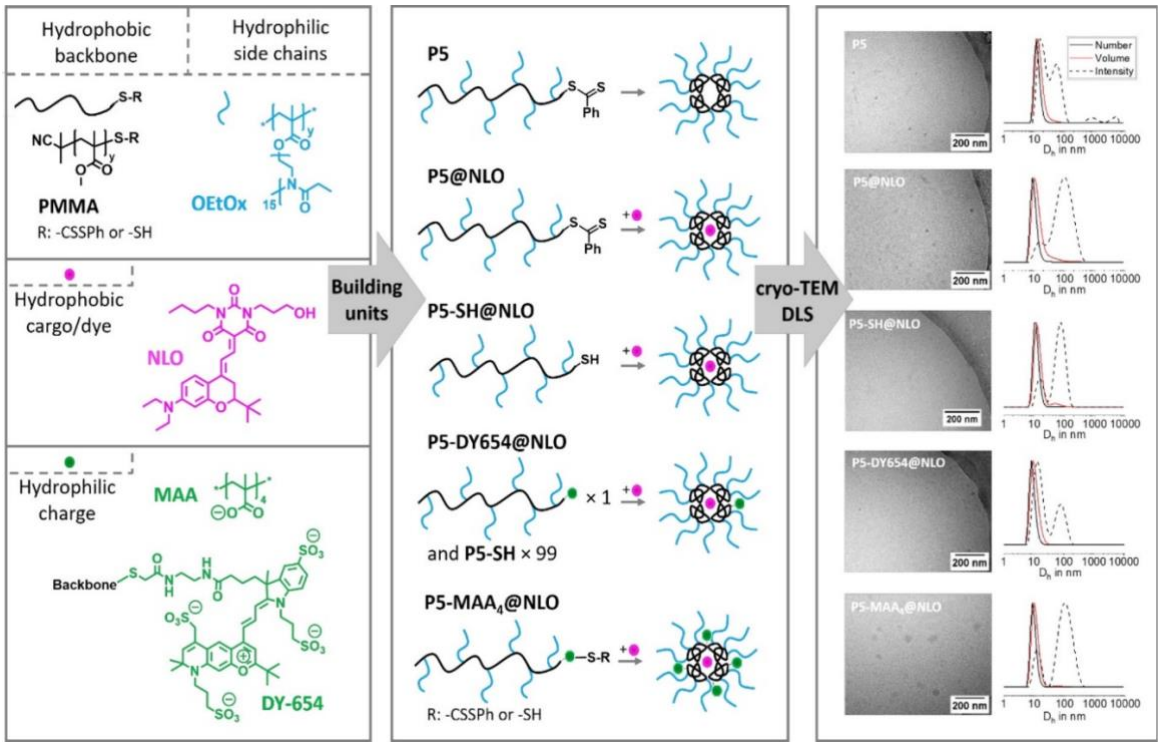

Figure 28: Left: Schematic representation of the building units used to form micelles with different moieties situated between core and shell. PMMA: Poly(methyl methacrylate). OEtOx15: Oligo(2-ethyl-2-oxazoline). NLO: Neutral lipid orange. MAA: Methacrylic acid. Middle: Simplified schematic overview of the polymer structures and the proposed micelles formed in aqueous solutions. Right: Aqueous cryo-TEM of micelles of P5 and dye-loaded micelles (concentration of polymer c = 10 mg/ml in aqueous solution). Dynamic light scattering plots of micelles of P5 and dye-loaded micelles with the number (solid black line), volume (red line), and intensity (dashed line) distributions (concentration of polymer c = 1 mg/ml in aqueous solution). Reprinted with permission from [72]. Copyrights 2021, American Chemical Society.

In contrast, the Raman spectroscopy showed the different molecular arrangement within the micelles. To obtain the fine differences in Raman spectroscopy, the principal component analysis (PCA) was done. PCA utilizes the Raman spectral features such as Raman band position, intensity, band shape, or noise to cluster Raman spectra according to similarity. The results obtained as 3D score plot clearly indicated that all the micelle types formed distinct clusters and were well separated from each other (Figure 29).

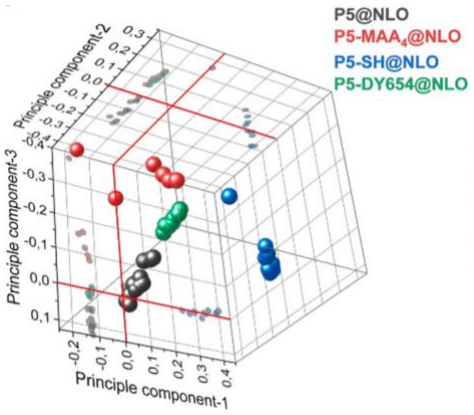

Figure 29: Hydrophilicity induces changes in the micellar confirmation. Raman spectra from micelles were obtained in liquid-state. The principal component analysis (PCA) of the Raman spectra of P5@NLO and the more hydrophilic micelles P5 DY654@NLO, P5-MAA4@NLO, and P5-SH@NLO. The spectral differences in the micelles can be visualized in the 3D-PC score plot obtained using PC-1, PC-2, and PC-3. Reprinted with permission from [72]. Copyrights 2021, American Chemical Society.

The end group effect was further investigated in in vitro and in vivo experiments by testing cellular uptake and stealth properties of the micelles (by intravital microscopy of the liver in mice). The efficient stealth properties were observed for polymers with anionically charged or thiol end groups i.e. P5-MAA4 and P5-SH. So this study confirm that how a small change in chemical structure can alter the micelles structure which can then further impact the cell type specificity and stealth properties of the nanocarriers.

Like many other studies reported in the literature [125, 126] very recently Jancura and the coworkers investigated the impact of increasing hydrophobic side chain length on the self-assembly of gradient copolymer composed of hydrophilic pEtOx and various 2-(4-alkyloxyphenyl)-2-oxazolines as hydrophobic blocks [127]. Initially the monomers were synthesized i.e. 2-(4-methyloxyphenyl)-2-oxazoline (MeOPhOx), 2-(4-ethyloxyphenyl)-2-oxazoline (EtOxPhOx), 2-(4-hexyloxyphenyl)-2-oxazoline (HePhOx), followed by polymerization (Figure 30 a) and formulation development by dialysis method using hypericin as model compound (used for photodiagnostics and photo dynamic therapy). The T_g of the resultant polymers was decreased with the increasing side chain length i.e. methyl to ethyl to hexyl, the T_g was 62, 61 and 53°C, respectively. The similar trend was also observed in the case of cmc values i.e. 0.4, 0.3 and 0.06 g/L, respectively. In the case of unloaded micelles, with the increasing side chain length i.e. methyl, ethyl and hexyl, the R_h was decreasing from 358, 81 to 75 nm, respectively (Figure 30 c, upper panel). The presence of hypericin (0.05 mg/ml) caused the rearrangement of the architecture and the R_h was significantly reduced in all the three cases i.e. 16, 12 and 11-33 nm for methyl, ethyl and hexyl, respectively (Figure 30 c, lower panel). At polymer/hypericin feed of 4/1 g/L, the LC and LE was found to be 16 wt.% and 85%,

respectively (Figure 30 d). No further higher hypericin feeds were tested in this study. An inverse relationship was observed between the hydrophobic side chain and drug release (in vitro) (Figure 30 b). The hypericin uptake was monitored in U87 MG and SK BR 3 cell lines for 24 h. The highest uptake was in the following order in both cell lines i.e. pristine hypericin > methyl > ethyl > hexyl (Figure 30 e). The intracellular distribution of hypericin in U87 MG cell lines was also visualized after 3 h of exposure. The fluorescence intensity of hypericin was significantly weaker in hexyl based polymer (Figure 30 f). The hexyl based polymer formulation was found to be most promising for in vivo delivery. This formulation retained the hypericn in the assemblies for longer time and prevented its redistribution to the serum proteins. Moreover, this formulation also exhibited delayed release in the chick chorioallantoic membrane (CAM) models.

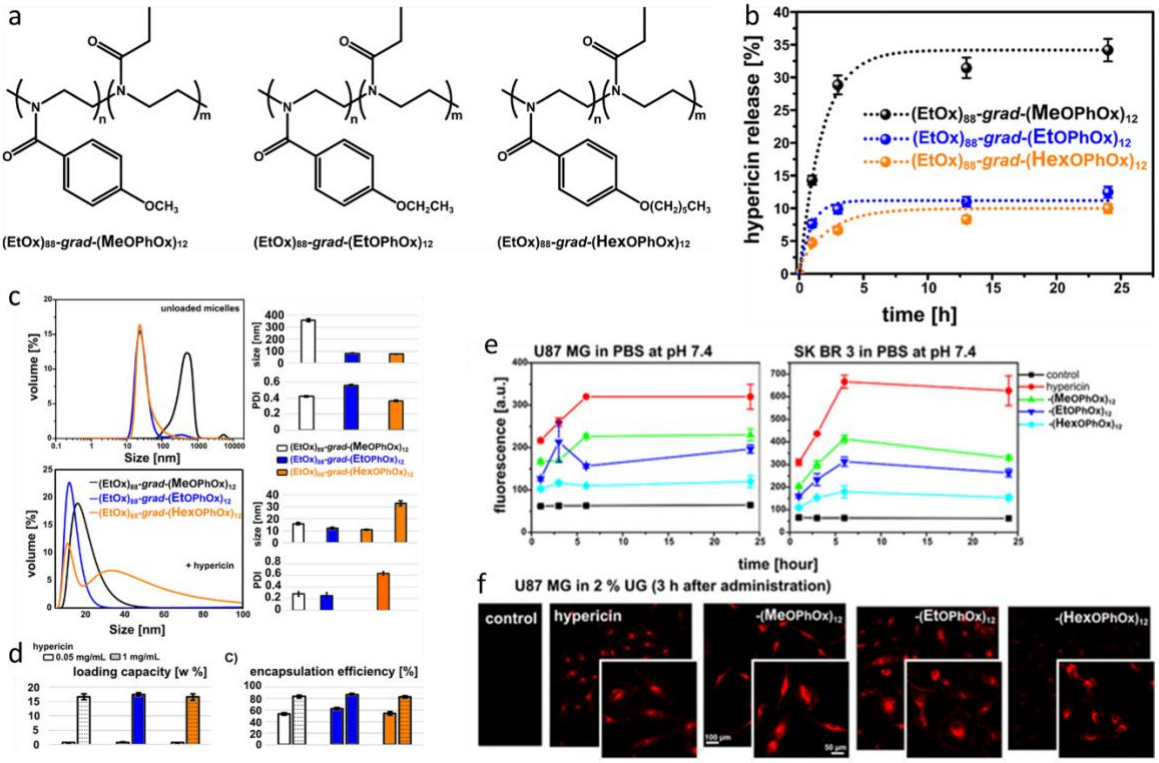

Figure 30: a) Structures of copolymers used in this study: $(EtOx)_{88}$-grad-$(MeOPhOx)_{12}$, $(EtOx)_{88}$-grad-$(EtOPhOx)_{12}$, and $(EtOx)_{88}$-grad-$(HexOPhOx)_{12}$. B) Release of hypericin from the nanoparticles toward 15 mg/mL BSA solution at pH = 7.4. The % of released hypericin molecules represents the average value (triplicates) with the standard deviations represented as error bars. c) Graphical representation of dynamic light scattering on unloaded and hypericin-loaded (hypericin feed concentration is 0.05 mg/mL) $(EtOx)_{88}$-grad-$(MeOPhOx)_{12}$ (black line), $(EtOx)_{88}$-grad- $(EtOPhOx)_{12}$ (blue line), and $(EtOx)_{88}$-grad-$(HexOPhOx)_{12}$ (orange line) nanoparticles. The size (hydrodynamic radius) and the polydispersity index (PDI) are represented in histograms. The bimodal distribution of hypericin-loaded $(EtOx)_{88}$-grad-$(HexOPhOx)_{12}$ nanoparticles was observed. d) Loading capacity of nanoparticles and hypericin encapsulation efficiency detected in the nanoparticles. In all nanoparticles, the feeding concentrations of hypericin were 0.05 (columns without patterns) and 1 mg/mL (columns with dotted patterns), and the feeding concentration of polymers

was 4 mg/mL. The uptake of 10 µM hypericin delivered into the U87 MG and SK BR 3 cells by the $(EtOx)_{88}$-grad-$(MeOPhOx)_{12}$, $(EtOx)_{88}$-grad-$(EtOPhOx)_{12}$, and $(EtOx)_{88}$-grad-$(HexOPhOx)_{12}$ nanoparticles, detected with e) fluorescence reader of 96-well plates and f) confocal fluorescence microscopy. The insets in f) represent zoomed images to better recognize hypericin distribution in cells. The intensity of hypericin in the $(EtOx)_{88}$-grad-$(HexOPhOx)_{12}$ nanoparticles was amplified. Modified and reprinted with permission from [127]. Copyrights 2021, American Chemical Society.

As discussed previously, besides the instinct SPR of the amphiphiles, the nature of guest molecules, its interaction and total concentration in the nanocarriers also play a very important role to tune the properties of final product for drug delivery applications [128, 129]. The various quality parameters such as drug loading, stability of formulation, overall morphology, release of cargo and in vivo fate are mainly governed by these factors. One early attempt to better understand the interplay of the structure of a polymer amphiphile and a hydrophobic guest/solute is a paper by Kabanov et al. meticulously studying the partitioning of hydrophobic molecules in Pluronic micelles (polyethylene oxide-polypropylene oxide-polyethylene oxide, PEP-PPO-PEO). The authors showed that the micelle formation and hydrophobic partitioning into the micelles are favored by the hydrophobic interactions in the micelle inner layers, which increase when PPO length increases or PEO length decreases [130]. Along these lines, Guo and Lu et al. also demonstrated that increasing the chain length of the hydrophobic block has a positive impact on drug loading [131, 132]. Wiest et al. showed that increasing the imatinib (an anticancer drug) concentration in taurocholate/lecithin micelles above a critical value, not only causes a morphology transition from vesicles to micelles but also leads to colloidal collapse, i.e. aggregation and precipitation [133].

The amount of loaded drug in the nanocarriers also play very important role in the therapeutic efficacy of the final product. However, in the literature very little attention has been given to this aspect. In this regard, Stenzel and the coworkers tried to answer this question that how a drug loading content can affect the biological activity [134]. However, the study was limited only to in vitro results. Initially a glycopolymer i.e. poly(1-O-methycryloyl-ß-D-fructopyranose)-block-poly(methyl methacrylate) (poly(1-O-MAFru)$_{36}$-b-$PMMA_{145}$) was synthesized. The model drug PTX was loaded by two different methods i.e. method 1 (PTX was loaded during self-assembly process) and method 2 (the preformed micelles were exposed to the PTX solution). In the case of method 1, the diameter of the micelles increased from 25 to 50 nm with the increasing PTX concentration (LC increased from 3.6 to 7.3 wt.%) (Figure 31 a). According to authors and further literature support, the micelles diameter around 50 nm display maximum cellular uptake. The similar results were obtained for these micelles, when tested for MDA-MB-231 and MCF-7 cell lines (Figure 31 b). The enhanced update was then coincided with higher toxicity.

a Size of Self-Assembled Drug-Loaded Poly(1-*O*-MAFru)$_{36}$-*b*-PMMA$_{145}$ Micelles at Different PTX Feed Amounts

micelles	[PTX] (mg/mL)	drug-loading efficiency (%)	drug-loading capacity (%)	D_h (nm) (DLS)	PDI	zeta potential (mV)
no drug	0	0	0	24.7 ± 1.2	0.112 ± 0.023	−9.9 ± 2.7
low drug	0.25	29.0	3.6	27.8 ± 3.8	0.213 ± 0.035	−22.3 ± 3.4
high drug	0.50	29.2	7.3	45.6 ± 2.6	0.178 ± 0.047	−21.2 ± 1.5

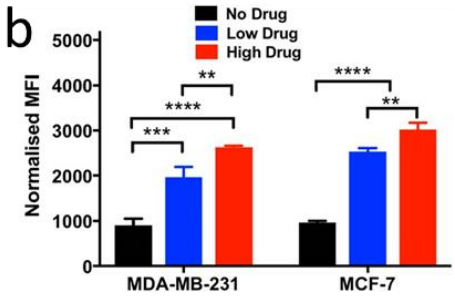

Figure 31: a) Table showing the various physico-chemical properties of the formulations. The drug was encapsulated during the self-assembly process. b) Flow cytometry on MDA-MB-231 and MCF-7 cell lines. The polymer concentrations were set to 0.2 mg/mL, and the concentration of loaded drug ranged from 0 to 0.015 mg/ml. Data are presented as mean ± SD (n = 3). Modified and reprinted with permission from [134]. Copyrights 2019, American Chemical Society.

The LC with the second method was even lower. Five different formulation (M1 to M5, with the increasing PTX feed) were prepared and in all of the case, LC never exceed above 2 wt.%. (Figure 32 a). However, the size of micelles remain in closer range i.e. 20 nm for all the formulations. In the cellular uptake experiments (MDA-MB-231 and MCF-7 cell lines), the results showed that the relatively higher PTX loaded micelles showed the least cellular uptake and vice versa (Figure 32 b). As the size of all the formulation are in close window so this finding gave a hint that the concentration and location of PTX is playing role in varied cellular uptake. To investigate the morphology and location of PTX in the micelles, small angle scattering experiments were performed. A core-shell model was used to fit the data. The radius of the PMMA core was almost independent of the PTX loading while the thickness of the shell decreased with the increasing PTX feed i.e. 3.7 to 2.9 nm (M0 to M5, respectively) (Figure 32 c). According to scattering length densities (SLD) change of shell in the presence of PTX, the volume fraction of water in the shell was calculated. It was concluded that the water content of the shell decreases with the increasing PTX concentration (Figure 32 d). Therefore, the author concluded that the nature of the hydrophilic shell and its hydration is a defining feature for the cellular uptake of the nanocarriers. Particularly, in the case of POx based amphiphile, the relevant phenomena was also observed in the case of A-pBuOx-A/PTX and A-pPrOzi-A/CUR loaded micelles [88, 106, 109], where the presence and concentration of guest molecule significantly affected the morphology of the micelles and the drug feed concertation caused the micelles to agglomerate and precipitate.

a **Size of Self-Assembled Drug-Loaded Poly(1-*O*-MAFru)$_{36}$-*b*-PMMA$_{145}$ Micelles with the Different Amounts of PTX after Loading of a Micelle Solution Prepared Using a Polymer Concentration of 2 mg/mL**

micelles	PTX solution added (μL)	actual amount of loaded drug (μg/mL)	drug loading efficiency (%)	drug loading capacity (%)	D_h (nm) (DLS)	PDI	zeta potential (mV)
M0	0	0	0	0	24.7 ± 1.2	0.112 ± 0.023	−9.9 ± 2.7
M1	10	2.63	26.30	0.13	21.2 ± 1.4	0.116 ± 0.045	−11.3 ± 2.4
M2	20	6.00	30.00	0.30	20.5 ± 2.1	0.154 ± 0.042	−12.2 ± 5.3
M3	40	19.76	49.40	0.99	19.2 ± 1.4	0.131 ± 0.034	−13.1 ± 3.2
M4	80	20.71	25.90	1.04	17.5 ± 1.6	0.142 ± 0.012	−14.0 ± 5.5
M5	160	26.56	16.60	1.33	19.4 ± 2.1	0.127 ± 0.024	−11.1 ± 4.6

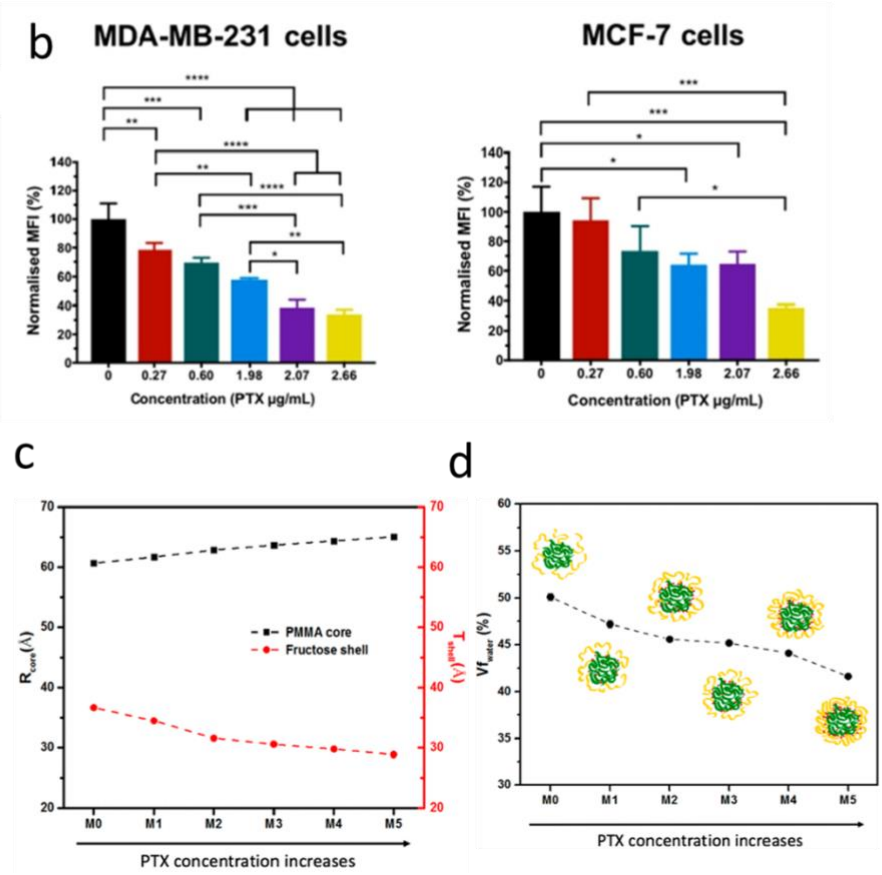

Figure 32: a) Table showing the various physico-chemical properties of the formulations. The drug encapsulation was done by exposing the preformed micelles to various drug concentrations. b) Flow cytometry on MDA-MB-231 cell line (left) and MCF-7 cell line (Right). The polymer concentrations were set to 0.1 mg/mL, and the concentration of loaded drug ranged from 0 to 2.65 µg/ml. Data are presented as mean ± SD (n = 3). c) Variation of core radius and the thickness of shell with drug loading. The lines are only to guide the eye. d) Volume fraction of water (D2O) in the fructose shell with respect to the different amounts of loaded drug. Modified and reprinted with permission from [134]. Copyrights 2019, American Chemical Society.

In this regards, Pöppler and the co-workers present the most notable work [113]. Utilizing the solid state NMR spectroscopy and complimentary analytical tools, Pöppler et al. investigated the ultra-high drug loaded A-pPrOzi-A/CUR formulations developed by Lübtow et al. [88] i.e. CUR-2-P, CUR-6-P and CUR-11-

P, each number is representing the solubility of curcumin in g/L, while the polymer was kept constant at 10 g/L. The results demonstrated that polymer carbonyl moieties acting as hydrogen bond acceptor are highly sensitive to presence of CUR (a proton donor). At relatively low drug loading (CUR-2-P), CUR with small molecular twist were mainly located in the core of micelles with the distribution of defined environment due to hydrogen bonding between phenolic OH moieties in CUR and the amide moiety of hydrophobic block (pPrOzi) (Figure 33). With the further increase in CUR loading (CUR-6-P), the preferred sites for such interactions were saturated and now the high CUR mass start to reside at core corona interface and start to interact with amide groups of hydrophilic corona (pMeOx). At this point sufficient number of amide moieties are still few and provide the hydration and colloidal stability to the micelles. With the further CUR feed, the interaction between pMeOx and CUR, lead to physical crosslinking and finally causing colloidal instability and precipitation of the whole system. These results were further corroborated with the dissolution profile of all the three formulations, an inverse relationship was observed between the high drug loading and dissolution rate.

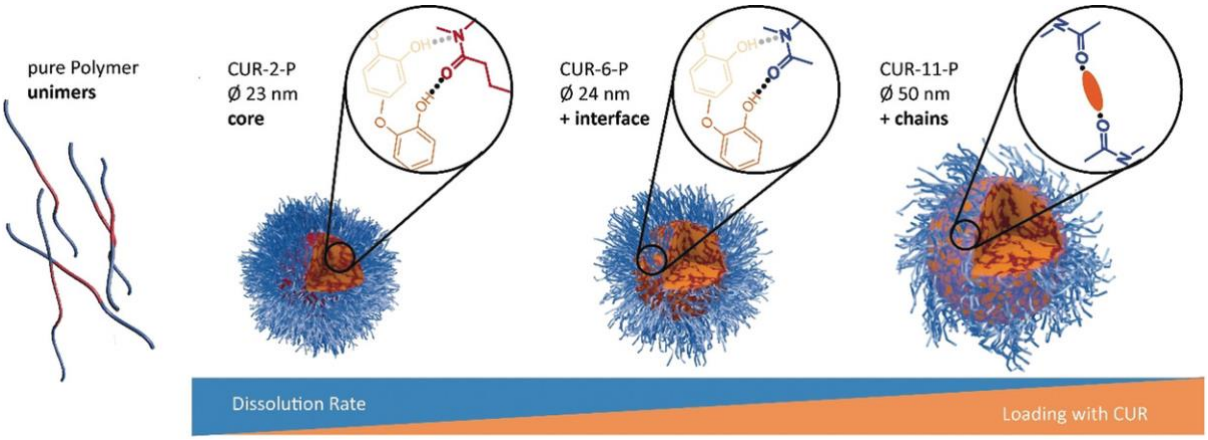

Figure 33: Schematic model of the structural changes of the polymeric micelles upon loading with curcumin based on the solid-state NMR data and complementary insights. For each loading stage, the additionally occurring interaction site is depicted [113]. Distributed under the Creative Commons Attribution License, CC BY-NC-ND 4.0. Published by Wiley-VCH Verlag GmbH & Co. KGaA.

In the follow study, to gain further insights into the morphology of the same micelles, the authors investigated the three different types of CUR loaded formulation i.e. with A-pPrOzi-A, A-pBuOx-A and A-pBuOzi-A by small angle neuron scattering (SANS). Two of the investigated polymers i.e. A-pBuOx-A and A-pBuOzi-A formed micelles without the presence of drug molecules, whereas the amphiphilic contrast of the third one i.e. A-pPrOzi-A was not pronounced enough, being present in aqueous solution mainly as single polymer chains (unimers). Important to note, the former two polymers formed rather spherical aggregates with no clear core-shell differentiation. However, after solubilization of small amounts of CUR

(polymer/CUR = 10/1 g/L), distinct core-shell spherical micelles appeared (also in the case of the A-pPrOzi-A). The SANS data showed that further increasing the CUR loading (polymer/CUR ≥ 10/3 g/L) lead to the formation of a second shell, i.e. spherical micelles with a core-shell-shell structure. This second, inner shell was found to be in good agreement with the participation of the hydrophilic polymer block (pMeOx) in the stabilization of ultra-high CUR loaded micelles, investigated by solid state NMR. Based on all the SANS data, the authors collectively summarized all the results and sketched them in figure 34.

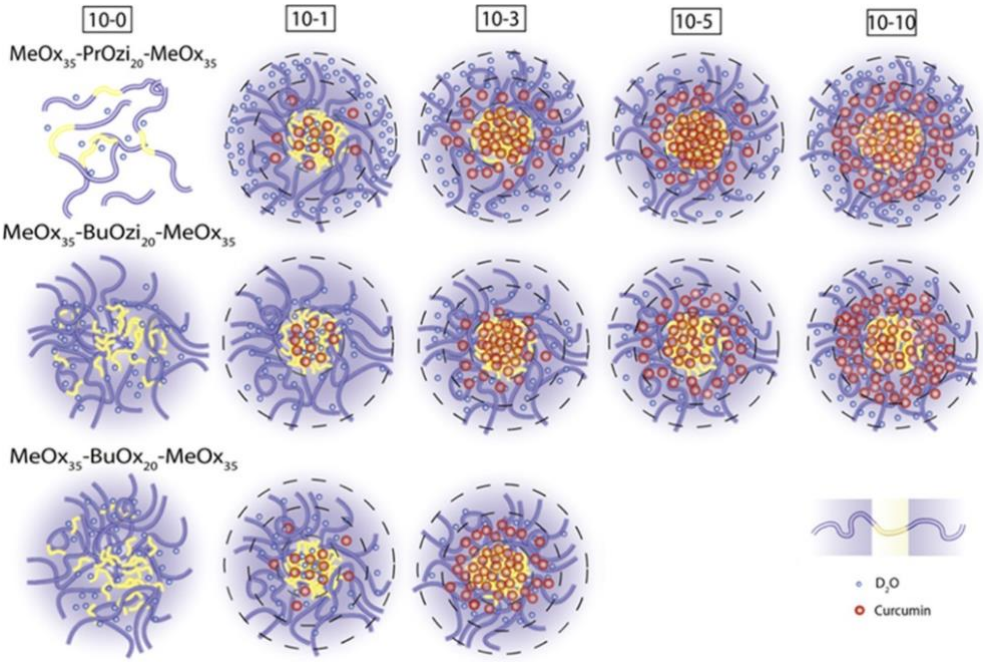

Figure 34: Schematic illustration of the different micellar morphologies at various CUR contents shown in. The sizes of the micelle compartments are not to scale to facilitate comparability. To visualize the amount of CUR in each micellar section, the number of red dots roughly represents the respective CUR concentration. The number on top of each panel is representing the polymer/CUR feed in g/L. Reprinted with permission from [115]. Copyright 2020, American Chemical Society.

From all of the studies cited here, it is now clear that structure property relationship play a very important role at every stage from product design to its development and until its final application.

3 References

[1] S.R. Bailey, M.V. Maus, Gene editing for immune cell therapies, Nature biotechnology 37(12) (2019) 1425-1434.
[2] R. Langer, J. Vacanti, Advances in tissue engineering, Journal of pediatric surgery 51(1) (2016) 8-12.
[3] D.-J. Cornelissen, A. Faulkner-Jones, W. Shu, Current developments in 3D bioprinting for tissue engineering, Current Opinion in Biomedical Engineering 2 (2017) 76-82.
[4] I. Matai, G. Kaur, A. Seyedsalehi, A. McClinton, C.T. Laurencin, Progress in 3D bioprinting technology for tissue/organ regenerative engineering, Biomaterials 226 (2020) 119536.
[5] S. Ali, K. Kolter, Challenges and opportunities in oral formulation development, American Pharmacuetical Review 15(7) (2012) 1.
[6] A.J. ten Tije, J. Verweij, W.J. Loos, A. Sparreboom, Pharmacological effects of formulation vehicles: implications for cancer chemotherapy, Clinical Pharmacokinetcs 42(7) (2003) 665-685.
[7] H. Cabral, K. Miyata, K. Osada, K. Kataoka, Block copolymer micelles in nanomedicine applications, Chemical Reviews 118(14) (2018) 6844-6892.
[8] B. Ghosh, S. Biswas, Polymeric micelles in cancer therapy: State of the art, Journal of Controlled Release 332 (2021) 127-147.
[9] N. Nishiyama, K. Kataoka, Current state, achievements, and future prospects of polymeric micelles as nanocarriers for drug and gene delivery, Pharmacology & Therapeutics 112(3) (2006) 630-648.
[10] H. Cabral, K. Kataoka, Progress of drug-loaded polymeric micelles into clinical studies, Journal of Controlled Release 190 (2014) 465-476.
[11] D. Hwang, J.D. Ramsey, A.V. Kabanov, Polymeric micelles for the delivery of poorly soluble drugs: from nanoformulation to clinical approval, Advanced Drug Delivery Reviews 156 (2020) 80-118.
[12] X. Zheng, J. Xie, X. Zhang, W. Sun, H. Zhao, Y. Li, C. Wang, An overview of polymeric nanomicelles in clinical trials and on the market, Chinese Chemical Letters (2020).
[13] W. Zhou, C. Li, Z. Wang, W. Zhang, J. Liu, Factors affecting the stability of drug-loaded polymeric micelles and strategies for improvement, Journal of Nanoparticle Research 18(9) (2016) 1-18.
[14] M. Yokoyama, Polymeric micelles as drug carriers: their lights and shadows, Journal of drug targeting 22(7) (2014) 576-583.
[15] A. Zahoranová, R. Luxenhofer, Poly(2-oxazoline)- and Poly(2-oxazine)-Based Self-Assemblies, Polyplexes, and Drug Nanoformulations-An Update., Advanced Healthcare Materials 10(6) (2021) 2001382.
[16] T. Lorson, M.M. Lübtow, E. Wegener, M.S. Haider, S. Borova, D. Nahm, R. Jordan, M. Sokolski-Papkov, A.V. Kabanov, R. Luxenhofer, Poly(2-oxazoline)s based biomaterials: A comprehensive and critical update, Biomaterials 178 (2018) 204-280.
[17] O. Sedlacek, B.D. Monnery, S.K. Filippov, R. Hoogenboom, M. Hruby, Poly(2-Oxazoline)s–Are They More Advantageous for Biomedical Applications Than Other Polymers?, Macromolecular Rapid communications 33(19) (2012) 1648-1662.
[18] S. Bahl, H. Nagar, I. Singh, S. Sehgal, Smart materials types, properties and applications: A review, Materials Today: Proceedings 28 (2020) 1302-1306.
[19] P.S. Kowalski, C. Bhattacharya, S. Afewerki, R. Langer, Smart biomaterials: recent advances and future directions, ACS Biomaterials Science & Engineering 4(11) (2018) 3809-3817.
[20] Q. Yang, C. Gao, X. Zhang, X. Zhao, Y. Fu, C. Tsou, C. Zeng, L. Yuan, Z. Pu, Y. Xia, Dual-responsive shape memory hydrogels with self-healing and dual-responsive swelling behaviors, Journal of Applied Polymer Science 138(13) (2021) 50308.
[21] J. Chen, J. Huang, Y. Hu, 3D printing of biocompatible shape-memory double network hydrogels, ACS Applied Materials & Interfaces 13(11) (2020) 12726-12734.

[22] X. Tong, W. Pan, T. Su, M. Zhang, W. Dong, X. Qi, Recent advances in natural polymer-based drug delivery systems, Reactive and Functional Polymers 148 (2020) 104501.
[23] V. Perez-Puyana, M. Jiménez-Rosado, A. Romero, A. Guerrero, Polymer-based scaffolds for soft-tissue engineering, Polymers 12(7) (2020).
[24] F. Perin, A. Motta, D. Maniglio, Amphiphilic copolymers in biomedical applications: synthesis routes and property control, Materials Science and Engineering: C 123 (2021) 111952.
[25] B.R. Hassan, Overview on drug delivery system, Pharmaceutica Analytica Acta 3(10) (2012) 4172.
[26] K.K. Jain, Drug delivery systems-an overview, Drug delivery systems 437 (2008) 1-50.
[27] M. Rodriguez-Aller, D. Guillarme, J.-L. Veuthey, R. Gurny, Strategies for formulating and delivering poorly water-soluble drugs, Journal of drug delivery science and technology 30 (2015) 342-351.
[28] D. Sikarra, V. Shukla, A.A. Kharia, D. Chatterjee, Techniques for solubility enhancement of poorly soluble drugs: an overview, Journal of medical pharmaceutical and allied sciences 1 (2012) 1-22.
[29] Z. He, A. Schulz, X. Wan, J. Seitz, H. Bludau, D.Y. Alakhova, D.B. Darr, C.M. Perou, R. Jordan, I. Ojima, A. Kabanov, R. Luxenhofer, Poly(2-oxazoline) based micelles with high capacity for 3rd generation taxoids: Preparation, in vitro and in vivo evaluation, Journal of Controlled Release 208 (2015) 67-75.
[30] B.Y. Kim, J.T. Rutka, W.C. Chan, Nanomedicine, New England Journal of Medicine 363(25) (2010) 2434-2443.
[31] C. Zhang, L. Yan, X. Wang, S. Zhu, C. Chen, Z. Gu, Y. Zhao, Progress, challenges, and future of nanomedicine, Nano Today 35 (2020) 101008.
[32] M. Germain, F. Caputo, S. Metcalfe, G. Tosi, K. Spring, A.K. Åslund, A. Pottier, R. Schiffelers, A. Ceccaldi, R. Schmid, Delivering the power of nanomedicine to patients today, Journal of Controlled Release 326 (2020) 164-171.
[33] K. Park, The beginning of the end of the nanomedicine hype, Journal of controlled release: official journal of the Controlled Release Society 305 (2019) 221-222.
[34] M. Ghezzi, S. Pescina, C. Padula, P. Santi, E. Del Favero, L. Cantù, S. Nicoli, Polymeric micelles in drug delivery: An insight of the techniques for their characterization and assessment in biorelevant conditions, Journal of Controlled Release 332 (2021) 312-336.
[35] S. Kalepu, V. Nekkanti, Insoluble drug delivery strategies: review of recent advances and business prospects, Acta Pharmaceutica Sinica B 5(5) (2015) 442-453.
[36] O. Wichterle, D. Lim, Hydrophilic gels for biological use, Nature 185(4706) (1960) 117-118.
[37] S.J. Buwalda, K.W. Boere, P.J. Dijkstra, J. Feijen, T. Vermonden, W.E. Hennink, Hydrogels in a historical perspective: From simple networks to smart materials, Journal of Controlled Release 190 (2014) 254-273.
[38] A. Mandal, J.R. Clegg, A.C. Anselmo, S. Mitragotri, Hydrogels in the clinic, Bioengineering & Translational Medicine 5(2) (2020) e10158.
[39] S. Aswathy, U. Narendrakumar, I. Manjubala, Commercial hydrogels for biomedical applications, Heliyon 6(4) (2020) e03719.
[40] A.H. Karoyo, L.D. Wilson, Physicochemical properties and the gelation process of supramolecular hydrogels: A review, Gels 3(1) (2017).
[41] K. Al Khateb, E.K. Ozhmukhametova, M.N. Mussin, S.K. Seilkhanov, T.K. Rakhypbekov, W.M. Lau, V.V. Khutoryanskiy, In situ gelling systems based on Pluronic F127/Pluronic F68 formulations for ocular drug delivery, International journal of pharmaceutics 502(2) (2016) 70-79.
[42] H. Ye, C. Owh, X.J. Loh, A thixotropic polyglycerol sebacate-based supramolecular hydrogel showing UCST behavior, Rsc Advances 5(60) (2015) 48720-48728.
[43] L. Hahn, M. Maier, P. Stahlhut, M. Beudert, V. Flegler, S. Forster, A. Altmann, F. Töppke, K. Fischer, S. Seiffert, B. Böttcher, T. Lühmann, R. Luxenhofer, Inverse thermogelation of aqueous triblock copolymer solutions into macroporous shear-thinning 3D printable inks, ACS Applied Materials & Interfaces 12(11) (2020) 12445-12456.
[44] S. Wellinghoff, J. Shaw, E. Baer, Polymeric materials from the gel state.: The development of fringed micelle structure in a glass, Macromolecules 12(5) (1979) 932-939.

[45] H. Tan, K.G. Marra, Injectable, biodegradable hydrogels for tissue engineering applications, Materials 3(3) (2010) 1746-1767.
[46] M. Liu, X. Zeng, C. Ma, H. Yi, Z. Ali, X. Mou, S. Li, Y. Deng, N. He, Injectable hydrogels for cartilage and bone tissue engineering, Bone Research 5(1) (2017) 1-20.
[47] H.J. Chung, T.G. Park, Self-assembled and nanostructured hydrogels for drug delivery and tissue engineering, Nano Today 4(5) (2009) 429-437.
[48] B. Maiti, D. Diaz Diaz, 3D printed polymeric hydrogels for nerve regeneration, Polymers 10(9) (2018) 1041.
[49] G. Janarthanan, I. Noh, Overview of Injectable Hydrogels for 3D Bioprinting and Tissue Regeneration, Royal Society of Chemistry2021.
[50] M. Champeau, D.A. Heinze, T.N. Viana, E.R. de Souza, A.C. Chinellato, S. Titotto, 4D printing of hydrogels: a review, Advanced Functional Materials 30(31) (2020) 1910606.
[51] D.W. Van Krevelen, K. Te Nijenhuis, Properties of polymers: their correlation with chemical structure; their numerical estimation and prediction from additive group contributions, fourth ed., Elsevier2009.
[52] B.C. Hancock, P. York, R.C. Rowe, The use of solubility parameters in pharmaceutical dosage form design, International journal of pharmaceutics 148(1) (1997) 1-21.
[53] C.M. Hansen, Hansen solubility parameters: a user's handbook, second ed., CRC press, Boca Raton, 2007.
[54] Y. Kobayashi, S. Tokishita, H. Yamamoto, Determination of Hansen Solubility Parameters of Ionic Liquids by Using Walden Plots, Industrial & Engineering Chemistry Research 59(32) (2020) 14217-14223.
[55] A. Alanazi, S. Alshehri, M. Altamimi, F. Shakeel, Solubility determination and three dimensional Hansen solubility parameters of gefitinib in different organic solvents: Experimental and computational approaches, Journal of Molecular Liquids 299 (2020) 112211.
[56] D.P. Faasen, A. Jarray, H.J. Zandvliet, E.S. Kooij, W. Kwiecinski, Hansen solubility parameters obtained via molecular dynamics simulations as a route to predict siloxane surfactant adsorption, Journal of colloid and interface science 575 (2020) 326-336.
[57] A. Alhalaweh, A. Alzghoul, W. Kaialy, Data mining of solubility parameters for computational prediction of drug–excipient miscibility, Drug development and industrial pharmacy 40(7) (2014) 904-909.
[58] A. Benazzouz, L. Moity, C. Pierlot, V. Molinier, J.-M. Aubry, Hansen approach versus COSMO-RS for predicting the solubility of an organic UV filter in cosmetic solvents, Colloids and Surfaces A: Physicochemical and Engineering Aspects 458 (2014) 101-109.
[59] A.J. Guenthner, K.R. Lamison, L.M. Lubin, T.S. Haddad, J.M. Mabry, Hansen solubility parameters for octahedral oligomeric silsesquioxanes, Industrial & engineering chemistry research 51(38) (2012) 12282-12293.
[60] J. Liu, Y. Xiao, C. Allen, Polymer–drug compatibility: a guide to the development of delivery systems for the anticancer agent, ellipticine, Journal of Pharmaceutical Sciences 93(1) (2004) 132-143.
[61] A.O. Kasimova, G.M. Pavan, A. Danani, K. Mondon, A. Cristiani, L. Scapozza, R. Gurny, M. Möller, Validation of a novel molecular dynamics simulation approach for lipophilic drug incorporation into polymer micelles, The Journal of Physical Chemistry B 116(14) (2012) 4338-4345.
[62] V.M. Alves, D. Hwang, E. Muratov, M. Sokolsky-Papkov, E. Varlamova, N. Vinod, C. Lim, C.H. Andrade, A. Tropsha, A.V. Kabanov, Cheminformatics-driven discovery of polymeric micelle formulations for poorly soluble drugs, Science Advances 5 (2019) 9784-9797.
[63] Y. Seo, A. Schulz, Y. Han, Z. He, H. Bludau, X. Wan, J. Tong, T.K. Bronich, M. Sokolsky, R. Luxenhofer, R. jordan, A. Kabanov, Poly(2-oxazoline) block copolymer based formulations of taxanes: effect of copolymer and drug structure, concentration, and environmental factors, Polymers for Advanced Technologies 26 (2015) 837-850.
[64] L. Trachsel, M. Zenobi-Wong, E.M. Benetti, The role of poly(2-alkyl-2-oxazoline)s in hydrogels and biofabrication, Biomaterials Science 9(8) (2021) 2874-2886.

[65] R. Luxenhofer, Y. Han, A. Schulz, J. Tong, Z. He, A.V. Kabanov, R. Jordan, Poly(2-oxazoline)s as Polymer Therapeutics, Macromolecular Rapid communications 33(19) (2012) 1613-1631.
[66] T.R. Dargaville, J.R. Park, R. Hoogenboom, Poly(2-oxazoline) Hydrogels: State-of-the-Art and Emerging Applications, Macromolecular Bioscience 18(6) (2018) 1800070.
[67] T. Bassiri, A. Levy, M. Litt, Polymerization of cyclic imino ethers. I. Oxazolines, Journal of Polymer Science Part B: Polymer Letters 5(9) (1967) 871-879.
[68] K.L. Eskow Jaunarajs, D.G. Standaert, T.X. Viegas, M.D. Bentley, Z. Fang, B. Dizman, K. Yoon, R. Weimer, P. Ravenscroft, T.H. Johnston, Rotigotine polyoxazoline conjugate SER-214 provides robust and sustained antiparkinsonian benefit, Movement Disorders 28(12) (2013) 1675-1682.
[69] R.W. Moreadith, T.X. Viegas, M.D. Bentley, J.M. Harris, Z. Fang, K. Yoon, B. Dizman, R. Weimer, B.P. Rae, X. Li, Clinical development of a poly(2-oxazoline)(POZ) polymer therapeutic for the treatment of Parkinson's disease–Proof of concept of POZ as a versatile polymer platform for drug development in multiple therapeutic indications, European Polymer Journal 88 (2017) 524-552.
[70] N. Vinod, D. Hwang, S.H. Azam, A.E. Van Swearingen, E. Wayne, S.C. Fussell, M. Sokolsky-Papkov, C.V. Pecot, A.V. Kabanov, High-capacity poly(2-oxazoline) formulation of TLR 7/8 agonist extends survival in a chemo-insensitive, metastatic model of lung adenocarcinoma, Science Advances 6(25) (2020) 5542.
[71] D. Hwang, T. Dismuke, A. Tikunov, E.P. Rosen, J.R. Kagel, J.D. Ramsey, C. Lim, W. Zamboni, A.V. Kabanov, T.R. Gershon, Poly(2-oxazoline) nanoparticle delivery enhances the therapeutic potential of vismodegib for medulloblastoma by improving CNS pharmacokinetics and reducing systemic toxicity, Nanomedicine: Nanotechnology, Biology and Medicine 32 (2021) 102345.
[72] I. Muljajew, S. Huschke, A. Ramoji, Z. Cseresnyés, S. Hoeppener, I. Nischang, W. Foo, J.r. Popp, M.T. Figge, C. Weber, M. Bauer, S.U. Schubert, A.T. Press, Stealth Effect of Short Polyoxazolines in Graft Copolymers: Minor Changes of Backbone End Group Determine Liver Cell-Type Specificity, ACS Nano 15(7) (2021) 12298-12313.
[73] Y. You, K. Kobayashi, B. Colak, P. Luo, E. Cozens, L. Fields, K. Suzuki, J. Gautrot, Engineered cell-degradable poly (2-alkyl-2-oxazoline) hydrogel for epicardial placement of mesenchymal stem cells for myocardial repair, Biomaterials 269 (2021) 120356.
[74] C. Hu, T. Ahmad, M.S. Haider, L. Hahn, P. Stahlhut, J. Groll, R. Luxenhofer, A thermogelling organic-inorganic hybrid hydrogel with excellent printability, shape fidelity and cytocompatibility for 3D bioprinting, Biofabrication 14(2) (2022) 025005.
[75] H. Witte, W. Seeliger, Cyclische imidsäureester aus nitrilen und aminoalkoholen, Leibigs Ann. 1974 (1974) 996-1009.
[76] G. Delecourt, L. Plet, V. Bennevault, P. Guegan, Synthesis of double hydrophilic block copolymers poly (2-oxazoline-b-ethylenimine) in a two-step procedure, ACS Applied Polymer Materials 2(7) (2020).
[77] N. Oleszko-Torbus, A. Utrata-Wesołek, M. Bochenek, D. Lipowska-Kur, A. Dworak, W. Wałach, Thermal and crystalline properties of poly(2-oxazoline)s, Polymer Chemistry 11(1) (2020) 15-33.
[78] F.C. Gaertner, R. Luxenhofer, B. Blechert, R. Jordan, M. Essler, Synthesis, biodistribution and excretion of radiolabeled poly(2-alkyl-2-oxazoline)s, Journal of Controlled Release 119(3) (2007) 291-300.
[79] M. Barz, R. Luxenhofer, R. Zentel, M.J. Vicent, Overcoming the PEG-addiction: well-defined alternatives to PEG, from structure–property relationships to better defined therapeutics, Polymer Chemistry 2 (2011) 1900-1918.
[80] O. Sedlacek, B.D. Monnery, J. Mattova, J. Kucka, J. Panek, O. Janouskova, A. Hocherl, B. Verbraeken, M. Vergaelen, M. Zadinova, Poly(2-ethyl-2-oxazoline) conjugates with doxorubicin for cancer therapy: in vitro and in vivo evaluation and direct comparison to poly [N-(2-hydroxypropyl) methacrylamide] analogues, Biomaterials 146 (2017) 1-12.
[81] M. Grube, M.N. Leiske, U.S. Schubert, I. Nischang, POx as an alternative to PEG? A hydrodynamic and light scattering study, Macromolecules 51(5) (2018) 1905-1916.
[82] F.C. Gaertner, R. Luxenhofer, B. Blechert, R. Jordan, M. Essler, Synthesis, biodistribution and excretion of radiolabeled poly (2-alkyl-2-oxazoline) s, Journal of Controlled Release 119(3) (2007) 291-300.

[83] P. Goddard, L.E. Hutchinson, J. Brown, L.J. Brookman, Soluble polymeric carriers for drug delivery. Preparation and in vivo behaviour of N-acylethylenimine copolymers, Journal of Controlled Release 10(1) (1989) 5-16.
[84] M.C. Woodle, C.M. Engbers, S. Zalipsky, New amphipathic polymer-lipid conjugates forming long-circulating reticuloendothelial system-evading liposomes, Bioconjugate Chemistry 5(6) (1994) 493-496.
[85] S. Zalipsky, C.B. Hansen, J.M. Oaks, T.M. Allen, Evaluation of blood clearance rates and biodistribution of poly(2-oxazoline)-grafted liposomes, Journal of pharmaceutical sciences 85(2) (1996) 133-137.
[86] D. Hwang, J.D. Ramsey, N. Makita, C. Sachse, R. Jordan, M. Sokolsky-Papkov, A.V. Kabanov, Novel poly(2-oxazoline) block copolymer with aromatic heterocyclic side chains as a drug delivery platform, Journal of Controlled Release 307 (2019) 261-271.
[87] M.M. Lübtow, M.S. Haider, M. Kirsch, S. Klisch, R. Luxenhofer, Like Dissolves Like? A Comprehensive Evaluation of Partial Solubility Parameters to Predict Polymer-Drug Compatibility in Ultra-High Drug Loaded Polymer Micelles, Biomacromolecules 20(8) (2019) 3041-3056.
[88] M.M. Lübtow, L.C. Nelke, J. Seifert, J. Kühnemundt, G. Sahay, G. Dandekar, S.L. Nietzer, R. Luxenhofer, Drug induced micellization into ultra-high capacity and stable curcumin nanoformulations: Physico-chemical characterization and evaluation in 2D and 3D in vitro models, Journal of Controlled Release 303 (2019) 162-180.
[89] X. Wan, J.J. Beaudoin, N. Vinod, Y. Min, N. Makita, H. Bludau, R. Jordan, A. Wang, M. Sokolsky, A.V. Kabanov, Co-delivery of paclitaxel and cisplatin in poly (2-oxazoline) polymeric micelles: Implications for drug loading, release, pharmacokinetics and outcome of ovarian and breast cancer treatments, Biomaterials 192 (2019) 1-14.
[90] M.S. Haider, J. Schreiner, S. Kendl, M. Kroiss, R. Luxenhofer, A Micellar Mitotane Formulation with High Drug-Loading and Solubility: Physico-Chemical Characterization and Cytotoxicity Studies in 2D and 3D In Vitro Tumor Models, Macromolecular Bioscience 20(1) (2020) 1900178.
[91] M.M. Lübtow, S. Oerter, S. Quader, E. Jeanclos, A. Cubukova, M. Krafft, M.S. Haider, C. Schulte, L. Meier, M. Rist, O. Sampetrean, H. Kinoh, A. Gohla, K. Kataoka, A. Appelt Menzel, R. Luxenhofer, In Vitro Blood–Brain Barrier Permeability and Cytotoxicity of an Atorvastatin-Loaded Nanoformulation Against Glioblastoma in 2D and 3D Models, Molecular Pharmaceutics 17(6) (2020) 1835-1847.
[92] O. Sedlacek, R. Hoogenboom, Drug Delivery Systems Based on Poly(2-Oxazoline)s and Poly(2-Oxazine)s, Advanced Therapeutics 3(1) (2020).
[93] H. Lukas, K. Larissa, P. Lando, F. Lars, H. Holger, L. Robert, ABA Type Amphiphiles with Poly(2-Benzhydryl-2-Oxazine) Moieties: Synthesis, Characterization and Inverse Thermogelation, (2021, 10.26434/chemrxiv.14322194.v1).
[94] R. Konradi, B. Pidhatika, A. Mühlebach, M. Textor, Poly-2-methyl-2-oxazoline: a peptide-like polymer for protein-repellent surfaces, Langmuir 24(3) (2008) 613-616.
[95] N. Zhang, T. Pompe, R. Luxenhofer, C. Werner, R. Jordan, Poly(2-oxazoline) bottle-rush brushes for the control of protein adsorption and cell adhesion, Polymer Preprints 53(1) (2012) 301.
[96] G. Morgese, B. Verbraeken, S.N. Ramakrishna, Y. Gombert, E. Cavalli, J.G. Rosenboom, M. Zenobi-Wong, N.D. Spencer, R. Hoogenboom, E.M. Benetti, Chemical Design of Non-Ionic Polymer Brushes as Biointerfaces: Poly (2-oxazine)s Outperform Both Poly (2-oxazoline)s and PEG, Angewandte Chemie 57 (2018) 11667-11672.
[97] R. Luxenhofer, A. Schulz, C. Roques, S. Li, T.K. Bronich, E.V. Batrakova, R. Jordan, A.V. Kabanov, Doubly amphiphilic poly(2-oxazoline)s as high-capacity delivery systems for hydrophobic drugs, Biomaterials 31 (2010) 4972-4979.
[98] Y. Han, Z. He, A. Schulz, T.K. Bronich, R. Jordan, R. Luxenhofer, A.V. Kabanov, Synergistic combinations of multiple chemotherapeutic agents in high capacity poly(2-oxazoline) micelles, Molecular Pharmaceutics 9(8) (2012) 2302-2313.
[99] M.M. Lübtow, L. Keßler, A. Appelt-Menzel, T. Lorson, N. Gangloff, M. Kirsch, S. Dahms, R. Luxenhofer, More Is Sometimes Less: Curcumin and Paclitaxel Formulations Using Poly(2-oxazoline) and Poly(2-

oxazine)-Based Amphiphiles Bearing Linear and Branched C9 Side Chains, Macromolecular Bioscience 18 (2018) 1800155-1800172.
[100] L. Hahn, M.M. Lübtow, T. Lorson, F. Schmitt, A. Appelt-Menzel, R. Schobert, R. Luxenhofer, Investigating the Influence of Aromatic Moieties on the Formulation of Hydrophobic Natural Products and Drugs in Poly(2-oxazoline)-Based Amphiphiles, Biomacromolecules 19(7) (2018) 3119.
[101] Z. He, X. Wan, A. Schulz, H. Bludau, M.A. Dobrovolskaia, S.T. Stern, S.A. Montgomery, H. Yuan, Z. Li, D. Alakhova, A high capacity polymeric micelle of paclitaxel: Implication of high dose drug therapy to safety and in vivo anti-cancer activity, Biomaterials 101 (2016) 296-309.
[102] Z. He, X. Wan, A. Schulz, H. Bludau, M.A. Dobrovolskaia, S.T. Stern, S.A. Montgomery, H. Yuan, Z. Li, D. Alakhova, A High Capacity Polymeric Micelle of Paclitaxel: Implication of High Dose Drug Therapy to Safety and In Vivo Anti-Cancer Activity, Biomaterials (2016).
[103] D. Hwang, N. Vinod, S.L. Skoczen, J.D. Ramsey, K.S. Snapp, S.A. Montgomery, M. Wang, C. Lim, J.E. Frank, M. Sokolsky-Papkov, Bioequivalence assessment of high-capacity polymeric micelle nanoformulation of paclitaxel and Abraxane® in rodent and non-human primate models using a stable isotope tracer assay, Biomaterials 278 (2021) 121140.
[104] Y. Han, Z. He, A. Schulz, T.K. Bronich, R. Jordan, R. Luxenhofer, A.V. Kabanov, Synergistic combinations of multiple chemotherapeutic agents in high capacity poly (2-oxazoline) micelles, Molecular pharmaceutics 9(8) (2012) 2302-2313.
[105] X. Wan, Y. Min, H. Bludau, A. Keith, S.S. Sheiko, R. Jordan, A.Z. Wang, M. Sokolsky Papkov, A.V. Kabanov, Drug Combination Synergy in worm-like Polymeric Micelles Improves Treatment Outcome for Small Cell and Non-Small Cell Lung Cancer, ACS Nano 12 (2018) 2426-2439.
[106] M.M. Lübtow, L. Hahn, M.S. Haider, R. Luxenhofer, Drug specificity, synergy and antagonism in ultrahigh capacity poly(2-oxazoline)/poly(2-oxazine) based formulations, Journal of the American Chemical Society 139(32) (2017) 10980-10983.
[107] B.L. Farrugia, K. Kempe, U.S. Schubert, R. Hoogenboom, T.R. Dargaville, Poly(2-oxazoline) hydrogels for controlled fibroblast attachment, Biomacromolecules 14(8) (2013) 2724-2732.
[108] K.P. Kohn, S.M. Underwood, M.M. Cooper, Connecting structure–property and structure–function relationships across the disciplines of chemistry and biology: Exploring student perceptions, CBE—Life Sciences Education 17(2) (2018).
[109] A. Schulz, S. Jaksch, R. Schubel, E. Wegener, Z. Di, Y. Han, A. Meister, J. Kressler, A.V. Kabanov, R. Luxenhofer, Drug-induced morphology switch in drug delivery systems based on poly (2-oxazoline)s, ACS nano 8 (2014) 2686-2696.
[110] J. Noolandi, K.M. Hong, Theory of block copolymer micelles in solution, Macromolecules 16(9) (1983) 1443-1448.
[111] S. Cammas, K. Suzuki, C. Sone, Y. Sakurai, K. Kataoka, T. Okano, Thermo-responsive polymer nanoparticles with a core-shell micelle structure as site-specific drug carriers, Journal of Controlled Release 48(2-3) (1997) 157-164.
[112] M.M. Lübtow, H. Marciniak, A. Schmiedel, M. Roos, C. Lambert, R. Luxenhofer, Ultra-high to ultra-low drug loaded micelles: Probing host-guest interactions by fluorescence spectroscopy, Chemistry-A European Journal 25 (2019) 12601-12610.
[113] A.C. Pöppler, M.M. Lübtow, J. Schlauersbach, J. Wiest, L. Meinel, R. Luxenhofer, Loading-Dependent Structural Model of Polymeric Micelles Encapsulating Curcumin by Solid-State NMR Spectroscopy, Angewandte Chemie International Edition 58(51) (2019) 18540-18546.
[114] M.S. Haider, M.M. Lübtow, S. Endres, S. Forster, V.J. Flegler, B. Böttcher, V.O. Aseyev, A.-C. Pöppler, R. Luxenhofer, Think beyond the core: The impact of the hydrophilic corona on the drug solubilization using polymer micelles, ACS Applied Materials & Interfaces 12(22) (2020) 24531–24543.
[115] B. Sochor, Ö. Düdükcü, M.M. Lübtow, B. Schummer, S. Jaksch, R. Luxenhofer, Probing the Complex Loading Dependent Structural Changes in Ultra-High Drug Loaded Polymer Micelles by Small-Angle Neutron Scattering, Langmuir 36 (2020) 3494-3503.

[116] G. Slor, A.R. Olea, S. Pujals, A. Tigrine, V.R. De La Rosa, R. Hoogenboom, L. Albertazzi, R.J. Amir, Judging Enzyme-Responsive Micelles by Their Covers: Direct Comparison of Dendritic Amphiphiles with Different Hydrophilic Blocks, Biomacromolecules 22(3) (2021) 1197–1210.
[117] C. Cao, J. Zhao, F. Chen, M. Lu, Y.Y. Khine, A. Macmillan, C.J. Garvey, M.H. Stenzel, Drug-Induced Morphology Transition of Self-Assembled Glycopolymers: Insight into the Drug–Polymer Interaction, Chemistry of Materials 30(15) (2018) 5227-5236.
[118] S.J. Holder, N.A. Sommerdijk, New micellar morphologies from amphiphilic block copolymers: disks, toroids and bicontinuous micelles, Polymer Chemistry 2(5) (2011) 1018-1028.
[119] A. Schulz, S. Jaksch, R. Schubel, E. Wegener, Z. Di, Y. Han, A. Meister, J.r. Kressler, A.V. Kabanov, R. Luxenhofer, Drug-induced morphology switch in drug delivery systems based on poly(2-oxazoline)s, ACS Nano 8(3) (2014) 2686-2696.
[120] F.M. Veronese, A. Mero, The impact of PEGylation on biological therapies, BioDrugs 22(5) (2008) 315-329.
[121] J.M. Harris, R.B. Chess, Effect of pegylation on pharmaceuticals, Nature Reviews Drug Discovery 2(3) (2003) 214-221.
[122] C. Lawatscheck, M. Pickhardt, S. Wieczorek, A. Grafmüller, E. Mandelkow, H.G. Börner, Generalizing the concept of specific compound formulation additives towards non-fluorescent drugs: a solubilization study on potential anti-alzheimer-active small-molecule compounds, Angewandte Chemie International Edition 55(30) (2016) 8752-8756.
[123] C. Lawatscheck, M. Pickhardt, S. Wieczorek, A. Grafmüller, E. Mandelkow, H.G. Börner, Generalizing the Concept of Specific Compound Formulation Additives towards Non-Fluorescent Drugs: A Solubilization Study on Potential Anti-Alzheimer-Active Small-Molecule Compounds, Angew. Chem. Int. Ed. 55(30) (2016) 8752-8756.
[124] S. Wieczorek, D. Remmler, T. Masini, Z. Kochovski, A.K. Hirsch, H.G. Börner, Fine-tuning nanocarriers specifically toward cargo: a competitive study on solubilizing related photosensitizers for photodynamic therapy, Bioconjugate Chemistry 28(3) (2017) 760-767.
[125] J. Yan, Z. Ye, M. Chen, Z. Liu, Y. Xiao, Y. Zhang, Y. Zhou, W. Tan, M. Lang, Fine tuning micellar core-forming block of poly (ethylene glycol)-block-poly (ε-caprolactone) amphiphilic copolymers based on chemical modification for the solubilization and delivery of doxorubicin, Biomacromolecules 12(7) (2011) 2562-2572.
[126] A. Takahashi, Y. Ozaki, A. Kuzuya, Y. Ohya, Impact of core-forming segment structure on drug loading in biodegradable polymeric micelles using PEG-b-poly (lactide-co-depsipeptide) block copolymers, BioMed research international 2014 (2014).
[127] V. Huntošová, S. Datta, L. Lenkavská, M. Máčajová, B. Bilčík, B. Kundeková, I. Čavarga, J. Kronek, A. Jutková, P. Miškovský, Alkyl Chain Length in Poly (2-oxazoline)-Based Amphiphilic Gradient Copolymers Regulates the Delivery of Hydrophobic Molecules: A Case of the Biodistribution and the Photodynamic Activity of the Photosensitizer Hypericin, Biomacromolecules 10(22) (2021) 4199-4216.
[128] A. Chroni, T. Mavromoustakos, S. Pispas, Biocompatible PEO-b-PCL nanosized micelles as drug carriers: Structure and drug–polymer interactions, Nanomaterials 10(9) (2020) 1872.
[129] A. Chroni, T. Mavromoustakos, S. Pispas, Poly (2-oxazoline)-Based Amphiphilic Gradient Copolymers as Nanocarriers for Losartan: Insights into Drug–Polymer Interactions, Macromol 1(3) (2021) 177-200.
[130] M.Y. Kozlov, N.S. Melik-Nubarov, E.V. Batrakova, A.V. Kabanov, Relationship between pluronic block copolymer structure, critical micellization concentration and partitioning coefficients of low molecular mass solutes, Macromolecules 33 (2000) 3305-3313.
[131] W. Lu, F. Li, R.I. Mahato, Poly (ethylene glycol)-block-poly (2-methyl-2-benzoxycarbonyl-propylene carbonate) micelles for rapamycin delivery: in vitro characterization and biodistribution, Journal of pharmaceutical sciences 100 (2011) 2418-2429.
[132] X.D. Guo, Y. Qian, C.Y. Zhang, S.Y. Nie, L.J. Zhang, Can drug molecules diffuse into the core of micelles?, Soft Matter 8 (2012) 9989-9995.

[133] J. Wiest, M. Saedtler, B. Böttcher, M. Grüne, M. Reggane, B. Galli, U. Holzgrabe, L. Meinel, Geometrical and structural dynamics of Imatinib within biorelevant colloids, Molecular Pharmaceutics 15 (2018) 4470-4480.
[134] C. Cao, J. Zhao, M. Lu, C.J. Garvey, M.H. Stenzel, Correlation between Drug Loading Content and Biological Activity: The Complexity Demonstrated in Paclitaxel-Loaded Glycopolymer Micelle System, Biomacromolecules 20(4) (2019) 1545-1554.

4 Results

The research findings of present thesis are compiled in the following sequence. The publications as co-auhtor are briefly presented while all the first-author publications are presented in full form (excluding, a review article about mitotane). Collectively, all the publications are mingled in way to make one plot for the better understanding of overall project development. The results section begin with review article for better introduction to the polymer classes of POx and POzi. Following this, the formulations of hydrophobic drugs with POx and POzi based amphiphiles are discussed with special emphasis on, solubility enhancement of hydrophobic drugs, polymer-drug compatibility and their estimation by solubility parameters. The latter publication will mainly express the formulation development of 21 different hydrophobic drugs with four different POx/POzi based amphiphiles. The estimation of polymer drug compatibility by solubility parameters has also remain the major focus. To get further insights into extraordinary high drug loadings, pronounced polymer-drug specificities and structure property relationship, a new library of polymers was synthesized where only the hydrophilic block pMeOx was exchanged with another pEtOx based hydrophilic block. This contribution explains the importance of pMeOx as hydrophilic block for ultra-high drug loading.

To investigate the therapeutic applications of POx/POzi based formulations, selected formulation were further evaluated. Among 21 different formulations, mitotane and BT-44 were extensively characterized. Mitotane is drug of choice for adrenocortical carcinoma. It is very difficult to achieve the necessary plasma concentration even at the very high dosage regimen (6 - 12 tablets/day) administered for months. The problem is a combination of poor aqueous solubility, low oral bioavailability and unpredictable pharmacokinetic profile. The POx based micellar formulation is capable to solubilize around 6 g/L of the MT. With this formulation, the idea of injectable MT administration is presented for the first time, which can potentially overcome the issue of low bioavailability and give better control over pharmacokinetics The BT-44 is the lead compound, under investigation for neurodegenerative disorders, was formulated and thoroughly characterized for its physico-chemical properties and in vivo efficacy.

Applying the similar approach i.e. replacing the pMeOx with pEtOx, a novel thermosensitive AB diblock copolymer (A = pEtOx) was synthesized, this is the second of its kind polymer which is based on POx/POzi, exhibiting LCST type behavior (the first POx/POzi AB di-block (A=pMeOx) was also synthesized in our lab. The hydrogel was thoroughly characterized for rheology and 3D bio printing and compared with pMeOx based hydrogels. The EtOx based hydrogel can potentially be used as hydrogel-bioink, injectable hydrogels or fugitive support material.

4.1 Poly(2-oxazoline)s and Poly(2-oxazine)s Based Biomaterials – an Overview

Biomaterials 178 (2018) 204–280

Contents lists available at ScienceDirect

Biomaterials

journal homepage: www.elsevier.com/locate/biomaterials

Poly(2-oxazoline)s based biomaterials: A comprehensive and critical update

Thomas Lorson [a, 1], Michael M. Lübtow [a, 1], Erik Wegener [b], Malik S. Haider [a], Solomiia Borova [a], Daniel Nahm [a, c], Rainer Jordan [b], Marina Sokolski-Papkov [d], Alexander V. Kabanov [d], Robert Luxenhofer [a, *]

[a] Functional Polymer Materials, Chair for Advanced Materials Synthesis, Department Chemistry and Pharmacy, Julius-Maximilians-University Würzburg, Röntgenring 11, 97070 Würzburg, Germany
[b] Chair of Macromolecular Chemistry, Faculty of Chemistry and Food Chemistry, School of Science, Technische Universität Dresden, Mommsenstr. 4, 01069 Dresden, Germany
[c] Department of Functional Materials in Medicine and Dentistry, University of Würzburg, Würzburg, 97070, Germany
[d] Center for Nanotechnology in Drug Delivery, Division of Pharmacoengineering and Molecular Pharmaceutics, Eshelman School of Pharmacy, University of North Carolina at Chapel Hill, 125 Mason Farm Road, Chapel Hill, NC, 27599, United States

Abstract

Poly(2-oxazoline)s have been investigated for decades as biomaterials. Pioneering early work suggested that hydrophilic poly(2-oxazoline)s are comparable to poly(ethylene glycol) regarding their potential as biomaterials, but the ready commercial availability of the latter has led to its meteoric rise to become the gold standard of hydrophilic synthetic biomaterials. In contrast, poly(2-oxazoline)s almost fell into oblivion. However, in the last decade, this family of polymers has gained much more interest in general and as biomaterials in particular. The rich chemistry and comparably straightforward synthesis of poly(2-oxazoline)s gives many opportunities for tailoring the properties of the resulting biomaterials, allowing the chemist to explore new conjugation chemistry, and to fine-tune the molar mass, hydrophilic lipophilic balance as well as architecture. Thus, the wide range of demands for various applications of biomaterials can be suitably addressed. This review aims to give a comprehensive and critical update of the development of poly(2-oxazoline) based biomaterials, focusing on the last 5 years, which have seen an explosive increase of interest. We believe that the research regarding this diverse family of polymers will remain strong and will keep growing, in particular after the promising first-in-human studies of a poly(2-oxazoline) drug conjugate. This review aims at researchers and students new to this polymer family and seasoned poly(2-oxazoline) experts alike and attempts to showcase how the chemical diversity of poly(2-oxazoline)s allows a relatively facile and broad access to biomaterials of all kinds.

4.2 Estimation of Polymer Drug Compatibility between 18 Polymers and 5 Drugs

Summary: The chemical versatility of POx/POzi based triblock copolymers facilitated the development of polymeric drug carriers enabling extremely high drug loadings > 50 wt.% in selective cases. In combination with some intuition and empirical knowledge, generally, the selection of suitable delivery vehicles is mainly based on trial and error. In order to investigate the effect of increasing side chain length (rendering the system more hydrophobic) on drug loading and to check the applicability of solubility parameters, we synthesized a library of 18 different POx/POzi based ABA triblock copolymers. Where A is always pMeOx while varying the hydrophobic B block from series of linear branched (aliphatic POx with varying side chain lengths; C4-C9) or an aromatic ringside chains. The polymers with shorter side chain length (C3 and C4) appeared to be the best solubilizer for various drugs. At this time point, A-pBuOx-A based ABA triblock copolymer has already been proved to be best solubilizer for many drugs, however the underlying mechanism or the SPR was under investigation. The solubilization experiments were performed with relatively small library of five different hydrophobic drugs. The polymer drug compatibility was estimated by theoretical group contribution methods (Flory-Huggins interaction and solubility parameters) or experimentally, by the determining the solubility of drugs and polymers in selected list of solvents. Surprisingly, SPs were indeed able to correctly estimate some trends regarding good and poor solubilizers, particularly for amphiphiles, which strongly differed in their chemical structure such as C3 or C4 vs strongly hydrophobic C9 sidechains. In contrast, the effect of e.g. branching or cyclization in the side-chain could not be predicted. Interestingly, drugs which were selectively soluble mainly in solvents comprising a high amount of hydrogen-bond acceptors also yielded the highest loading capacity and *vice versa* in case of formulation. Following this, initially we assumed that this is in accordance with the chemical structure of the POx and POzi based amphiphiles, comprising a high density of tertiary amides, which also act as hydrogen-bond acceptors, thus resulting in high drug loading. However, in the next study, where we have explored a library of 21 different drugs, no such trend was apparent.

BioMACROMOLECULES

Article

Cite This: Biomacromolecules 2019, 20, 3041−3056

pubs.acs.org/Biomac

Like Dissolves Like? A Comprehensive Evaluation of Partial Solubility Parameters to Predict Polymer−Drug Compatibility in Ultrahigh Drug-Loaded Polymer Micelles

Michael M. Lübtow, Malik Salman Haider, Marius Kirsch, Stefanie Klisch, and Robert Luxenhofer*

Functional Polymer Materials, Chair for Advanced Materials Synthesis, Department of Chemistry and Pharmacy and Bavarian Polymer Institute, University of Würzburg, Röntgenring 11, 97070 Würzburg, Germany

Abstract

Despite decades of research, our understanding of the molecular interactions between drugs and polymers in drug-loaded polymer micelles does not extend much beyond concepts such as “like-dissolves-like” or hydrophilic/hydrophobic. However, polymer−drug compatibility strongly affects formulation properties and therefore the translation of a formulation into the clinics. Specific interactions such as hydrogen-bonding, π−π stacking, or coordination interactions can be utilized to increase drug loading. This is commonly based on trial and error and eventually leads to an optimized drug carrier. Unfortunately, due to the unique characteristics of each drug, the deduction of advanced general concepts remains challenging. Furthermore, the introduction of complex moieties or specifically modified polymers hampers systematic investigations regarding polymer−drug compatibility as well as clinical translation. In this study, we reduced the complexity to isolate the crucial factors determining drug loading. Therefore, the compatibility of 18 different amphiphilic polymers for five different hydrophobic drugs was determined empirically. Subsequently, the obtained specificities were compared to theoretical compatibilities derived from either the Flory−Huggins interaction parameters or the Hansen solubility parameters. In general, the Flory−Huggins interaction parameters were less suited to correctly estimate the experimental drug solubilization compared to the Hansen solubility parameters. The latter were able to correctly predict some trend regarding good and poor solubilizers, yet the overall predictive strength of Hansen solubility parameters is clearly unsatisfactory.

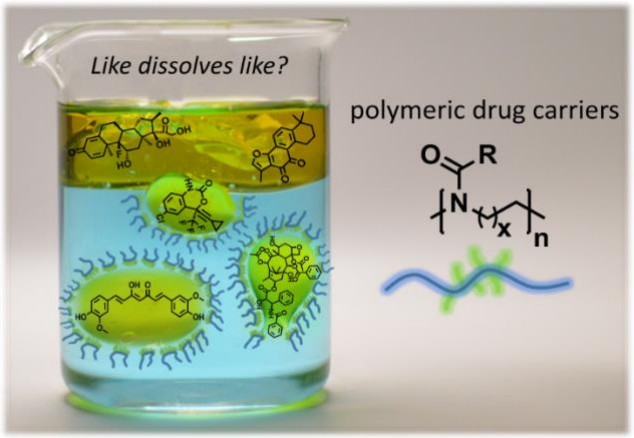

4.3 Estimation of Polymer Drug Compatibility between 4 polymers and 21 Drugs

Summary: For the cure of pathologies, it is desirable that the drug reaches its site of action at a particular concentration within the therapeutic window to mitigate the illness. As discussed previously, the action of APIs is limited by various factors like poor water solubility, poor pharmacokinetic profile and their incapacity to penetrate tissues because of their unique physicochemical properties resulting in an incomplete cure. A lot of efforts have been directed into improving the solubility of hydrophobic APIs, but the success remained limited and the loading capacity, i.e. how much drug can be formulated per amount of polymer, falls below 30 wt.% in the majority of cases. Such relatively low drug loading requires large amounts of excipient (polymer) to achieve the desired dose, which in turn limit the use during clinical translation (because of potential excipient toxicity). The results shown above clearly indicate that in case of POx based amphiphiles a minor amphiphilic contrast is beneficial for high drug loading. Additionally, the strong structure property relationship exist between the hydrophobic block for the same drug. To further achieve, the goal of project i.e. to increase the aqueous solubility of hydrophobic drugs and enhance the ease of their administration, we selected four ABA triblock copolymers with the shorter side chain length in hydrophobic block (B), namely poly(2-butyl-2-oxazoline) (pBuOx), poly(2-pentyl-2-oxazoline) (pPentOx), poly(2-proyl-2-oxazine) (pPrOzi), poly(2-butyl-2-oxazine) (pBuOzi), where A is always poly(2-methyl-2-oxazine) (pMeOx). The formulation experiments were performed with 21 different hydrophobic drugs. In this study, we also further investigated the applicability of solubility parameters. The theoretical and experimental SPs of different homo-/triblock copolymers and 21 different hydrophobic drugs were calculated by two group contribution methods (i.e. hoftyzer Van-Krevelen and Yamamoto molecular break method) and by solubility testing in list of selective solvents (for polymers only). The results confirmed that the compatibility estimation by SPs is a non-suitable tool, particularly for POx/POzi based systems.

Development of Poly(2-oxazoline)s and poly(2-oxazine)s based formulation library and estimation of polymer/drug compatibility.

Malik Salman Haider[1], Robert Luxenhofer[2*]

[1]*Functional Polymer Materials, Chair for Advanced Materials Synthesis, Institute for Functional Materials and Biofabrication, Department of Chemistry and Pharmacy, Julius-Maximilians-University Würzburg, Röntgenring 11, 97070 Würzburg, Germany*

[2*]*Soft Matter Chemistry, Department of Chemistry, and Helsinki Institute of Sustainability Science, Faculty of Science, University of Helsinki, PB 55, 00014 Helsinki, Finland*

Correspondence to: robert.luxenhofer@helsinki.fi

Keywords: hydrophobic drugs, solubility enhancement, micelles, polymer-drug interaction

Abstract

The main objective of this study is to formulate a library of difficult to solubilize drugs with four slightly different poly(2-oxazoline)s (POx) and poly(2-oxazine)s (POzi) based amphiphilic triblock copolymers and to elucidate whether the drug-polymer compatibility, as estimated by solubility parameters (SPs) might be used as tool to guide formulation development. The theoretical and experimental SPs of different homo-/triblock copolymers and 21 different hydrophobic drugs were calculated by two group contribution methods (i.e. Hoftyzer Van-Krevelen and Yamamoto molecular break method) and determined experimentally by solubility testing in list of selective solvents (for polymers only). The obtained SPs were further utilized to calculate the distance between polymers and drugs (Ra) in 3 dimensional Hansen space. Out of 21 structurally diverse drugs, the loading capacity (LC) was found to be higher than 40, 30, 20 and 10 wt.% for 4, 4, 3 and 5 drugs, respectively. In the remaining of 5 drugs the maximum achievable LC was found below 10 wt.%. The experimental results obtained by formulation development were not in accordance with the results predicted by Ra calculation. In contrast to several reports found in the literature, the determination of SPs and concurrent compatibility estimation appeared not to be a suitable tool to predict polymer-drug compatibility in the present system. As the predictive power of SPs is based on simple mathematical calculations, limiting the precise prediction of overall polarity, hydrogen bonding ability of molecules and interplay between the hydrophilic and hydrophobic domains

resulting in differing deviations than predicted interactions thus might compromise the predictive power of SPs.

1. Introduction

The technological innovations in drug discovery have led to the development of larger, more complex and more hydrophobic compounds as lead candidates and active pharmaceutical ingredients. According to an estimate, 40% of the drugs in market and 90% of the new chemical entities are considered hydrophobic [1]. These molecules require specialized processing and safe vehicles for solubilisation to overcome the instinct issues, including problems at various levels from discovery to processing and formulations development until consumption to therapeutic outcomes [2]. However, many vehicles available do either not have an ideal safety profile, e.g. Cremophor EL (CrEL) for paclitaxel (PTX) administration [3] or are not as good solubilizers as would be desired. Even with the pre-medication including corticosteroids and anti-histamines, CrEL induced hypersensitivity reactions are commonly observed [4] and most vehicles/excipients do not allow for solubilization of more than 20 wt. – 25 wt.% and the overall increase in apparent solubility is limited. Thus, for the delivery of these agents, there is clear need to find alternative formulations and vehicles.

Polymeric micelles (PMs) have long been investigated as a promising drug delivery platform. They are nanoscopic architectures formed by the self-assembly of amphiphilic polymers [5, 6]. During (or after) the self-assembly process, PMs are capable to encapsulate/solubilize additional hydrophobic molecules. Several PMs formulations are already in clinical use or have been in clinical trials, for example NK911 and Genexol-PM [7-10]. However, PMs often suffer from intrinsic issues such as low drug loading, instability [11] and poor permeability across cell membranes or other biological barriers [12]. The loading capacity (LC) and stability can directly be correlated to intrinsic properties of polymers, drugs or/and their compatibility with each other [13]. In the past decades, poly(2-oxazoline)s (POx) and poly(2-oxazine)s (POzi) have gained significant attention for their biomedical and pharmaceutical applications [14-16]. Unlike many other systems, the POx/POzi based ABA triblock copolymer (A and B, hydrophilic and hydrophobic block, respectively) have shown particular potential for development of ultra-high drug loaded micellar formulations [14]. In particular, ABA triblock copolymers featuring poly(2-methyl-2-oxazoline) (pMeOx) as hydrophilic A block and moderately hydrophobic poly(2-*n*-butyl-2-oxazoline) (pBuOx), poly(2-*n*-butyl-2-oxazine)

(pBuOzi) or poly(2-*n*-propyl-2-oxazoline) (pPrOx) show very promising properties such as high drug loading, excellent cytocompatibility and are very well tolerated upon *in vivo* administration [17, 15, 18].

For the development of a successful PMs system, the primary mission is to select a polymer which is not only compatible with the cargo but also provide colloidal stability even at high relative and absolute cargo concentrations. There are a variety of physicochemical techniques available to determine the compatibility between polymer and drugs, but most of these are time-consuming, expensive and laborious [19-22]. For the development of cost-effective and efficient drug delivery system, it is usually desirable to predict theoretically the extent of compatibility between polymer and drugs before any experimentation. For many years, Hansen solubility parameters (HSPs) were routinely employed for estimation of compatibility between solute and solvent especially in paint/polymer industry [23]. More recently, HSPs are used in other areas like cosmetics [24], drugs [25], oligomers [26] or gel formation [27] and nanoparticles [28]. To guide formulation development, Allen and the co-workers calculated HSPs to estimate the compatibility between model drug ellipticine and a variety of chemically diverse polymers. Overall, a good correlation was observed between theoretical compatibility profile and experimental results of the formulation[29]. Importantly, as the HSPs are calculated by various group contribution methods so the polymers which are closely related or structural isomers would yield the same HSPs values and in turn represent the similar compatibility for the drugs. In contrary, Lübtow et al. observed the distinct polymer-drug specificities in POx/POzi based micellar formulation, although the polymers differed by only one methylene unit in the side chain or the backbone (structural isomers) of hydrophobic block [30].

In order to investigate the effect of increasing side chain length (rendering the system more hydrophobic) on drug loading and to check the applicability of HSPs, previously, previously a library of 18 different POx/POzi based ABA triblock copolymers was synthesized, comprising pMeOx as A, while varying the hydrophobic B block from series of linear [31, 32], branched (aliphatic POx with varying side chain lengths; C4-C9) [33, 34] or an aromatic side chains [35, 29]. The polymers with shorter side chain length (C3 and C4) appeared to be the best solubilizer for various drugs, while overall predictive power of HSPs was found to be unsatisfactory. Thus, the main aim of the present study is to establish an effective, rapid and

simple method for the rational design of drug formulations. Therefore, the goal was to develop a formulation library with high drug loading as well as the comparison of calculated HSPs, to identify if they can be used as means to predict the polymer drug compatibility in these systems. Accordingly, from the previously synthesized library, we selected the best performing polymers and tested their solubilizing capacity with a library of 21 different hydrophobic drugs. The HSPs were also estimated theoretically and experimentally to guide formulation development and to check their applicability for such systems.

2. Materials and Methods

All substances for the preparation of the homo-/triblock copolymers were purchased from *Sigma-Aldrich* (Steinheim, Germany) or *Acros* (Geel, Belgium) and were used as received unless otherwise stated. The monomers 2-*n*-butyl-2-oxazoline (BuOx), 2-*n*-pentyl-2-oxazoline (PentOx), 2-*n*-propyl-2-oxazine (PrOzi), 2-*n*-butyl-2-oxazine (BuOzi), and 2-methyl-2-oxazoline (MeOx) were prepared following the procedure by Seeliger [36]. All substances used for polymerization, specifically methyl trifluoromethylsulfonate (MeOTf), MeOx, BuOx, PentOx, PrOzi, BuOzi and benzonitrile (PhCN), were refluxed over CaH_2 and distilled and stored under argon.

Axitinib, Brefeldine, Dasatinib, Erlotinib, Sunitinib, Crizotinib, Vorinostat Bexarotene, Cabazitaxel, Bortezomib, Celecoxib, Genistein, Lapatinib, Sorafenib, Vismodegib were purchased from LC Laboratories (Woburn, MA, USA). Clofazimine, carbamazepine and cannabidiol crystals were purchased from Sigma-Aldrich, ACROS and Meet Harmony, London UK, respectively. The Clotrimazole and mitotane was purchased from TCI, Germany and ISP Chemical products, Columbus, USA, respectively.

2.1. General Synthetic Procedure for Homopolymers

The polymerization and work-up procedures were carried out as described previously. Briefly, 1 eq. of initiator (MeOtF) was added to a dried and argon flushed flask and dissolved in the respective amount of solvent (PhCN). The monomer was added and the reaction mixture was heated to 110°C (POx) or 120°C (POzi) for approximately 4-6 hours. Reaction progress was controlled by ^{1}H-NMR spectroscopy. After complete consumption of the monomer, termination was carried out by the addition of 3 eq. of Boc-pip and the mixture was stirred at 50°C for additional 4 hours. PhCN was removed under reduced pressure. In the case of four hydrophobic homopolymers (pBuOx, pPentOx, pPrOzi and pBuOzi), after PhCN removal, the

thick polymer mass was dissolved in chloroform and extracted three times against water followed by chloroform removal under reduced pressure.

While in the case of pMeOx, hydrophilic homopolymer, the thick polymer mass was dissolved in 1:1 mixture of chloroform and methanol. The polymer solution was added dropwise into the ice cold diethyl ether under continuous stirring. After polymer precipitation, the diethyl ether was decanted. The residual diethyl ether was removed at rotary evaporator. The polymer mass was dissolved in deionized (DI) water and lyophilized.

2.2. Nuclear Magnetic Resonance Spectroscopy (NMR)

NMR spectra were recorded on a Fourier 300 (300.12 MHz), *Bruker Biospin* (Rheinstetten, Germany) at 298 K. The spectra were calibrated to the signal of residual protonated solvent ($CDCl_3$ at 7.26 ppm) and analyzed using MestReNova software (version 6.0.2-5475).

2.3. Gel Permeation Chromatography (GPC)

Gel permeation chromatography (GPC) was performed on SECurity GPC Agilent 1260 Infinity System (*Polymer Standard Service)* Mainz, Germany with HFIP containing 3 g/L potassium trifluoroacetate; precolumn: 50 x 8 mm PSS PFG linear M; 2 columns: 300 x 8 mm PSS PFG linear M (particle size 7 µm; pore size 0.1 – 1,000 kDa). The columns were kept at 40°C and flow rate was 0.7 ml/min, prior to each measurement, samples were filtered through 0.2 µm PTFE filters, *Roth* (Karlsruhe, Germany). Conventional calibration was performed using poly(ethylene glycol) standards (0.1 – 1,000 kg/mol) and data was processed with Win-GPC software and further plotted in OriginPro 2015 Sr2 software (version b9.2.272).

2.4. Solubility Parameters

The theoretical solubility parameters were calculated by group contribution methods (GCM) from Hoftyzer Van-Krevelen's (HnV) and Yamamoto Molecular break method (YMB) by commercially available HSPiP software (5^{th} edition, version 5.0.05). In case of GCM (HnV), each functional or structural group in a compound contribute towards certain molar attractive force and hydrogen bonding energy. In contrast to one dimensional Hildebrand solubility parameters, the Hansen solubility parameters (HSPs) divide the total solubility parameter *(δ_T)* into three individual components arising from dispersion *(δ_d)*, polar *(δ_p)* and hydrogen bonding contributions *(δ_h).* The δ_d, δ_p and δ_h can be calculated by HnV method by using the following equations:

$$\delta_d = \frac{\sum Fdi}{V} \qquad \delta_p = \frac{(\Sigma F_{pi}^2)^{1/2}}{V} \qquad \delta_h = (\Sigma \frac{E_{hi}}{V})^{1/2} \qquad V = \sum Vi \qquad (1, 2, 3, 4)$$

Where F_{di}, F_{pi} and E_{hi} are the molar dispersion, polar attraction constant and hydrogen bonding energy, respectively and *Vi* is the group specific volume. Each structural group in the molecule contribute towards the F_{di}, F_{pi} and *Ehi* and the respective values were obtained from literature [37]. Where, V is the molar volume of drug calculated by Fedor's method [38]. Accordingly, each functional group contribute towards the molar volume and can be calculated by following equation 4. The δ_{drug} and $\delta_{polymer}$ are representing the δ_T for drug and polymer, respectively. The δ_T is the sum of dispersion (δ_d), polar (δ_p) and hydrogen bonding contributions (δ_h) and can be calculated by following equations:

$$\delta_{drug}^2 = \delta_d^2 + \delta_p^2 + \delta_h^2 \qquad \delta_{polymer}^2 = \delta_d^2 + \delta_p^2 + \delta_h^2 \qquad (5, 6)$$

The second method used for HSPs calculation is YMB. This is a sub-program of commercially available HSPiP software. In comparison to HnV, this is relatively simpler method to obtain HSPs. The HSPs can be obtained by inserting SMILES code into the software. The SMILES codes were obtained by drawing the structures in the ChemDraw Professional, version 20.0.0.41. YMB is also a GCM with a larger set of functional groups. However, there is also a limitation that it can not process structures greater than 120 heavy atoms.

The software HSPiP also provides a method to semi-empirically determine the HSPs values by dissolving the compound in a wide range of different solvents. Therefore, the solubility profiles of homo-/triblock copolymers were checked in 31 different solvents at concentration of 20 g/L by shaking at 25°C for 24 hours. The results were recorded as binary score of 0 and 1, corresponding to insoluble and soluble, respectively. These results were further incorporated into HSPiP software and experimental HSPs values were obtained.

The extent of compatibility between drugs and polymers was estimated by using the Hildebrand-Scatchard equation [39].

$$\chi_{drug-polymer} = (\delta_{drug} - \delta_{polymer})^2 \frac{V}{RT} \qquad (7)$$

Where $\chi_{drug\text{-}polymer}$ (χ_{dp}) represents the Flory-Huggins interaction parameter, δ_{drug} and $\delta_{polymer}$ are the δ_T for the drug and polymer, respectively. *V* is the molar volume of calculated by Fedor's method [38], *R* is the gas constant and *T* is the temperature in K.

Besides Hildebrand-Scatchard equation, the compatibility was also estimated by correlating δ_d, δ_p and δ_h in three dimensional (3D) Hansen space by using the following equation:

$$Ra^2 = (4(\delta_{d1} - \delta_{d2})^2 + \left(\delta_{p1} - \delta_{p2}\right)^2 + (\delta_{h1} - \delta_{h2})^2 \quad (8)$$

The subscripts 1 and 2 represent the two material of interest i.e. polymer and drug. The lower Ra value represent the higher compatibility between polymer and drug.

2.5. Drug Formulation

Drug loaded polymer micelles were prepared using the thin film hydration method. Depending upon solubility of drugs in organic solvents, polymer and drug stock solutions were mixed in desired ratios. After complete removal of the solvent at 50°C under a mild stream of argon, the films were further dried *in vacuo* (≤ 0.2 mbar) for at least 30 minutes to remove the traces of organic solvent (if any). Subsequently, preheated (37°C) DI water was added to obtain desired final polymer (10 g/L) and drug concentrations. To ensure complete solubilisation, the solutions were shaken at 55°C for 15 to 30 min at 1250 rpm with a Thermomixer comfort (*Eppendorf AG,* Hamburg, Germany). Non-solubilized drug was removed by centrifugation for 5 min at 10.000 rpm with a 3-Speed micro centrifuge, (*neoLab,* Heidelberg, Germany). Solubilisation experiments were performed in 3 individually prepared samples and results are presented as mean ± standard deviation (SD).

2.6. High Performance Liquid Chromatography (HPLC)

HPLC analysis was carried out on a LC-20A Prominence HPLC (*Shimadzu,* Duisburg, Germany) equipped with a system controller CBM-20A, a solvent delivery unit LC-20 AT (double plunger), an on-line degassing unit DGU-20A, an auto-sampler SIL-20AC, a photo diode array detector SPD-M20A. As stationary phase, a ZORBAX Eclipse Plus (*Agilent,* Santa Clara, CA, USA) C18 column (4.6 x 100 mm; 3.5 µm) was used. Quantification of drugs was performed with a stepwise gradient using acetonitrile and water with 0.05% TFA. Initially the HPLC methods were developed for individual drugs. After that, the series of standard solutions of different known concentrations were measured to obtain the standard curve followed by the drug quantification at their respective lambda max. For all the HPLC data, please refer to Figure S8-S28.

2.7. Loading Capacity and Loading Efficiency (LC & LE)

The following equations were used to calculate the loading capacity (LC) and loading efficiency (LE) of the drug loaded formulations:

$$LC = \frac{m_{drug}}{m_{drug}+m_{excipient}} * 100\% \quad (9)$$

$$LE = \frac{m_{drug}}{m_{drug,added}} * 100\% \quad (10)$$

where m_{drug} and $m_{excipient}$ are the weight amounts of the solubilized drug and polymer excipient in solution and $m_{drug,added}$ is the weight amount of the drug initially added to the dispersion. No loss of polymer during micelles preparation was assumed.

2.8. UV-Vis spectroscopy

Clofazimine (CFZ) quantification was performed by UV-Vis absorption on a BioTek Microplate spectrophotometer, *Thermo Fischer Scientific* (MA, USA) using a calibration curve with the known amounts of CFZ (Figure S14). Samples were prepared Rotilabo F-Type 96 well plates, *Carl Roth GmbH and Co. KG* (Karlsruhe, Germany) with the constant volume of 200 µl. Spectra were recorded from 300 to 600 nm at 298 k. CFZ absorption was detected at 450 nm. Prior to UV-Vis absorption measurements, the aqueous formulations were diluted with ethanol.

3. Results and Discussions

3.1. Synthesis of Homopolymers

From a previously investigated library of 18 different ABA triblock copolymers [34], we selected 3 best performing polymers with respect to drug solublization. In all the selected polymers the hydrophilic block A is always poly(2-methyl-2-oxazoline) and comprising moderately hydrophobic block B i.e. poly(2-*n*-butyl-2-oxazoline) (pBuOx), poly(2-*n*-propyl-2-oxazine) (pPrOzi) and poly(2-*n*-butyl-2-oxazine) (pBuOzi). All of these polymers were previously investigated for drug formulation and have shown promising results [40, 9, 41-43]. As all the triblock copolymers comprised of pMeOx as A, so they are represented according to hydrophobic block i.e. A-pBuOx-A, A-pPrOzi-A, and A-BuOzi-A. To this mini-library, we added a fourth polymer (less commonly explored) comprised of hydrophobic poly(2-*n*-pentyl-2-oxazoline) (pPentOx) block. Recently, the polymer A-pPentOx-A was reported to have ultra-high LC of 47 wt.% for new investigational molecule i.e. BT-44 (BT44 ChemRxiv). The targeted block length for each block in triblock copolymer is A_{35}-B_{20}-A_{35}. For synthesis and characterization of four triblock copolymers, the readers are referred to previous reports [30, 34] (BT44 ChemRxiv). These four polymers represent two pairs of structural isomers. i.e. they differ from each other by one methylene unit which is shifted from polymer backbone to the

side of hydrophobic block and vice versa (A-pBuOx-A/A-pPrOzi-A and A-PentOx-A/A-pBuOzi-A).

To gain insights into theoretical and experimental solubility parameters (SPs) while keeping in mind the general assumption that mainly hydrophobic block is responsible for drug loading, initially, we synthesized five different homopolymers which collectively comprised our triblock copolymers represented as hydrophobic pBuOx, pPentOx, pPrOzi, pBuOzi and hydrophilic pMeOx (Figure 1a). All of the homopolymers were synthesized by living cationic ring opening polymerization (LCROP) as previously described [36]. The homopolymers were characterized by ^{1}H-NMR and GPC. The end-group analysis via ^{1}H-NMR gave a degree of polymerization of around 20 and 35 for hydrophobic and hydrophilic block, respectively (Figure S1 to S5) which is very close to targeted block length. GPC elugram showed that purified homopolymers appeared essentially 9onomodal with reasonably low dispersity (Đ < 1.1) (Figure S6).

a

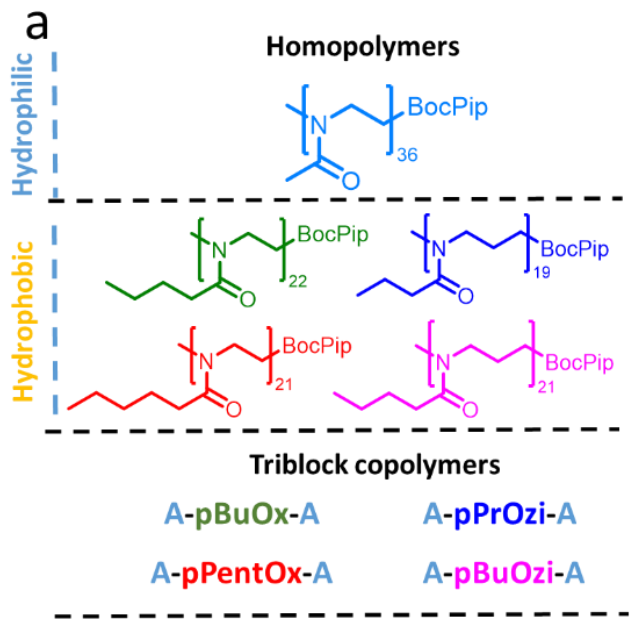

b

Characterization of all synthesized homopolymers including the molecular weight M_n and dispersity Đ

Polymer	M_n [a)] [kg/mol]	M_n [b)] [kg/mol]	Đ [b)] HFIP
$pMeOx_{35}$	3.3	2.7	1.07
$pBuOx_{22}$	3.0	2.1	1.04
$pPentOx_{21}$	3.2	2.3	1.05
$pPrOzi_{19}$	2.6	2.1	1.05
$pBuOzi_{21}$	3.2	2.3	1.06

[a)]Obtained by ^{1}H-NMR analysis ($CDCl_3$; 300 MHz), [b)]obtained by GPC analysis (eluent is HFIP).

Figure 1: a) Chemical structures of the synthesized hydrophilic (pMeOx) and hydrophobic (pBuOx, pPentOx, pPrOzi and pBuOzi) homopolymers and representation of corresponding triblock copolymers. B) ^{1}H-NMR and GPC characterization of all five synthesized homopolymers.

3.2. Solubility Parameters of Homo-/Triblock Copolymers and Drugs

After successful homopolymer and triblock copolymers synthesis , we determined the theoretical and experimental Hansen solubility parameters (HSPs). Initially, the molar volume was calculated by Fedor's method (Table S1) followed by theoretical SPs calculations by

Hoftyzer Van-Krevelen (HnV) (Table S3-S24) and Yamamoto molecular break method (YMB) (Table S26). The SPs values obtained by HnV method were not affected by degree of polymerization (DP), in contrast, in case of YMB, with the increasing DP, the SPs of selected homopolymer showed exponential increase and became physically unreasonable [34]. For the sake of comparison with HnV method, a single repeat unit was used for YMB method.

HnV is a group contribution method, where every single group in the chemical structure contributes towards the SPs of the compound. The δ_d, δ_p, δ_h, δ_T and molar volume V were calculated by using equation 1 to 6 (Table S1 and Table S3-S24). Expectedly, and as reported for a library of 18 different triblock copolymers [34], the HnV could not differentiate between the structural isomers i.e. pBuOx/pPrOzi and pPentOx/pBuOzi resulting in similar δ_d, δ_p, δ_h, δ_T (Figure 2a, Table S2) and molar volume values (Figure 3a). Generally, with the exception of δ_d value, the δ_p, δ_h *and* δ_T values of hydrophilic pMeOx remained significantly higher in comparison to all four hydrophobic blocks (Figure 2a). Overall, the SPs values for all the hydrophobic blocks by HnV method remained in close range. Interestingly, the YMB method was able to differentiate between the structural isomers with respect to δ_d, δ_p, δ_h values. However, the obtained δ_T (20.80 $MPa^{1/2}$) (Table S2) and molar volume values (145.60 cm^3/mol) (Figure 3a) for pPentOx/pPrOzi and pBuOx/pPrOzi, respectively, were identical. Additionally, the δ_d value for the 4 hydrophobic blocks was found to be the same i.e. 16.8 $MPa^{1/2}$ while a slightly higher δ_d value for the pMeOx was obtained i.e. 17.2 $MPa^{1/2}$ (Table S2). In comparison to HnV, a significant drop in δ_d and δ_T values (obtained by YMB) was noted for all five blocks while δ_p, δ_h values obtained by both methods remained in close range (Figure 2a).

Semi-empirical determination of SPs was also performed by dissolving the synthesized homo-/triblock copolymers at 20 g/L concentration in a library of solvents ranging from polar (protic and aprotic) to non-polar solvents (Figure 2b). Initially, the solubility profile of all the homopolymers was obtained. The POx based hydrophobic polymers i.e. pBuOx and pPentOx showed similar solubility profile with an exception to one solvent i.e. pBuOx and pPentOx were not soluble in toluene and sulfolane, respectively (Figure 2b, column 1 and 2). For the POzi based homoplymers i.e. pPrOzi and pBuOzi, both exhibited a very similar solubility profile with only one exception; dimethoxy methane, in which pPrOzi was not soluble (Figure 2b, column 3). The pMeOx homopolymer being hydrophilic, exhibited slightly different solubility

profile as compared to hydrophobic homopolymers (Figure 2b, column 5). Additionally, the solubility profile of all the selected ABA triblock copolymers was also obtained. Not surprisingly, the results showed that the solubility of triblock copolymers is strongly affected by the presence of hydrophilic pMeOx block. The solubility profile of both POx based triblocks (i.e. A-pBuOx-A and A-pPentOx-A) (Figure 2b, column 6 and 7) was the same as that of pMeOx homopolymer. The POzi based triblocks (i.e. A-pPrOzi-A and A-pBuOzi-A) also followed the same pattern with a notable single exception to butyronitrile, where both POzi based triblocks were found soluble too (Figure 2b, column 8 and 9).

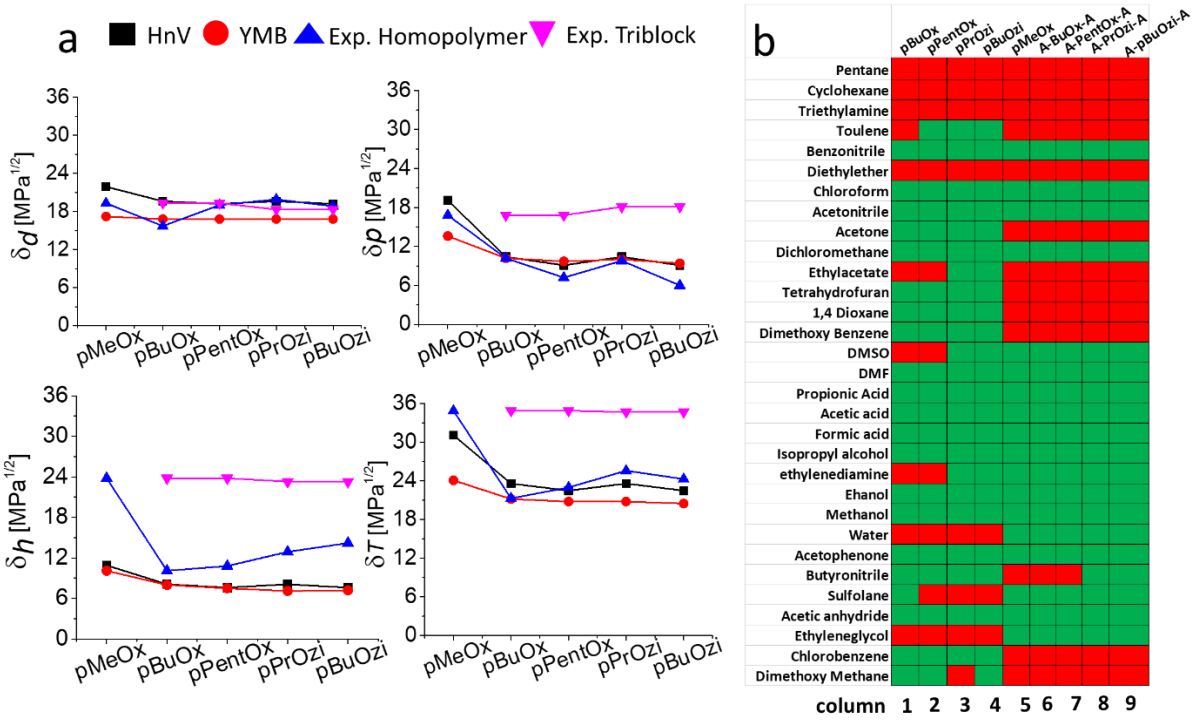

Figure 2: a) The theoretical (Hoftyzer van-Krevelen (HnV) and Yamamoto molecular break method (YMB)) and experimental (exp.) partial and total solubility parameters of homo-/triblock copolymer, calculated by group contribution methods i.e. (HnV, black squares) and (YMB, red circles) and obtained experimentally (blue triangle and inverted magenta triangle for homopolymer and triblocks, respectively). b) Solubility profile of five homopolymers and their respective four triblock copolymers in 31 different solvents at a concentration of 20 g/L and at 25°C (green: soluble, red: insoluble). This solubility score was utilized in HSPiP software to obtain the experimental solubility parameters shown in Figure 2a.

The semi-empirical SPs were obtained by utilizing the solubility score obtained as binary code, i.e. 0 (insoluble, red) and 1 (soluble, green) (Figure 2b) in the HSPiP software. The polymer concentration used for solubility testing was randomly chosen (i.e. 20 g/L), unfortunately, there is no defined rule for that. Important to note, different concentrations/temperatures and shaking time, may result in different solubility profile and in turn varied SPs. The semi-

empirical SPs determination was capable to differentiate between hompolymers which are structural isomers, because of minor differences in obtained solubility profile (Figure 2b, column 1-4 and Table S2). Within pure POx and POzi based triblock copolymers, identical SPs values were obtained because of identical solubility profile (Figure 2b, column 6-9, Table S2). Overall, no correlation was observed in the experimental SPs values of homo- and triblock copolymers. This already gave a hint that while determining the compatibility between amphiphilic polymers and drugs, the only consideration of hydrophobic block, which is most commonly practiced method in the literature [44], may lead to unrealistic results.

We selected a list of hydrophobic drugs for formulation development and compatibility estimation. The main criteria for the selection of drugs was their hydrophobicity and associated concerns, which can limit therapeutic outcomes. The physicochemical properties of the selected drugs are shown in table 1.

Table 1: Physicochemical properties of the investigated active pharmaceutical ingredients as taken from www.drugbank.com

entry	Drug	mol. weight [g/mol]	aqueous solubility [g/L]	Log P	H-bond donors	H-bond acceptor	polar surface area [Å^2]	Rotatable bond count
1	Axitinib	386.5	0.0005	4.17	2	3	70.67	5
2	Brefeldine	280.4	0.8	1.73	2	3	66.76	0
3	Carbamazepine	236.3	0.1	2.7	1	1	46.33	0
4	Dasatanib	488.0	0.01	2.7	3	8	106.51	7
5	Erlotinib	393.4	0.008	3.13	1	7	74.73	10
6	Sunitinib	398.5	0.03	3.24	3	3	77.23	7
7	Clofazimine	473.4	0.001	7.39	1	4	39.99	4
8	Crizotinib	450.3	0.006	3.82	2	5	77.99	5
9	Ezetimibe	409.4	0.008	4.14	2	3	60.77	6
10	Vorinostat	264.3	0.07	1.88	3	3	78.43	8
11	Bexarotene	348.5	0.0001	6.86	1	2	37.3	3
12	Cabazitaxel	835.9	0.004	3.69	3	10	202.45	15
13	Bortezomib	384.2	0.05	1.53	4	6	124.44	9
14	Cannabidiol	314.5	0.01	6.1	2	2	40.46	6
15	Celecoxib	381.4	0.005	3.99	1	3	77.98	4
16	Clotrimazole	344.8	0.001	5.48	0	1	17.82	4
17	Genistein	270.2	0.1	3.04	3	5	86.99	1
18	Lapatinib	581.1	0.02	5.18	2	7	106.35	1
19	Sorafenib	464.8	0.001	4.12	3	3	92.35	11
20	Vismodegib	421.3	0.001	3.93	1	4	76.13	6
21	Mitotane	320.0	0.000001	6.08	0	0	0	3

At first, SPs of the drugs were calculated by HnV and YMB method. To proceed, initially, the molar volume of the drugs were calculated by Fedor's method [38] and by HSPiP software. The molar volume of drugs and polymers obtained by YMB method was higher than HnV

(Figure 3a). The SPs of the drug library were obtained by HnV method using equation 1 to 6 and for YMB methods, the drugs SMILES were obtained by drawing the structures in ChemDraw followed by further processing in HSPiP software. The δ_d, δ_p, δ_h and δ_T of all the drugs generally followed similar trend irrespective of method i.e. HnV or YMB with the single exception of Genistein, where δ_d, δ_h and δ_T were found higher in case of HnV method (Figure 3b). Overall, the HSPs values obtained by YMB are slightly lower than HnV, except for δ_p, where the values are very close to each other for both methods.

a The molar volume was calculated by Fedors method and by HSPiP software

S.No	Drugs/Polymers	Molar volume cm³/mol	
		HnV	YMB
1	Axitinib	257.3	291.0
2	Brefeldine	233.0	289.2
3	Carbamazepine	157.1	187.5
4	Dasatanib	301.5	351.6
5	Erlotinib	257.8	362.2
6	Sunitinib	282.3	325.9
7	Clofazimine	313.7	350.5
8	Crizotinib	284.8	338.9
9	Ezetimibe	262.2	319.1
10	Vorinostat	162.6	222.5
11	Bexarotene	295.6	319.3
12	Cabazitaxel	575.2	-
13	Bortezomib	246.6	384.2
14	Cannabidiol	298.8	325.0
15	Celecoxib	226.4	278.0
16	Clotrimazole	252.5	292.2
17	Genistein	135.4	211.5
18	Lapatinib	361.3	430.9
19	Sorafenib	305.9	316.5
20	Vismodegib	225.9	288.4
21	Mitotane	240.8	233.8
1	MeOx	58.0	93.8
2	BuOx	106.3	145.6
3	PentOx	122.4	161.5
4	PrOzi	106.3	145.6
5	BuOzi	122.4	162.9

b

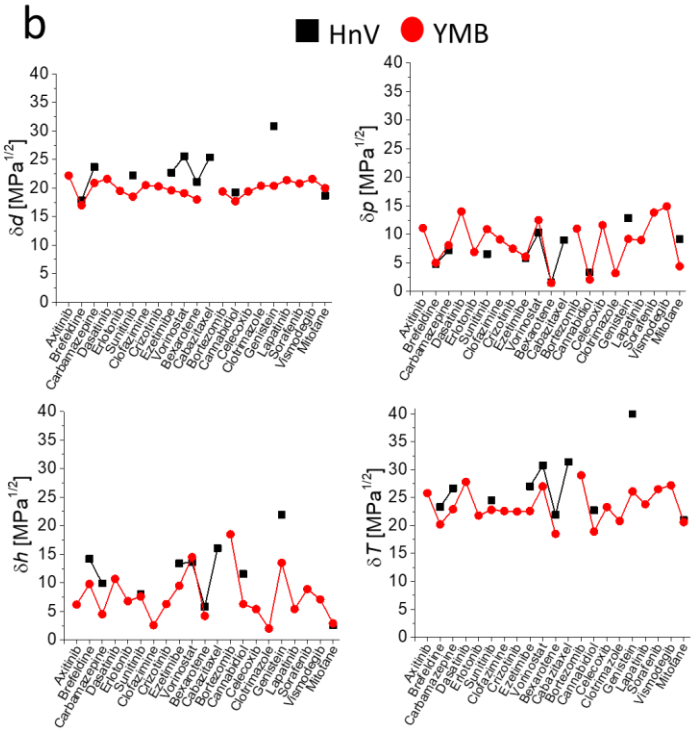

Figure 3: a) The molar volume of 21 hydrophobic drugs (blue) and individual blocks of triblock copolymers (gray) obtained by Fedor's method (used further for HnV method) and by HSPiP software (used further in YMB method calculations). The molar volume of cabazitaxel was not possible to obtain by HSPiP software indicated as (-) in the table. b) The partial and total solubility parameters of hydrophobic drugs obtained by Hoftyzer van-Krevelen (HnV, black squares, 10 drugs) and Yamamoto molecular break method (YMB, red circles, 20 drugs). The solubility parameters of 11 drugs by HnV were not calculated because of unavailability of F_{di}, F_{pi} and E_{hi} values for certain groups in the chemical structures. The lines are added only for eye guidance.

Both of the group contribution methods have certain limitations. In case of HnV, the most obvious is a small number of functional groups with designated molar attractions constants. Out of 21 drugs, the SPs determination by HnV was not possible for 11 drugs (missing black squares in Figure 3b) e.g. for the drugs Erlotinib, Axitinib and Bortezomib, as the F_{di}, F_{pi} and E_{hi} values for C-C triple bond, -N= and borane, respectively are not available. For a better comparison of SPs values obtained by HnV and YMB for the 10 drugs both methods were

suitable, the SPs values were replotted and presented in the supporting information (Figure S7). As stated previously, no major differences were observed for both group contribution methods. The calculation of molar volume for all the drugs was possible by Fedor's method because of the large number of groups enlisted with their respective values in the literature (Figure 3a) [38]. The YMB method also has limitations like, it is unable to process the molecules larger than 120 heavy atoms. However, in the case of Cabazitaxel, after inserting the SMILES in the HSPiP software, the HSPs values could not be obtained, although the compound is smaller than the specified limit. The experimental determination of SPs of drugs was revoked as it would not be worthy to determine, especially when the experimental SPs values of the POx and POzi based triblock copolymer have shown the similar results (Figure 2a and Table S2).

3.3. Estimation of Compatibility and Formulation Studies

The SPs values obtained by HnV and by experimental determination were not further processed for compatibility estimation because of the similar SPs values for the polymers (Figure 2a and Table S2). Only the SPs values obtained by the YMB method were further utilized to estimate the compatibility between polymers and drugs either by Flory-Huggins interaction parameter ($\chi_{drug\text{-}polymer,}$ χ_{dp}) or by Ra calculation (equation 7 and 8, respectively). Here, a lower value of χ_{dp} (ideally = 0) suggests a better polymer-drug compatibility. For χ_{dp} calculation (equation no. 7), the total solubility parameters (δ_T) of drug and polymer is needed. As noted previously, the YMB method gave the similar δ_T values (for PrOzi and PentOx polymer) (Table S2) and molar volume values (for BuOx and PrOzi polymer) i.e. 20.8 $MPa^{1/2}$ and 145.60 cm^3/mol, respectively (Figure 3a). This already gave a hint that Flory-Huggins interaction parameter would not be an appropriate method to estimate the compatibility, because of the same δ_T and molar volume values. Therefore, the measurement of Ra (equation no. 8), which involves the utilization of individual δ_d, δ_p, δ_h values was only considered for compatibility estimation. The smaller distance between polymers and drugs in Hansen space represent the higher compatibility. Importantly, Ra of the two substances in the Hansen space only provide the qualitative information of compatibility.

Initially, the solubility of drugs was tested in various solvents to select the best solvent for thin film-hydration method. In our previous studies, depending upon the solubility of the drug, the most commonly used solvent is EtOH. Herein, most of the enlisted drugs were also

soluble in ethanol (EtOH) with the exception of dasatinib, clofazimine and lapatinib for which mixture of EtOH/Acetonitrile (ACN) and methanol (MeOH) were used, respectively. All the information about solubility of drugs in organic solvents is presented in Table S28. The drug formulations included in this study were prepared as reported previously [17, 30]. Briefly, the polymer and drug solutions (prepared in organic solvent) were mixed in desired ratios (the targeted polymer concentration was kept constant at 10 g/L while the drug concentration was increased from 2 to 10 g/L) followed by solvent removal and the subsequent hydration of resultant thin-film by deionized (DI) water. A total of 1260 formulations were prepared with the in-house developed formulation assembly capable to make 24 thin films in one session (Figure S29). The (dissolved) drug in the micellar formulation was quantified by HPLC, after removal of (if any) non-solubilized drug by centrifugation. All the HPLC related details i.e. standard curve, elugrams and HPLC method can be found in Figure S8-S28. The aqueous solubility of pristine drugs was also determined and the results are presented in Table 2. For the ease of readers and for better comparison, the theoretical compatibility profiles (obtained by Ra calculation) and the practical formulation results are discussed together, individually for each drug with respect to four amphiphilic triblock copolymers. Additionally, the solubility of drugs in formulations is presented in g/L to better compare with the solubility of pristine drugs (determined in-house), however for maximum solubility achieved for each drug, the corresponding loading capacities and loading efficiencies are also presented.

3.3.1. Axitinib (AXT): AXT is tyrosine kinase inhibitor (TKI), use to treat a variety of cancers such as renal cell carcinoma [45]. It also has anti-angiogenic effect [46]. The aqueous solubility of AXT was determined in-house to be 0.005 g/L (Table 2). The compatibility estimation by Ra showed that all the 4 hydrophobic blocks and, surprisingly, the hydrophilic block has similar compatibility (Figure 4a). To the best of our knowledge, no POx/POzi based AXT formulations are reported so far. At the AXT feed of 2 g/L, all the four triblock copolymer yielded in similar apparent AXT solubility, i.e. ≈ 0.2 g/L (LC ≈ 2 wt.% and LE ≈ 10%). With the increasing AXT feed, the differences in solubilizing capacity for triblock became apparent, especially between A-pBuOx-A and A-pPentOx-A. Like for many other drugs, A-pBuOx-A was found to be the best solubilizer and the maximum achievable solubility was around 1 g/L at 4 g/L AXT feed (LC ≈ 7 wt.% and LE ≈ 25%) while its higher homologue A-pPentOx-A was found to be the least efficient in solubilizing AXT (≈ 0.25 g/L) ((Figure 4b). Shi et al. recently reported polyethylene

glycol-polycaprolactone (PEG-PCL) micelles which were capable to solubilize only 0.01 g/L of AXT [47], two orders of magnitude lower than the solubility achieved here. In the selected list of four polymers, A-pPentOx-A, which is comparatively least efficient AXT solubilizer, performed better than a previously reported PEG-PCL system. No marked differences in the solubilizing capacity of A-pPrOzi-A and A-pBuOzi-A were observed. Increasing the AXT feed did not improve the aqueous solubility. From the AXT formulation results, we can conclude that the compatibility estimation was not helpful in optimizing this formulation and stronger structure-solubilization difference was observed in case of POx than POzi based formulations.

3.3.2. Brefeldine (BRF): BRF is lactone antiviral drug, produced by fungus, *Penicillium brefeldianum*. It is capable to inhibit the protein transport across endoplasmic reticulum and Golgi complex [48]. According to Ra calculation, the structural isomers i.e. A-pBuOx-A/A-pPrOzi-A and A-pPentOx-A/A-BuOzi-A exhibited similar compatibility for BRF, while the later pair are supposedly better solubilizer than former (Figure 4a). As expected, pMeOx being hydrophilic showed the least compatibility. In this case, the formulation results were in accordance with the compatibility profile. The structural isomer pair, A-pPentOx-A/A-BuOzi-A were found to be better and capable to solubilize ≈ 0.40/0.33 g/L BRF (LC ≈ 4/3 wt.% and LE ≈ 20/8%), respectively (Figure 4c). The in-house BRF aqueous solubility was found to be 0.15 g/L (Table 2). For the treatment of metastatic breast cancer, Yu et al. reported the nanoparticles based co-formulation of Brefeldine and celecoxib, where solubility of BRF was found to be ≈ 0.29 g/L [49]. Unlike other, ultra-high drug loaded POx/POzi formulations [50, 17], we can say that for the BRF, POx/POzi based amphiphiles are hardly solubilizers, but still performed better than previously published systems.

3.3.3. Carbamazepine (CAR): CAR is an anticonvulsant drug, primarily used for the treatment of neuropathic pain and epilepsy [51]. Based on the calculated Ra, CAR compatibility with the four different hydrophobic blocks was in the following order i.e. pBuOzi > pPrOzi ≈ pPentOx > pBuOx (Figure 4a). The experimentally determined solubility of CAR was found to be 0.005 g/L (Table 2). At 2 g/L CAR feed, no significant difference in solubility (≈ 0.7 g/L) (LC ≈ 6.5 wt.% and LE ≈ 35%) was observed for all four triblock copolymers (Figure 4d). However with the further increase in CAR feed, slight improvement in solubilizing capacity of A-pPrOzi-A (≈ 1.5 g/L at 6 g/L CAR feed) (LC ≈ 13 wt.% and LE ≈ 25%) was observed, the rest of the picture did not change significantly. The study by Kadam et al. showed the maximum solubilizing capacity

of Pluronics micelles for CAR to be 1.18 g/L [52]. It is apparent that no correlation was observed between compatibility estimation and formulation results.

3.3.4. Dasatinib (DSA): Like AXT, DSA is also a TKI, used for the treatment of variety of cancers such as leukemia [53]. The Ra calculation revealed that the hydrophilic block pMeOx has supposedly the highest compatibility with DSA while for the hydrophobic blocks, the compatibility was in the following order, pBuOx > pPentOx ≈ pPrOzi > pBuOzi (Figure 4a). Experimentally, the best solubilizer was found to be A-pBuOzi-A (solubility of DSA ≈ 2.8 g/L at 4 g/L DSA feed) (LC ≈ 22 wt.% and LE ≈ 70%), diametrially opposite to the prediction. The aqueous solubility of DSA was found to be 0.003 g/L (Table 2), meaning a 930- fold increase of the apparent solubility could be achieved. For A-pBuOx-A, increase in DSA feed did not improve the solubility (remained ≈ 2 g/L at all DSA feeds), on the contrary, a weak trend was observed with respect to decrease in solubility of DSA for A-pPentOx-A and A-pBuOzi-A with the increasing DSA feed (Figure 4e). The A-pPrOzi-A was found to be the least efficient solubilizer for DSA (solubility ≈ 0.2 g/L at 4 g/L DSA feed) (LC ≈ 2 wt.% and LE ≈ 5%). According to Li et al., PEG-PCL micelles were capable to solubilize only 0.19 g/L of DSA [54]. A strong polymer-drug specificity is apparent for A-pBuOzi-A and A-pPrOzi-A, although both differ from each other by just one methylene unit in the side chain of the hydrophobic block. Again, the obtained formulation results were not in line with compatibility trend expected from Ra calculation.

3.3.5. Erlotinib (ERL): ERL is epidermal growth factor receptor (EGFR) inhibitor used for the treatment of variety of cancers like non-small cell lung carcinoma or pancreatic cancer [55]. The Ra calculation suggests a compatibility in the following order: pBuOzi > pPrOzi ≈ pPentOx > pBuOx (Figure 4a). The experimental formulation results showed that A-pPentOx-A and A-pPrOzi-A formulation completely precipitated and ERL amounts were below the limit of detection in HPLC. For A-pBuOx and A-pBuOzi-A, the solubilizing capacity was also very low. The maximum achievable soluble ERL was found to be 0.2 g/L by A-pBuOzi-A triblock copolymer at 4 g/L ERL feed (LC ≈ 2 wt.% and LE ≈ 5%) (Figure 4f) while the in-house ERL aqueous solubility was found to be 0.007 g/L (Table 2). Overall, the Ra, successfully identified the (comparatively) best solubilizer (i.e. A-pBuOzi-A) but the overall picture was not consistent with the compatibility estimation. The presently employed POx/POzi polymers and thin film hydration are clearly not well suited for ERL solubilisation.

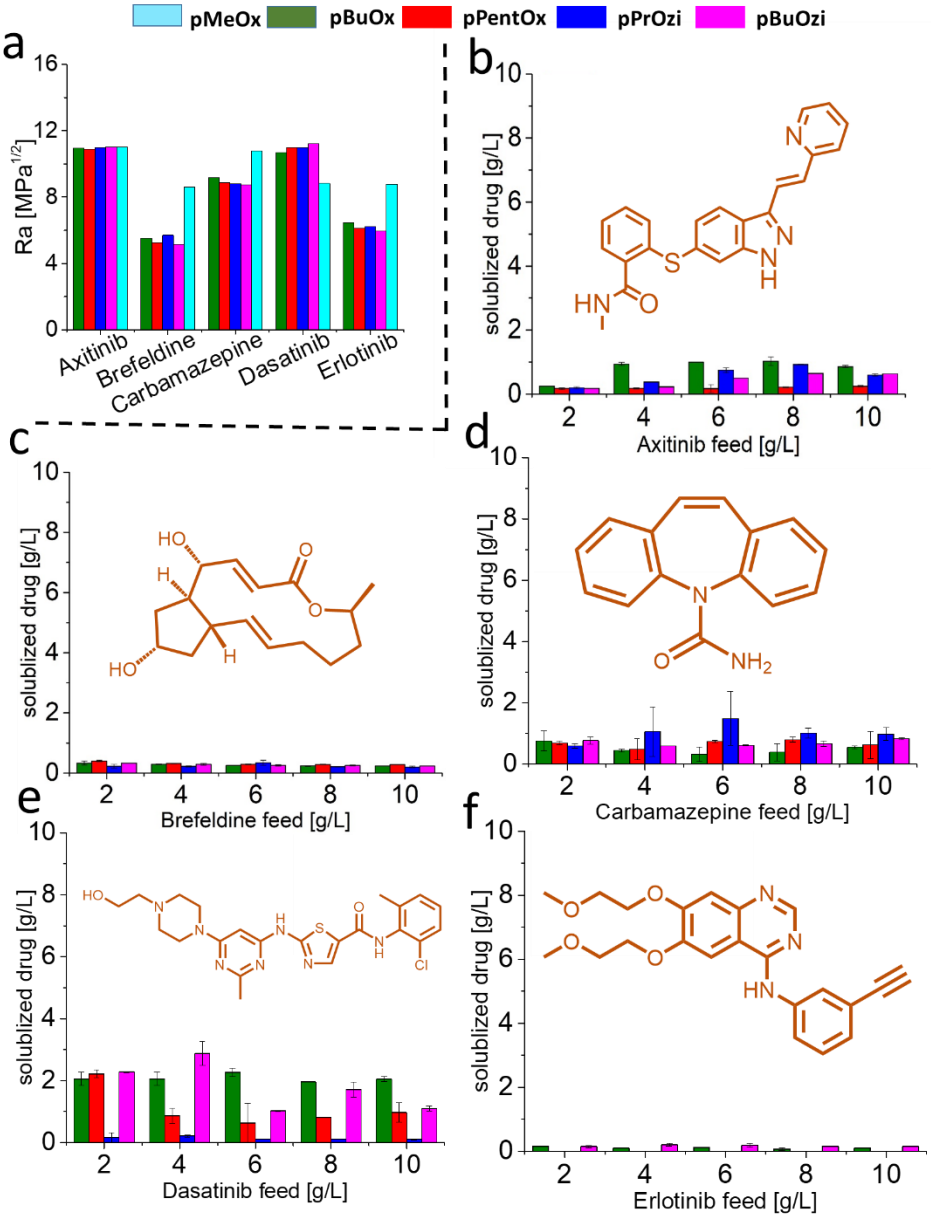

Figure 4: a) The predicted compatibility estimated by YMB method with calculating distance between polymer and drug in 3D-Hansen space (Ra) by equation no. 8. The lower Ra value represents the higher compatibility qualitatively. The maximum achieved, experimental aqueous concentrations of b) axitinib c) brefeldine d) carbamazepine e) dasatinib and f) erlotinib, directly after formulation development. The triblock copolymer concentration was kept constant at 10 g/L with the increasing feed of drug from 2 to 10 g/L. The triblock copolymers are represented according to their hydrophobic blocks only. All the formulation were prepared in triplicate and the results are presented as means ± standard deviation.

3.3.6. Sunitinib (SUN): The SUN is also a multi-targeted TKI used for treatment of cancers like renal cell carcinoma [56]. The Ra calculation showed the following compatibility estimation

with the increasing order, i.e. pBuOx > pPrOzi > pPentOx > pBuOzi (Figure 5a). Like ERL, the formulation results showed that none of the triblock copolymer were capable to significantly solubilize SUN (Figure 5b). Maximum apparent solubility was observed for A-pBuOx-A triblock copolymer (≈0.6 g/L at 6 g/L SUN feed) (LC ≈ 5.5 wt.% and LE ≈ 10%). The aqueous solubility of SUN was determined in-house to be 0.023 g/L (Table 2). Streets et al. reported methoxy-PEG-PCL nanoparticles, which were capable to solubilize 0.32 g/L of SUN [57]. The A-pPrOzi-A triblock was found to be a non-solubilizer for SUN. Overall, the Ra, successfully identified the (comparatively) better solubilizer, but the rest of the trend was not consistent with the compatibility estimation.

3.3.7. Clofazimine CFZ: Along with rifampicin and dapsone, the CFZ is used for the treatment of leprosy [58]. CFZ has dark brown colour. According to Ra calculation, both POzi based hydrophobic blocks showed higher and equal compatibility for CFZ (Figure 5a), when compared to POx based polymers. The order of compatibility was found to be, i.e. pPrOzi ≈ pBuOzi > pPentOx > pBuOx. The maximum achievable formulation solubility of CFZ was 0.2 g/L by A-pBuOzi-A, A-pPentOx-A and A-pBuOx-A at 4, 4 and 6 g/L CFZ feed, respectively (Figure 5c). The in-house aqueous solubility determination was not possible, because CFZ was found completely insoluble in water (Table 2). The A-pPrOzi-A triblock was found to be the worst solubilizer. Once again, the compatibility results are not consistent with the formulation profile.

3.3.8. Crizotinib (CRI): The CRI is a protein kinase inhibitor, used for the treatment of variety of cancers like non-small cell lung carcinoma [59]. The order of compatibility was found to be i.e. pBuOzi > pPrOzi ≈ pPentOx > pBuOx (Figure 5a). The formulation results showed A-pBuOx-A to be the best solubilizer for CRI (≈ 1.15 g/L at 2 g/L feed) (LC ≈ 10 wt.% and LE ≈ 57%) (Figure 5d), which according to Ra calculation should be the least efficient in solubilizing CRI. The in-house CRI aqueous solubility was found to be 0.08 g/L (Table 2). No increase in solubility was observed with the further increase in CRI feed. At CRI feed of 4 to 10 g/L, A-pPentOx-A and A-pBuOzi-A, being structural isomers, exhibited similar solubilizing capacity i.e. ≈ 0.6 to 0.8 g/L. As for CFZ, A-pPrOzi-A also displayed least efficiency for solubilizing CRI. However, a strong polymer drug specificity could be observed in the case of A-pBuOx-A (best solubilizer) and A-pPrOzi-A (worst solubilizer) being structural isomers of each other. No correlation was observed between compatibility estimation and formulation results.

3.3.9. Ezetimibe (EZE): In combination with statins, EZE is administered to treat lipid abnormalities [60]. Both of the structural isomers, A-pPentOx-A and A-pBuOzi-A has a suggested higher and similar compatibility for EZE as compared to their lower homologue pair (Figure 5a). However, the formulation results presented a slightly different picture, where all the four triblock copolymer showed somewhat similar solubilizing capacity for EZE (≈ 1.4 - 1.6 g/L at 2 g/L EZE feed) (LC ≈ 12-14 wt.% and LE ≈ 70-80%) (Figure 5e). The EZE aqueous solubility was determined in-house to be 0.01 g/L (Table 2). With further increase in EZE feed, solubility was decreased and remained in the range of 0.4 – 0.7 g/L for all the tested ratios except for A-pPrOzi-A, where apparent solubility significantly dropped to 0.02 g/L. No clear correlation between compatibility estimation and formulation results was observed.

3.3.10. Vorinostat (VOR): VOR is histone deacetylase inhibitor (HDI) and used for the treatment of skin related manifestations like cutaneous T-cell lymphoma [61]. Like DAS, VOR also exhibited higher compatibility for hydrophilic pMeOx as compared to hydrophobic blocks. The increase in compatibility for the hydrophobic blocks was observed in following order, i.e. pBuOx > pPentOx > pPrOzi > pBuOzi (Figure 5a). The maximum achievable aqueous solubility of VOR was found to be 2 g/L (LC ≈ 16 wt.% and LE ≈ 100%) with A-pPentOx-A triblock copolymer while its structural isomer, A-pBuOzi-A (appearing as least efficient solubilizer by compatibility estimation) could solubilize 1.8 g/L (at 2 g/L VOR feed) (LC ≈ 15 wt.% and LE ≈ 90%) while the second structural isomer pair i.e. A-pBuOx-A/A-pPrOzi-A exhibited similar solubilizing capacity (i.e. ≈ 1.7/1.7 g/L, respectively) (LC ≈ 14 wt.% and LE ≈ 85%) (Figure 5f). The in-house VOR aqueous solubility was found to be 0.07 g/L (Table 2). Rompicharla et al. also showed that PEG-PLGA micelles are capable to solubilize around 1.8 g/L of VOR [62], similar, albeit lower than achieved here. Further increase in VOR feed, did not improve the solubility, in fact it fell below 2 g/L. For A-pBuOx-A, the solubility of VOR remained around 2g/L while a slight decrease was observed in the case of A-pPentOx-A (≈ 1.1 g/L) and A-pBuOzi-A (≈ 1.0 g/L) at higher VOR feed. For A-pPrOzi-A, a dramatic decrease was observed from 2 to 6 g/L VOR feed (solubility dropped from 1.7 to 0.4 g/L). Further increase in VOR feed led to complete precipitation of formulation and no further quantification was possible.

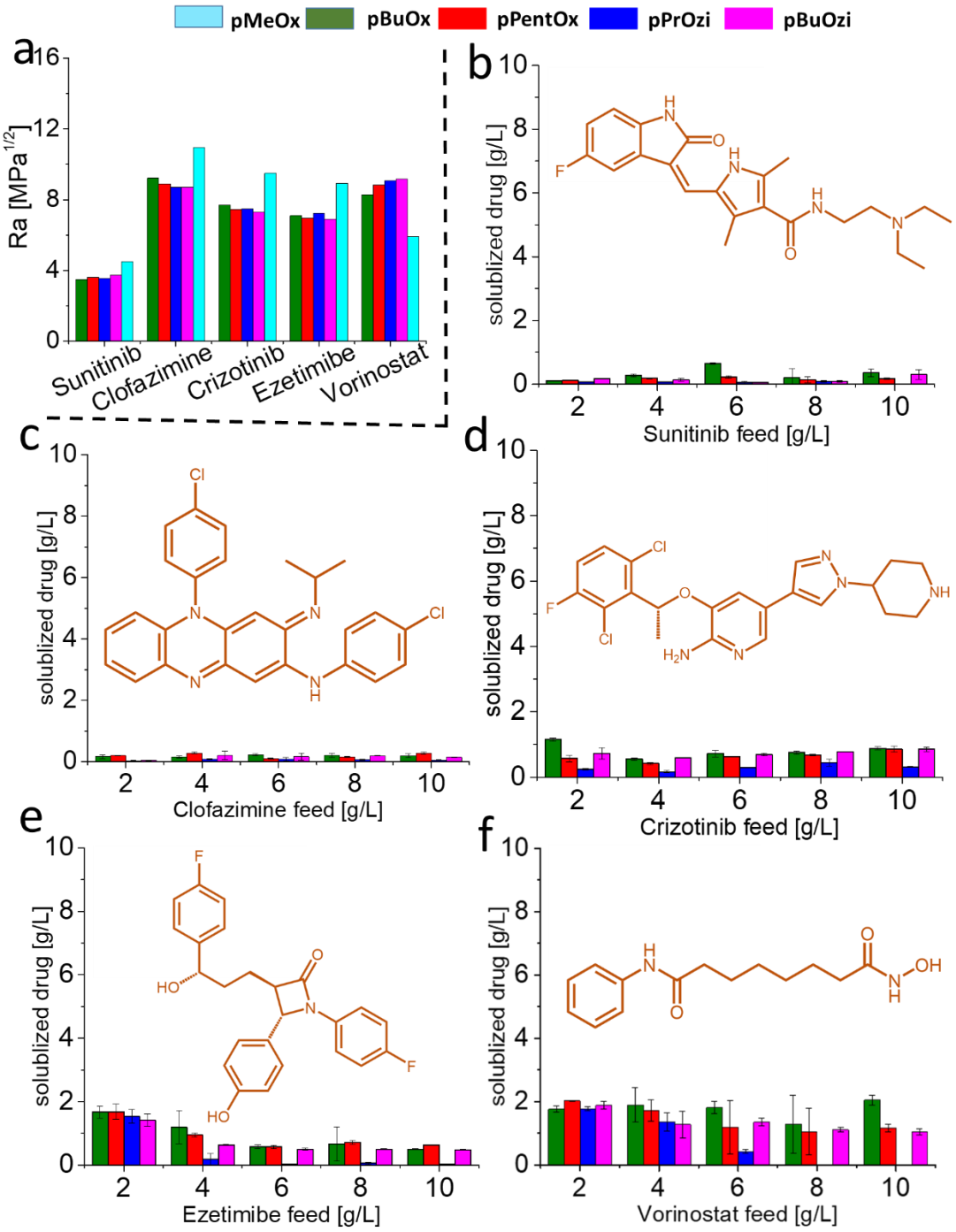

Figure 5: a) The predicted compatibility estimated by YMB method with calculating distance between polymer and drug in 3D-Hansen space (Ra) by equation no. 8. The lower Ra value represents the higher compatibility qualitatively. The maximum achieved soluble concentrations of b) sunitinib c) clofazimine d) crizotinib e) ezetimibe and f) vorinostat, directly after formulation development. The triblock copolymer concentration was kept constant at 10 g/L with the increasing feed of drug from 2 to 10 g/L. The triblock copolymers are represented according to their hydrophobic blocks only. All the formulation were prepared in triplicate and the results are presented as means ± standard deviation.

3.3.11. Bexarotene (BEX): Like VOR, BEX being a third generation retinoid is also an anticancer agent used for the treatment of cutaneous T-cell lymphoma [63]. According to Ra calculation, the compatibility should be in the order pBuOzi > pPentOx > pPrOzi > pBuOx (Figure 6a). In contrast, experiment showed that pBuOx based triblock showed the highest solubilizing capacity for BEX (≈ 1.1 g/L at 4 g/L BEX feed) (LC ≈ 10 wt.% and LE ≈ 55%) (Figure 6b). The aqueous solubility of BEX was found to be 0.004 g/L (Table 2). In all other triblock copolymers, solubility of BEX fell below 0.5 g/L. No clear trend between the four individual polymers was observed in formulation experiments when compared to compatibility estimation.

3.3.12. Cabazitaxel (CBZ): CBZ, being 3rd generation, semi-synthetic derivative of natural taxoids, is a microtubule inhibitor and is used for the treatment of various cancers like prostate cancer [64]. As mentioned previously, the compatibility estimation of CBZ was not possible because of limitation in HSPiP software, incapable to process large size SMILES. The formulation results revealed that A-pBuOx-A was capable to solubilize all provided drug, i.e. up to 10 g/L (Figure 6c) (LC ≈ 50 wt.% and LE ≈ 100%). The crash point of this formulation was not determined by further increasing the CBZ feed. The aqueous solubility of CBZ was found to be 0.007 g/L (Table 2). For A-pPentOx-A and A-pBuOzi-A, the CBZ solubility also kept on increasing with the increasing feed (until 8 g/L feed) and the achievable soluble CBZ was ≈ 6.8 g/L, while at 10 g/L CBZ feed, A-pPentOx-A gave 8.5 g/L and for A-pBuOzi-A, the solubility dropped to 5.3 g/L. Like for many other tested drugs, A-pPrOzi-A displayed comparatively, poor performance to solubilize the CBZ and the maximum soluble CBZ obtained was 1.5 g/L and also significant decrease in solubility was observed with the increasing CBZ feed. Thus, a strong polymer drug specificity was observed for the structural isomer pair i.e. A-pBuOx-A/A-pPrOzi-A, where the former appeared to be best solubilizer while the latter showed poor performance, very similar to the situation with paclitaxel, the first generation taxoid.

3.3.13. Bortezomib (BTZ): BTZ is a proteasome inhibitor, used for treatment of various cancers like multiple myeloma and mantle cell lymphoma [65]. Like DSA and VOR, upon Ra calculation, the hydrophilic pMeOx supposedly exhibits a higher compatibility for BTZ in comparison to hydrophobic blocks. Amongst those, , the estimated compatibility was in the order of pBuOx > pPentOx > pBuOzi ≈ pPrOzi (Figure 6a). Previously, Schulz et al. reported the A-pBuOx-A based formulations are capable to solubilize around 3.1 g/L BTZ [50]. Here, we obtained similar results for the A-pBuOx-A triblock (i.e. 3.1 g/L soluble BTZ at 6 g/L feed). At

8 g/L BTZ feed, A-pBuOx-A gave BTZ solubility of around 3.9 g/L. However, the A-PentOx-A, its higher homologue, was found to be the best solubilizer, giving a BTZ solubility of 4.7 g/L (at 10 g/L feed) (LC ≈ 32 wt.% and LE ≈ 47%) (Figure 6d). The BTZ solubility in plain water was found to be relatively high with 0.75 g/L (Table 2). A-pBuOzi-A showed a similar performance like A-pBuOx-A and gave a BTZ solubility of 3.8 g/L (at 10 g/L feed). Compared to other drugs, A-pPrOzi-A performed better in solubilizing BTZ, but the achieved solubility (≈ 2.7 g/L) was less than other polymers in the series. The suggested compatibility profile was not corroborated by formulation experiments, instead of A-pBuOx-A, the A-pPentOx-A was found to be best solubilizer and A-pPrOzi-A and A-pBuOzi-A showed differences in solubilizing BTZ, which became more apparent at higher BTZ feed.

3.3.14. Cannabidiol (CBD): CBD is phyto-cannabinoid used for the treatment of epileptic seizures and in neuropathic pains [66]. CBD solubility was below our limit of detection, and therefore practically insoluble in plain water (Table 2). According to Ra calculation, the order of compatibility is pBuOzi > pPentOx > pPrOzi > pBuOx (Figure 6a). In general, the POzi based triblocks were found to be better solubilizer for CBD. The formulation results also revealed A-pBuOzi-A to be the best solubilizer for CBD, i.e. 3.3 g/L CBD (at 4 g/L feed), (LC ≈ 25 wt.% and LE ≈ 82%). However, with the further increase in CBD feed, a dramatic decrease in solubility was observed (i.e 0.1 g/L soluble CBD at 6 g/L feed) (Figure 6e). While, the Berrocoso et al. reported the CBD loaded PEG-PLGA nanoparticles with the LC of 12 wt.% [67]. Instead of A-pPentOx-A, as estimated by Ra calculation, the second best solubilizer was found to be A-pPrOzi-A (3 g/L soluble CBD at 4 g/L feed). The maximum achievable soluble CBD with A-pBuOx-A triblock was around 2 g/L at 8 g/L CBD feed. The A-pPentOx-A was found to be the least efficient solubilizer and gave only 1 g/L soluble CBD at 2 g/L feed. At 10 g/L CBD feed, all the four triblock formulations precipitated and, the soluble CBD level fell below 0.2 g/L. The results obtained by compatibility estimation are partially consistent with the formulation results.

3.3.15. Celecoxib (CXB): CXB is a cyclooxygenase (COX2) inhibitor and a nonsteroidal anti-inflammatory drug [68]. According to Ra calculation, pPrOzi hydrophobic block was supposed to be most compatible, pPentOx/pBuOzi showed similar and intermediate while pBuOx should exhibit the least compatibility for CXB (Figure 6a). On the contrary, the A-pBuOx-A gave the maximum achievable aqueous solubility for CXB i.e. 4.8 g/L (at 6 g/L CXB feed) (LC ≈

32 wt.% and LE ≈ 80%) (Figure 6f). The solubility of CXB was experimentally found to be 0.004 g/L (Table 2). At 2 and 4 g/L CXB feed, all the triblock copolymers gave the similar solubility, except for A-pPentOx-A, which showed a slight decrease (≈ 3.8 g/L) in solubilizing CXB at 4 g/L feed. Above 6 g/L feed, all the four triblock copolymer showed different solubilizing capacity and a general decrease in solubility for CXB was observed. Compared to other triblock copolymers, a dramatic decrease was observed in the case of A-pPrOzi-A triblock copolymer (solubility of CXB dropped to 0.1 g/L). The compatibility results for CXB are not consistent with the formulation experiments.

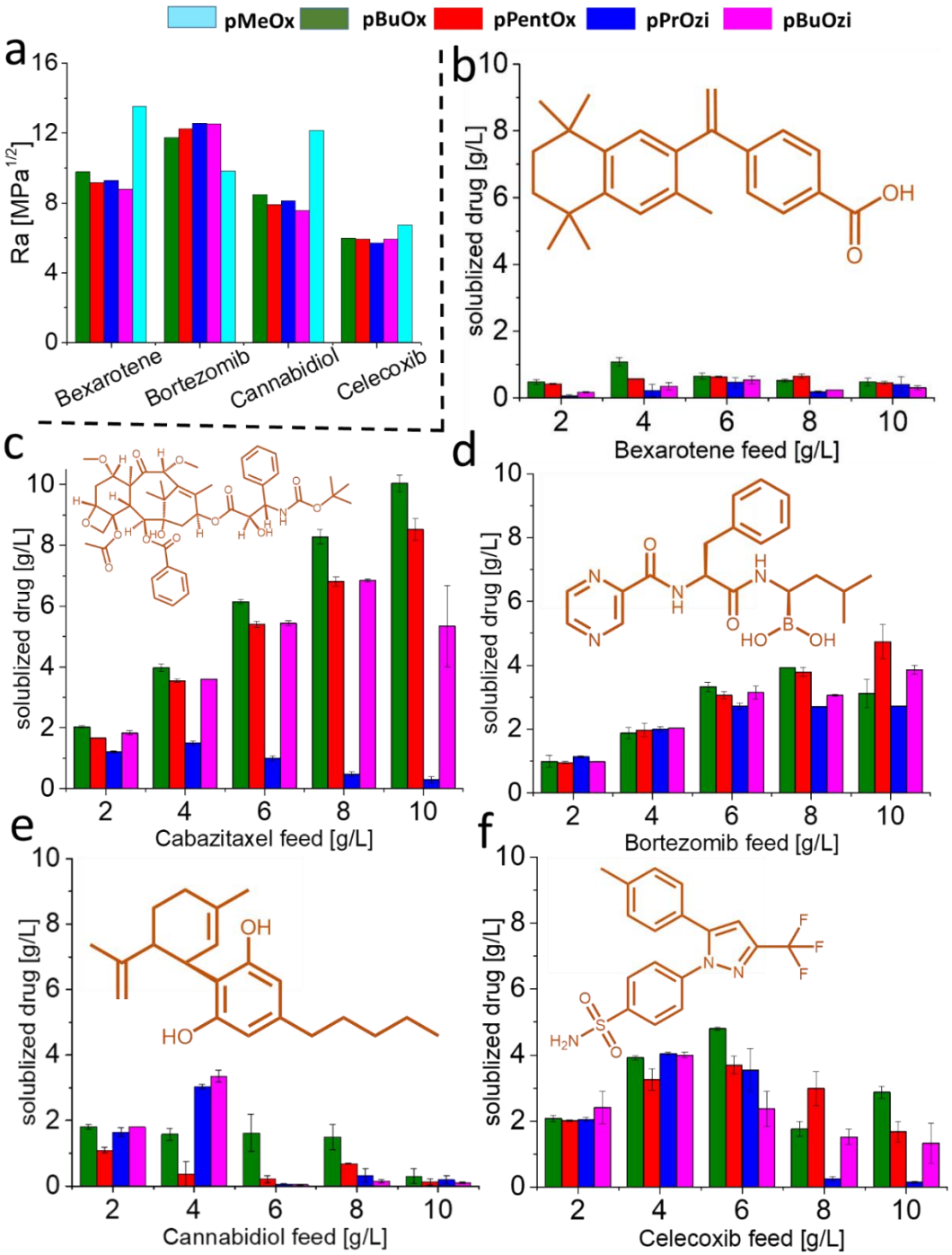

Figure 6: a) The predicted compatibility estimated by YMB method with calculating distance between polymer and drug in 3D-Hansen space (Ra) by equation no. 8. The lower Ra value represents the higher compatibility qualitatively. The maximum achieved soluble concentrations of b) bexarotene c) cabazitaxel d) bortezomib e) cannabidiol and f) celecoxib, directly after formulation development. The triblock copolymer concentration was kept constant at 10 g/L with the increasing feed of drug from 2 to 10 g/L. The triblock copolymers are represented according to their hydrophobic blocks only. All the formulation were prepared in triplicate and the results are presented as means ± standard deviation.

3.3.16. Clotrimazole (CTZ): CTZ is an imidazole derivative with antifungal activity. It is used for the treatment of various infections like pityriasis and vaginal yeast infection [69]. The estimation with Ra displayed the following decreasing order of compatibility, i.e. pBuOzi > pPrOzi ≈ pPentOx > pBuOx (Figure 7a). Our experiments showed that the CTZ is essentially insoluble in plain water (Table 2). The formulation experiments revealed A-pPentOx-A to be the best solubilizer for CTZ. At the highest tested feed ratio of 10 g/L, the formulation was completely clear and all of the added drug was solubilized (LC ≈ 50 wt.% and LE ≈ 100%) (Figure 7b). In contrast, the A-pPrOzi-A was found to be the least efficient in solubilizing CTZ and at all tested CTZ feed ratios, solubility fell below 0.2 g/L. Catenacci et al. recently reported the CTZ loaded hyaluronic acid capable to solubilize 0.018 g/L CTZ [70], 3.5 orders of magnitude lower compared to the apparent solubility achieved here. Again, the CTZ formulation results obtained are completely opposite to the compatibility estimation, where a similar level of compatibility for A-pPrOzi-A/A-pPentOx-A was observed. The A-pBuOx-A and A-pBuOzi-A showed intermediate solubilizing capacity for CTZ i.e. 2.6 and 4.4 g/L, respectively and with the increasing drug feed minor increase in solubility was observed.

3.3.17. Genistein (GEN): The GEN is a naturally occurring isoflavone. It is TKI and topoisomerase II inhibitor. It also exhibits anti-tumor, anthelmintic and anti-inflammatory properties [71]. Like DSA, VOR and BTZ, upon Ra calculation, the hydrophilic pMeOx was supposed to show higher compatibility for GEN in comparison to hydrophobic blocks while for hydrophobic blocks, the estimated compatibility was in the order of pBuOx > pPentOx > pBuOzi > pPrOzi (Figure 7a). The experimentally determined GEN solubility in water was found to be 0.007 g/L (Table 2). The formulation experiments revealed, at 6 g/L feed, both A-pBuOx-A and A-pBuOzi-A were capable to solubilize around 4.2 (LC ≈ 29 wt.% and LE ≈ 70%) and 4.3 g/L (LC ≈ 30 wt.% and LE ≈ 71%) of GEN, respectively (Figure 7c). A direct relationship was observed between GEN feed and solubilized GEN up to 6 g/L feed for all the triblock copolymers, with the exception of A-pPentOx-A (for which a slight decrease in GEN solubility was observed), while with the further GEN increase, the solubilizing capacity for all the triblock copolymer dropped to around 1.3 g/L. At 2, 8 and 10 g/L GEN feed, no significant differences in solubility was observed for all the four triblock copolymers. However, at 4 and 6 g/L GEN feed, higher level of polymer drug specificity can be observed. The compatibility results obtained by Ra calculation are partially consistent with the formulation results. As

predicted, the A-pBuOx-A exhibited higher solubilizing capacity for GEN, but at the same time A-pBuOzi-A, which was predicted as third best solubilizer also showed similar solubilizing capacity like A-pBuOx-A at 6 g/L feed. While the A-pPentOx-A being predicted as second best solubilizer, appeared last in the row with the least formulation efficiency.

3.3.18. Lapatinib (LAP): LAP is another TKI, used for the treatment of metastatic or advanced breast cancer [72]. The LAP aqueous solubility was determined to be 0.016 g/L (Table 2). According to Ra calculations, A-pBuOx-A is supposed to be the least compatible, while all other three triblock copolymer showed somewhat similar compatibility (Figure 7a). Experimentally, the formulation results revealed significant differences in solubilizing capacities of all triblock copolymer at varying LAP feed. The A-pPentOx-A gave maximum solubility of 5.5 g/L at 6 g/L feed (LC ≈ 35 wt.% and LE ≈ 91%) (Figure 7d). The further increase in the LAP feed did not improve the solubility, and it remain between 5 and 6 g/L. The similar behaviour was observed for A-pBuOx-A and A-pBuOzi-A, however the maximum achievable soluble LAP was 3.4 and 2.8 g/L, respectively. The A-pPrOzi-A was found to be least efficient in solubilizing LAP (≈ 1.5 g/L). The obtained formulation results are not in correspondence with the estimated compatibility profile.

3.3.19. Sorafenib (SRF): The kinase inhibitor SRF is used for the treatment of renal and hepatocellular carcinoma [73]. It is practically insoluble in plain water (Table 2). According to Ra, the hydrophilic pMeOx should exhibit a higher compatibility with SRF than hydrophobic blocks. For the hydrophobic blocks, the order of compatibility was found to be pBuOx > pPrOzi > pPentOx > pBuOzi (Figure 7a). On the contrary, the formulation results showed that the best solubilizer for SRF is A-pPrOzi-A giving a solubility of 5.6 g/L at 8 g/L SRF feed (LC ≈ 36 wt.% and LE ≈ 70%) (Figure 7e). A-pBuOzi-A, the higher homologue of A-pPrOzi-A appeared to be least efficient solubilizer for SRF and solubility fell below 0.7 g/L at all the employed feed of SRF. The A-pPentOx-A appeared to be the second best solubilizer (4.1 g/L) while A-pBuOx-A, being best solubilizer for paclitaxel and many other drug herein, could solubilize SRF only to 1.6 g/L Overall, no correlation was observed between the estimated compatibility and formulation results.

3.3.20. Vismodegib (VSM): The VSM is a hedgehog signalling inhibitor used for the treatment of basal cell carcinoma [74]. Like DSA, VOR, GEN and BTZ, upon Ra calculation, the hydrophilic pMeOx showed higher compatibility for VSM in comparison to hydrophobic blocks while for

hydrophobic blocks, the estimated compatibility was in the order of pBuOx ≈ pPrOzi > pPentOx > pBuOzi (Figure 7a). Experimentally, VSM was essentially insoluble in plain water (Table 2) but with the A-pPentOx-A triblock copolymer, we were capable to solubilize around 8.8 g/L (at 10 g/L VSM feed) (LC ≈ 47 wt.% and LE ≈ 88%) (Figure 7f). The A-pBuOx-A and A-pBuOzi-A also exhibited very high solubilizing capacity of 7.2 and 7.5 g/L, respectively, albeit less than A-pPentOx-A. Utilizing the A-pBuOx-A triblock, very recently, Hwang et al. also reported the VSM formulation capable to solubilize around 7.5 g/L VSM (at 8 g/L feed) [43], indicating that the A-pBuOx-A/VSM formulation is quite reproducible. The A-pPrOzi-A exhibited somewhat lower VSM solubility of around 4.8 g/L. For the VSM formulations, we can conclude that the compatibility estimation is not consistent with the formulation results.

3.3.21. Mitotane (MT): MT is a drug of choice for adrenocortical carcinoma [75]. According to Ra calculation, the extent of compatibility between MT and triblocks was supposed to be in following order i.e. pBuOzi > pPrOzi ≈ pPentOx > pBuOx (Figure 7a). The measured aqueous MT solubility was found to be 0.0004 g/L (Table 2). The formulation results revealed A-pPentOx-A to be the best solubilizer, yielding an aqueous MT solubility of around 7.2 g/L at 10 g/L MT feed (LC ≈ 42 wt.% and LE ≈ 72%) (Figure 7g). The second and third best solubilizer was found to A-pBuOx-A and A-pBuOzi-A with MT solubility of around 5.7 and 4.3 g/L (at 10 g/L MT feed) (LC ≈ 36 and 30 wt.%). The A-pPrOzi-A displayed relatively low solubility for MT i.e. 1.4 g/L (at 6 g/L feed) [29]. Apparently, there is no correlation between compatibility estimation and formulation results.

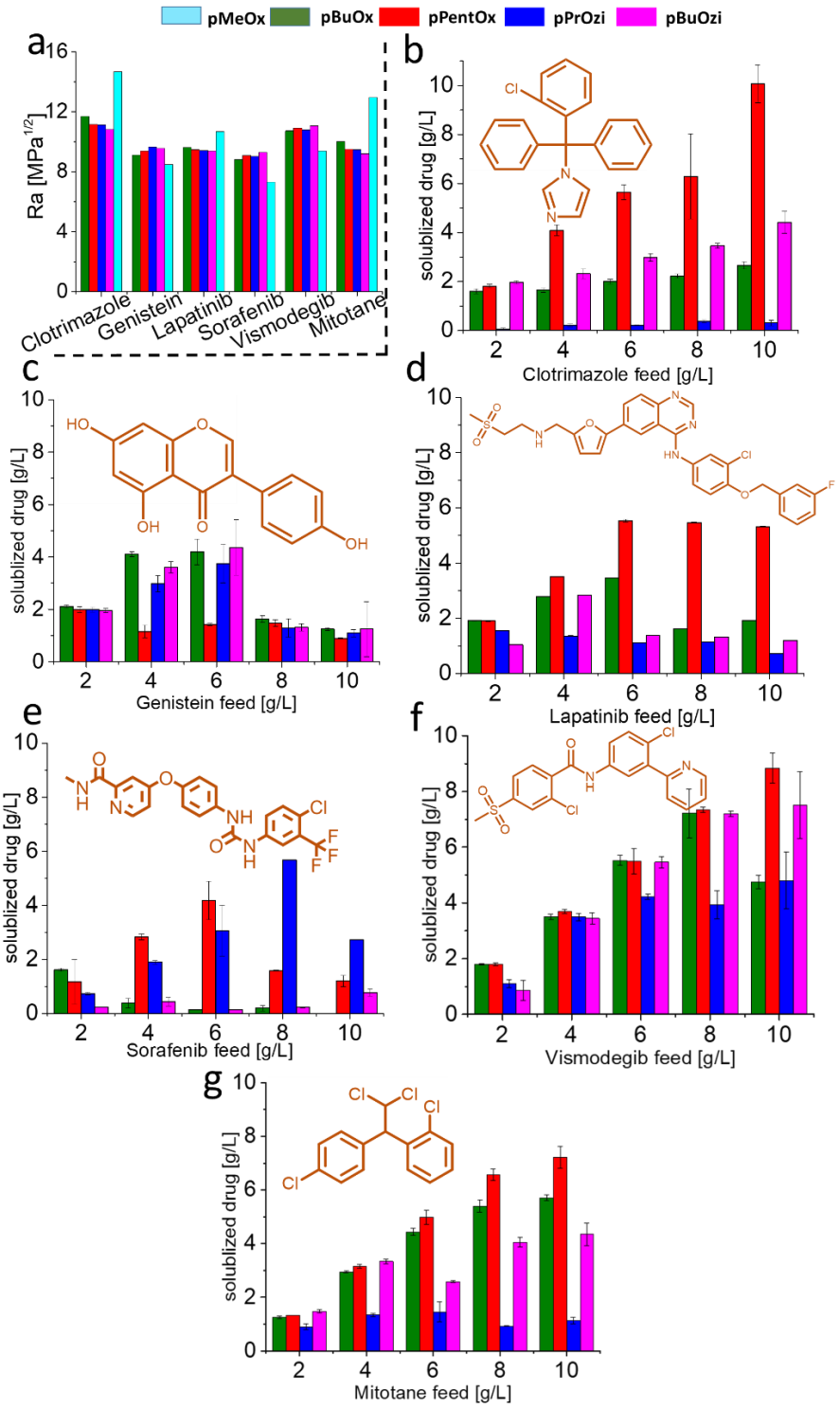

Figure 7: a) The predicted compatibility estimated by YMB method with calculating distance between polymer and drug in 3D-Hansen space (Ra) by equation no. 8. The lower Ra value represents the higher compatibility qualitatively. The maximum achieved soluble concentrations of b) clotrimazole c) genistein d) lapatinib e) sorafenib f) vismodegib and g) mitotane, directly after formulation development. The triblock copolymer concentration was kept constant at 10 g/L with the increasing feed of drug from 2 to 10 g/L. The triblock copolymers are represented according to their hydrophobic blocks only. All the formulation were prepared in triplicate and the results are presented as means ± standard deviation.

Table 2: The values of in-house determined aqueous solubility of drugs library, solubility enhancement after formulation development, respective loading capacity and best performing polymer.

Entry	Drug	In-house solubility [g/L]	Formulation solubility [g/L]	Loading capacity [wt.%]	Best Polymer
1	Axitinib	0.005	1.00	7	pBuOx
2	Brefeldine	0.153	0.40	4	pPentOx
3	Carbamazepine	0.005	1.50	13	pPrOzi
4	Dasatanib	0.003	2.80	22	pBuOzi
5	Erlotinib	0.007	0.20	2	pBuOzi
6	Sunitinib	0.023	0.60	5	pBuOx
7	Clofazimine	Insoluble	0.20	2	pBuOx/pPentOx/ pBuOzi
8	Crizotinib	0.08	1.15	10	pBuOx
9	Ezetimibe	0.01	1.4-1.6	12-14	pBuOx/pPentOx/ pPrOzi/pBuOzi
10	Vorinostat	0.07	2.00	16	pPentOx
11	Bexarotene	0.004	1.10	10	pBuOx
12	Cabazitaxel	0.007	10.0	50	pBuOx
13	Bortezomib	0.75	4.70	32	pPentOx
14	Cannabidiol	Insoluble	3.30	25	pBuOzi
15	Celecoxib	0.004	4.80	32	pBuOx
16	Clotrimazole	Insoluble	10.0	50	pPentOx
17	Genistein	0.007	4.2-4.3	29	pBuOx/pBuOzi
18	Lapatinib	0.016	5.50	35	pPentOx
19	Sorafenib	Insoluble	5.60	36	pPrOzi
20	Vismodegib	Insoluble	8.80	47	pPentOx
21	Mitotane	0.0004	7.20	42	pPentOx

So far, the correlation between HSP based predicted compatibility and experimental formulation results for four polymers *vs* one drug were presented. To analyse the compatibility of 21 drugs for single polymer, the obtained results were replotted to present this trend to the readers (Figure S30). On the left Y-axis Ra values are plotted with the decreasing order of compatibility between each polymer and drugs, while on the right Y-axis the actual solubility of drugs (as a formulation) is plotted. No correlation was observed between Ra based compatibility trend and the formulation results of 21 drugs with individual polymer.

The non-covalent supramolecular affinities (such as hydrogen bonding, hydrophobic interaction, π- π stacking and van der Waals interactions) [76, 77] between polymers and drugs play a very important role in overall organization and colloidal stability of such assemblies. The efficient and stable encapsulation of cargo into the micelles is not only governed by cargo polymer interaction, but certain innate properties of cargo like chemical composition, rigidity, conformation, molecular weight (Table 1) and/or most importantly interfacial structure between cargo and polymer also play a very important role. It is becoming more evident that the ultra-high drug loading reported for the majority of the

tested drugs with POx/POzi based amphiphiles [17, 35, 40, 29, 9, 41] is partly because of hydrophilic pMeOx [78]. The A-pPrOzi-A/curcumin [79] and A-pBuOx-A/paclitaxel [80] have been investigated thoroughly in this regard. Previously, investigating the ultra-high curcumin loaded A-pPrOzi-A formulation with solid state NMR spectroscopy [79], Pöppler et al. demonstrated that polymer carbonyl moieties acting as hydrogen bond acceptor were highly sensitive to presence of curcumin (a proton donor). After a certain curcumin feed, the amide groups of hydrophilic corona also start to involve in solubilizing the cargo, leading to physical crosslinking and finally causing colloidal instability and precipitation of the whole system. In the case of POx/POzi based amphiphiles library, Lübtow et al. observed that the drugs with higher proton donor count yielded the highest drug loading and vice versa, however the library was relatively small consisting of only 5 hydrophobic compounds [34]. Herein, no correlation was observed between high proton donor count in drugs structure and higher drug loading. Out of 21 drugs, bortezomib which has the highest number of proton donor group i.e. 4 (Table 1) has shown the intermediate loading capacity of 32 wt.% (Table 2) while the two other drugs i.e. clotrimazole and mitotane having zero proton donor groups (Table 1) have shown the highest loading capacity of 50 and 42 wt.%, respectively (Table 2). The six drugs i.e. dasatinib, sunitinib, vorinostat, cabazitaxel, genistein and sorafenib with three proton donor groups (Table 1) have shown a varied loading capacity of 22, 5, 16, 50, 30 and 36 wt.%, respectively (Table 2). Additionally, water molecules also have strong influence on the conformation and aggregation morphology of many drug delivery vehicle [81, 82]. The simple mathematical calculations like solubility parameters determination for such kind of complex system is obviously insufficient to get realistic compatibility profile. So the discrepancy between experiment formulation results and the compatibility estimation by aforementioned group contribution methods are likely due, in part, to the absence of such factors in general calculation.

4. Stability Studies of Drug Formulations

To investigate the shelf-life, the freshly prepared formulations were stored at ambient conditions with the initial precipitate (if any). The samples were collected at day 0, 1, 5 and 30 and quantified by HPLC. The drugs which exhibited very poor loading capacity were excluded from this study. Accordingly, the stability studies of six drugs is presented namely cabazitaxel, celecoxib, clotrimazole, cannabidiol, lapatinib and mitotane. Previously, we had

observed A-pBuOx-A/paclitaxel [50, 17] and A-pPrOzi-A/curcumin [40] exhibited an excellent stability for several months. However, in few cases, POx/POzi based formulation were also found to be less stable [35].

In case of cabazitaxel formulations, initially a slight reduction in solubility (≈ 10-15 %) was observed in all the four triblock copolymers from day 0 to day 1 (24 h) (Figure S31). The A-pBuOx-A and A-pBuOzi-A showed relatively stable formulations until day 30 and gradual minor decrease in solubility was observed, i.e. 10 to 7.2 g/L and 5.3 to 3.9 g/L, respectively at 10 g/L cabazitaxel feed. In contrast, in the case of A-pPentOx-A formulation the dramatic decrease in solubility of cabazitaxel was observed i.e. 8.5 to 3.25 g/L in the time span of 30 days.

In the case of celecoxib formulation, all the four triblock copolymer (at all the tested celecoxib ratios) exhibited very good stability and only minor loss in solubility was observed until day 30 (Figure S32). In the case of A-pBuOx-A, A-pPentOx-A and A-pPrOzi-A (at 6 g/L celecoxib feed) the solubility decreased from 4.8 to 4.3, 3.7 to 2.5, 3.5 to 3.2 g/L, respectively from day 0 to 30 while in the case of A-pBuOzi-A formulation (at 4 g/L celecoxib feed), the solubility decreased from 4.0 to 2.7 g/L. In the case of clotrimazole formulations, the A-pBuOx-A triblock copolymer presented as highly stable formulation at all the tested ratios and a minor loss in solubility was observed (< 5%) although the solubility never exceeded ≈ 2 g/L at any of the employed clotrimazole feed (Figure S33). A-pBuOzi-A based formulations followed the similar trend until day 5, however slightly higher loss in solubility was observed at day 30 (≈ 30-40 %). The A-pPrOzi-A displayed very poor solubilizing capacity for clotrimazole so it was not further considered for long term stability study. In the case of A-pPentOx-A triblock copolymer, all the employed clotrimazole was completely solubilized in freshly prepared formulation. However, the formulation tend to agglomerate or precipitate fast and at day 1, a solubility loss of around 50% was observed and until day 30 this loss further increased to 90%.

The cannabidiol formulations followed a somewhat similar pattern like celecoxib formulations, i.e. minor loss in solubility (< 5%) was observed at day 1 at all the tested ratios and until day 30 no significant loss was further observed (Figure S34). However, in freshly prepared formulations, the solubility of cannabidiol never exceeded 1.5 and 3.4 g/L in POx and POzi based triblock copolymers, respectively.

For lapatinib, the A-pPentOx-A triblock also exhibited the similar stability pattern as for clotrimazole i.e. rapid reduction in solubility was observed at day 1 and until day 30, an 80% decrease in lapatinib solubility was observed (Figure S35). In contrast, for A-pBuOx-A, A-pBuOzi-A and A-pPrOzi-A triblock copolymers, a minor loss in solubility (< 10%) was observed until day 30.

In the case of POx/POzi based formulations, it is becoming more evident that the after a certain threshold drug feed, the hydrophilic corona start to interact with the hydrophobic drug and this association may lead to high drug loading and/or eventually the formulation agglomeration and precipitation. In majority cases, the drug was found to be amorphous in these agglomerate/precipitates [33, 40, 78] with the exception of A-pBuOx-A/mitotane formulation [29] where at 6 g/L mitotane feed, the rapid crystallization of drug was observed. The differential scanning calorimetry (DSC) measurement further confirmed the presence of crystalline mitotane. Herein, for mitotane formulations, we can also speculate the similar phenomena, particularly for A-pBuOzi-A triblock based formulations, where a rapid formulation instability can be observed even at lower mitotane feed i.e. 4 g/L (Figure S36). While, the poor instability in the case of the A-pPentOx-A triblock copolymer might hint towards different mechanism, as we have observed this poor stability problem in most of the other drug presented herein.

Compared to the other triblock copolymers used in this study, A-pPentOx-A has been been much less explored for formulation development. Recently, an ultra-high drug loaded A-pPentOx-A/BT-44 formulations (BT-44 solubility ≈ 9 g/L at 10 g/L polymer feed) (BT-44 chemRxiv) was reported. At all the tested ratios, the solubility of BT-44 was decreased by 90% by day 30. This poor stability was further investigated in detail to confirm, if the drug BT-44 is crystallizing like previously reported A-pBuOx-A/mitotane formulation [29] or this decreased in solubility is because of the formulation agglomeration. The DSC measurements confirmed the presence of amorphous BT-44. Additionally, the dynamic light scattering experiments (at 173°, at room temperature) revealed the relatively bigger hydrodynamic diameter (D_h) of 115 nm for plain polymer at 10 g/L concentration. The results obtained by DLS were further corroborated by cryo-TEM analysis where the plain polymer at 10 g/L and BT-44 formulation at 10/2 g/L polymer/BT-44 feed, appeared as worm like structures. In general, based on these recent findings, the poor stability of A-pPentOx-A formulation for the majority of drugs tested

here, can be correlated to the polymer aggregation/agglomeration behaviour. Recently, depending upon the drug feed, Lim et al. observed the transition of freshly prepared A-pBuOx-A/Olaparib spherical micelles (D_h ≈ 10-30 nm) to worm like structures (D_h ≈ 200 nm) in the time span of 72 hours [83]. While, the small angle neutron scattering (SANS) revealed the core shell morphologies in the case of plain A-pBuOx-A polymer [84].

In general, it is now evident that, such morphology transition is usually driven by presence of certain level of hydrophobic environment in the whole system assembling together, which in the case of A-pBuOx-A triblock copolymer is provided by a specific threshold drug concentration while in the case of A-pPentOx-A triblock copolymer, the hydrophobicity of pPentOx block is sufficient to induce this transition which is further substantiated with the drug addition leading to rapid formulation agglomeration. The direct comparison of A-pBuOx-A and A-pPentOx-A micellar formulations utilizing the analytical tools like solid state NMR and SANS can give us much deeper understanding of polymer drug interactions resulting in specialized micellar architecture, however such analysis is beyond the scope of current contribution.

5. Conclusion

A considerable library of structurally diverse 21 hydrophobic drugs was tested with four POx/POzi based triblock copolymer which differ from each other by one methylene unit (shuffling either in the side chain or backbone) rendering them the structural isomers of each other (i.e. pBuOx/pPrOzi and pPentOx/pBuOzi, respectively). The results obtained by compatibility estimation (by group contribution method i.e. HnV and YMB) were not in accordance with the obtained formulation results with only a few exceptions, which can be considered as more coincidental rather than systematic. The practical weakness of this approach is the limited number of functional groups available in the literature and most importantly the impact of secondary factors like thermodynamics, hydrophilic lipophilic balance, drug structure, drug rigidity, interfacial tension, polymer and drug concentration, the solvent and the method for formulation development which are not taken into consideration in such approaches. Thus, the theoretical prediction based on the assumption that majority of the drug is located in the core of polymeric micelles is not comprehensive and should be practised with caution. Therefore, it is extremely essential to build a theoretical method,

capable to bring most of the factor discussed above into consideration, for drug-polymer compatibility evaluation to guide the formulation design of polymeric micelles.

Nevertheless, we have successfully solubilized the majority of the hydrophobic drugs in the library specifically, 11 out of 21 drugs exhibited the loading capacity > 20 wt.% (Table 2), which is typical upper limit for many systems reported in the literature. Similar to previously reported POx based triblock copolymers formulation [29, 41-43, 40], we anticipate that variety of formulations presented here will allow the parenteral administration and will help to alleviate the problem associated with the use of hydrophobic drugs like, poor pharmacokinetics and use of toxic excipients for parenteral administration, overall improving the therapeutic outcomes of treatment.

Associated Content:

Supporting information

Author Information

Corresponding author: E.mail: robert.luxenhofer@helsinki.fi

ORCID: Robert Luxenhofer: 0000-0001-5567-7404

Notes: R.L. is listed as co-inventors on a patent pertinent to some materials in the present work and is co-founder of DelAqua Pharmaceutical Inc. intending commercial development of poly(2-oxazoline)s based drug delivery system.

Acknowledgement

Malik Salman Haider is grateful to higher education commission of Pakistan and German academic exchange services (HEC-DAAD Pakistan) for the award of PhD scholarship. This work was supported by Deutsche Forschungsgemeinschaft (DFG) German Research Foundation, Project no. 398461692 awarded to Robert Luxenhofer

References:

1. Ali S, Kolter K. Challenges and opportunities in oral formulation development. American Pharmacuetical Review. 2012;15(7):1.
2. Ten Tije AJ, Verweij J, Loos WJ, Sparreboom A. Pharmacological effects of formulation vehicles: implications for cancer chemotherapy. Clinical Pharmacokinetics. 2003;42(7):665-85.
3. Dye D, Watkins J. Suspected anaphylactic reaction to Cremophor EL. British medical journal. 1980;280(6228):1353.
4. Lee KS, Chung HC, Im SA, Park YH, Kim CS, Kim S-B et al. Multicenter phase II trial of Genexol-PM, a Cremophor-free, polymeric micelle formulation of paclitaxel, in patients with metastatic breast cancer. Breast cancer research and treatment. 2008;108(2):241-50.
5. Cabral H, Miyata K, Osada K, Kataoka K. Block copolymer micelles in nanomedicine applications. Chemical Reviews. 2018;118(14):6844-92.
6. Ghosh B, Biswas S. Polymeric micelles in cancer therapy: State of the art. Journal of Controlled Release. 2021;332:127-47.
7. Nishiyama N, Kataoka K. Current state, achievements, and future prospects of polymeric micelles as nanocarriers for drug and gene delivery. Pharmacology & Therapeutics. 2006;112(3):630-48.
8. Cabral H, Kataoka K. Progress of drug-loaded polymeric micelles into clinical studies. Journal of Controlled Release. 2014;190:465-76.
9. Hwang D, Ramsey JD, Kabanov AV. Polymeric micelles for the delivery of poorly soluble drugs: From nanoformulation to clinical approval. Advanced Drug Delivery Reviews. 2020;156:80-118. doi:10.1016/j.addr.2020.09.009.
10. Zheng X, Xie J, Zhang X, Sun W, Zhao H, Li Y et al. An overview of polymeric nanomicelles in clinical trials and on the market. Chinese Chemical Letters. 2020.
11. Zhou W, Li C, Wang Z, Zhang W, Liu J. Factors affecting the stability of drug-loaded polymeric micelles and strategies for improvement. Journal of Nanoparticle Research. 2016;18(9):1-18.
12. Yokoyama M. Polymeric micelles as drug carriers: their lights and shadows. Journal of drug targeting. 2014;22(7):576-83.
13. Callari M, De Souza PL, Rawal A, Stenzel MH. The Effect of Drug Loading on Micelle Properties: Solid-State NMR as a Tool to Gain Structural Insight. Angewandte Chemie. 2017;129(29):8561-5.
14. Zahoranová A, Luxenhofer R. Poly(2-oxazoline) and Poly(2-oxazine)-Based Self-Assemblies, Polyplexes, and Drug Nanoformulations-An Update. Advanced Healthcare Materials. 2021;10(6):2001382.
15. Lorson T, Lübtow MM, Wegener E, Haider MS, Borova S, Nahm D et al. Poly(2-oxazoline)s based biomaterials: A comprehensive and critical update. Biomaterials. 2018;178:204-80.
16. Sedlacek O, Monnery BD, Filippov SK, Hoogenboom R, Hruby M. Poly(2-Oxazoline)s–Are They More Advantageous for Biomedical Applications Than Other Polymers? Macromolecular Rapid communications. 2012;33(19):1648-62.
17. He Z, Schulz A, Wan X, Seitz J, Bludau H, Alakhova DY et al. Poly(2-oxazoline) based micelles with high capacity for 3rd generation taxoids: Preparation, in vitro and in vivo evaluation. Journal of Controlled Release. 2015;208:67-75.
18. Sedlacek O, Hoogenboom R. Drug Delivery Systems Based on Poly(2-Oxazoline)s and Poly(2-Oxazine)s. Advanced Therapeutics. 2020;3(1):1900168.
19. Wu C, McGinity JW. Non-traditional plasticization of polymeric films. International Journal of Pharmaceutics. 1999;177(1):15-27.
20. Hossin B, Rizi K, Murdan S. Application of Hansen Solubility Parameters to predict drug–nail interactions, which can assist the design of nail medicines. European Journal of Pharmaceutics and Biopharmaceutics. 2016;102:32-40.
21. Lin S-Y, Lee C-J, Lin Y-Y. Drug-polymer interaction affecting the mechanical properties, adhesion strength and release kinetics of piroxicam-loaded Eudragit E films plasticized with different plasticizers. Journal of controlled release. 1995;33(3):375-81.
22. El-Houssiny A, Ward A, Mostafa D, Abd-El-Messieh S, Abdel-Nour K, Darwish M et al. Drug–polymer interaction between glucosamine sulfate and alginate nanoparticles: FTIR, DSC and

dielectric spectroscopy studies. Advances in Natural Sciences: Nanoscience and Nanotechnology. 2016;7(2):025014.
23. Barton AF. Solubility parameters. Chemical Reviews. 1975;75(6):731-53.
24. Benazzouz A, Moity L, Pierlot C, Molinier V, Aubry J-M. Hansen approach versus COSMO-RS for predicting the solubility of an organic UV filter in cosmetic solvents. Colloids and Surfaces A: Physicochemical and Engineering Aspects. 2014;458:101-9.
25. Alhalaweh A, Alzghoul A, Kaialy W. Data mining of solubility parameters for computational prediction of drug–excipient miscibility. Drug development and industrial pharmacy. 2014;40(7):904-9.
26. Guenthner AJ, Lamison KR, Lubin LM, Haddad TS, Mabry JM. Hansen solubility parameters for octahedral oligomeric silsesquioxanes. Industrial & engineering chemistry research. 2012;51(38):12282-93.
27. Bonnet J, Suissa G, Raynal M, Bouteiller L. Organogel formation rationalized by Hansen solubility parameters: dos and don'ts. Soft Matter. 2014;10(18):3154-60.
28. Doktorovova S, Souto EB, Silva AM. Hansen solubility parameters (HSP) for prescreening formulation of solid lipid nanoparticles (SLN): In vitro testing of curcumin-loaded SLN in MCF-7 and BT-474 cell lines. Pharmaceutical development and technology. 2018;23(1):96-105.
29. Haider MS, Schreiner J, Kendl S, Kroiss M, Luxenhofer R. A Micellar Mitotane Formulation with High Drug-Loading and Solubility: Physico-Chemical Characterization and Cytotoxicity Studies in 2D and 3D In Vitro Tumor Models. Macromolecular Bioscience. 2020;20(1):1900178.
30. Lübtow MM, Hahn L, Haider MS, Luxenhofer R. Drug specificity, synergy and antagonism in ultrahigh capacity poly(2-oxazoline)/poly(2-oxazine) based formulations. Journal of the American Chemical Society. 2017;139(32):10980-3.
31. Luxenhofer R, Schulz A, Roques C, Li S, Bronich TK, Batrakova EV et al. Doubly amphiphilic poly(2-oxazoline)s as high-capacity delivery systems for hydrophobic drugs. Biomaterials. 2010;31:4972-9.
32. Han Y, He Z, Schulz A, Bronich TK, Jordan R, Luxenhofer R et al. Synergistic combinations of multiple chemotherapeutic agents in high capacity poly(2-oxazoline) micelles. Molecular Pharmaceutics. 2012;9(8):2302-13.
33. Lübtow MM, Keßler L, Appelt-Menzel A, Lorson T, Gangloff N, Kirsch M et al. More Is Sometimes Less: Curcumin and Paclitaxel Formulations Using Poly(2-oxazoline) and Poly(2-oxazine)-Based Amphiphiles Bearing Linear and Branched C9 Side Chains. Macromolecular Bioscience. 2018;18:1800155-72.
34. Lübtow MM, Haider MS, Kirsch M, Klisch S, Luxenhofer R. Like Dissolves Like? A Comprehensive Evaluation of Partial Solubility Parameters to Predict Polymer-Drug Compatibility in Ultra-High Drug Loaded Polymer Micelles. Biomacromolecules. 2019;20(8):3041-56.
35. Hahn L, Lübtow MM, Lorson T, Schmitt F, Appelt-Menzel A, Schobert R et al. Investigating the Influence of Aromatic Moieties on the Formulation of Hydrophobic Natural Products and Drugs in Poly(2-oxazoline)-Based Amphiphiles. Biomacromolecules. 2018;19(7):3119.
36. Witte H, Seeliger W. Cyclische imidsäureester aus nitrilen und aminoalkoholen. Leibigs Ann. 1974;1974:996-1009.
37. Van Krevelen DW, Te Nijenhuis K. Properties of polymers: their correlation with chemical structure; their numerical estimation and prediction from additive group contributions. Elsevier; 2009.
38. Fedors RF. A method for estimating both the solubility parameters and molar volumes of liquids. Polymer Engineering & Science. 1974;14(2):147-54.
39. Letchford K, Liggins R, Burt H. Solubilization of hydrophobic drugs by methoxy poly(ethylene glycol)-block-polycaprolactone diblock copolymer micelles: Theoretical and experimental data and correlations. Journal of Pharmaceutical Sciences. 2008;97(3):1179-90.
40. Lübtow MM, Nelke LC, Seifert J, Kühnemundt J, Sahay G, Dandekar G et al. Drug induced micellization into ultra-high capacity and stable curcumin nanoformulations: Physico-chemical

characterization and evaluation in 2D and 3D in vitro models. Journal of Controlled Release. 2019;303:162-80.
41. Lübtow MM, Oerter S, Quader S, Jeanclos E, Cubukova A, Krafft M et al. In Vitro Blood–Brain Barrier Permeability and Cytotoxicity of an Atorvastatin-Loaded Nanoformulation Against Glioblastoma in 2D and 3D Models. Molecular Pharmaceutics. 2020;17(6):1835-47.
42. Vinod N, Hwang D, Azam SH, Van Swearingen AE, Wayne E, Fussell SC et al. High-capacity poly(2-oxazoline) formulation of TLR 7/8 agonist extends survival in a chemo-insensitive, metastatic model of lung adenocarcinoma. Science Advances. 2020;6(25):eaba5542.
43. Hwang D, Dismuke T, Tikunov A, Rosen EP, Kagel JR, Ramsey JD et al. Poly(2-oxazoline) nanoparticle delivery enhances the therapeutic potential of vismodegib for medulloblastoma by improving CNS pharmacokinetics and reducing systemic toxicity. Nanomedicine: Nanotechnology, Biology and Medicine. 2021;32:102345.
44. Raveendran R, Mullen KM, Wellard RM, Sharma CP, Hoogenboom R, Dargaville TR. Poly (2-oxazoline) block copolymer nanoparticles for curcumin loading and delivery to cancer cells. European Polymer Journal. 2017;93:682-94.
45. Sonpavde G, Hutson TE, Rini BI. Axitinib for renal cell carcinoma. Expert opinion on investigational drugs. 2008;17(5):741-8.
46. Choueiri TK. Axitinib, a novel anti-angiogenic drug with promising activity in various solid tumors. Current opinion in investigational drugs (London, England: 2000). 2008;9(6):658-71.
47. Shi S, Peng F, Zheng Q, Zeng L, Chen H, Li X et al. Micelle-solubilized axitinib for ocular administration in anti-neovascularization. International journal of pharmaceutics. 2019;560:19-26.
48. Nebenführ A, Ritzenthaler C, Robinson DG. Brefeldin A: deciphering an enigmatic inhibitor of secretion. Plant physiology. 2002;130(3):1102-8.
49. Yu R-Y, Xing L, Cui P-F, Qiao J-B, He Y-J, Chang X et al. Regulating the Golgi apparatus by co-delivery of a COX-2 inhibitor and Brefeldin A for suppression of tumor metastasis. Biomaterials science. 2018;6(8):2144-55.
50. Schulz A, Han Y, He Z, Bronich TK, Kabanov AV, Luxenhofer R et al. Poly(2-oxazoline)s as high-capacity multi-drug delivery systems. Polymer Preprints. 2012;53:305.
51. Kravitz HM, Fawcett J. Carbamazepine in the treatment of affective disorders. Medical Science Research. 1987;15:1-8.
52. Kadam Y, Yerramilli U, Bahadur A. Solubilization of poorly water-soluble drug carbamezapine in Pluronic® micelles: effect of molecular characteristics, temperature and added salt on the solubilizing capacity. Colloids and Surfaces B: Biointerfaces. 2009;72(1):141-7.
53. Olivieri A, Manzione L. Dasatinib: a new step in molecular target therapy. Annals of Oncology. 2007;18:vi42-vi6.
54. Li Q, Lai KL, Chan PS, Leung SC, Li HY, Fang Y et al. Micellar delivery of dasatinib for the inhibition of pathologic cellular processes of the retinal pigment epithelium. Colloids and surfaces B: biointerfaces. 2016;140:278-86.
55. Cohen MH, Johnson JR, Chen YF, Sridhara R, Pazdur R. FDA drug approval summary: erlotinib (Tarceva®) tablets. The oncologist. 2005;10(7):461-6.
56. Méjean A, Ravaud A, Thezenas S, Colas S, Beauval J-B, Bensalah K et al. Sunitinib alone or after nephrectomy in metastatic renal-cell carcinoma. New England Journal of Medicine. 2018;379(5):417-27.
57. Streets J, Bhatt P, Bhatia D, Sutariya V. Sunitinib-Loaded MPEG-PCL Micelles for the Treatment of Age-Related Macular Degeneration. Scientia Pharmaceutica. 2020;88(3):30.
58. Arbiser JL, Moschella SL. Clofazimine: a review of its medical uses and mechanisms of action. Journal of the American Academy of Dermatology. 1995;32(2):241-7.
59. Curran MP. Crizotinib. Drugs. 2012;72(1):99-107.
60. Cannon CP, Blazing MA, Giugliano RP, McCagg A, White JA, Theroux P et al. Ezetimibe added to statin therapy after acute coronary syndromes. New England Journal of Medicine. 2015;372(25):2387-97.

61. Mann BS, Johnson JR, Cohen MH, Justice R, Pazdur R. FDA approval summary: vorinostat for treatment of advanced primary cutaneous T-cell lymphoma. The oncologist. 2007;12(10):1247-52.
62. Rompicharla SVK, Trivedi P, Kumari P, Muddineti OS, Theegalapalli S, Ghosh B et al. Evaluation of anti-tumor efficacy of vorinostat encapsulated self-assembled polymeric micelles in solid tumors. AAPS PharmSciTech. 2018;19(7):3141-51.
63. Duvic M, Hymes K, Heald P, Breneman D, Martin AG, Myskowski P et al. Bexarotene is effective and safe for treatment of refractory advanced-stage cutaneous T-cell lymphoma: multinational phase II-III trial results. Journal of clinical oncology. 2001;19(9):2456-71.
64. Paller CJ, Antonarakis ES. Cabazitaxel: a novel second-line treatment for metastatic castration-resistant prostate cancer. Drug design, development and therapy. 2011;5:117.
65. San Miguel JF, Schlag R, Khuageva NK, Dimopoulos MA, Shpilberg O, Kropff M et al. Bortezomib plus melphalan and prednisone for initial treatment of multiple myeloma. New England Journal of Medicine. 2008;359(9):906-17.
66. Ibegbu A, Mullaney I, Fyfe L, MacBean D. Therapeutic potentials and uses of cannabinoid agonists in health and disease conditions. British Journal of Pharmacology and Toxicology. 2012;3(2):76-88.
67. Berrocoso E, Rey-Brea R, Fernández-Arévalo M, Micó JA, Martín-Banderas L. Single oral dose of cannabinoid derivate loaded PLGA nanocarriers relieves neuropathic pain for eleven days. Nanomedicine: Nanotechnology, Biology and Medicine. 2017;13(8):2623-32.
68. Frampton JE, Keating GM. Celecoxib. Drugs. 2007;67(16):2433-74.
69. Crowley P, Gallagher H. Clotrimazole as a pharmaceutical: past, present and future. Journal of applied microbiology. 2014;117(3):611-7.
70. Catenacci L, Marrubini G, Sorrenti M, Rossi S, Sandri G, Ferrari F et al. Design of Experiments-Assisted Development of Clotrimazole-Loaded Ionic Polymeric Micelles Based on Hyaluronic Acid. Nanomaterials. 2020;10(4):635.
71. Polkowski K, Mazurek AP. Biological properties of genistein. A review of in vitro and in vivo data. Acta Poloniae Pliarmaceutica—Drug Research. 2000;57(2):l35-l55.
72. Moy B, Goss PE. Lapatinib: current status and future directions in breast cancer. The oncologist. 2006;11(10):1047-57.
73. Wilhelm S, Carter C, Lynch M, Lowinger T, Dumas J, Smith RA et al. Discovery and development of sorafenib: a multikinase inhibitor for treating cancer. Nature reviews Drug discovery. 2006;5(10):835-44.
74. Gould SE, Low JA, Marsters Jr JC, Robarge K, Rubin LL, de Sauvage FJ et al. Discovery and preclinical development of vismodegib. Expert opinion on drug discovery. 2014;9(8):969-84.
75. Hahner S, Fassnacht M. Mitotane for adrenocortical carcinoma treatment. Current opinion in investigational drugs (London, England: 2000). 2005;6(4):386-94.
76. Kothari K, Ragoonanan V, Suryanarayanan R. The role of drug–polymer hydrogen bonding interactions on the molecular mobility and physical stability of nifedipine solid dispersions. Molecular pharmaceutics. 2015;12(1):162-70.
77. Mistry P, Mohapatra S, Gopinath T, Vogt FG, Suryanarayanan R. Role of the strength of drug–polymer interactions on the molecular mobility and crystallization inhibition in ketoconazole solid dispersions. Molecular pharmaceutics. 2015;12(9):3339-50.
78. Haider MS, Lübtow MM, Endres S, Forster S, Flegler VJ, Böttcher B et al. Think beyond the core: The impact of the hydrophilic corona on the drug solubilization using polymer micelles. ACS Applied Materials & Interfaces. 2020;12(22):24531–43.
79. Pöppler AC, Lübtow MM, Schlauersbach J, Wiest J, Meinel L, Luxenhofer R. Loading-Dependent Structural Model of Polymeric Micelles Encapsulating Curcumin by Solid-State NMR Spectroscopy. Angewandte Chemie International Edition. 2019;58(51):18540-6.
80. Grüne M, Luxenhofer R, Iuga D, Brown SP, Pöppler A-C. 14 N–1 H HMQC solid-state NMR as a powerful tool to study amorphous formulations–an exemplary study of paclitaxel loaded polymer micelles. Journal of Materials Chemistry B. 2020;8(31):6827-36.

81. Deshmukh SA, Solomon LA, Kamath G, Fry HC, Sankaranarayanan SK. Water ordering controls the dynamic equilibrium of micelle–fibre formation in self-assembly of peptide amphiphiles. Nature communications. 2016;7(1):1-11.
82. Moilanen DE, Fenn EE, Wong D, Fayer MD. Water dynamics in large and small reverse micelles: From two ensembles to collective behavior. The Journal of chemical physics. 2009;131(1):014704.
83. Lim C, Ramsey JD, Hwang D, Teixeira SCM, Poon C-D, Strauss JD et al. Drug-dependent morphological transitions in spherical and worm-like polymeric micelles define stability and pharmacological performance of micellar drugs. bioRxiv. 2021:2021.06.10.447962. doi:10.1101/2021.06.10.447962.
84. Sochor B, Düdükcü Ö, Lübtow MM, Schummer B, Jaksch S, Luxenhofer R. Probing the Complex Loading Dependent Structural Changes in Ultra-High Drug Loaded Polymer Micelles by Small-Angle Neutron Scattering. Langmuir. 2020;36:3494-503.

4.4 Impact of Hydrophobic block on Structure Property Relationship of Micelles for Drug Loading

Summary: From previous contributions, we generally concluded that the polymers with shorter side chain length (in hydrophobic block) (C3 and C4) appeared to be the best solubilizer for various drugs. So they were further harnessed to explore the structure property relationship. The impact of the smallest changes in the chemical structure of the polymeric drug carrier on the drug loading capacity became further apparent when the solubilizing capacity of (short side chain) POx and POzi based amphiphiles were tested to solubilize highly hydrophobic anticancer drug PTX and a natural compound CUR. By formally shifting a single methylene unit from the polymer sidechain (POx) to the polymer main chain (POzi) of the hydrophobic block caused distinct specificities for both hydrophobic compounds. Moreover, the co-formulation, i.e. simultaneous solubilization of both compounds with the same drug carrier, resulted in either synergistic or antagonistic solubilization patterns depending on the chemical structure of the polymer amphiphile. In the presence of PTX, solvatochromic Reichardt's dye showed a remodeling of the micellar microenvironment. Unexpectedly, highly hydrophobic PTX seemed to establish a more polar microenvironment which was attributed to the large number of polar moieties present in PTX. This gave first hints that the common perception of hydrophobic drugs being more or less unspecifically incorporated into the hydrophobic core should be regarded with great care. Apart from that, the extraordinary high LCs and small micellar sizes even at high drug loading suitable for IV administration showed the therapeutic potential of the first ever reported POzi based drug formulations.

JACS
JOURNAL OF THE AMERICAN CHEMICAL SOCIETY
Communication
pubs.acs.org/JACS

Drug Specificity, Synergy and Antagonism in Ultrahigh Capacity Poly(2-oxazoline)/Poly(2-oxazine) based Formulations

Michael M. Lübtow, Lukas Hahn, Malik Salman Haider, and Robert Luxenhofer*

Functional Polymer Materials, Chair for Chemical Technology of Material Synthesis and the Bavarian Polymer Institute, University of Würzburg, Röntgenring 11, 97070 Würzburg, Germany

Abstract

Polymer micelles offer the possibility to create a nanoscopic environment that is distinct from the bulk phase. They find applications in catalysis, drug delivery, cleaning, etc. Often, one simply distinguishes between hydrophilic and hydrophobic, but fine-tuning of the microenvironment is possible by adjusting the structure of the polymer amphiphile. Here, we investigated a small library of structurally similar amphiphiles based on poly(2-oxazoline)s and poly(2-oxazine)s with respect to their solubilization capacity for two extremely water insoluble drugs, curcumin and paclitaxel. We found very significant and orthogonal specificities even if only one methylene group is exchanged between the polymer backbone and side chain. More strikingly, we observed profound synergistic and antagonistic solubilisation patterns for the coformulation of the two drugs. Our findings shed new light on host–guest interaction in polymer micelles and such pronounced host–guest specificities in polymer micelles may not only be interesting in drug delivery but for applications such as micellar catalysis.

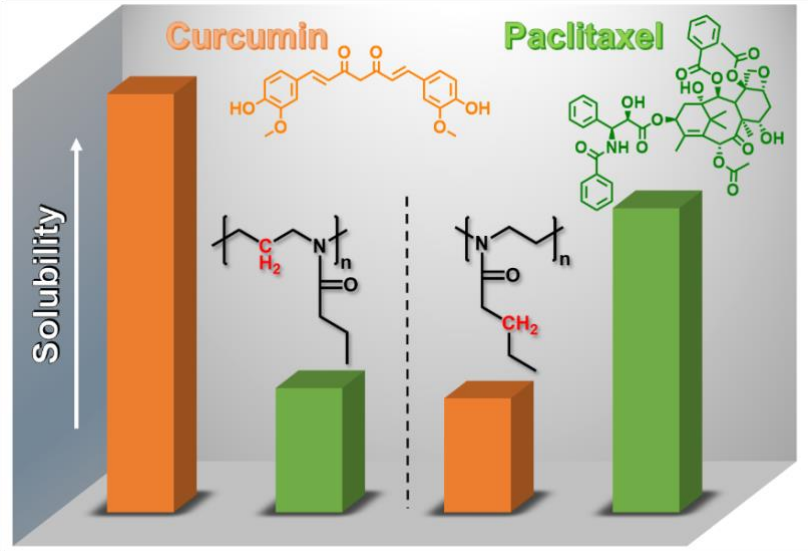

4.5 Impact of Hydrophilic block on Structure Property Relationship of Micelles for Drug Loading

Summary: After successful solubilization experiments and investigating the impact of hydrophobic block the drug loading, the next question was to find what makes our system ultra-high drug loaded. The standard model of drug loaded micelles is that of a core-shell structure, where core is responsible for drug encapsulation and shell provide the colloidal stability and some level of protection for the drug. In the case of ultra-high drug loading, theoretical consideration suggest that it is impossible that the amount of solubilized drug in one micelle could be accommodated merely in the hydrophobic block. We hypothesized that also the hydrophilic block/corona could have an effect on the drug solubilisation, which has not been systematically studied to date. A library of new ABA triblock copolymers which differ only in their hydrophilic blocks were synthesized (A= pMeOx or pEtOx). The drug loading capacities and various analytical techniques confirmed that besides the hydrophobic block, the hydrophilic blocks of the amphiphiles also play very important role in drug solubilisation. These results show for the first time that the hydrophilic corona of polymer micelles may not only be involved in providing colloidal stability, but also that a minor change in the hydrophilic block of a polymer amphiphile can have a significant impact on drug loading. These results shed new light and give clear instructions on how to design and optimize drug delivery system polymeric excipients in general. Jun-Prof. Ann-Christin Pöppler from Organic Chemistry department, University of Würzburg is further exploring these system to better understand the overall packing of micelles and all the findings support the hypothesis. This work shows that a simple core-shell architecture is an oversimplification of micellar architecture and selection of hydrophilic block play a decisive role in the drug solubilisation and stability of micelles.

ACS APPLIED MATERIALS & INTERFACES

www.acsami.org Research Article

Think Beyond the Core: Impact of the Hydrophilic Corona on Drug Solubilization Using Polymer Micelles

Malik Salman Haider, Michael M. Lübtow, Sebastian Endres, Stefan Forster, Vanessa J. Flegler, Bettina Böttcher, Vladimir Aseyev, Ann-Christin Pöppler, and Robert Luxenhofer*

Cite This: *ACS Appl. Mater. Interfaces* 2020, 12, 24531−24543 Read Online

ACCESS | Metrics & More | Article Recommendations | Supporting Information

ABSTRACT: Polymeric micelles are typically characterized as core−shell structures. The hydrophobic core is considered as a depot for hydrophobic molecules, and the corona-forming block acts as a stabilizing and solubilizing interface between the core and aqueous milieu. Tremendous efforts have been made to tune the hydrophobic block to increase the drug loading and stability of micelles, whereas the role of hydrophilic blocks is rarely investigated in this context, with poly(ethylene glycol) (PEG) being the gold standard of hydrophilic polymers. To better understand the role of the hydrophilic corona, a small library of structurally similar A−B−A-type amphiphiles based on poly(2-oxazoline)s and poly(2-oxazine)s is investigated by varying the hydrophilic block A utilizing poly(2-methyl-2-oxazoline) (pMeOx; A) or poly(2-ethyl-2-oxazoline) (pEtOx; A*). In terms of hydrophilicity, both polymers closely resemble PEG. The more hydrophobic block B bears either a poly(2-oxazoline) and poly(2-oxazine) backbone with C3 (propyl) and C4 (butyl) side chains. Surprisingly, major differences in loading capacities from A−B−A > A*−B−A > A*−B−A* is observed for the formulation with two poorly water-soluble compounds, curcumin and paclitaxel, highlighting the importance of the hydrophilic corona of polymer micelles used for drug formulation. The formulations are also characterized by various nuclear magnetic resonance spectroscopy methods, dynamic light scattering, cryogenic transmission electron microscopy, and (micro) differential scanning calorimetry. Our findings suggest that the interaction between the hydrophilic block and the guest molecule should be considered an important, but previously largely ignored, factor for the rational design of polymeric micelles.

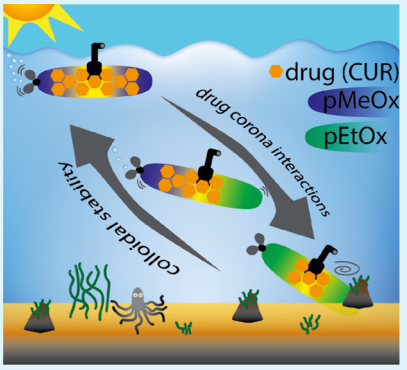

KEYWORDS: *poly(2-oxazoline)s, amphiphilic block copolymers, hydrophobic drugs, nanoformulations, corona−drug interactions*

INTRODUCTION

Amphiphilic block copolymers can self-assemble to form polymeric micelles (PMs), vesicles, and many other forms of self-assemblies in selective solvents above their critical micelle concentration (cmc).[1] Such nanostructures can be employed for a variety of applications such as drug delivery,[2] viscosity modifications, catalysis, and toughening of plastics.[3] The size, morphology, stability, and surface chemistry of PMs can be easily adjusted by fine tuning the hydrophilic/hydrophobic ratios and block lengths.[4] PMs are capable of encapsulating hydrophobic molecules, increasing their apparent solubility and stability. It is frequently postulated and sometimes confirmed that micelles have core−shell structures, where the core (comprised of the hydrophobic polymer block) hosts the hydrophobic guest molecules, and the shell (comprised of the hydrophilic block) provides the solubility and colloidal stability in aqueous medium.[5] One early attempt to better understand the interplay of the structure of a polymer amphiphile and a hydrophobic guest/solute was a paper by Kabanov et al., meticulously studying the partitioning of hydrophobic solutes in Pluronic micelles. The micelle formation and hydrophobic partitioning of the hydrophobic solute into the micelles are "favored by the hydrophobic interactions in the micelle inner layers, which increase when the poly(propylene oxide) length increases or poly(ethylene oxide) length decreases."[6] Along these lines, Guo and Lu et al. demonstrated that increasing the chain length of the hydrophobic block has a positive impact on drug loading.[7,8] However, the interplay between polymer self-assemblies and hydrophobic guests can be quite complex. On the one hand, drug loading can affect the morphologies of self-assemblies, which was shown, among others, by Schulz et al. and Cao et al.[4,9] On the other hand, Lübtow et al. reported a case where micelle formation of A−B−A triblock copolymers was triggered only by the presence of a hydrophobic guest molecule.[10] More recently, Wiest et al. showed that increasing the imatinib (an anticancer drug) concentration in taurocholate/lecithin micelles above a critical value not only causes a

Received: December 18, 2019
Accepted: May 7, 2020
Published: May 7, 2020

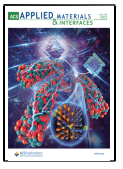

https://dx.doi.org/10.1021/acsami.9b22495
ACS Appl. Mater. Interfaces 2020, 12, 24531−24543

morphology transition from vesicles to micelles but also leads to colloidal collapse, that is, aggregation and precipitation.[11] PMs have been studied intensively for decades with respect to their physicochemical properties and general behavior in biological systems.[12,13] However, despite thousands of research papers on the use of PMs for drug delivery, little information can be found on the impact of the hydrophilic block on the drug loading of PMs, the localization of the drug within the micelles,[4] or the colloidal stability[14] of such a drug-delivery system.

In the vast majority of described systems for drug delivery, the hydrophilic corona is comprised of poly(ethylene glycol) (PEG).[15−17] However, for several years, alternatives for PEG as the gold standard for a hydrophilic, nonfouling, stealth, nontoxic, and nonimmunogenic synthetic biomaterial have been heavily investigated.[18] One particularly debated issue is the potential immunogenicity of PEG.[19] This discussion notwithstanding, alternative polymers[20] used for the hydrophilic corona of PMs may be useful to tailor the properties of the corona. One such alternative are hydrophilic poly(2-oxazoline)s (POx), in particular, poly(2-methyl-2-oxazoline) (pMeOx) and poly(2-ethyl-2-oxazoline) (pEtOx). More recently, poly(2-oxazine)s, POx's higher main-chain homologues, have also raised some interest.[21−25] For the formulation of hydrophobic drugs, A−B−A-type triblock copolymers have been intensively investigated recently and are also in the focus of the present contribution (Scheme 1). In fact, the POx-based amphiphiles have demonstrated their unusual drug loading capacity (LC)[26−29] and excellent therapeutic potential in various challenging tumor models.[30−36] Luxenhofer and co-workers reported an ultrahigh paclitaxel (PTX)-loaded POx-based micellar formulation (LC ≈ 50 wt %) ($m_{Drug}/(m_{Drug} + m_{Polymer})$)[37] with excellent *in vivo* antitumor efficacy.[31,32] The lead amphiphile was an A−B−A type triblock copolymer, poly(2-methyl-2-oxazoline)-*b*-(poly(2-*n*-butyl-2-oxazoline)-*b*-poly(2-methyl-2-oxazoline) (pMeOx-*b*-pBuOx-*b*-pMeOx = A−pBuOx−A). For variation of the more hydrophobic central B block, Lübtow et al. tested a library of structurally related amphiphiles with a variety of extremely poorly water-soluble molecules such as curcumin (CUR),[38−40] tanshinone IIa, and various hydrophobic drugs such as efavirenz, dexamethasone, and mitotane.[41,42]

Notably, the small structural difference of only one methylene group switching between the polymer backbone and the sidechain in A−pBuOx−A and A−pPrOzi−A [poly(2-methyl-2-oxazoline)-*b*-poly(2-*n*-propyl-2-oxazine)-*b*-poly(2-methyl-2-oxazoline)] resulted in profound specificities in drug loading.[43] We and others have spent considerable efforts to elucidate the structure−property relationships for different drugs and polymer in this system. However, the preparation and finding of the best polymer/drug combinations are very tedious. To accelerate the development of effective drug-delivery systems, Alves and co-workers built models predicting LC and loading efficiency (LE) of POx-based polymer platform for hydrophobic drugs.[44]

A closer look at the ultrahigh loadings (LC ≈ 50 wt %), which were previously observed for this polymer platform and different drugs, including PTX and CUR, from a stoichiometric perspective, shows how unlikely such high drug loading should be. For example, at the maximum CUR loading of A−pPrOzi−A (LC ≈ 54 wt %; 12 g L^{-1} CUR for 10 g L^{-1} polymer), 1.3 molecules of CUR ($C_{21}H_{20}O_6$, M = 368 g mol^{-1}) for every repeat unit of the hydrophobic block pPrOzi ($C_7H_{13}NO$, M = 127 g mol^{-1}) are solubilized in the micelles, assuming that essentially all polymer molecules contribute. Therefore, one could hypothesize that not only the hydrophobic repeat units interact with the drug but also the hydrophilic ones. In fact, very recently, we conducted solid-state nuclear magnetic resonance (NMR) spectroscopy[45,46] as well as small-angle neutron scattering experiments,[47,48] which clearly showed the interactions of the hydrophilic corona forming pMeOx and CUR or PTX and its detrimental effect on the dissolution rate of lyophilized drug formulations. Also, Cao and co-workers[4] reported recently in a different polymeric system that at higher drug loading, CUR started to reside in the shell-forming block, leading to a reduction in the shell hydration. With the ultrahigh drug loading and structure−property relationships investigated in detail with respect to the hydrophobic block,[38,43] we now turn our attention on the variations of the hydrophilic block. Accordingly, this work investigates the impact of chemically distinct hydrophilic blocks (pMeOx and pEtOx) on the drug loading (CUR and PTX), solubilization, and colloidal stability of POx-based A−B−A triblock copolymer micelles.

Scheme 1. (a) Chemical Structures of the A−B−A Triblock Copolymers Used in This Study, Where Hydrophilic Blocks (i.e., Corona-Forming Blocks) Are Either pMeOx (A) and/or pEtOx (A*) and the Hydrophobic Block (i.e., Core-Forming Block) Is Either pBuOx, pBuOzi, pPrOx, or pPrOzi. Please Note, One Important Feature of These Hydrophobic Blocks Is the Presence of the a Highly Polar Tertiary Amide Moiety in Every Repeat Unit, Rendering the Polymer Backbone Polar Also in the Hydrophobic Block; (b) Chemical Structure, Molecular Weight, and log *P* Value of the Model Drugs Used in This Study, paclitaxel (PTX) and curcumin (CUR)

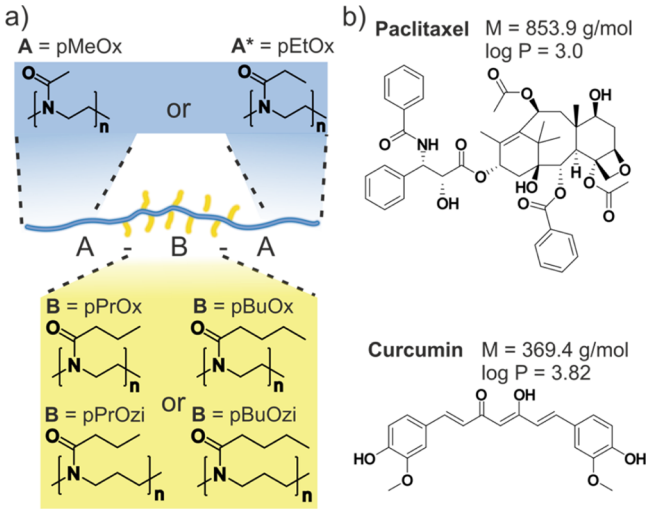

METHODS AND MATERIALS

All triblock copolymers were synthesized by living cationic ring opening polymerization[49] followed by characterization with ^{1}H NMR spectroscopy, gel permeation chromatography (GPC), differential scanning calorimetry (DSC), thermogravimetric analysis (TGA), and fluorescence spectroscopy for the determination of cmc. The synthesis of A−pPrOx−A, A−pPrOzi−A, A−pBuOx−A, and A−pBuOzi−A was reported previously.[49] A*−pPrOx−A*, A*−pPrOzi−A*, A*−pBuOx−A*, and A*−pBuOzi−A* triblock copolymers as well as A*−pPrOzi−A and A*−pBuOx−A triblock terpolymers were synthesized for this study; synthetic details and full characterization can be found

https://dx.doi.org/10.1021/acsami.9b22495
ACS Appl. Mater. Interfaces 2020, 12, 24531−24543

Table 1. Physicochemical Characterization of All Synthesized Polymers Including the Molecular Weight M_n, Dispersity $Đ$, Glass Transition Temperature T_g, and cmc as Well as Maximum LC for CUR and PTX

		M_n[b] [kg/mol]		$Đ$[b]			cmc[d]		max. LC (%)	
polymer	M_n[a] [kg/mol]	HFIP	DMF	HFIP	DMF	T_g[c] [°C]	[mg/L]	[mM]	CUR	PTX
A^*_{35}–pBuOx$_{20}$–A^*_{35}	9.5	4.1	6.6	1.11	1.02	48	263	0.027	18	29
A^*_{29}–pPrOzi$_{18}$–A^*_{29}	8.2	3.9	6.5	1.12	1.14	42	▲		28	8
A^*_{38}–pBuOzi$_{23}$–A^*_{38}	10	3.4	6.3	1.15	1.12	37	130	0.013	24	16
A^*_{39}–pPrOx$_{29}$–A^*_{39}	10	3.7	6.0	1.10	1.11	50	▲		5	1.7
A^*_{32}–pPrOzi$_{19}$–A_{31}	8.5	4.1	n.d.	1.11	n.d.	45	▲		29	22
A^*_{34}–pBuOx$_{20}$–A_{31}	8.7	3.6	n.d.	1.18	n.d.	54	485	0.056	27	39
pMeOx$_{35}$	3.0	1.7	n.d.	1.09	n.d.	73	n.a.		2.2	n.d.
pEtOx$_{35}$	3.5	1.6	n.d.	1.08	n.d.	52	n.a.		0.5	n.d.

[a]Obtained by ^{1}H NMR analysis ($CDCl_3$; 300 MHz). [b]Obtained by GPC analysis [eluents are hexafluoroisopropanol (HFIP) and dimethylformamide (DMF)]. [c]Obtained by DSC (from the third heating curve). [d]Obtained by the pyrene assay at 25 °C. ▲—unable to apply the fit to obtain the cmc values.

in the Supporting Information. All CUR and PTX formulations were prepared by the thin-film hydration method. The quantification for drug loading was done with high-performance liquid chromatography and ultraviolet–visible (UV–vis) spectroscopy. All drug formulations were further characterized by DSC, ^{1}H NMR, ^{1}H diffusion ordered spectroscopy (DOSY), ^{1}H–^{1}H nuclear Overhauser effect spectroscopy (NOESY), dynamic light scattering (DLS), cryogenic transmission electron microscopy (cryo-TEM), and micro-DSC studies. The details of each method or procedure are described in the Supporting Information and referred to in the corresponding sections of the following section.

RESULTS AND DISCUSSION

Synthesis and Drug Formulation. Initially, four structurally similar A–B–A triblock copolymers were synthesized (Table 1 and Scheme 1a), in which we replaced the previously employed pMeOx (A) with another highly hydrophilic POx, that is, pEtOx (A*), resulting in A*–pPrOx–A*, A*–pPrOzi–A*, A*–pBuOx–A*, and A*–pBuOzi–A* triblock copolymer amphiphiles. For the detailed characterization (^{1}H NMR, GPC, TGA, DSC, and fluorescence spectroscopy for cmc determination), the reader is referred to Table 1 and the Supporting Information (Figures S1–S9, S18–S21, S23, and S25).

These four polymers were tested for their solubilizing capacity for PTX and CUR as well-known representatives for poorly water-soluble guest molecules of medical interest (Figure 1b) by using the thin-film method (Figures S26–S30). Briefly, the polymer and drug are dissolved in ethanol, which is subsequently removed. The resulting polymer–drug film is dissolved by addition of water or other aqueous media. Compared to the polymers bearing a pMeOx hydrophilic block (Figure 1a and Table S1),[43] a very significant drop in the LC was observed for all A*–B–A* amphiphiles, and LC values never exceeded 30 wt % (Figure 1b and Table S2). Interestingly, 20–30 wt % is typically the upper limit for micellar LC found in the literature.[50−52] It should be noted though, that despite the considerable drop in LC compared to A–pPrOzi–A, the LC of A*–pPrOzi–A*-based amphiphiles is still much higher than that of most CUR formulations found in the literature, including POx-based ones.[53] For the A–pBuOx–A triblock, being the best solubilizer for PTX,[31] the LC dropped from 48 wt % (9 g L^{-1}) to 30 wt % (4 g L^{-1}) for A*–pBuOx–A*. Similarly, for A–pPrOzi–A, being the best solubilizer for CUR,[43] a drop from 54 wt % (11.9 g L^{-1}) to 28 wt % (3.9 g L^{-1}) for A*–pPrOzi–A* was observed. However, both remained the best solubilizers for PTX and CUR in the

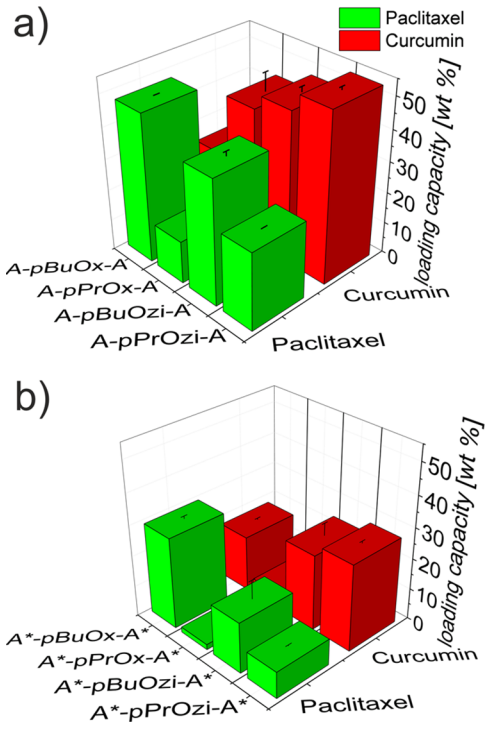

Figure 1. Maximum LC for PTX (green) and CUR (red) concentrations using four different A–B–A triblock copolymers with (a) pMeOx (A) and (b) pEtOx (A*) as hydrophilic blocks (polymer feed 10 g L^{-1}). Data is given as means ± SD (n = 3). The data shown in (a) is taken from ref 43. See Tables S1 and S2 for tabulated values.

A*–B–A* series, that is, the previously observed drug specificities with respect to the hydrophobic block remained valid. In the case of A*–pBuOzi–A*, again a dramatic decrease in LC was observed, that is, 48 to 24 wt % (9.4–3.2 g L^{-1}) for CUR and 40 to 16 wt % (6.7–2.1 g L^{-1}) for PTX (Tables S1 and S2). It is important to note that the restricted solubilization capacity cannot be attributed to poor solubility of the newly synthesized A*–B–A* triblock copolymers themselves as the aqueous solubility of the neat polymers well exceeded 100 g L^{-1}. In all cases with A*–B–A* copolymers, the thin-film method resulted in an undissolved gel-like agglomerate after film hydration once a critical LC is reached. ^{1}H NMR in the nonselective $CDCl_3$ revealed that the agglomerate clearly contains both the polymer and the drug

https://dx.doi.org/10.1021/acsami.9b22495
ACS Appl. Mater. Interfaces 2020, 12, 24531–24543

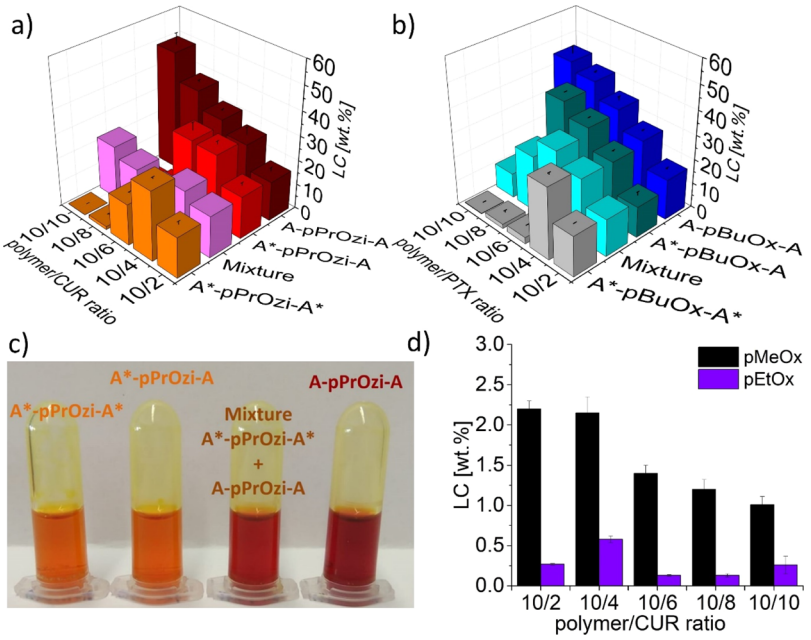

Figure 2. Achieved LC at different ratios (w/w in g/L) of (a) CUR and (b) PTX and triblock co- and terpolymers with pPrOzi and pBuOx as the hydrophobic block and four different setups of hydrophilic blocks, i.e., A−B−A, A*−B−A, A*−B−A*, and a mixture (A−B−A and A*−B−A* 1:1 w/w) (A = pMeOx and A* = pEtOx). (c) Visual appearance of CUR aqueous formulation prepared with four different setups of hydrophilic blocks at the polymer/CUR feed ratio of 10/2 g L^{-1}. (d) CUR-solubilizing capacity of the corona-forming blocks as homopolymers pMeOx (black) and pEtOx (violet). In all cases, the polymer feed was 10 g L^{-1}, and the drug feed was 0 to 10 g L^{-1}. Data is given as means ± SD (n = 3). See Tables S5−S7 for tabulated values.

itself[54] (Figures S32 and S33). For further characterization, pristine CUR, PTX, and freeze-dried agglomerate for both PTX and CUR formulations with A*−pBuOx−A*and A*−pPrOzi−A* amphiphiles, respectively, were analyzed using DSC.

Clearly, the sharp endothermic peaks appearing as the melting point of pristine CUR (175 °C) and solid−solid transition of PTX (170 °C)[55], respectively, were absent in the DSC thermograms of both agglomerates, confirming their amorphous character (Figures S34 and S35). To further understand the influence of the hydrophilic corona on drug formulation, two new A*−B−A triblock terpolymers with two different hydrophilic blocks were synthesized (for detailed characterization, see Table 1 and Figures S10−S13, S18−S19, S23, and S25), selecting the two best performing hydrophobic blocks, pBuOx and pPrOzi (highest LC for PTX and CUR, respectively). The resulting triblock terpolymers are denoted as A*−pBuOx−A and A*−pPrOzi−A.

Drug formulation experiments revealed that the LC of A*−pPrOzi−A and A*−pBuOx−A for CUR (Figure 2a) and PTX (Figure 2b) fall between A−B−A and A*−B−A*, respectively. In the case of CUR, immediate differences could be noted by virtue of the solvatochromicity of CUR.[56] The formulations with A*−pPrOzi−A* and A*−pPrOzi−A appeared orange, whereas A−pPrOzi−A-based formulations appeared dark red (Figure 2c), indicating the different microenvironment for the guest molecule. It is clear that CUR solvatochromicity is not only limited to hydrophobic blocks[10,54] but also affected by the hydrophilic blocks in these particular micellar formulations. The LC for PTX with A*−pBuOx−A (39 wt %, 6.5 g L^{-1}), is comparable with that for A−pBuOx−A (41 wt %, 7.1 g L^{-1}), up to a polymer/PTX feed of 10/8 g L^{-1}. Upon further increase in the drug feed, the LC significantly dropped to 3 wt % (0.24 g L^{-1}), and A−pBuOx−A kept solubilizing increasing amounts of PTX (LC ≈ 45 wt %, 8.2 g L^{-1}) (Figure 2b and Table S6). Similarly, for A*−pPrOzi−A/CUR formulations, a dramatic decrease in LC was observed at a polymer/CUR feed > 10/6 g L^{-1} (Figure 2a and Table S5). The formulation completely agglomerated (and sedimented) upon further increase in the drug feed. Therefore, the maximal LC for both drugs follows the order of A−B−A > A*−B−A > A*−B−A*. Considering the macromolecular structure of the A*−B−A triblock terpolymers, the resulting micelles must inevitably have a mixed pMeOx/pEtOx corona. In contrast, if the corresponding individual A−B−A and A*−B−A* triblock copolymers are mixed, the system could form mixed micelles or phase separate into two distinct sets of micelles or some kind of intermediate. Accordingly, the two pairs of triblock copolymers were mixed in a 1/1 ratio (w/w), and CUR/PTX formulations were prepared. Interestingly, at first glance, the solubilization results neither resemble the picture expected for mixed micelles nor two separate types of micelles (Figure 2a,b; magenta and cyan bars). The formulation experiments were also performed for the drugs and the hydrophobic blocks, which are not preferred, that is, CUR and PTX with pBuOx- and pPrOzi-based amphiphiles, respectively (Figure S31, Tables S3 and S4), and a similar picture was obtained.

The hydration and, thus, the water solubility of many water-soluble polymers is strongly temperature-dependent and shows a lower critical solution temperature (LCST). Both pMeOx and pEtOx are highly water-soluble, but while pMeOx does not show a LCST in water,[57] whereas pEtOx can exhibit a LCST depending on the molar mass and polymer architecture with a cloud point temperature (T_{cp}) as low as 61−69 °C.[58] However, Schubert et al. reported that at least 100 repeat units are required for linear pEtOx to observe the T_{cp} below 100 °C.[59] During thin-film dissolution, our standard protocol involves heating to 55 °C, and it could be hypothesized that

https://dx.doi.org/10.1021/acsami.9b22495
ACS Appl. Mater. Interfaces 2020, 12, 24531−24543

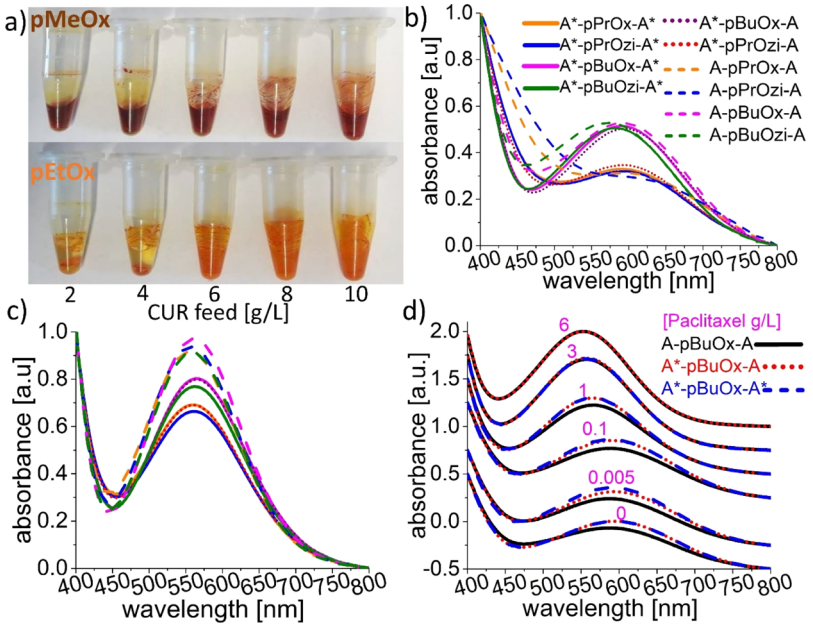

Figure 3. (a) Visual appearance of CUR formulations prepared with pMeOx (upper row) and pEtOx (lower row) homopolymers (polymer feed 10 g L^{-1} and drug feed 0 to 10 g L^{-1}). Normalized UV−vis absorption spectra of RD in the (b) absence (polymer/dye 10/0.5 g L^{-1}) and (c) presence of PTX (polymer/dye/PTX 10/0.5/1 g L^{-1}). (d) Normalized absorption spectra of RD coformulated with PTX into PMs of either A−pBuOx−A (black), A*−pBuOx−A (red), or A*−pBuOx−A* with increasing PTX feed (0−6 g L^{-1}) (purple numbers above the graph) and with the constant polymer/dye feed of 10/0.5 g L^{-1}. For better visibility, the absorption spectra were shifted along the *y*-axis.

pEtOx undergoes a LCST transition at this temperature because of steric crowding in the micellar corona leading to the observed, low LC values. Therefore, formulation experiments were also performed at room temperature, but no significant differences in drug loading were observed (Table S5). To aid with the solubilization or supersaturation of water-insoluble active pharmaceutical ingredients, water-soluble homopolymers are also regularly employed.[60,61] Indeed, pEtOx has been considered in this context with some success.[62] Here, pMeOx and pEtOx homopolymers (35 repeat units) were synthesized (Table 1 and Figures S14−S17, S22, and S24) and compared for CUR solubilization (Figure 2d and Table S7). It was found that pMeOx is capable of solubilizing 8 times more CUR (0.23 g L^{-1}) than pEtOx (0.03 g L^{-1}), suggesting that pMeOx is a profoundly superior excipient to pEtOx and also to other commonly employed polymer excipients such as polyvinylpyrrolidone (0.18 g L^{-1} at pH 5.2)[61,63] and hydroxypropyl methylcellulose. Interestingly, CUR solvatochromicity was also observed when using the homopolymers pEtOx (orange) and pMeOx (dark red) for formulation development (Figure 3a). A recent and excellent study by Nischang and co-workers suggested that both pEtOx and pMeOx are good alternatives to PEG from the perspective of hydrodynamic invariants.[64] However, our results highlight important differences between pMeOx and pEtOx for pharmaceutical applications, which is in line with a recent report by Morgese et al. They compared polymer brushes of PEG, pEtOx, and pMeOx as well as mixtures thereof. When compared to pMeOx, pEtOx-based polymer brushes have shown the least hydration and the highest amount of physisorbed proteins.[65] Likewise, it can be assumed that the profound differences observed in the LC with different hydrophilic blocks are also connected to a difference in hydration between pMeOx and pEtOx, and the previously mentioned work by Cao and co-workers[4] clearly suggests that this effect could be relevant for many other polymers, such as the gold standard PEG. This would be of greatest relevance for the development of drug-delivery systems and a parameter that has been all but ignored previously.

Physicochemical Characterization of Drug Formulations. *Probing Micellar Microenvironment with Reichardt's Dye.* The observed solvatochromicity of CUR in the different micelles shows the presence of different micellar microenvironments. To further probe this, the hydrophobic and solvatochromic Reichardt's dye (RD) was employed to obtain the solvent polarity parameter $E_T(30)$,[66] which has been widely used to measure the polarity of different systems[67] (Figures S36 and S37). RD clearly allowed to distinguish between the polymer sidechain and to a lesser extent the polymer backbone in all investigated samples (polymer/RD 10/0.5 g L^{-1}) (Figure 3b). Albeit somewhat less obvious, the different hydrophilic blocks can also be distinguished. A−pPrOx−A and A−pPrOzi−A showed broad and comparably featureless UV−vis spectra,[43] whereas A*−pPrOzi−A* and A*−pPrOzi−A featured better resolved local maxima. The latter may be attributed to a more defined molecular environment. A more pronounced difference was observed for polymers featuring a butyl side chain, irrespective of the hydrophilic block. Very clearly distinguishable local maxima between 585 and 595 nm were observed. Upon coencapsulating PTX and RD (polymer/RD/PTX 10/0.5/1 g L^{-1}), all spectra narrowed and aligned with the local maxima around 560 nm, indicating the remodeling of the micellar microenvironment (Figure 3c). With an increase in the PTX feed (from 0 to 6 g L^{-1}), λ_{max} gradually decreased to 557, 554, and 552 nm for A*−pBuOx−A*, A*−pBuOx−A, and A−pBuOx−A (Figure 3d and Table S9), respectively, with the corresponding $E_T(30)$ values of 51.3, 51.6, and 51.8. High $E_T(30)$ values correspond to high solvent polarity and vice versa (Table S8). Interesting to note, at low PTX loading, the UV−vis spectrum of A−pBuOx−A is clearly separated from A*−pBuOx−A and A*−pBuOx−A*,

https://dx.doi.org/10.1021/acsami.9b22495
ACS Appl. Mater. Interfaces 2020, 12, 24531−24543

which are essentially identical up to 9 wt % (10/1 g L^{-1}). In contrast, at 23 wt % (10/3 g L^{-1}), the spectra of all three formulations superimpose.

At first sight, this seems to contradict the influence of the polymer corona. However, it should be kept in mind that the microenvironment is probed with RD while increasing the PTX feed. The present data can be interpreted that at low loading, the RD molecules can interact with both the hydrophilic corona and the hydrophobic core. Above a critical loading (9 wt % < LC < 23 wt %), the RD only interacts with the core, presumably because PTX starts to interact more and preferably with the corona. This observation coincides with the formation of the raspberry-like morphology observed at similar LC values for A−pBuOx−A/PTX formulations, which can be explained in the light of the present work with the start of the interaction of PTX with the micellar corona.[9] However, this interpretation should be viewed with considerable care, as we cannot know for sure the location of RD. Unfortunately, a similar analysis using RD is not possible for the CUR formulations, as CUR itself is highly colored and dominates the UV−vis spectrum over RD.

^{1}H NMR Spectroscopy. To gain more insights into the structure of CUR-loaded PMs, pure polymers and lyophilized CUR formulations prepared with A−pPrOzi−A, A*−pPrOzi−A, A*−pPrOzi−A* triblocks, and a mixture of A−pPrOzi−A/A*−pPrOzi−A* (1/1, w/w) were dispersed in D_2O and subsequently analyzed by ^{1}H NMR spectroscopy (Figures 4a,b, 5a,b, and S38−S49). Please note that any precipitate that occurred in the formulation was removed and does not contribute to the NMR spectra. Nevertheless, all data is discussed with respect to the CUR feed, not the actual concentration, which can be found in the Supporting Information (Table S5). In the absence of CUR, the ^{1}H NMR spectra of A*−pPrOzi−A* and A*−pPrOzi−A in D_2O clearly present all signals from the polymers with the expected intensities (Figures S38 and S39), suggesting that the polymers exist as unimers in a nonaggregated form. The pyrene assay also confirmed the absence of micelles in the case of pPrOzi-based amphiphiles (Table 1 and Figure S25). These observations corroborate recent results, which showed that A−pPrOzi−A self-assembles only in the presence of hydrophobic molecules.[10] In the formulations, the characteristic signals for CUR were not observed.[10,54] This can be attributed to a hindered mobility, resulting in short T_2 relaxation times. In contrast, the polymer signals were clearly distinguishable for all samples, but individual signal intensities strongly varied with CUR loading.[68] For the A−pPrOzi−A/CUR formulation, comparison of signals attributed to the hydrophilic block versus the hydrophobic block provides clear evidence for reduced mobility in the latter (Figure S44). However, after a strong initial increase of the integral ratio between I_1/I_8 (CH_2^{MeOx}/CH_3^{PrOzi}) and I_5/I_8 (CH_3^{MeOx}/CH_3^{PrOzi}), the ratio decreases again at a CUR feed ≥ 6 g L^{-1}, suggesting also lowered mobility of the hydrophilic block (Figure S45, blue and magenta triangles). This corroborates that the hydrophilic block becomes involved in the coordination of CUR above a certain CUR concentration. This is in line with a recent, more extensive solid-state NMR analysis of A−pPrOzi−A/CUR formulations.[45] In contrast, for A*−pPrOzi−A*/CUR formulations, the integral ratios I_1/I_9 (pEtOx backbone/CH_3^{PrOzi}) and I_8/I_9 (CH_3^{EtOx}/CH_3^{PrOzi}) kept on increasing with increasing CUR feed (Figures S46 and S47, blue triangle and green diamond), even while overall drug solubilization deteriorated.

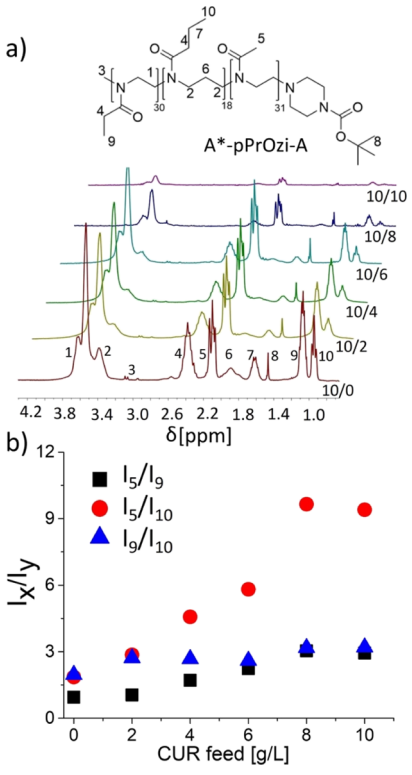

Figure 4. (a) ^{1}H NMR spectra (D_2O, 300 MHz, 298 K) with signal assignment and (b) NMR integral ratios (I_x/I_y) of terpolymer (A*−pPrOzi−A)/CUR formulations as a function of the CUR feed (0−10 g L^{-1}). For better visibility, enlarged sections are added as insets.

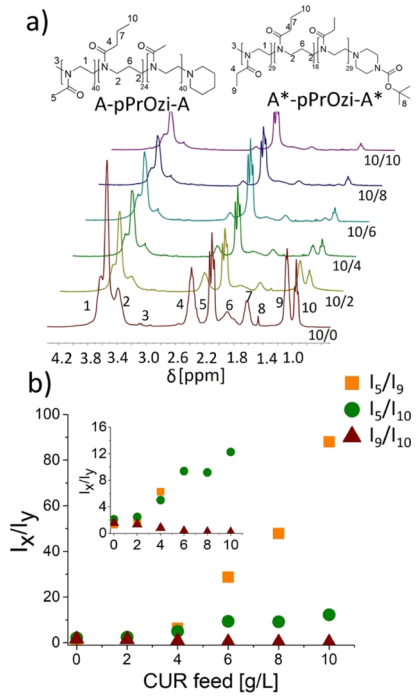

Figure 5. (a) ^{1}H NMR spectra (D_2O, 300 MHz, 298 K) with signal assignment and (b) NMR integral ratios (I_x/I_y) of mixture (1:1 w/w) A−pPrOzi−A/A*−pPrOzi−A*/CUR formulation as a function of the CUR feed (0−10 g L^{-1}). For better visibility, enlarged sections are added as insets.

https://dx.doi.org/10.1021/acsami.9b22495
ACS Appl. Mater. Interfaces 2020, 12, 24531−24543

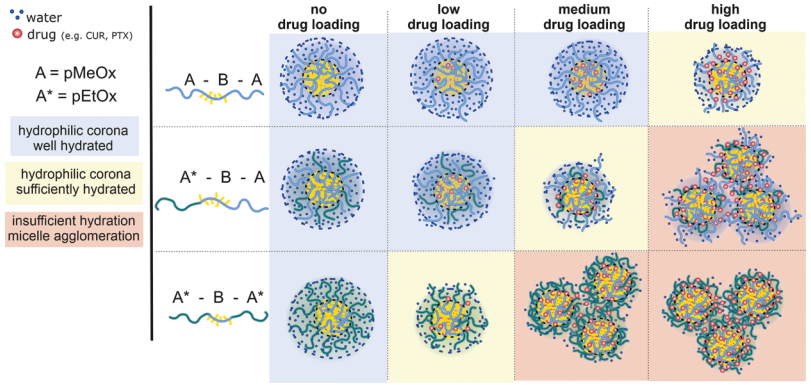

Figure 6. Schematic illustration of the effect of drug loading on the corona of drug-loaded micelles according to the corona composition. Without the added drug, pMeOx and pEtOx coronas are well hydrated. When the drug is added, it also interacts with polymer chains comprising the hydrophilic corona, reducing the hydration of the polymer chains. This apparently affects pEtOx chains more profoundly compared to pMeOx, which is more hydrophilic. While the polymer micelles featuring pMeOx coronas remain hydrated and colloidally stable even at high drug loading, the colloidal stability of pEtOx-bearing micelles is compromised a comparably low drug loading.

Comparing the spectra of the terpolymer A*−pPrOzi−A formulations (Figure 4) and those employing the mixture A*−pPrOzi−A*/A−pPrOzi−A (Figure 5) shows us in more detail the involvement of different moieties of the hydrophilic coronas and their interactions with CUR.

In the case of the A*−pPrOzi−A/CUR formulation (Figures 4a,b and S4), the increase in the integral ratio I_5/I_{10} (CH_3^{MeOx}/CH_3^{PrOzi}, red circles) again indicates the higher mobility of pMeOx compared to pPrOzi with the increasing CUR feed, whereas the integral ratio I_9/I_{10} (CH_3^{EtOx}/CH_3^{PrOzi}, blue triangles) did not change significantly (Figure 4b). This suggests that the mobility of EtOx and PrOzi units decreases in a similar manner, while MeOx remains more mobile. More interestingly, in the case of the A*−pPrOzi−A*/A−pPrOzi−A mixture, the integral ratio I_5/I_9 (CH_3^{MeOx}/CH_3^{EtOx}, orange squares) (Figures 5a,b and S4) increased much more than the ratio I_5/I_{10} (CH_3^{MeOx}/CH_3^{PrOzi}, green circles) with increasing drug content. The signal of the Boc-protected piperazine terminating reagent (signal 8) attached either at the pMeOx (A*−pPrOzi−A) or pEtOx (A*−pPrOzi−A*) block further corroborates this picture. While the signal remains clearly visible when attached to pMeOx (Figure 4a), it essentially vanishes already at low drug loading when attached to pEtOx (Figure 5a). It appears that a slightly lower hydration of the pEtOx shell compared to pMeOx is exacerbated with increased drug loading. The mobility of the hydrophilic pEtOx blocks suffers much more compared to pMeOx for both the terpolymer and the polymer mixture. Quantitatively, however, the increase in the ratio pMeOx side chain/pEtOx side chain with increasing drug feed was much lower in the case of the triblock terpolymer (Figure 4, black square) versus the triblock copolymer mixture (Figure 5, orange square), especially as the polymer/drug ratio exceeded 10/4 g L^{-1} and was 30 times higher at 10/10 g L^{-1} (Figure 5b, orange squares). The ^{1}H NMR analysis of the lyophilized supernatant in $CDCl_3$ revealed also the presence of both components of the mixture in the expected ratio up to the polymer/CUR feed of 10/4 g L^{-1} (Figure S52). Upon further increase in the CUR feed, the signal for the EtOx side chain (signal 9) starts to decrease but does not completely vanish even at a maximum CUR feed (10 g L^{-1}).

This profound loss in the pEtOx signal intensity can have two reasons. First, the pEtOx moieties become more solidlike because of strong interactions with CUR and loss of mobility and probably also segregate more toward the interior of the micelles. Second, the polymers in the mixture could undergo phase separation, and micelles that contain more pEtOx agglomerate/precipitate preferentially, which also let them appear more solidlike but also removes them from the analysis of the supernatant. To elucidate this, the precipitate of the A*−pPrOzi−A*/A−pPrOzi−A/CUR formulation was analyzed (after freeze-drying and dissolution in the nonselective solvent $CDCl_3$). Strikingly, the ^{1}H NMR analysis revealed exclusively A*−pPrOzi−A* and CUR (Figure S50). This means that the mixture indeed phase separates and A*−pPrOzi−A*/CUR precipitates, whereas micelles enriched in A−pPrOzi−A remain in solution. In contrast, in the case of the A*-pPrOzi-A terpolymer, pMeOx and pEtOx are covalently linked and cannot separate. The characteristic signal of the methyl group of pMeOx in the case of the A*−pPrOzi−A/CUR formulation is clearly distinguishable in the ^{1}H NMR spectrum (in $CDCl_3$ at 2 ppm) of the redissolved lyophilized agglomerate (Figure S51). It is therefore obvious that the increasing CUR feed leads to stronger interaction with A*−pPrOzi−A*, resulting in agglomeration of pure A*−pPrOzi−A*/CUR, whereas A−pPrOzi−A remains in solution and is available to solubilize CUR along with a few A*−pPrOzi−A* chains. However, it appears that CUR has much higher affinity for pEtOx as most of the added CUR is agglomerated with A*−pPrOzi−A*; therefore, CUR solubilized by A−pPrOzi−A did not increase with higher feeding ratio (Table S5). In the light of this, the formulation with an excessive CUR feed (polymer/CUR = 10/16 g L^{-1}) (Table S5) was also prepared and expected to saturate A*−pPrOzi−A*. However, no significant increase in solubilized CUR was observed. Again, the ^{1}H NMR analysis of the agglomerate (in $CDCl_3$) formed during formulation development showed the massive amount of CUR (polymer/CUR ≈ 5/12 w/w) (Figure S53), further indicating the concentration-dependent higher interaction of pEtOx with CUR than pMeOx.

Based on these results, we can build a tentative model of the micelle architecture with different hydrophilic coronas and drug loadings (Figure 6). At no or very low drug loading, no major difference is observable as the corona-forming polymers are well-hydrated and give excellent colloidal stability for the micelles. However, with increasing drug loading, pEtOx

https://dx.doi.org/10.1021/acsami.9b22495
ACS Appl. Mater. Interfaces 2020, 12, 24531−24543

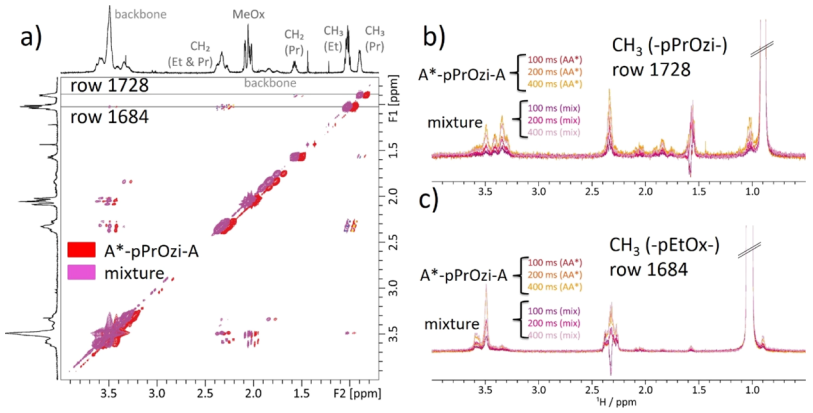

Figure 7. (a) Overlay of the ^{1}H−^{1}H NOESY spectra of CUR formulation based on A*−pPrOzi−A (terpolymer) (red) and the mixture of A−pPrOzi−A/A*−pPrOzi−A* (magenta) (1:1 w/w) with a CUR feed of 2 g L^{-1}, recorded with a mixing time of 100 ms. For easier comparison, the red spectrum is slightly shifted to the right. (b,c) Overlay of the slices from ^{1}H−^{1}H NOESY experiments at different mixing times extracted for the two spectral rows as indicated by the gray dashed lines in (a).

interacts stronger with the hydrophobic guest molecules, compromising its hydration and mobility. Upon further increase of drug loading, the A*−B−A* micelles undergo collapse of their hydrophilic corona and agglomerate/precipitate. In contrast, A*−B−A micelles still have hydrated pMeOx chains, stabilizing and solubilizing them at somewhat higher drug loading. However, eventually, its capacity is reached, and the A*−B−A micelles precipitate earlier than the A−B−A micelles containing only pMeOx, which remain colloidally stable even at ca. 50 wt %.

Diffusion and NOE Data. To support the findings based on the comparison of ^{1}H NMR and integrations as well as to gain more insights into the assembly of the micelles, ^{1}H diffusion ordered (DOSY) NMR spectroscopy was performed for formulations (polymer/CUR 10/2 g L^{-1}) based on four different setups of hydrophilic blocks, that is, A−pPrOzi−A, A*−pPrOzi−A, A*−pPrOzi−A*, and mixture (A*−pPrOzi−A*/A−pPrOzi−A). Please note that at this CUR feed, solubilization in all formulations was quantitative. From agreement of the diffusion coefficients for water (residual protonated solvent, HDO signal) and comparison between a stimulated BPP-LED pulse sequence (longitudinal eddy current delay sequence with bipolar gradient pulse pairs for diffusion and additional spoil gradients after the second and fourth 90° pulse) and a double stimulated echo pulse sequence for all four samples, differences in viscosity or convection effects could be excluded. The diffusion coefficients were determined by fitting the experimental diffusion data with a log normal function,[69] and the values are in comparable range for all four samples, indicating similar hydrodynamic radii (Table S10). From comparison of the averaged diffusion coefficients over the functional groups for each sample, the smallest value (and thus largest particles size) was observed for A*−pPrOzi−A* and increases in the order A*−pPrOzi−A ≈ polymer mixture < A−pPrOzi−A, which thus shows the smallest hydrodynamic volume. The individual diffusion coefficients for the moieties in the terpolymer and the polymer mixture do not differ in a significant or systematic way. This hints at the presence of mixed micelles for the polymer mixture at 10/2 drug loading. This was further supported by the direct comparison of the respective ^{1}H (Figure S54) and ^{1}H−^{1}H NOESY NMR spectra (Figure 7a). ^{1}H−^{1}H NOESY spectra were recorded with different mixing times d_8 = 50 (Figure S55), 100, 200, and 400 ms (Figure 7b,c). The similarity of the two NOESY spectra (Figure 7a) confirms that, for low CUR loading, the mixture formed mixed micelles. The cross-peaks observed in the spectra are largely identical. At strongly increased intensity, cross-peaks between the CH_3 groups of EtOx and the PrOzi fragments start to appear. As this cross-peak is very close to the intense diagonal signal, a series of NOESY spectra with increasing mixing time (100, 200, and 400 ms) were recorded. For each of these spectra, the rows 1728 and 1684 corresponding to the CH_3 groups of PrOzi and EtOx, respectively, were extracted (Figure 7b,c). For the overlay of these one-dimensional extracted slices, the spectra were scaled to equal height of the diagonal peak to compare the relative intensity of the cross-peak. CH_3^{PrOzi} indeed shows a cross-peak with the EtOx signal at 1.02 ppm, which increases with increasing mixing time. In fact, this cross-peak is observed for both the terpolymer (A*−pPrOzi−A) and the mixture. CH_3^{EtOx} also exhibits clearly visible cross-peaks to the adjacent CH_2 group and to the POx backbone but also a low intensity signal to the CH_2^{PrOzi} side chain at 1.57 ppm (Figure 7c).

Interestingly, for neither CH_3^{EtOx} nor CH_3^{PrOzi}, contact to MeOx at 2.05 ppm can be observed at 100 ms mixing time, and only a low intensity signal barely above the noise is detected for the two longer mixing times (200 and 400 ms). Presumably, this weak residual contact results from the direct connection of the polymer blocks. All NOESY data strongly suggest that while EtOx units are in close proximity of PrOzi units, the MeOx units remain more separated. This could be understood as a sign of increased core/corona separation because of the larger hydrophilicity/hydrophobicity contrast.

DLS and Cryo-TEM. To support the results from DOSY NMR spectroscopy, the polymer/CUR (10/2 g L^{-1}) formulations with four different setups of hydrophilic coronas (A*−pPrOzi−A*, A*−pPrOzi−A, A−pPrOzi−A, and mixture of A*−pPrOzi−A*/A−pPrOzi−A) were analyzed by DLS (at 90°). All tested aqueous formulations self-assemble to form micelles with the hydrodynamic radii (R_h) ranging between 12 and 15 nm (Figure S56a). At these subcritical concentrations, the formulations proved to be very stable. After eight months storage under ambient conditions, no precipitate could be observed by visible inspection, and no significant change in the size or size distribution was observed (Figure S56b). Previously, it was observed that A−pBuOx−A/PTX- and A−pPrOzi−A/CUR-based formulations (with polymer/drug feed of 10/2 and 10/3 g L^{-1}, respectively) exhibit R_h of 8 and 11

https://dx.doi.org/10.1021/acsami.9b22495
ACS Appl. Mater. Interfaces 2020, 12, 24531−24543

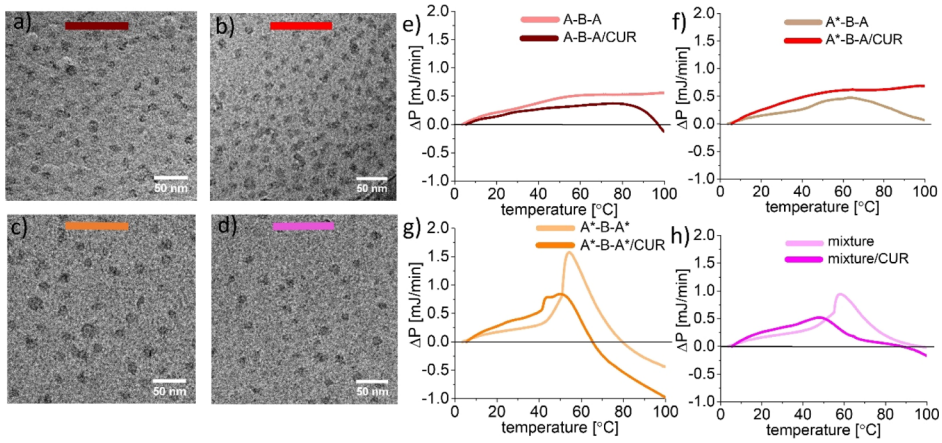

Figure 8. Cryo-TEM images of CUR formulations with four different setups of hydrophilic blocks. (a) A−pPrOzi−A (brown), (b) A*−pPrOzi−A (red), (c) A*−pPrOzi−A* (orange), and (d) mixture (magenta) (A−pPrOzi−A/A*−pPrOzi−A* 1:1 w/w) at 10/2 g L^{-1} polymer/CUR feed (A* = pEtOx and A = pMeOx). Raw microcalorimetry heating curves (e−h) obtained for plain polymers and their respective CUR formulations (10/2 g L^{-1}) with four different setups of hydrophilic blocks (with heating rate of 60 °C/h). ΔP represents the measured heat flow difference, the difference between the sample solution and the solvent reference (DI water) (n = 1).

nm, respectively.[9,10] In short, at a CUR feed of 2 g L^{-1}, where all employed CUR formulations were colloidally stable, no significant differences in the size of the micelles were observed for different hydrophilic coronas. The freshly prepared similar samples were also imaged by cryo-TEM to get better insight into the morphology of the micelles. At first glance, all four samples (polymer/CUR 10/2 g L^{-1}) (Figure 8a−d) present as small fairly spherical assemblies with an apparent diameter of 13−16 nm. In contrast, cryo-TEM images of A−pBuOx−A/PTX formulations that exhibited a more electron-dense core with a less dense, presumably better hydrated pMeOx corona appeared as gray haloes,[9] and the pPrOzi-based polymers and CUR formulation appeared as fairly uniform spheres with no clearly discernible internal structure. For comparison, a similar morphology was observed by Bacher et al. for celecoxib-loaded casein micelles.[70] Lübtow et al. found that both at higher (10/8 g L^{-1}) and lower drug loadings (10/3 g L^{-1}), spherical and wormlike structures coexist for the A−pPrOzi−A/CUR formulation, whereas in this case, utilizing a different polymer batch, the A−pPrOzi−A/CUR formulation at 10/2 g L^{-1} presents only as rather spherical assemblies.[10] It can be concluded that the factors such as the composition of an amphiphile including hydrophilic and hydrophobic blocks, the chain length of each block, and the nature and concentration of the drug[4,10] can significantly impact the self-assembly process resulting in defined architectures.

Microcalorimetry Studies (Micro-DSC). Differences in hydration of the hydrophilic corona may exacerbate with increasing temperature. Therefore, microcalorimetric studies were conducted for pure polymers with four different setups of hydrophilic corona and their respective CUR formulations (polymer/CUR 10/2 g L^{-1}). Samples were heated from 5 to 100 °C with a heating rate of 60 °C/h, and the heat flow difference (ΔP) between the reference [deionized (DI) water] and the sample was recorded (Figure 8e−h). Clearly, in all cases, the pure polymers showed distinct thermograms when compared to their respective CUR formulations. The thermogram of A−B−A plain polymer did not show any evidence of thermal transition up to the measured temperature of 100 °C (Figure 8e). Interestingly, A−pPrOzi−A/CUR formulations showed a sharp decrease in the ΔP value above 80 °C, probably due to the interaction of CUR with the pMeOx hydrophilic block in A−pPrOzi−A, which decreases the pMeOx strength in the interaction with water, leading to a loss of hydration and a decrease in the ΔP value. In the case of the A*−pPrOzi−A plain terpolymer (Figure 8f), a thermal transition was observed around 60 °C. In contrast, for the A*−pPrOzi−A/CUR formulation, no evidence of any transition was observed. Besides pMeOx, pEtOx is also present as a hydrophilic block in the A*−pPrOzi−A terpolymer. Because of the higher affinity of pEtOx to CUR compared to pMeOx, pMeOx hydration is not affected at this loading, and the system does not undergo any thermal transition. This further corroborates the results from NMR experiments showing the preferential condensation and dehydration of the pEtOx over pMeOx blocks upon CUR addition. Most interestingly, the pure A*−pPrOzi−A* polymer showed a sharp thermal transition around 60 °C, with the highest ΔP value followed by negative ΔP around 80 °C (Figure 8g). This indicates the dehydration and reorganization of relatively less hydrophilic pEtOx blocks at 60 °C, followed by polymer precipitation around 80 °C. Similarly, A*−pPrOzi−A*/CUR formulations show the most pronounced thermal transition and profound negative ΔP values above 60 °C. Notably, A*−pPrOzi−A*/CUR was the only formulation in this series that showed macroscopic agglomeration and precipitation at this loading with increased temperature, which is in line with the strong negative values of ΔP. Notably, the observed bimodal peak supports the idea that the pEtOx corona dehydrates. Such bimodality maybe attributed to the dynamics/kinetics of the transition of the chains in the micellar corona. Such behavior has been reported for core−shell particles and was found to be more pronounced for thermoresponsive polymers of higher molar mass in the corona[71] or the reorganization of the polymer in the corona. It should be noted that the cooling curves of A−pPrOzi−A/A*−pPrOzi−A*/CUR formulations also showed this bimodality (Figure S57).

Unexpectedly, the thermogram of the A−pPrOzi−A/A*−pPrOzi−A* mixture (Figure 8h) showed close resemblance to the pure A*−pPrOzi−A* polymer (Figure 8g) and an entirely different picture compared to A*−pPrOzi−A (Figure 8f), although they comprise the same building blocks. Most interestingly, the mixture of the A−pPrOzi−A/A*−pPrOzi−A*/CUR formulation showed an entirely different picture

https://dx.doi.org/10.1021/acsami.9b22495
ACS Appl. Mater. Interfaces 2020, 12, 24531−24543

from the terpolymer/CUR formulation. Initially, the obtained curves are similar, but in the temperature range of 36−60 °C, a small but distinct peak is observed in the case of the mixture/CUR formulation (Figure 8h). We attribute this thermal transition to the dehydration of predominantly pEtOx chains interacting with CUR and concomitant reorganization of the hydrophilic corona. In contrast to the situation with the terpolymer A*−pPrOzi−A formulation, the mixture/CUR formulation can undergo phase separation, which is in fact observed at higher drug loading as previously discussed. At this lower loading, during the measurement, the phase separation is induced by the increase in temperature. In addition, at a very high temperature, the microcalorimetric trace of the mixture/CUR formulation resembles the trace for the A−pPrOzi−A/CUR formulation, suggesting also in the mixture that CUR remains to some extent in the corona of A−pPrOzi−A micelles and decrease pMeOx hydration. Again, this corroborates the data obtained by ^{1}H NMR for higher loading of CUR.

SUMMARY

In summary, it is shown conclusively using a range of complementary analytical tools that the hydrophilic corona of polymer micelles plays a decisive role in the solubilization of hydrophobic cargo. Already a minor change in the hydrophilic block of a polymer amphiphile (pMeOx vs pEtOx vs pMeOx/pEtOx) can have a significant impact on the drug loading and/or colloidal stability of the micelles. These findings further suggest that a simple core−shell architecture, where the core incorporates the drug and the corona stabilizes the micelle, can be an oversimplification. Clearly, the nature of the hydrophobic block and the guest molecule (exemplified here with CUR and PTX) are not the only determinants, and more scrutiny must be applied to the interactions between cargo and hydrophilic corona. These interactions can affect the system in various ways, which can ultimately modulate the physicochemical properties of nanocarriers. In fact, the highly unusual ultrahigh drug loading now well-established for POx-based micelles is apparently in part possible because of the choice of the hydrophilic pMeOx. These results shed new light and give clearer instructions on how to design and optimize drug-delivery systems and polymeric excipients in general. Considering that the vast majority of drug-delivery systems contain PEG as a hydrophilic polymer, which is very similar to pEtOx in its amphiphilicity, a question can be raised whether the limited drug loading of PMs found in the literature may be strongly correlated with the choice of PEG as the hydrophilic polymer. In addition, our finding may also suggest that major differences in the interaction between different hydrophilic polymers and drugs in polymer−drug conjugates or even polymer−protein conjugates can be expected, just as it has been observed for lipopolymers and how they interact with lipid bilayers.[72]

ASSOCIATED CONTENT

Supporting Information

The Supporting Information is available free of charge at https://pubs.acs.org/doi/10.1021/acsami.9b22495.

Materials and methods, NMR spectroscopy and GPC studies, dialysis, synthesis, DSC, TGA, and fluorescence spectroscopy studies, drug formulation by the thin-film method, drug quantification, UV−vis spectroscopy, LC and LE calculations, formulation with RD, NMR studies, DOSY, NOESY, DLS, and cryo-TEM measurements, and micro-DSC studies (PDF)

AUTHOR INFORMATION

Corresponding Author

Robert Luxenhofer − *Functional Polymer Materials, Chair for Chemical Technology of Material Synthesis and Bavarian Polymer Institute, Faculty of Chemistry and Pharmacy, University of Würzburg, 97070 Würzburg, Germany; Department of Chemistry, University of Helsinki, Helsinki FIN-00014, Finland;* orcid.org/0000-0001-5567-7404; Email: robert.luxenhofer@uni-wuerzburg.de, robert.luxenhofer@helsinki.fi

Authors

Malik Salman Haider − *Functional Polymer Materials, Chair for Chemical Technology of Material Synthesis and Bavarian Polymer Institute, Faculty of Chemistry and Pharmacy, University of Würzburg, 97070 Würzburg, Germany*

Michael M. Lübtow − *Functional Polymer Materials, Chair for Chemical Technology of Material Synthesis and Bavarian Polymer Institute, Faculty of Chemistry and Pharmacy, University of Würzburg, 97070 Würzburg, Germany*

Sebastian Endres − *Institute of Organic Chemistry, Faculty of Chemistry and Pharmacy, University of Würzburg, 97074 Würzburg, Germany*

Stefan Forster − *Functional Polymer Materials, Chair for Chemical Technology of Material Synthesis and Bavarian Polymer Institute, Faculty of Chemistry and Pharmacy, University of Würzburg, 97070 Würzburg, Germany*

Vanessa J. Flegler − *Biocenter and Rudolf Virchow Centre, University of Würzburg, 97080 Würzburg, Germany*

Bettina Böttcher − *Biocenter and Rudolf Virchow Centre, University of Würzburg, 97080 Würzburg, Germany;* orcid.org/0000-0002-7962-4849

Vladimir Aseyev − *Department of Chemistry, University of Helsinki, Helsinki FIN-00014, Finland*

Ann-Christin Pöppler − *Institute of Organic Chemistry, Faculty of Chemistry and Pharmacy, University of Würzburg, 97074 Würzburg, Germany;* orcid.org/0000-0002-0624-1708

Complete contact information is available at: https://pubs.acs.org/10.1021/acsami.9b22495

Author Contributions

M.S.H. and R.L. designed overall study, M.S.H. and M.M.L. carried out polymer synthesis and characterization as well as formulation preparation and characterization. M.S.H, S.E. and A.-C.P. performed NMR spectroscopy experiments and their analysis. S.F., V.J.F. and B.B. carried out electron microscopy and analyzed data, V.A. carried out micro-DSC experiments and analysis. M.S.H and R.L. composed manuscript with the help of all authors.

Notes

The authors declare the following competing financial interest(s): M.M.L. and R.L. are listed as inventors on a patent application pertinent to some of the materials discussed in this contribution. R.L. is co-founder and has a financial interest in DelAqua Pharmaceuticals Inc. which is intent on commercializing poly(2-oxazoline) based excipients.

https://dx.doi.org/10.1021/acsami.9b22495
ACS Appl. Mater. Interfaces 2020, 12, 24531−24543

■ ACKNOWLEDGMENTS

This work was supported by Deutsche Forschungsgemeinschaft (DFG, project no. 398461692 awarded to R.L.). Moreover, M.S.H. and M.M.L. are grateful to the Higher Education Commission of Pakistan and German academic exchange services (HEC-DAAD Pakistan) (M.S.H.) and Evonik Foundation (M.M.L.), respectively, for the PhD scholarships. Financial support from the Fonds der Chemischen Industrie (FCI) in the form of a material cost allowance is acknowledged (A.-C. P.). We thank Lukas Hahn and Dr. Matthias Grüne for valuable discussion.

■ REFERENCES

(1) Wang, E.; Lu, J.; Bates, F. S.; Lodge, T. P. Effect of Corona Block Length on the Structure and Chain Exchange Kinetics of Block Copolymer Micelles. *Macromolecules* **2018**, *51*, 3563−3571.

(2) García Daza, F. A.; Colville, A. J.; Mackie, A. D. Chain architecture and micellization: A mean-field coarse-grained model for poly (ethylene oxide) alkyl ether surfactants. *J. Chem. Phys.* **2015**, *142*, 114902−114910.

(3) Li, T.; Zhang, J.; Schneiderman, D. K.; Francis, L. F.; Bates, F. S. Toughening glassy poly (lactide) with block copolymer micelles. *ACS Macro Lett.* **2016**, *5*, 359−364.

(4) Cao, C.; Zhao, J.; Chen, F.; Lu, M.; Khine, Y. Y.; Macmillan, A.; Garvey, C. J.; Stenzel, M. H. Drug-Induced Morphology Transition of Self-Assembled Glycopolymers: Insight into the Drug−Polymer Interaction. *Chem. Mater.* **2018**, *30*, 5227−5236.

(5) Adair, J. H.; Parette, M. P.; Altınoğlu, E. İ.; Kester, M. Nanoparticulate alternatives for drug delivery. *ACS Nano* **2010**, *4*, 4967−4970.

(6) Kozlov, M. Y.; Melik-Nubarov, N. S.; Batrakova, E. V.; Kabanov, A. V. Relationship between pluronic block copolymer structure, critical micellization concentration and partitioning coefficients of low molecular mass solutes. *Macromolecules* **2000**, *33*, 3305−3313.

(7) Lu, W.; Li, F.; Mahato, R. I. Poly (ethylene glycol)-block-poly (2-methyl-2-benzoxycarbonyl-propylene carbonate) micelles for rapamycin delivery: in vitro characterization and biodistribution. *J. Pharm. Sci.* **2011**, *100*, 2418−2429.

(8) Guo, X. D.; Qian, Y.; Zhang, C. Y.; Nie, S. Y.; Zhang, L. J. Can drug molecules diffuse into the core of micelles? *Soft Matter* **2012**, *8*, 9989−9995.

(9) Schulz, A.; Jaksch, S.; Schubel, R.; Wegener, E.; Di, Z.; Han, Y.; Meister, A.; Kressler, J.; Kabanov, A. V.; Luxenhofer, R.; Papadakis, C. M.; Jordan, R. Drug-induced morphology switch in drug delivery systems based on poly (2-oxazoline)s. *ACS Nano* **2014**, *8*, 2686−2696.

(10) Lübtow, M. M.; Nelke, L. C.; Seifert, J.; Kühnemundt, J.; Sahay, G.; Dandekar, G.; Nietzer, S. L.; Luxenhofer, R. Drug induced micellization into ultra-high capacity and stable curcumin nanoformulations: Physico-chemical characterization and evaluation in 2D and 3D in vitro models. *J. Controlled Release* **2019**, *303*, 162−180.

(11) Wiest, J.; Saedtler, M.; Böttcher, B.; Grüne, M.; Reggane, M.; Galli, B.; Holzgrabe, U.; Meinel, L. Geometrical and structural dynamics of Imatinib within biorelevant colloids. *Mol. Pharm.* **2018**, *15*, 4470−4480.

(12) Cabral, H.; Matsumoto, Y.; Mizuno, K.; Chen, Q.; Murakami, M.; Kimura, M.; Terada, Y.; Kano, M. R.; Miyazono, K.; Uesaka, M.; et al. Accumulation of sub-100 nm polymeric micelles in poorly permeable tumours depends on size. *Nat. Nanotechnol.* **2011**, *6*, 815−823.

(13) Win, K. Y.; Feng, S.-S. Effects of particle size and surface coating on cellular uptake of polymeric nanoparticles for oral delivery of anticancer drugs. *Biomaterials* **2005**, *26*, 2713−2722.

(14) Li, Z.; Lenk, T. I.; Yao, L. J.; Bates, F. S.; Lodge, T. P. Maintaining hydrophobic drug supersaturation in a micelle corona reservoir. *Macromolecules* **2018**, *51*, 540−551.

(15) Gref, R.; Domb, A.; Quellec, P.; Blunk, T.; Müller, R. H.; Verbavatz, J. M.; Langer, R. The controlled intravenous delivery of drugs using PEG-coated sterically stabilized nanospheres. *Adv. Drug Delivery Rev.* **1995**, *16*, 215−233.

(16) Diao, L. H.; Fu, H. M.; Hu, Y.; Jiang, T.; Wei, C. D.; Gao, J. Doxorubicin-loaded PEG-PCL copolymer micelles enhance cytotoxicity and intracellular accumulation of doxorubicin in adriamycin-resistant tumor cells. *Int. J. Nanomed.* **2011**, *6*, 1955−1963.

(17) Sill, K. N.; Sullivan, B.; Carie, A.; Semple, J. E. Synthesis and Characterization of Micelle-Forming PEG-Poly (Amino Acid) Copolymers with Iron-Hydroxamate Cross-Linkable Blocks for Encapsulation and Release of Hydrophobic Drugs. *Biomacromolecules* **2017**, *18*, 1874−1884.

(18) Barz, M.; Luxenhofer, R.; Zentel, R.; Vicent, M. J. Overcoming the PEG-addiction: well-defined alternatives to PEG, from structure−property relationships to better defined therapeutics. *Polym. Chem.* **2011**, *2*, 1900−1918.

(19) Schellekens, H.; Hennink, W. E.; Brinks, V. The immunogenicity of polyethylene glycol: facts and fiction. *Pharm. Res.* **2013**, *30*, 1729−1734.

(20) Thomas, A.; Müller, S. S.; Frey, H. Beyond poly (ethylene glycol): linear polyglycerol as a multifunctional polyether for biomedical and pharmaceutical applications. *Biomacromolecules* **2014**, *15*, 1935−1954.

(21) Bloksma, M. M.; Paulus, R. M.; van Kuringen, H. P. C.; van der Woerdt, F.; Lambermont-Thijs, H. M. L.; Schubert, U. S.; Hoogenboom, R. Thermoresponsive Poly(2-oxazine)s. *Macromol. Rapid Commun.* **2012**, *33*, 92−96.

(22) Klein, T.; Parkin, J.; Jongh, P. A. J. M.; Esser, L.; Sepehrizadeh, T.; Zheng, G.; Veer, M.; Alt, K.; Hagemeyer, C. E.; Haddleton, D. M.; et al. Functional Brush Poly(2-ethyl-2-oxazine)s: Synthesis by CROP and RAFT, Thermoresponsiveness and Grafting onto Iron Oxide Nanoparticles. *Macromol. Rapid Commun.* **2019**, *40*, 1800911−1800917.

(23) Morgese, G.; Verbraeken, B.; Ramakrishna, S. N.; Gombert, Y.; Cavalli, E.; Rosenboom, J. G.; Zenobi-Wong, M.; Spencer, N. D.; Hoogenboom, R.; Benetti, E. M. Chemical Design of Non-Ionic Polymer Brushes as Biointerfaces: Poly (2-oxazine) s Outperform Both Poly (2-oxazoline) s and PEG. *Angew. Chem.* **2018**, *57*, 11667−11672.

(24) Lorson, T.; Jaksch, S.; Lübtow, M. M.; Jüngst, T.; Groll, J.; Lühmann, T.; Luxenhofer, R. A thermogelling supramolecular hydrogel with sponge-like morphology as a cytocompatible bioink. *Biomacromolecules* **2017**, *18*, 2161−2171.

(25) Lorson, T.; Lübtow, M. M.; Wegener, E.; Haider, M. S.; Borova, S.; Nahm, D.; Jordan, R.; Sokolski-Papkov, M.; Kabanov, A. V.; Luxenhofer, R. Poly (2-oxazoline) s based biomaterials: A comprehensive and critical update. *Biomaterials* **2018**, *178*, 204−280.

(26) Lübtow, M. M.; Marciniak, H.; Schmiedel, A.; Roos, M.; Lambert, C.; Luxenhofer, R. Ultra-high to ultra-low drug loaded micelles: Probing host-guest interactions by fluorescence spectroscopy. *Chem.—Eur. J.* **2019**, *25*, 12601−12610.

(27) Lübtow, M. M.; Oerter, S.; Quader, S.; Jeanclos, E.; Cubukova, A.; Krafft, M.; Haider, M. S.; Schulte, C.; Meier, L.; Rist, M.; et al. In vitro blood-brain-barrier permeability and cytotoxicity of atorvastatin-loaded nanoformulation against glioblastoma in 2D and 3D models. *Mol. Pharm.* **2020**, DOI: 10.1021/acs.molpharmaceut.9b01117.

(28) Salgarella, A. R.; Zahoranová, A.; Šrámková, P.; Majerčíková, M.; Pavlova, E.; Luxenhofer, R.; Kronek, J.; Lacík, I.; Ricotti, L. Investigation of drug release modulation from poly (2-oxazoline) micelles through ultrasound. *Sci. Rep.* **2018**, *8*, 9893.

(29) Seo, Y.; Schulz, A.; Han, Y.; He, Z.; Bludau, H.; Wan, X.; Tong, J.; Bronich, T. K.; Sokolsky, M.; Luxenhofer, R.; et al. Poly (2-oxazoline) block copolymer based formulations of taxanes: effect of copolymer and drug structure, concentration, and environmental factors. *Polym. Adv. Technol.* **2015**, *26*, 837−850.

(30) Han, Y.; He, Z.; Schulz, A.; Bronich, T. K.; Jordan, R.; Luxenhofer, R.; Kabanov, A. V. Synergistic combinations of multiple

chemotherapeutic agents in high capacity poly(2-oxazoline) micelles. *Mol. Pharm.* **2012**, *9*, 2302−2313.
(31) Luxenhofer, R.; Schulz, A.; Roques, C.; Li, S.; Bronich, T. K.; Batrakova, E. V.; Jordan, R.; Kabanov, A. V. Doubly amphiphilic poly(2-oxazoline)s as high-capacity delivery systems for hydrophobic drugs. *Biomaterials* **2010**, *31*, 4972−4979.
(32) He, Z.; Schulz, A.; Wan, X.; Seitz, J.; Bludau, H.; Alakhova, D. Y.; Darr, D. B.; Perou, C. M.; Jordan, R.; Ojima, I.; et al. Poly(2-oxazoline) based micelles with high capacity for 3rd generation taxoids: Preparation, in vitro and in vivo evaluation. *J. Controlled Release* **2015**, *208*, 67−75.
(33) He, Z.; Wan, X.; Schulz, A.; Bludau, H.; Dobrovolskaia, M. A.; Stern, S. T.; Montgomery, S. A.; Yuan, H.; Li, Z.; Alakhova, D.; et al. A high capacity polymeric micelle of paclitaxel: Implication of high dose drug therapy to safety and in vivo anti-cancer activity. *Biomaterials* **2016**, *101*, 296−309.
(34) Paál, K.; Müller, J.; Hegedûs, L. High affinity binding of paclitaxel to human serum albumin. *Eur. J. Biochem.* **2001**, *268*, 2187−2191.
(35) Wan, X.; Min, Y.; Bludau, H.; Keith, A.; Sheiko, S. S.; Jordan, R.; Wang, A. Z.; Sokolsky-Papkov, M.; Kabanov, A. V. Drug Combination Synergy in worm-like Polymeric Micelles Improves Treatment Outcome for Small Cell and Non-Small Cell Lung Cancer. *ACS Nano* **2018**, *12*, 2426−2439.
(36) Zinger, A.; Koren, L.; Adir, O.; Poley, M.; Alyan, M.; Yaari, Z.; Noor, N.; Krinsky, N.; Simon, A.; Gibori, H.; Krayem, M.; et al. Collagenase nanoparticles enhance the penetration of drugs into pancreatic tumors. *ACS Nano* **2019**, *13*, 11008−11021.
(37) Ma, P.; Mumper, R. J. Paclitaxel nano-delivery systems: a comprehensive review. *J. Nanomed. Nanotechnol.* **2013**, *4*, 1000164.
(38) Esatbeyoglu, T.; Huebbe, P.; Ernst, I. M. A.; Chin, D.; Wagner, A. E.; Rimbach, G. Curcumin—from molecule to biological function. *Angew. Chem.* **2012**, *51*, 5308−5332.
(39) Naksuriya, O.; Okonogi, S.; Schiffelers, R. M.; Hennink, W. E. Curcumin nanoformulations: a review of pharmaceutical properties and preclinical studies and clinical data related to cancer treatment. *Biomaterials* **2014**, *35*, 3365−3383.
(40) Baell, J. B. Feeling nature's PAINS: natural products, natural product drugs, and pan assay interference compounds (PAINS). *J. Nat. Prod.* **2016**, *79*, 616−628.
(41) Lübtow, M. M.; Haider, M. S.; Kirsch, M.; Klisch, S.; Luxenhofer, R. Like Dissolves Like? A Comprehensive Evaluation of Partial Solubility Parameters to Predict Polymer-Drug Compatibility in Ultra-High Drug Loaded Polymer Micelles. *Biomacromolecules* **2019**, *20*, 3041−3056.
(42) Haider, M. S.; Schreiner, J.; Kendl, S.; Kroiss, M.; Luxenhofer, R. A Micellar Mitotane Formulation with High Drug-Loading and Solubility: Physico-Chemical Characterization and Cytotoxicity Studies in 2D and 3D In Vitro Tumor Models. *Macromol. Biosci.* **2020**, *20*, 1900178.
(43) Lübtow, M. M.; Hahn, L.; Haider, M. S.; Luxenhofer, R. Drug specificity, synergy and antagonism in ultrahigh capacity poly(2-oxazoline)/poly(2-oxazine) based formulations. *J. Am. Chem. Soc.* **2017**, *139*, 10980−10983.
(44) Alves, V. M.; Hwang, D.; Muratov, E.; Sokolsky-Papkov, M.; Varlamova, E.; Vinod, N.; Lim, C.; Andrade, C. H.; Tropsha, A.; Kabanov, A. V. Cheminformatics-driven discovery of polymeric micelle formulations for poorly soluble drugs. *Sci. Adv.* **2019**, *5*, No. eaav9784.
(45) Pöppler, A. C.; Lübtow, M. M.; Schlauersbach, J.; Wiest, J.; Meinel, L.; Luxenhofer, R. Loading-Dependent Structural Model of Polymeric Micelles Encapsulating Curcumin by Solid-State NMR Spectroscopy. *Angew. Chem.* **2019**, *58*, 18540−18546.
(46) Grüne, M.; Luxenhofer, R.; Iuga, D.; Brown, S. P.; Pöppler, A.-C.; $^{14}N-^{1}H$ HMQC solid-state NMR Investigation of Amorphous PTX Formulations. *J. Mat. Chem. B*, **2020**, accepted.
(47) Sochor, B.; Düdükcü, Ö.; Lübtow, M. M.; Schummer, B.; Jaksch, S.; Luxenhofer, R. Probing the Complex Loading Dependent Structural Changes in Ultra-High Drug Loaded Polymer Micelles by Small-Angle Neutron Scattering. *Langmuir* **2020**, *36*, 3494−3503.
(48) Geisel, K.; Rudov, A. A.; Potemkin, I. I.; Richtering, W. Hollow and core−shell microgels at oil−water interfaces: Spreading of soft particles reduces the compressibility of the monolayer. *Langmuir* **2015**, *31*, 13145−13154.
(49) Witte, H.; Seeliger, W. Cyclische imidsäureester aus nitrilen und aminoalkoholen. *Leibigs Ann.* **1974**, *1974*, 996−1009.
(50) Yu, Y.; Chen, C.-K.; Law, W.-C.; Weinheimer, E.; Sengupta, S.; Prasad, P. N.; Cheng, C. Polylactide-graft-doxorubicin nanoparticles with precisely controlled drug loading for pH-triggered drug delivery. *Biomacromolecules* **2014**, *15*, 524−532.
(51) Cheetham, A. G.; Zhang, P.; Lin, Y.-a.; Lock, L. L.; Cui, H. Supramolecular nanostructures formed by anticancer drug assembly. *J. Am. Chem. Soc.* **2013**, *135*, 2907−2910.
(52) Maksimenko, A.; Dosio, F.; Mougin, J.; Ferrero, A.; Wack, S.; Reddy, L. H.; Weyn, A.-A.; Lepeltier, E.; Bourgaux, C.; Stella, B. A unique squalenoylated and nonpegylated doxorubicin nanomedicine with systemic long-circulating properties and anticancer activity. *Proc. Natl. Acad. Sci. U.S.A.* **2014**, *111*, E217−E226.
(53) Raveendran, R.; Mullen, K. M.; Wellard, R. M.; Sharma, C. P.; Hoogenboom, R.; Dargaville, T. R. Poly (2-oxazoline) block copolymer nanoparticles for curcumin loading and delivery to cancer cells. *Eur. Polym. J.* **2017**, *93*, 682−694.
(54) Lübtow, M. M.; Keßler, L.; Appelt Menzel, A.; Lorson, T.; Gangloff, N.; Kirsch, M.; Dahms, S.; Luxenhofer, R. More is sometimes less: curcumin and paclitaxel formulations using Poly (2-oxazoline) and Poly (2-oxazine)-based amphiphiles bearing linear and branched C9 side chains. *Macromol. Biosci.* **2018**, *18*, 1800155.
(55) Liggins, R. T.; Hunter, W. L.; Burt, H. M. Solid-state characterization of paclitaxel. *J. Pharm. Sci.* **1997**, *86*, 1458−1463.
(56) Patra, D.; Barakat, C. Synchronous fluorescence spectroscopic study of solvatochromic curcumin dye. *Spectrochim. Acta, Part A* **2011**, *79*, 1034−1041.
(57) Hoogenboom, R.; Schlaad, H. Thermoresponsive poly (2-oxazoline) s, polypeptoids, and polypeptides. *Polym. Chem.* **2017**, *8*, 24−40.
(58) Lin, P.; Clash, C.; Pearce, E. M.; Kwei, T. K.; Aponte, M. A. Solubility and miscibility of poly(ethyl oxazoline). *J. Polym. Sci., Part B: Polym. Phys.* **1988**, *26*, 603−619.
(59) Hoogenboom, R.; Thijs, H. M. L.; Jochems, M. J. H. C.; van Lankvelt, B. M.; Fijten, M. W. M.; Schubert, U. S. Tuning the LCST of poly(2-oxazoline)s by varying composition and molecular weight: alternatives to poly (N-isopropylacrylamide)? *Chem. Commun.* **2008**, *44*, 5758−5760.
(60) Li, B.; Konecke, S.; Wegiel, L. A.; Taylor, L. S.; Edgar, K. J. Both solubility and chemical stability of curcumin are enhanced by solid dispersion in cellulose derivative matrices. *Carbohydr. Polym.* **2013**, *98*, 1108−1116.
(61) Paradkar, A.; Ambike, A. A.; Jadhav, B. K.; Mahadik, K. R. Characterization of curcumin−PVP solid dispersion obtained by spray drying. *Int. J. Pharm.* **2004**, *271*, 281−286.
(62) Bender, J. C. M. E.; Hoogenboom, R.; Van Vliet, P. A. A. Drug Delivery System Comprising Polyoxazoline and a Bioactive Agent. WO 2011002285 A1, 2014.
(63) Hernandez-Patlan, D.; Solis-Cruz, B.; Pontin, K. P.; Latorre, J. D.; Baxter, M. F. A.; Hernandez-Velasco, X.; Merino-Guzman, R.; Méndez-Albores, A.; Hargis, B. M.; Lopez-Arellano, R. Evaluation of a solid dispersion of curcumin with polyvinylpyrrolidone and boric acid against Salmonella Enteritidis infection and intestinal permeability in broiler chickens: A pilot study. *Front. Microbiol.* **2018**, *9*, 1289.
(64) Grube, M.; Leiske, M. N.; Schubert, U. S.; Nischang, I. POx as an alternative to PEG? A hydrodynamic and light scattering study. *Macromolecules* **2018**, *51*, 1905−1916.
(65) Morgese, G.; Gombert, Y.; Ramakrishna, S. N.; Benetti, E. M. Mixing Poly (ethylene glycol) and Poly (2-alkyl-2-oxazoline) s Enhances Hydration and Viscoelasticity of Polymer Brushes and Determines Their Nanotribological and Antifouling Properties. *ACS Appl. Mater. Interfaces* **2018**, *10*, 41839−41848.

https://dx.doi.org/10.1021/acsami.9b22495
ACS Appl. Mater. Interfaces 2020, 12, 24531−24543

(66) Reichardt, C. Solvatochromic dyes as solvent polarity indicators. *Chem. Rev.* **1994**, *94*, 2319−2358.
(67) Cerón-Carrasco, J. P.; Jacquemin, D.; Laurence, C.; Planchat, A.; Reichardt, C.; Sraïdi, K. Solvent polarity scales: determination of new ET (30) values for 84 organic solvents. *J. Phys. Org. Chem.* **2014**, *27*, 512−518.
(68) de Graaf, A. J.; Boere, K. W. M.; Kemmink, J.; Fokkink, R. G.; van Nostrum, C. F.; Rijkers, D. T. S.; van der Gucht, J.; Wienk, H.; Baldus, M.; Mastrobattista, E.; Vermonden, T.; Hennink, W. E. Looped structure of flowerlike micelles revealed by 1H NMR relaxometry and light scattering. *Langmuir* **2011**, *27*, 9843−9848.
(69) Guo, X.; Laryea, E.; Wilhelm, M.; Luy, B.; Nirschl, H.; Guthausen, G. Diffusion in Polymer Solutions: Molecular Weight Distribution by PFG-NMR and Relation to SEC. *Macromol. Chem. Phys.* **2017**, *218*, 1600440−1600450.
(70) Bachar, M.; Mandelbaum, A.; Portnaya, I.; Perlstein, H.; Even-Chen, S.; Barenholz, Y.; Danino, D. Development and characterization of a novel drug nanocarrier for oral delivery, based on self-assembled β-casein micelles. *J. Controlled Release* **2012**, *160*, 164−171.
(71) Shan, J.; Chen, J.; Nuopponen, M.; Tenhu, H. Two phase transitions of poly (N-isopropylacrylamide) brushes bound to gold nanoparticles. *Langmuir* **2004**, *20*, 4671−4676.
(72) Magarkar, A.; Róg, T.; Bunker, A. A computational study suggests that replacing PEG with PMOZ may increase exposure of hydrophobic targeting moiety. *Eur. J. Pharm. Sci.* **2017**, *103*, 128−135.

https://dx.doi.org/10.1021/acsami.9b22495
ACS Appl. Mater. Interfaces 2020, 12, 24531−24543

4.6 Therapeutic Potential of Poly(2-oxazoline)s and Poly(2-oxazine)s based Micellar Formulations

In this project we have also investigated the therapeutic potential of selective POx/POzi based formulation. Among the library of 21 drugs, the mitotane (MT) and BT-44 formulations were investigated in more detail.

Summary: MT is the drug of choice and only possible pharmaceutical intervention for adrenocortical carcinoma (ACC) and has an extremely low aqueous solubility of 0.0001 g/L. More importantly, using the current, approved clinical dosage form (lysodren tablets 500 mg), it is very difficult to achieve the necessary plasma concentration even at the very high dosage regimen (6 - 12 tablets/day) administered for months. The problem is a combination of poor aqueous solubility, low oral bioavailability and unpredictable pharmacokinetic (PK) profile. In this regard, we have presented for the first time (as a review article), the idea of injectable MT administration, which can potentially overcome the issue of low bioavailability and give better control over PK. This review aimed to give a concise update about the clinical challenges associated with the administration of high dose mitotane oral therapy, which encompass the issues of poor bioavailability, difficult-to-predict pharmacokinetics and associated adverse events. Moreover, we presented recent efforts to develop/improve mitotane formulations. The success of these formulations was limited and we therefore propose an injectable mitotane formulation instead of oral administration, which could bypass many of the main issues associated with high dose oral mitotane therapy and associated side effects with better therapeutic outcomes. A parenteral administration of mitotane could help to alleviate not only the adverse effects but also circumvent the variable oral absorption, give better control over therapeutic plasma mitotane concentration, and potentially shortens the time to achieve therapeutic drug plasma concentrations considerably.

European Journal of Drug Metabolism and Pharmacokinetics (2021) 46:575–593
https://doi.org/10.1007/s13318-021-00700-5

LEADING ARTICLE

The Challenging Pharmacokinetics of Mitotane: An Old Drug in Need of New Packaging

Malik Salman Haider[1] · Taufiq Ahmad[2] · Jürgen Groll[2] · Oliver Scherf-Clavel[3] · Matthias Kroiss[4,6] · Robert Luxenhofer[1,5]

Accepted: 24 June 2021 / Published online: 21 July 2021

Abstract: Adrenocortical carcinoma (ACC) is a malignant tumor originating from the adrenal gland cortex with a heterogeneous but overall dismal prognosis in advanced stages. For more than 50 years, mitotane has remained a cornerstone for the treatment of ACC as adjuvant and palliative therapy. It has a very poor aqueous solubility of 0.1 mg/l and high partition coefficient in octanol/water (log *P*) value of 6. The commercially available dosage form is 500 mg tablets (LysodrenR). Even at doses up to 6 g/day (12 tablets in divided doses) for several months, > 50% patients do not achieve therapeutic plasma concentration > 14 mg/l due to poor water solubility, large volume of distribution and inter/intra individual variability in bioavailability. This article aims to give a concise update of the clinical challenges associated with the administration of high-dose mitotane oral therapy which encompass the issues of poor bioavailability, difficult-to-predict pharmacokinetics and associated adverse events. Moreover, we present recent efforts to improve mitotane formulations. Their success has been limited, and we therefore propose an injectable mitotane formulation instead of oral administration, which could bypass many of the main issues associated with high-dose oral mitotane therapy. A parenteral administration of mitotane could not only help to alleviate the adverse effects but also circumvent the variable oral absorption, give better control over therapeutic plasma mitotane concentration and potentially shorten the time to achieve therapeutic drug plasma concentrations considerably.

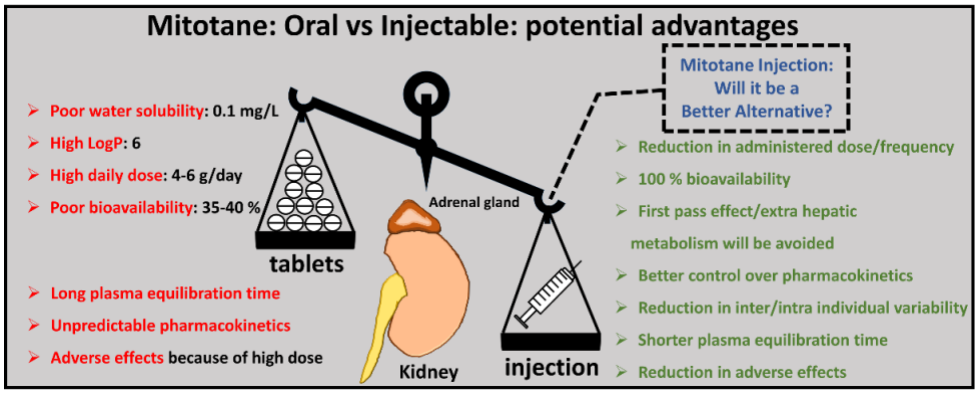

4.6.1 Mitotane formulation

Summary: Utilizing our POx/POzi based platform, we developed nanoformulation for MT, capable to solubilize around 6-7 g/L of the MT, representing several thousands fold increase in apparent solubility. In this regard, POx based mitotane encapsulated formulation was developed and extensively, (physico-chemically) characterized. The small micellar sizes, high loadings as well as sufficient long-term stabilities and redispersibility of lyophilized formulations make it promising candidate for intravenous administration. The anti-tumoral activity of the MT formulation was evaluated in conventional 2D cell culture as well as more sophisticated 3D tumor spheroids. The cytocompatibility of polymer excipient was also tested on various cell lines.

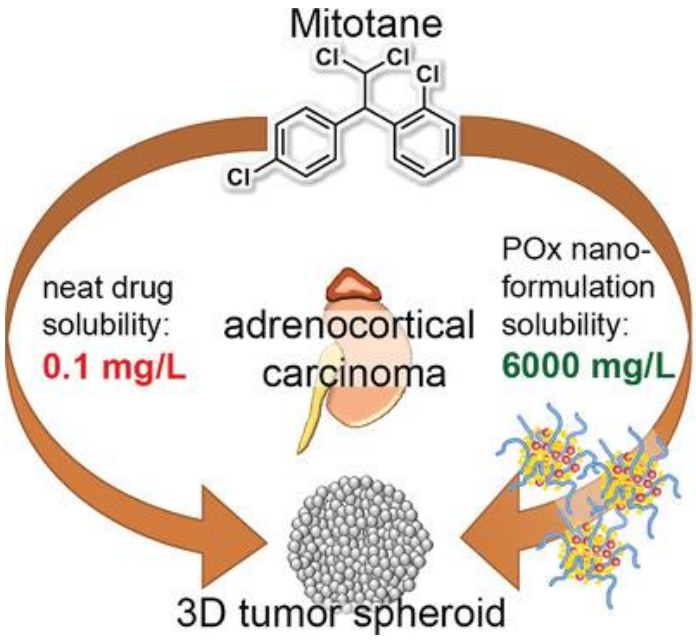

Macromolecular Bioscience
www.mbs-journal.de

A Micellar Mitotane Formulation with High Drug-Loading and Solubility: Physico-Chemical Characterization and Cytotoxicity Studies in 2D and 3D In Vitro Tumor Models

Malik Salman Haider, Jochen Schreiner, Sabine Kendl, Matthias Kroiss, and Robert Luxenhofer**

Adrenocortical carcinoma (ACC) is a rare tumor and prognosis is overall poor but heterogeneous. Mitotane (MT) has been used for treatment of ACC for decades, either alone or in combination with cytotoxic chemotherapy. Even at doses up to 6 g per day, more than half of the patients do not achieve targeted plasma concentration (14–20 mg L^{-1}) even after many months of treatment due to low water solubility, bioavailability, and unfavorable pharmacokinetic profile. Here a novel MT nanoformulation with very high MT concentrations in physiological aqueous media is reported. The MT-loaded nanoformulations are characterized by Fourier transform infrared spectroscopy, differential scanning calorimetry, and powder X-ray diffraction which confirms the amorphous nature of the drug. The polymer itself does not show any cytotoxicity in adrenal and liver cell lines. By using the ACC model cell line NCI-H295 both in monolayers and tumor cell spheroids, micellar MT is demonstrated to exhibit comparable efficacy to its ethanol solution. It is postulated that this formulation will be suitable for i.v. application and rapid attainment of therapeutic plasma concentrations. In conclusion, the micellar formulation is considered a promising tool to alleviate major drawbacks of current MT treatment while retaining bioactivity toward ACC in vitro.

1. Introduction

Adrenocortical carcinoma (ACC) is a highly aggressive malignant disease with a high risk of recurrence even after complete resection and heterogeneous but generally poor prognosis in advanced stages.[1–3] In the majority of the cases, patients with ACC present with hormonal excess, mostly Cushing's syndrome and symptoms of sex steroid excess. Patients without hormone overproduction generally are diagnosed due to symptoms of local tumor growth or symptomatic metastases. The therapeutic challenge is to both control hormone excess and to combat tumor progression.[4]

The only approved treatment for ACC is the adrenolytic drug 1,1-dichloro-2-(o-chlorophenyl)-2-(p-chlorophenyl)ethane, better known by its trivial name mitotane (MT). MT is used both as adjuvant therapy after complete tumor resection and as palliative treatment in case of advance disease. Only recently, the presumed key molecular mechanism of action was shown to be inhibition of sterol-O-acyl transferase 1[5] but additional drug effects, for example, at the level of mitochondria have been reported.[6,7] Based on the results obtained from a large randomized phase III clinical trial, the combination of oral MT with intravenous administration of etoposide, doxorubicin, and cisplatin is currently considered as treatment standard for advanced ACC.[8,9] Mitotane 500 mg tablets are marketed in Europe as Lysodren by HRA Pharma, Paris and in the U.S. by Bristol-Myers Squibb. Treatment with MT is hampered by its severe side effects to the central nervous system (dizziness, speech difficulties, stroke-like symptoms), liver, and gastrointestinal tract.[10–12] While serum concentrations above 14 mg L^{-1} have been reported to be associated with the therapeutic response,[13–16] the incidence of toxic effects increases beyond 20 mg L^{-1} leading to a narrow therapeutic window and the requirement of therapeutic drug monitoring. Management is further complicated by unfavorable pharmacokinetic properties of MT. Even at high cumulative doses of 4 to 6 g per day for a consecutive of 3 months, more than half of the patients do not achieve targeted plasma concentration.[3,17] Overall, MT pharmacokinetics exhibit large inter-individual variability which appears to be due in part due intestinal[18] and/or hepatic

M. S. Haider, Prof. R. Luxenhofer
Functional Polymer Materials
Chair for Chemical Technology of Material Synthesis
Faculty of Chemistry and Pharmacy
University of Würzburg
and Bavarian Polymer Institute
Röntgenring 11, 97070 Würzburg, Germany
E-mail: robert.luxenhofer@uni-wuerzburg.de

J. Schreiner, S. Kendl, Dr. M. Kroiss
University Hospital Würzburg
Department of Internal Medicine I
Division of Endocrinology/Diabetology
Oberdürrbacher Str. 6, 97080 Würzburg, Germany
E-mail: Kroiss_M@ukw.de

The ORCID identification number(s) for the author(s) of this article can be found under https://doi.org/10.1002/mabi.201900178.

DOI: 10.1002/mabi.201900178

metabolism.[19] The inactive metabolite o,p′-DDA is also found ten times higher in blood than the active parent compound MT.[20–22] The evidence that MT is strong inducer of hepatic cytochrome-P450 enzyme further strengthens its hepatic metabolism.[23–26]

MT's limited aqueous solubility of 0.1 mg L^{-1}[27] is likely the cause of poor and variable oral absorption[28] and high volume of distribution.[29] Efforts in the past have been undertaken to shorten the time interval to reach the therapeutic serum/plasma concentrations and reduce the gastrointestinal side effects. Attivi et al. reported a self-micro-emulsifying drug delivery system (SMEDDS). MT was dissolved in various oils and surfactants (in ratio of 1:16) as individual or in the various binary and ternary mixtures (33% caproyl, 33% tween, and 33% cremophore EL). The solubility of MT in individual vehicle was maximal with 409 g L^{-1} in cremophore EL. The relative bioavailability in rabbits at a dose of 100 mg kg^{-1} body weight was increased by a factor of 3.4 for the MT emulsion.[30] Battung and coworkers filed a patent about the development of an oily formulation (SMEDDS) of MT (based on propylene glycol monocaprylate, propylene glycol dicaprate and polyoxyethylene sorbitan monooleate). They were capable of solubilizing 0.4 g of MT per gram of oily vehicle (28 wt%). In vivo studies were conducted in Beagle dogs and the relative bioavailability was increased by factor of 3.2 for the oily formulation.[31,32]

Lipophilicity of MT has been shown to result in predominant association with serum lipoproteins (LPs)[33,34] and also chyle[18] but only free MT was demonstrated to be therapeutically active.[35,36] Collectively, poor aqueous solubility and difficult to predict PK profile of MT are the major obstacles in MT therapy. Here, we aimed at the development of a novel MT nanoformulations, which may enable both an injectable formulation and could increase bioavailability when administered orally and hence shorten the long lag time, which is arguably the biggest problem of MT in the clinics.

Micelles are formed by the self-assembly of amphiphilic molecules. Several polymeric micelles formulations have been widely studied in preclinical and clinical trials which have shown improved pharmacological activity and less systemic toxicity.[37–42] Poly(2-oxazoline)s (POx) have been discussed as potential biomaterial for decades but the major advancements have been seen in the last few years.[43,44] In particular, poly(2-methyl-2-oxazoline)-block-poly(2-butyl-2-oxazoline)-block-poly(2-methyl-2-oxazoline) (pMeOx-pBuOx-pMeOx) being the most investigated amphiphile of this polymer family has shown a huge potential for not only solubilizing hydrophobic drugs but also exhibited high cytocompatibility.[45,46] Accordingly, we set out to develop a novel pMeOx-pBuOx-pMeOx based MT nanoformulation with high drug loading. The formulation was comprehensively characterized and the bioactivity of the solubilized MT was assessed in 2D and 3D cell culture using NCI-H295 adrenocortical carcinoma cell line. Our results suggest that this novel MT nanoformulation is suitable for i.v. administration and thus may alleviate the biggest clinical problem of MT, its poor bioavailability and unfavorable pharmacokinetics.

2. Experimental Section

All substances for the preparation of polymer and bovine serum albumin (BSA) were purchased from *Sigma-Aldrich* (Steinheim, Germany) or *Acros* (Geel, Belgium) and were used as purchased unless stated otherwise. Mitotane was purchased from *ISP chemical products*, Columbus, USA. The monomer 2-*n*-butyl-2-oxazoline (BuOx) was prepared according to the original procedure by Seeliger et al.[47] as modified and reported recently.[48] All substances used for polymerization, methyl trifluoromethylsulfonate (MeOTf), 2-methyl-2-oxazoline and other solvents for polymer preparation were refluxed over CaH_2, while benzonitrile (PhCN) was refluxed over P_2O_5 and distilled under argon. Deuterated solvents for NMR analysis were purchased from *Deutero GmbH* (Kastellaun, Germany). Phosphate-buffered saline (PBS) was prepared by dissolving 8.0 g (137 mmol) NaCl, 0.2 g (2.7 mmol) KCl, 1.42 g (10 mmol) Na_2HPO_4, and 0.27 g (1.98 mmol) KH_2PO_4 in 1.0 L of deionized (DI) water (pH 7.4 at 25 °C). If necessary, pH was adjusted to 7.4 with aqueous HCl or NaOH solution.

2.1. Polymer Synthesis

The polymerizations and work-up procedures were carried out as described previously.[48–50] As an example, the synthesis of **A-pBuOx-A** was performed as follows.

The initiator, MeOTf was added to a dried and argon flushed flask and dissolved in PhCN. MeOx was added and the reaction mixture was heated to 110 °C for approximately 4 h. Reaction progress was controlled by Fourier-transform infrared (FT-IR) and ^{1}H-NMR-spectroscopy. After complete consumption of MeOx, the mixture was cooled to RT and the monomer for the second block (BuOx) was added. The reaction mixture was heated to 120 °C and kept on stirring overnight. The procedure was repeated for the third block (MeOx) and after full monomer consumption was confirmed, termination was carried out by addition of 5 eq. of 1 M NaOH solution in DI water (Polymer batch: P1) or 3 equivalents of piperidine (Polymer batch: P2) at 50 °C for 4 h. Subsequently, 1 eq. of K_2CO_3 (only in P2) was added and the mixture was stirred at 50 °C for 4 h. PhCN was removed under reduced pressure. The highly viscous residues were dissolved in DI water and transferred into a dialysis bag (MWCO 1 kDa, cellulose acetate) and dialyzed against DI water for 24 h. The solution was recovered from the bag and lyophilized. The products were obtained as colorless powders.

2.2. Nuclear Magnetic Resonance Spectroscopy

NMR spectra were recorded on a Fourier 300 (300.12 MHz), *Bruker Biospin* (Rheinstetten, Germany) at 298 K. The spectra were calibrated to the signal of residual protonated solvent ($CDCl_3$ at 7.26 ppm) using MestReNova software.

2.3. Dialysis

Dialysis was performed using Spectra/Por membranes with a molecular weight cutoff (MWCO) of 1 kDa (material: cellulose acetate) obtained from *neoLab* (Heidelberg, Germany). DI water was renewed after 1, 4, and every 12 h subsequently, until the end of dialysis.

2.4. Gel Permeation Chromatography

Gel permeation chromatography (GPC) was performed on an Agilent 1260 Infinity System, *Polymer Standard Service* (Mainz, Germany) with HFIP containing 3 g L^{-1} potassium trifluoroacetate; precolumn: 50 mm × 8 mm PSS PFG linear M; 2 columns: 300 mm × 8 mm PSS PFG linear M (particle size 7 µm; pore size 0.1–1000 kDa). The columns were kept at 40 °C and flow rate was 0.7 mL min^{-1}. Prior to each measurement, samples were filtered through 0.2 µm PTFE filters, *Roth* (Karlsruhe, Germany). Conventional calibration was performed with PEG standards (0.1–1000 kg mol^{-1}) and data was processed with Win-GPC software.

2.5. Drug Formulation

Drug loaded polymer micelles were prepared using the thin film method. Ethanolic polymer (10 g L^{-1}) and MT (10 g L^{-1}) stock solutions were mixed in desired ratios. After complete removal of the solvent at 50 °C under a mild stream of argon, the films were dried in vacuo (≤0.2 mbar) for at least 30 min. Subsequently, preheated (37 °C) DI water, PBS, or aqueous serum albumin solution (40 g L^{-1}) was added to obtain desired final polymer (10 g L^{-1}) and MT concentrations. To ensure complete solubilisation, the solutions were shaken at 55 °C for 15 min at 1250 rpm with a Thermomixer comfort (*Eppendorf AG,* Hamburg, Germany). Non-solubilized drug was removed by centrifugation for 5 min at 10.000 rpm with a 3-Speed micro centrifuge, (*neoLab,* Heidelberg, Germany). Solubilisation experiments were performed with three individually prepared samples and results are presented as means ± standard deviation (SD).

2.6. High Performance Liquid Chromatography

HPLC analysis was carried out on a LC-20A Prominence HPLC (*Shimadzu,* Duisburg, Germany) equipped with a system controller CBM-20A, a solvent delivery unit LC-20 AT (double plunger), an on-line degassing unit DGU-20A, an auto-sampler SIL-20AC, a photo diode array detector SPD-M20A. As stationary phase, a ZORBAX Eclipse Plus (*Agilent,* Santa Clara, CA, USA) C18 column (4.6 mm × 100 mm; 3.5 µm) was used. Quantification of MT was performed with a stepwise gradient. Within the first 10 min, the ratio of H_2O/ACN was decreased from 60/40 (v/v) to 40/60 (v/v). Solvent ratio was kept constant for 5 min, prior to increasing it to the initial ratio of 60/40 (v/v) within 0.5 min. This ratio was kept for 5 min. Flow rate was 1 mL min^{-1}. Detection was performed at 230 nm and the retention time was 3.9 min.

2.7. Loading Capacity and Loading Efficiency

The following equations were used to calculate the loading capacity (LC) and loading efficiency (LE) of the formulations:

$$\mathrm{LC} = \frac{m_{\mathrm{drug}}}{m_{\mathrm{drug}} + m_{\mathrm{excipient}}} * 100\%$$

$$\mathrm{LE} = \frac{m_{\mathrm{drug}}}{m_{\mathrm{drug,added}}} * 100\%$$

where m_{drug} and $m_{\mathrm{excipient}}$ are the weight amounts of the solubilized drug and polymer excipient in solution and $m_{\mathrm{drug,added}}$ is the weight amount of the drug initially added to the dispersion. No loss of polymer during micelles preparation was assumed.

2.8. Long Term Stability Studies

For long term stability studies, formulated MT was stored at ambient conditions (≈25 °C) under the exclusion of light. The samples were collected at day 0, 1, 2, 3, 4, 5, 10, 20, and day 30. Before the determination of the drug loading by HPLC, all samples were centrifuged for 5 min at 10 000 rpm with a 3-Speed micro centrifuge (*neoLab,* Heidelberg, Germany). Long-term stabilization experiments were performed with three individually prepared samples and results are presented as means ± SD, quantification was carried out as described above.

2.9. Redispersion Studies

The freshly prepared formulations were frozen in liquid nitrogen and subjected to 24 h lyophilization to obtain the dried powdered MT formulation for redispersion studies. The media used for the redispersion (keeping the polymer concentration 10 g L^{-1}) were DI water, cell culture medium, PBS, and PBS with 40 g L^{-1} BSA. The formulations were shaken at 1250 rpm with a Thermomixer comfort (*Eppendorf AG,* Hamburg, Germany) at room temperature for 10 min followed by HPLC analysis as stated in section long-term stability studies.

2.10. Polymer Drug Compatibility Evaluation by Hansen Solubility Parameters

The extent of compatibility between MT and the core forming block of the ABA triblock copolymers was calculated by employing the Hildebrand–Scatchard equation:[51]

$$\chi_{\mathrm{drug-polymer}} = (\delta_{\mathrm{drug}} - \delta_{\mathrm{polymer}})^2 \frac{V}{RT} \quad (1)$$

where $\chi_{\mathrm{drug-polymer}}$ (χ_{dp}) is Flory–Huggins interaction parameter, δ_{drug} and $\delta_{\mathrm{polymer}}$ are the total solubility parameter (δ_{total}) for the MT and the core forming block, respectively. V is the molar volume of MT calculated by Fedors methods,[52] while R is the gas constant and T is the temperature. The δ_{total} (also called as 3D solubility parameter) that is, δ_{drug} and $\delta_{\mathrm{polymer}}$ were further calculated by following equations:

$$\delta^2_{\mathrm{drug}} = \delta^2_d + \delta^2_p + \delta^2_h \quad (2)$$

$$\delta^2_{\mathrm{polymer}} = \delta^2_d = \delta^2_p + \delta^2_h \quad (3)$$

The δ_{total} is the sum of dispersion (δ_d), polar (δ_p), and hydrogen bonding forces (δ_h). The δ_d, δ_p, and δ_h were further calculated by Hoftyzer and Van Krevelen's additive group contribution method by employing the following equations:

$$\delta_d = \frac{\sum F_{di}}{V} \tag{4}$$

$$\delta_p = \frac{(\Sigma F_{pi}^2)^{1/2}}{V} \tag{5}$$

$$\delta_h = \left(\Sigma \frac{E_{hi}}{V}\right)^{1/2} \tag{6}$$

where F_{di}, F_{pi}, and E_{hi} are the molar dispersion, polar attraction constant and hydrogen bonding energy, respectively. Each structural group in the molecule contributes towards the F_{di}, F_{pi}, and $E_{hi.}$

2.11. Fourier Transform Infrared Spectroscopy

The FT-IR spectra were recorded on a FT-IR-4100 (Jasco, Gross-Umstadt, Germany), measuring from 500 to 4000 cm^{-1}. The aqueous MT formulations were lyophilized to obtain the dry powdered formulation prior to FT-IR measurements.

2.12. Differential Scanning Calorimetry

For DSC studies samples were placed into flat-bottom aluminum pans with the pierced lids. The aqueous MT formulations were lyophilized to obtain the dry powdered formulation prior to DSC measurements.

DSC was performed on DSC 204 F1 Phoenix equipped with a CC200 F1 Controller, (*NETZSCH,* Selb, Germany). The dynamic scans were recorded in nitrogen atmosphere with a heating rate of 10 K min^{-1} (25–200 °C) and subsequently cooled to −50 °C (10 K min^{-1}). The samples were heated and cooled two additional times from −50 to 200 °C (10 K min^{-1}) (three heating and two cooling cycles).

2.13. X-Ray Diffraction

Powder X-ray diffraction (XRD) was performed at STADI P from STOE (STOE & Cie GmbH, Darmstadt Germany). The setup is equipped with radiation source of Cu-Kα and the detector is linear PSD. Measurement were done at 0.15° steps each step lasting 180 s in transmission mode at 40 kV voltage and 30 mA current and 2Θ angle ranging from 5° to 60° were used.

2.14. Dynamic Light Scattering

Dynamic light scattering were measured on Zetasizer Nano ZSP from Malvern, (Malvern Instruments, Worcestershire, UK) in disposable cuvettes (UV cuvettes semi micro, BRAND GmbH, Wertheim, Germany) at ambient temperatures (≈25 °C). Data was analyzed by using zetasizer software 7.11. All the samples were measured after filtration using 0.45 µm PVDF syringe filter (Rotilabo, Karlsruhe). The filtered samples were further diluted (1:1 ratio with DI water) and measured again to exclude variation due to dilution effect (Figure S11, Supporting Information). The measurements were recorded as average of three test runs for two individually prepared samples.

2.15. Cell Culture

The adherent adrenocortical cell line NCI-H295R (ATCC, USA)[53] and HepG2 cell line (ATCC, USA) were grown in DEMEM/F-12 1:1 mix (Gibco, USA) supplemented with 1% insulin-transferrin-selenium (Gibco, USA) and 3% Nu-Serum (Corning, USA). Cells were cultured at 37 °C and 5% CO_2 humid atmosphere in flasks.

2.16. Monolayer Culture and Spheroid Formation

For monolayer cell culture, 1×10^5 cells were seeded in a flat bottom 96-well plate in 100 and 200 µL medium for cytocompatibility studies and cytotoxicity studies, respectively, and incubated for 24 h. For spheroid formation 5×10^4 cells were seeded in 96-well plates, coated with 50 µL 1.5% autoclaved agarose (Sigma-Aldrich, Germany) in a total volume of 200 µL culture medium. Initially, the spheroid formation was induced by centrifugation at 1 g for 3 min. Medium was refreshed after 48 h by exchanging 100 µL of supernatant. After 96 h spheroids were formed in each well.

2.17. Cytocompatibility Studies

The cytocompatibility studies of the polymer alone (both polymer batches, P1 and P2) were performed on monolayer culture of HepG2 cell line and NCI-H295R. The cells were cultured as stated, after 24 h incubation the monolayers were exposed to various polymer concentrations, that is, 1, 5, 10, 25, 50, and 100 g L^{-1} (prepared in cell culture medium). Treated plates were incubated for 6 and 24 h. Cell viability was assessed by WST1 (NCI-H295R and HepG2 cells) and cellTiter-Glo-3D-assay (Promega, Germany) (NCI-H295R). Briefly, after the incubation time of 6 and 24 h the treated plates (with HepG2 cells) were exposed to WST1 reagent (10 µL in each well). The plates were further incubated for 2 h followed by the absorbance measurement by multilabel plate reader Wallac Victor 1420 (PerkinElmer, USA). CellTiter-Glo-3D assay was performed according to the manufacturer's instructions. 150 µL of supernatant was removed and replaced with 50 µL of CellTiter-Glo-3D-Reagent. Cell lysis was induced by mixing with multichannel pipettes and the lysate was transferred to opaque plates. After 25 min of incubation luminescence was measured by multilabel plate reader Wallac Victor 1420 (PerkinElmer, USA).

2.18. Cytotoxicity Studies in 2D and 3D Cell Spheroids

The efficacy of MT formulated in micelles or MT dissolved in EtOH was comparatively assed in 2D cell culture and 3D cell spheroids. Mitotane treatment was performed after 24 h of culturing for monolayer and 96 h for spheroids culture in a 96 well-plate, by removing 100 µL medium and adding 100 µL culture medium containing either mitotane-EtOH or mitotane in micelles to attain final concentrations ranging from 5 to 75 µM and 50 to 200 µM for monolayer and spheroids, respectively. Various stock solutions of mitotane in micelles (2 mM stock solution, prepared in cell culture medium) and mitotane-EtOH (MT was dissolved in absolute ethanol in 500–20 mM stock solutions) were prepared. Stocks solutions were further diluted with cell culture medium to obtain final concentrations. EtOH concentration was 1% (v/v) in all mitotane-EtOH samples and controls. Treated plates were incubated for 24 and 48 h. All experiments were performed in triplicate with $n = 8$ in each replicate, unless specified otherwise.

2.19. Statistical Analysis

Statistical analysis was performed using two-way ANOVA using GraphPad prism software version 5.01. Statistical significance was calculated by applying Bonferroni post hoc tests.

3. Results and Discussions

3.1. Polymer Synthesis and Characterization

Block copolymers of POx are easily accessible by living cationic ring-opening polymerization (LCROP) and POx amphiphiles are highly tunable with respect to solubility, size, architecture as well chemical functionality.[54–57] All polymers in this study were also synthesized by LCROP using methyltriflate as an initiator (MeOTf) as previously described.[48,50] All ABA triblock copolymers comprised hydrophilic pMeOx as block A and poly(2-*n*-propyl-2-oxazoline) (pPrOx), poly(2-*n*-propyl-2-oxazine) (pPrOzi), poly(2-*n*-butyl-2-oxazoline) (pBuOx), poly(2-benzyl-2-oxazoline) (pBzOx), and poly(2-*n*-butyl-2-oxazine) (pBuOzi) as hydrophobic block B, respectively (**Table 1**). Two polymer batches of pBuOx based triblock copolymer (P1 and P2) were synthesized specifically for this contribution and terminated with NaOH/water and piperidine, respectively. In our previous work, we have observed relatively minor effect of the polymer termini in poly(2-oxazoline)/poly(2-oxazine) (POx/POzi) based ABA triblock copolymers, but this may have to be assessed on a case-by-case basis.[46,58] Both batches were characterized by ^{1}H-NMR and GPC. A satisfactory synthetic control was achieved in both batches of the polymer, supporting the excellent reproducibility for this polymer synthesis.[59] For further analytical details, please see Table 1 and supporting information (Figures S1–S7, Supporting Information).

Table 1. Physicochemical characterization of all the polymers used in this study including the molecular weight M_n and dispersity $Đ$.

Polymer	M_n[a)] [kg mol^{-1}]	M_n[b)] [kg mol^{-1}] HFIP	$Đ$[b)]
A_{41}-p$PrOx_{23}$-A_{40}	9.7	4.7	1.19
A_{35}-p$PrOzi_{20}$-A_{35}	8.7	5.4	1.19
A_{33}-p$BuOx_{20}$-A_{33} (P1)	8.1	3.6	1.10
A_{32}-p$BuOx_{20}$-A_{32} (P2)	8.0	5.6	1.10
A_{40}-p$BzOx_{20}$-A_{41}	10.3	5.2	1.25
A_{35}-p$BuOzi_{20}$-A_{35}	9.0	5.6	1.20

[a)]obtained by ^{1}H-NMR analysis ($CDCl_3$; 300 MHz); [b)]obtained by GPC analysis (eluent: HFIP, PEG calibration). The values are taken from the refs. [48,50].

3.2. Formulation Studies

3.2.1. Formulation Development

POx-based amphiphiles have tremendous potential for formulation development.[45,58,60,61] For example, Milonaki et al. reported very high drug loading with indomethacin using an (pseudo-diblock) copolymers from 2-methyl-2-oxazoline and 2-phenyl-2-oxazoline.[61] Luxenhofer et al.[58] reported the ultra-high paclitaxel (PTX)-loaded POx-based micellar formulation with very promising in vivo data. The lead amphiphile is a ABA triblock copolymer, A and B being comprised of hydrophilic poly(2-methyl-2-oxazoline) (pMeOx) and modestly hydrophobic poly(2-butyl-2-oxazoline) (pBuOx), respectively (pMeOx-pBuOx-pMeOx). The loading capacity (LC) was found to be 50 wt% corresponding to an increase of solubility of PTX over five order of magnitude to 50 g L^{-1}. PTX/POx formulation showed superior antitumor efficacy with the maximum tolerated dose (MTD) of 150 mg kg^{-1} when compared to commercially available formulations, that is, Taxol and Abraxane (MTD being 20 and 90 mg kg^{-1}, respectively).[60] Wan et al. recently reported the co-formulation of etoposide (ETO) and a hydrophobized cisplatin (Cis) using the similar amphiphile (pMeOx-pBuOx-pMeOx). This co-formulation demonstrated superior antitumor efficacy on various small cell and non-small cell lung cancer models as compared to single drug micelles or their combination as well as free drug combination.[62]

It is an usual assumption that the hydrophobic block is mainly responsible for solubilisation of hydrophobic drugs and that increasing the hydrophobicity of the core forming block (B) can increase the solubilisation capacity of an amphiphile. More recently, more specific interactions between polymers and their cargo have come into the focus of researchers.[63,64] In the case of POx-based amphiphiles an inverse relationship between the hydrophobicity of the micellar core and the drug-loading capacity has been observed repeatedly. Lübtow et al.[49] have recently reported a study on this behavior showing that POx- and POzi-based ABA triblock copolymer with long linear or branched side chains, that is (poly(2-nonyl-2-oxazoline) (pNonOx) or (poly(2-(3-ethylheptyl)-2-oxazoline) (pEtHepOx) rather negatively affect the LCs for hydrophobic drugs, curcumin (CUR) and PTX. Besides higher solubilizing capacity of short side chain core forming blocks, Lübtow et al.[48] further reported that minor changes in the chemical structure of short side chain core forming blocks, that is, a formal transition of one methylene unit from side chain (pBuOx) to the back bone

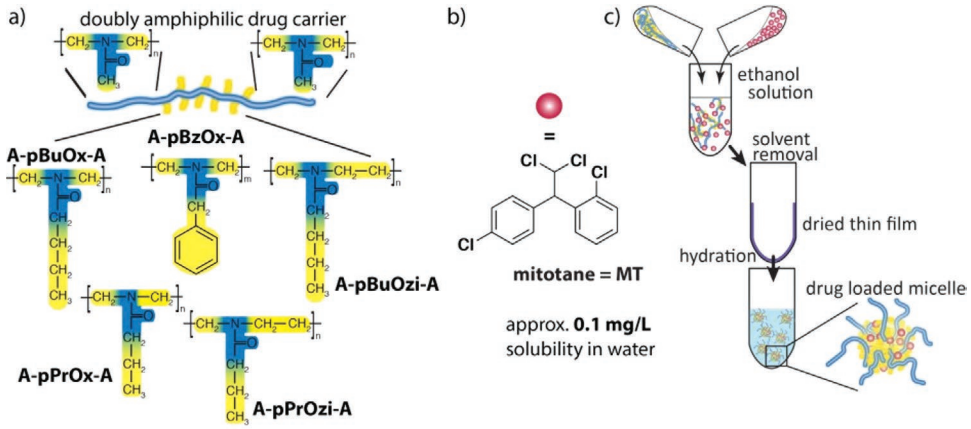

Figure 1. a) Schematic representation of the polymers used in this this study. b) Chemical structure of Mitotane and c) schematic illustration of thin film hydration method for formulation development.

(pPrOzi) or introduction of aromatic moieties[50] have significant impact on the LCs for hydrophobic drugs, indicating very strong polymer/drug specificities.

Accordingly, the solubilization of MT, which exhibits an extremely low water solubility,[27] zero H-bond donor groups, and higher aromatic character, was tested using five different ABA triblock copolymers including the most commonly investigated ABA triblock amphiphile, that is, A-pBuOx-A, and A-pPrOzi-A, A-pBuOzi-A, A-pPrOx-A, and A-pBzOx-A (**Figure 1**c and Table 1). The polymers with short linear side chain (which have been shown to optimally solubilize various hydrophobic drugs)[48,58] or with the aromatic content (inspired by a potential benefit of π-π stacking between drug and carrier)[50,65,66] were specifically selected to find a good MT solubilizer, for which only very few formulations are reported to date.[30,67] Using the thin-film approach (Figure 1b), we prepared micellar formulations of MT with the aforementioned amphiphilic triblock copolymers (Table S1, Supporting Information). Briefly, the polymer and MT were dissolved in ethanol, which was subsequently removed and the resulting thin-film was dissolved by adding DI water. We kept the targeted polymer concentration at 10 g L^{-1} and increased the targeted MT concentration from 2 to 10 g L^{-1}. The actual MT concentration achieved in the aqueous phase was assessed using HPLC (**Figure 2**a) after removal of non-solubilized drug.

Increasing the MT feed from 2 to 10 g L^{-1} raised the LC from 11 to 36 wt% (1.25 and 5.7 g L^{-1}, respectively) (Table S1–S3, Supporting Information). A-pBuOx-A being the best solubilizer for PTX,[58] also gives the highest MT loading among the tested amphiphiles. Up to 6 g L^{-1} (19 mM) MT could be obtained as a clear micellar solution with low viscosity (LC = 36 wt%). Therefore, the apparent solubility could be increased by a factor of 6×10^4. Notably, the loading efficiency (LE) did not change much while increasing the MT feed from 2 to 10 g L^{-1}, ranging between 55% and 75%. As stated previously, from a physiological perspective one possibility could be that, MT upon oral administration, because of its strong association to lipoproteins, enters the lipid transport pathway and MT bound to chylomicrons or their remnants are repeatedly exposed to hepatocytes resulting in higher rate of biotransformation and a much higher inactive metabolite concentration in blood. We postulate the administration of MT injectable formulation will render the optimal MT active metabolite concentration in blood by reducing its hepatic and extra hepatic metabolism. To the best of our knowledge, such high apparent MT aqueous solubility was never reported in the literature. Formulation experiments were performed with both polymer batches (P1 and P2) and no significant difference was observed in loading capacities (Tables S2 and S3, Supporting Information). In comparison to A-pBuOx-A, A-pBuOzi also gave good, somewhat lower LC of 27 wt% (≈3.7 g L^{-1}). In contrast, A-pPrOzi-A and A-pPrOx-A were much less effective in solubilizing MT with LC of 10 wt% (≈1.3 g L^{-1}) and 5 wt% (≈0.5 g L.) respectively. Also, the aromatic A-pBzOx-A was found less efficient than expected[50] but was slightly better than A-pPrOx-A and A-pPrOzi-A with LC ≈16 wt% (≈2 g L^{-1}) (Table S1, Supporting Information). Based on these results, we chose A-pBuOx-A based MT formulations for detailed physicochemical characterization and biological studies.

3.2.2. Stability and Redispersion Studies of the Formulation

To investigate the potential shelf-life of the formulations (A-pBuOx-A), the freshly prepared MT aqueous solutions were stored at ambient conditions containing the initial precipitate followed by the collection of samples at day 0, 1, 2, 3, 4, 5, and then at day 10, 20, 30. The formulations were centrifuged prior to each measurement. We have previously observed PTX-based A-pBuOx-A formulations have shown excellent stability up to several months[45,68]; however, other POx/PTX formulations were much less stable.[69] The formulations with the MT feed of 2 and 4 g L^{-1} resulted in relatively stable formulations (Figure 2b). After 24 h only a minor loss in the LC was observed in both cases (11 to 10 wt% and 22 to 21 wt%, respectively). However, after 30 days, the LC decreased to 3 and 10 wt%, respectively. In case of higher MT feed of 6, 8, and 10 g L^{-1} (Figure 2b) a dramatic decrease in the LC (30 to 3, 35 to 2, and 36 to 4 wt%, respectively) was observed within 24 h. It is becoming more and more evident that drug molecules can also

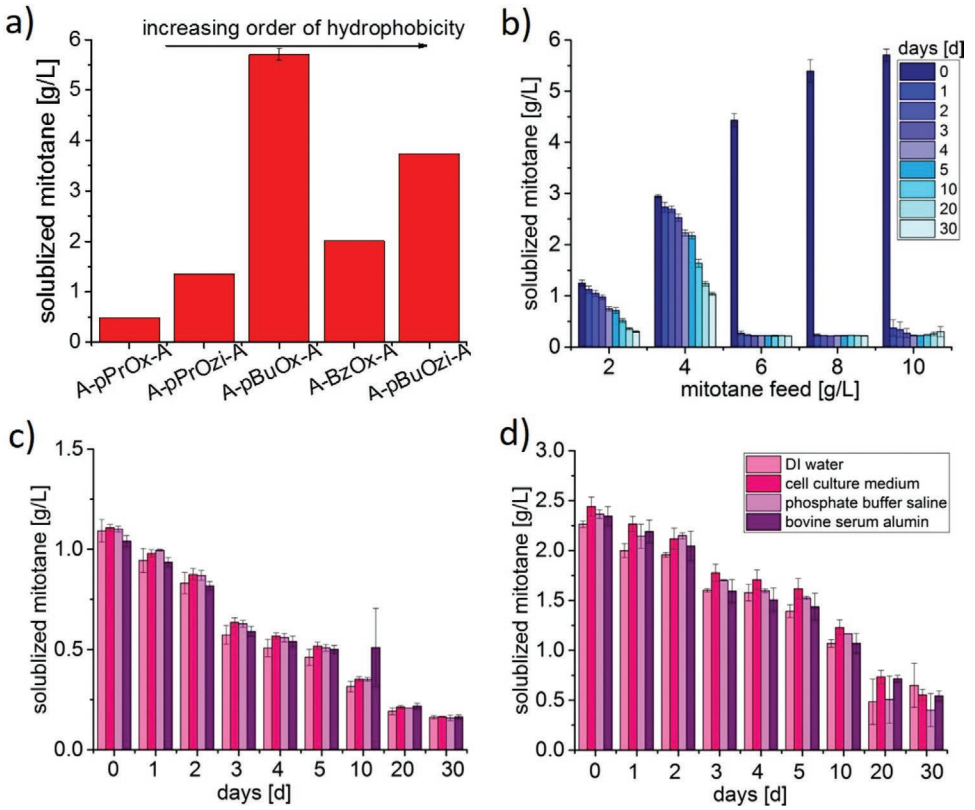

Figure 2. a) Maximum aqueous mitotane concentration obtained using different amphiphilic block copolymers (10 g L^{-1}) using the thin film method. Data is given as means ± SD ($n = 3$) only for A-pBuOx-A based formulation. b) Long term stability of mitotane formulation in dependence of mitotane feed concentration (polymer 10 g L^{-1}, mitotane 2–10 g L^{-1}). Data is given as means ± SD ($n = 3$). Formulation stability after redispersion of A-pBuOx-A: mitotane c) polymer to mitotane feed ratio of 10/2 and d) 10/4 formulation in different media, that is, deionized (DI) water, cell culture medium, phosphate buffer saline (PBS) of pH 7.4 and PBS of pH 7.4 with 40 g L^{-1} bovine serum albumin up to day 30.

coordinate with the micellar corona.[70,71] This drug–corona interaction can enable to ultra-high drug loading[71,72] or lead to colloidal instability of the formulation.[49,73] However, the drug corona interaction can also affect the morphology,[74] endocytosis,[75,76] or prolong supersaturation.[77] Interestingly, for the POx/POzi nanoformulations the drug was found fully amorphous in the precipitate, which also contains polymer.[49,70] It therefore appears that the micelles agglomerate and precipitate with the still amorphous drug embedded. However, the extremely rapid precipitation observed here at polymer/drug feed ≥10/6 g L^{-1} suggests at a different mechanism. Therefore, we investigated the precipitate after 24 h from a formulation with polymer/drug feed of 10/8 g L^{-1} by differential scanning calorimetry (DSC). The first heating cycle clearly showed the melting peak of MT at 78 °C (Figure S10, Supporting Information), indicative of MT rapid crystallization from the formulation above a critical feed of >10/4 g L^{-1}. In contrast, at 10/4, A-pBuOx-A acts as a rather effective crystallization inhibitor. This could be very promising for improving the bioavailability after oral administration.

Formulations with limited stability in an aqueous environment may be stored in lyophilized state. In this case, redispersibility is a key issue. Here, the A-pBuOx-A based MT formulation with the drug feed of 2 and 4 g L^{-1} were lyophilized and redispered in different media (Figure 2c,d). The lyophilized formulations were stored for 7 days at ambient conditions followed by redispersion in DI water, cell culture medium, PBS and PBS with 40 g L^{-1} BSA. Upon redispersion with DI water, initially a minor decrease in LC (11 to 10 and 22 to 18 wt% for 2 and 4 g L^{-1} MT feed, respectively) was observed. A similar pattern was observed in case of other redispersion mediums. However, long-term stability after redispersion followed a similar pattern as that for freshly prepared formulation showing time dependent gradual decrease in LC. It can be concluded that A-pBuOx-A based MT formulations should be stored as lyophilized powder and used freshly after redispersion. Even though this was not systematically studied at this point, the lyophilized powders seem to be quite stable at ambient conditions. No deterioration of re-dispersibility was observed over the time course of this study. Of course, these preliminary studies to not exclude the possibility to extend shelf-life, for example, by addition of other excipients.

3.2.3. Polymer Drug Compatibility Evaluation by Hansen Solubility Parameters

The physicochemical compatibility between an active pharmaceutical ingredient and the drug delivery system is believed to be a key factor in the formulation development process

Table 2. Hansen solubility parameters of mitotane and core forming blocks of the ABA triblock copolymers.

Polymer/drug	[a]δD	[a]δP	[a]δH	[b]δT	[c]Molar volume $cm^3\ mol^{-1}$	[d]Flory Huggins parameter
pPrOx 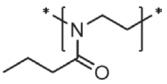	20.1	12.3	8.8	25.1	90.2	0.327
pPrOzi 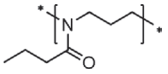	19.6	10.4	8.1	23.6	106.3	0.009
pBuOx 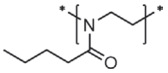	19.6	10.4	8.1	23.6	106.3	0.009
pBzOx 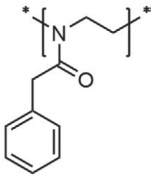	22.8	10.0	7.9	26.1	112.0	0.750
pBuOzi 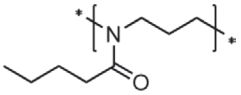	19.2	9.1	7.6	22.5	122.4	0.055
Mitotane 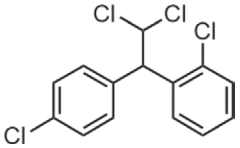	18.7	9.2	2.6	21.0	240.8	

[a]Calculated by Hoftyzer and Van Krevelen's method, Equations (4), (5), and (6); [b]calculated by Equations (2) and (3); [c]calculated by Fedor's method; [d]calculated by Equation (1).

to determine the suitability of the drug delivery system. Considering the plethora of drugs with unique physicochemical properties, a universal carrier for all the drugs seems impossible.[78] There are various ways to assess the drug polymer compatibility[79–82] which are thought to help to select a suitable carrier for a specific drug in time and cost effective manner. The extent of compatibility between MT and POx based carriers was calculated by the Hansen solubility parameter (HSP) (**Table 2**).[83,84] For the further details on HSPs calculations please refer to the Supporting Information (Tables S4–S5, Supporting Information).

The extent of compatibility between MT and the core forming blocks was estimated by Flory–Huggin's interaction parameters (χ_{dp}). The lower the value of χ_{dp} the better the polymer/drugs compatibility. Based on the calculated χ_{dp}, MT compatibility with five of selected amphiphiles was in the following order pBuOx=pPrOzi > pBuOzi > pPrOx > pBzOx. Interestingly, the core forming block pBuOx and pPrOzi are suggested to be best solubilizers for the MT. Being based on group contribution methods, the calculated solubility parameters of pBuOx and pPrOzi, which are structural isomers, yielded identical solubility parameter values and thus, compatibility for the drug MT. Experimentally, however, strong contrast in the solubilization capacities were found, similar to the situation reported for other drugs.[48] Interestingly, pBzOx was suggested to be the least compatible polymer, even though it features the aromatic system. It is apparent that the experimental results are only partially consistent with the calculated compatibility profile between MT and core forming blocks. It seems that the correct assignment of the best solubilizer, pBuOx is more coincidental and does not indicate that HSP can correctly predict compatibilities in the present system.

3.2.4. Physicochemical Characterization of MT Nanoformulations

A-pBuOx-A based MT nanoformulations were characterized using FT-IR, DSC, XRD, and DLS (polymer/drug 10/2 g L^{-1}). FT-IR spectroscopy (**Figure 3**a) of lyophilized formulation in comparison with the physical mixture, pure drug, and pure polymer was performed to characterize potential interactions between MT and polymer. Pure MT is characterized by a number of sharp signals, with particular strong signals in the range of 700–800 cm^{-1}, which are attributed to the −C−Cl stretching vibration. MT also exhibited a characteristic signal at 1490 cm^{-1}, which is attributed to −C=C− aromatic stretch. While in the physical mixture these signals can still be observed, they completely vanished in the case of nanoformulation. The broader signal at 1630 cm^{-1} is attributed to the stretching and bending vibration of carbonyl stretch and no noticeable change was observed between the spectra of physical mixture and nanoformulation. Overall, IR suggest very significant interaction between MT and the polymer. As the sharp signals of MT do not shift but significantly broaden to the point of becoming indiscernible these interactions are presumed to be versatile and undefined.

In order to investigate the thermal behavior of MT nanoformulations, DSC (Figure 3b) was conducted for pure polymer, pure drug, physical mixture, and the lyophilized nanoformulation. The thermogram of pure drug and its physical mixture with polymer showed an endothermic peak at 80 and 78 °C, respectively, which represents the characteristic melting peak of MT. The disappearance of the melting endothermic peak of the drug in the nanoformulation shows that MT is fully amorphous in the lyophilized nanoformulation. Therefore, the lyophilized nanoformulation can be considered a solid amorphous dispersion of MT in A-pBuOx-A.

For further analysis, pure polymer, pristine drug, physical mixture, and the lyophilized micellar formulation were analyzed by powder-XRD (Figure 3c). The XRD spectra of the pristine MT shows numerous reflexes in the 2Θ range of 5 to 40° corresponding to the crystalline nature of MT. The identical spectrum was observed for physical mixture of drug with polymer. In contrast, no signs of crystallinity were observed in case of lyophilized nanoformulation even after 15 days of storage at ambient conditions, confirming the amorphous nature of MT

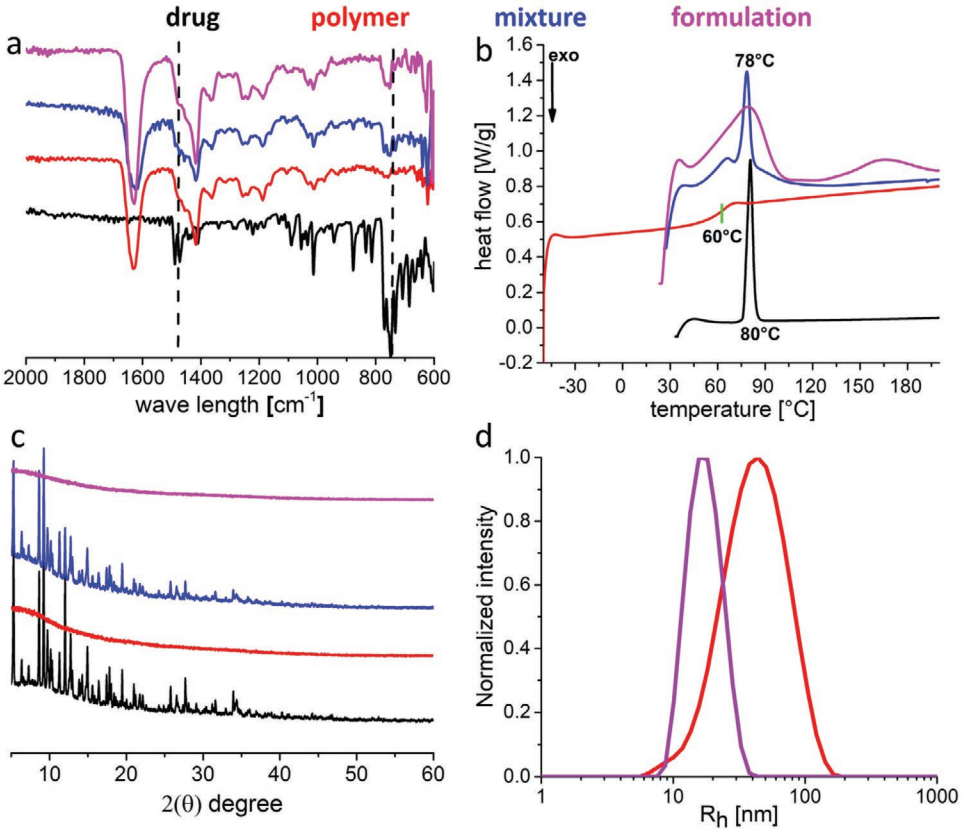

Figure 3. a) FT-IR spectra, b) DSC thermograms (first heating cycle for drug, mixture, formulation, and second heating cycle for pure polymer is shown) and c) XRD spectra of pure drug (black), polymer (red), physical mixture of drug, and polymer (blue) and nanoformulation (purple) for a polymer to drug ratio 10/2 (w/w). d) The size distribution by intensity of pure polymer (10 g L^{-1}) (red) and mitotane formulation (10/2 w/w) (purple) in deionized water after filtration through 0.45 µm PVDF filter.

in the nanoformulation. After redispersion, the hydrodynamic radii (R_h) of the micelles was estimated by zeta sizer (Figure 3d and Figure S11, Supporting Information) showing $R_h \approx 40$ nm for the pure polymer and $R_h \approx 20$ nm for the MT-encapsulated micelles.

3.3. Cell Studies

3.3.1. Cytocompatibility Studies on HepG2 and NCI-H295 Cell Lines

When it comes to the in vivo administration, the safety of the polymer excipients is of great interest. Even though cytocompatibility of POx based amphiphiles has been established several times,[46,58,85] cytocompatibility of the presently employed polymer was investigated in HepG2 and NCI-H295 cell lines using WST1 and CellTiter Glo assay (which reflects ATP content) after treatment with polymer solution at different concentrations for 6 and 24 h. We investigated both polymer batches, that is, P1 and P2 by WST1 assay in NCI-H295R and HepG2 cell lines at concentrations of up to 100 and 50 g L^{-1} for P2 and P1, respectively (**Figure 4**a,b and Figure S12, Supporting Information). No sign of cytotoxicity was observed and cell viability remained above 95% in all cases indicating its excellent cytocompatibility. Similar results were obtained using the CellTiter Glo assay (Figure 4c and Figure S12, Supporting Information).

3.3.2. In Vitro 2D and 3D Cytotoxicity Studies of Nanoformulations on NCI-H295 Cell Lines

The cytotoxicity of MT in EtOH and micellar formulation was determined by CellTiter Glo assay in both 2D (monolyer) and 3D (spheroids) NCI-H295R cell lines, for 24 and 48 h. In all the cases dose dependent cytotoxicity was observed.

For the monolayer culture, there was no significant difference in cytotoxicity between MT in EtOH and MT in micelles ($p > 0.05$) upon 24 h incubation (**Figure 5**a). The $IC_{50,24h}$ were 15 and 19 µM for MT in EtOH and micelles, respectively, which corresponds well with values found in the literature ($IC_{50,24h}$ = 15 µM.[18] The cell viability was less than 3% at 50 µM MT concentration (either in EtOH or micelles) consistent with the previous reports by Silveira et al. and others.[86,87] Prolonged incubation had no effect on IC_{50} values ($IC_{50,48h}$ = 15 and 18 µM for MT in EtOH and micelles, respectively ($p > 0.05$), Figure 5b).

There is growing evidence that cancerous cells grown as spheroids do more accurately mimic the 3D tumor microenvironment when compared to monolayer cultures.[88] Besides

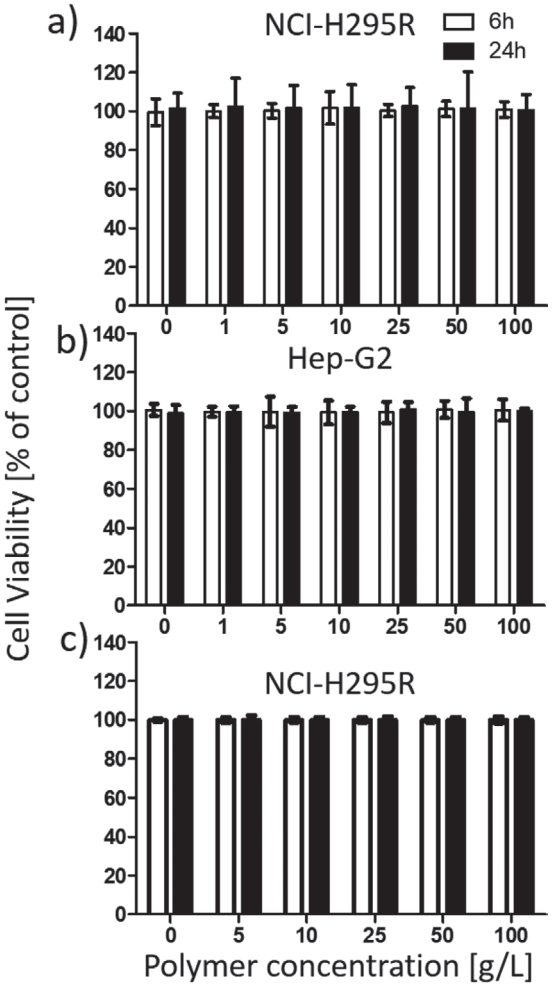

Figure 4. Cell viability of A-pBuOx-A (P2) in a) NCI-H295 and b) HepG2 cell line by WST1 assay and c) NCI-H295 cell line by CellTiter Glo assay after 6 h (white) and 24 h (black) incubation. Experiments were performed as duplicate (in case of WST1 assay) and as single experiment for the CellTiter Glo assay with $n = 8$ technical replicates. Data is expressed as means ± standard deviation.

activation of cell–cell and cell–matrix interactions, spheroids also simulate some in vivo tumor characteristics such as dormancy, hypoxia, and activation of anti-apoptotic signaling. After 96 h of incubation, we obtained single, uniformly sized, and dense spheroids of NCI-H295R cells (Figure S14, Supporting Information).[87] In general, when compared to 2D monolayer cells, cancer cells are less sensitive to drugs when analyzed in spheroids. This could be attributed to hypoxia and tight cell–cell interactions in spheroids leading to poor permeability, among other factors.[89] Accordingly, we used range of higher concentration (50 – 200 μM MT). Important to note, the MT in EtOH dilution (prepared in cell culture medium) at 200 μM turned milky, whereas A-pBuOx-A based MT micelles remained a clear solution. This suggests MT emulsion or precipitation and it follows that such high concentrations are feasible in vivo only when using a suitable drug carrier. In spheroids, we expectedly observed resistance to pharmacotherapy with $IC_{50,24h}$ values determined at 75 and 65 μM for MT in EtOH and micelles, respectively (Figure 5c), whereas IC_{50} was 15 and 19 μM in monolayer cultures. Cell viability was drastically reduced at 100 μM (<30%) and 150 μM (<7%) MT concentration either in ethanol or micelles. Almost no cells survived at 200 μM MT concentration (Figure 5c), irrespective whether MT was administered in EtOH or as nanoformulation.

Interesting to note, in case of spheroids, incubation time did affect cell viability. The $IC_{50,48h}$ was found to be 47 and 43 μM for MT in ethanol and micelles, respectively (Figure 5d). Data reported by Silveira et al. suggest that 72 h incubation time of NCI-H295 cell spheroids[87] led to 15 and 26% cell viability at 30 and 50 μM MT concentration (dissolved in ethanol), respectively. However, it is possible that different strains of NCI-H295 cells and culture conditions may affect the properties of spheroids cultivated in different laboratories.

When comparing the increase of IC_{50} values from 2D monolayer cultures to 3D spheroids we observed a more pronounced increase of IC_{50} values for MT in EtOH compared to our nanoformulation. At 24 h incubation, the increase was fivefold when using EtOH but only 3.4-fold in case of the nanoformulation. At 48 h, the IC_{50} values increased 3.1 (EtOH) and 2.4 (A-pBuOx-A) fold. This could potentially be attributed to a better penetration of the drug into the spheroids when nanoformulated, but this hypothesis will need to be tested thoroughly.

4. Conclusion

Motivated by the poor aqueous solubility (0.1 mg L^{-1}), extremely high daily dosage (up to 6 g per day in divided doses) and unfavorable pharmacokinetic profile of the adrenolytic drug mitotane (MT), we attempted the development of MT loaded micelles which may enable both improved oral administration and an injectable formulation to overcome critical clinical limitations. A poly(2-oxazoline) (POx) based formulation ($pMeOx_{35}$-$pBuOx_{20}$-$pMeOx_{35}$) was capable to increase the aqueous solubility of MT to around 6 g L^{-1} (LC ≈ 36 wt%). To the best of our knowledge, such high MT water solubility has never been reported in the literature. Various instrumental techniques confirmed the development of a stable nanoformulation. This formulation can be stored as lyophilized powder ready for re-dispersion. The polymer excipient was proven to be highly cytocompatible even at extremely high concentrations of 100 g L^{-1} in NCI-H295R and HepG2 cell lines (cell viability > 95%). The obtained IC_{50} values in conventional 2D monolayer cell cultures were comparable for MT dissolved in EtOH and micelles (15 and 19 μM, respectively) while in the case of 3D tumor spheroids higher doses were needed to obtained cytotoxic effects, which confirms an increased resistance of the tumor cells cultured in 3D. The IC_{50} at 24 h values were 75 and 65 μM for MT in EtOH and micelles, respectively. Time dependent decrease in IC_{50} after 48 h incubation was observed in case of spheroids (47 and 43 μM for MT in EtOH and micelles, respectively) which points to a diffusion limited process of tissue penetrance. It stands to reason that this nanoformulation, for the first time, might allow the parenteral administration of MT, which will help to alleviate not only the side effects associated with the use of high dose oral therapy of 6 g per day but also circumventing the variable oral absorption resulting in more predictable therapeutic plasma concentration and better

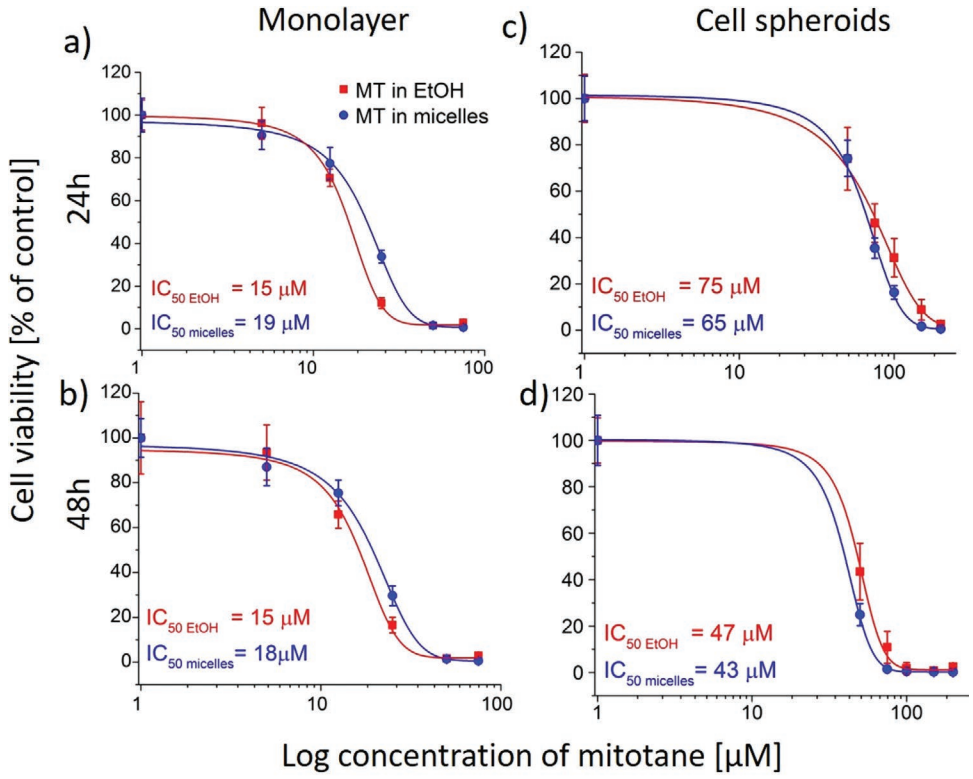

Figure 5. Cell viability and corresponding IC_{50} values of mitotane dissolved in ethanol (red) and as micelles formulation (blue) in NCI-H295R monolayer after incubation for a) 24 and b) 48 h and 3D tumor spheroids c) 24 h and d) 48 h) as determined by CellTiterGlo assay. Monolayer and tumor spheroids were treated with the range of mitotane concentrations dissolved in ethanol and as A-pBuOx-A nanoformulation. All the values are average of replicates expressed relative to cell viability values in control cells normalized to 100%. Data points represent average of $n = 3$ experiments with eight technical replicates per mitotane concentration for each experiment ± standard deviation.

pharmacokinetic profile. However, the safety and tolerability of this injectable formulation remain to be demonstrated.

Supporting Information

Supporting Information is available from the Wiley Online Library or from the author.

Acknowledgements

This work was supported by Deutsche Forschungsgemeinschaft (DFG), German Research Foundation Project no. 398461692 to R.L. and 314061271 – TRR205 and 237292849 to M.K). Moreover, Malik Salman Haider is grateful to the Higher education commission of Pakistan and German academic exchange services (HEC-DAAD Pakistan) for the award of Ph.D. scholarship. The authors thank Lukas Hahn for providing A-pBzOx-A triblock copolymer as well as André Muthig and Thomas Lorson technical support. Also, the authors are indebted to Prof. Ann-Christin Pöppler for measuring DOSY NMR spectra of P1 and very valuable discussions.

Conflict of Interest

R.L. is listed as co-inventor of several patents pertinent to the present contribution and is co-founder of Delaqua Pharmaceutical Inc. intending commercial development of poly(2-oxazoline)-based drug delivery systems.

Keywords

adrenocortical carcinoma, amphiphilic block copolymer, NCI-H295R, poly(2-oxazoline), solubility enhancement

Received: May 22, 2019
Revised: August 16, 2019
Published online:

[1] B. Allolio, M. Fassnacht, *J. Clin. Endocrinol. Metabol.* **2006**, *91*, 2027.
[2] E. Kebebew, E. Reiff, Q. Y. Duh, O. H. Clark, A. McMillan, *World J. Surg.* **2006**, *30*, 872.
[3] T. M. Kerkhofs, R. H. Verhoeven, J. M. Van der Zwan, J. Dieleman, M. N. Kerstens, T. P. Links, L. V. Van de Poll Franse, H. R. Haak, *Europ. J. Cancer* **2013**, *49*, 2579.
[4] I. Veytsman, L. Nieman, T. Fojo, *J. Clin. Oncol.* **2009**, *27*, 4619.
[5] S. Sbiera, E. Leich, G. Liebisch, I. Sbiera, A. Schirbel, L. Wiemer, S. Matysik, C. Eckhardt, F. Gardill, A. Gehl, *Endocrinology* **2015**, *156*, 3895.
[6] S. Hescot, L. Amazit, M. Lhomme, S. Travers, A. DuBow, S. Battini, G. Boulate, I. J. Namer, A. Lombes, A. Kontush, *Oncotarget* **2017**, *8*, 109924.

[7] S. Hescot, A. Slama, A. Lombes, A. Paci, H. Remy, S. Leboulleux, R. Chadarevian, S. Trabado, L. Amazit, J. Young, *Endocrine-Related Cancer* **2014**, *20*, 371.
[8] A. Berruti, E. Baudin, H. Gelderblom, H. Haak, F. Porpiglia, M. Fassnacht, G. Pentheroudakis, *Ann. Oncol.* **2012**, *23*, vii131.
[9] I. Bourdeau, J. M. Feder, A. Lacroix, *Current Opinion Endocrinol. Diabetes Obesity* **2013**, *20*, 192.
[10] M. Fassnacht, M. Kroiss, B. Allolio, *J. Clin. Endocrinol. Metabol.* **2013**, *98*, 4551.
[11] T. Else, A. C. Kim, A. Sabolch, V. M. Raymond, A. Kandathil, E. M. Caoili, S. Jolly, B. S. Miller, T. J. Giordano, G. D. Hammer, *Endocrine Rev.* **2014**, *35*, 282.
[12] M. Fassnacht, O. Dekkers, T. Else, E. Baudin, A. Berruti, R. R. De Krijger, H. Haak, R. Mihai, G. Assie, M. Terzolo, *Eur. J. Endocrinol.* **2018**, *179*, G1.
[13] E. Baudin, G. Pellegriti, M. Bonnay, A. Penfornis, A. Laplanche, G. Vassal, M. Schlumberger, *Cancer* **2001**, *92*, 1385.
[14] M. Terzolo, A. Baudin, A. Ardito, M. Kroiss, S. Leboulleux, F. Daffara, P. Perotti, R. Feelders, B. Zaggia, S. De Francia, *Eur. J. Endocrinol.* **2013**, *169*, 263.
[15] I. G. Hermsen, M. Fassnacht, M. Terzolo, S. Houterman, J. den Hartigh, S. Leboulleux, F. Daffara, A. Berruti, R. Chadarevian, M. Schlumberger, *J. Clin. Endocrinol. Metabol.* **2011**, *96*, 1844.
[16] F. Megerle, W. Herrmann, W. Schloetelburg, C. L. Ronchi, A. Pulzer, M. Quinkler, F. Beuschlein, S. Hahner, M. Kroiss, M. Fassnacht, *J. Clin. Endocrinol. Metabol.* **2018**, *103*, 1686.
[17] T. Kerkhofs, E. Baudin, M. Terzolo, B. Allolio, R. Chadarevian, H. Mueller, B. Skogseid, S. Leboulleux, F. Mantero, H. Haak, *J. Clin. Endocrinol. Metabol.* **2013**, *98*, 4759.
[18] M. Kroiss, D. Plonné, S. Kendl, D. Schirmer, C. L. Ronchi, A. Schirbel, M. Zink, C. Lapa, H. Klinker, M. Fassnacht, *Eur. J. Endocrinol.* **2016**, *174*, 343.
[19] U. Arshad, M. Taubert, M. Kurlbaum, S. Frechen, S. Herterich, F. Megerle, S. Hamacher, M. Fassnacht, U. Fuhr, M. Kroiss, *Eur. J. Endocrinol.* **2018**, *179*, 287.
[20] S. Hescot, A. Paci, A. Seck, A. Slama, S. Viengchareun, S. Trabado, S. Brailly Tabard, A. Al Ghuzlan, J. Young, E. Baudin, *Hormon. Cancer* **2014**, *5*, 312.
[21] V. Sreif, J. Sinsheimer, J. Ward, D. Schteingart, *J. Pharm. Sci.* **1974**, *63*, 1730.
[22] A. Mornar, M. Sertić, N. Turk, B. Nigović, M. Koršić, *Biomed. Chromatogr.* **2012**, *26*, 1308.
[23] N. P. van Erp, H. J. Guchelaar, B. A. Ploeger, J. A. Romijn, J. den Hartigh, H. Gelderblom, *Eur. J. Endocrinol.* **2011**, *164*, 621.
[24] M. Kroiss, M. Quinkler, W. K. Lutz, B. Allolio, M. Fassnacht, *Clin. Endocrinol.* **2011**, *75*, 585.
[25] V. Chortis, A. E. Taylor, P. Schneider, J. W. Tomlinson, B. A. Hughes, D. M. O'neil, R. Libé, B. Allolio, X. Bertagna, J. Bertherat, *J. Clin. Endocrinol. Metabol.* **2013**, *98*, 161.
[26] D. Theile, W. E. Haefeli, J. Weiss, *Endocrine* **2015**, *49*, 842.
[27] J. W. Biggar, R. L. Riggs, *Hilgardia* **1974**, *42*, 383.
[28] R. Takano, K. Furumoto, K. Shiraki, N. Takata, Y. Hayashi, Y. Aso, S. Yamashita, *Pharm. Res.* **2008**, *25*, 2334.
[29] H. v. Slooten, A. V. Seters, D. Smeenk, A. Moolenaar, *Cancer Chemother. Pharmacol.* **1982**, *9*, 85.
[30] D. Attivi, I. Ajana, A. Astier, B. Demore, S. Gibaud, *Drug Dev. Ind. Pharm.* **2010**, *36*, 421.
[31] F. Battung, E. Hassan, L. Sansoe, US8486445B2 **2013**.
[32] E. Hassan, WO2012071043A1 **2015**.
[33] D. Gebhardt, A. Moolenaar, A. V Seters, E. Van Der Velde, J. G. Leuven, *Cancer Chemother. Pharmacol.* **1992**, *29*, 331.
[34] R. C. Pohland, R. E. Counsell, *Toxicol. Appl. Pharmacol.* **1985**, *77*, 47.
[35] S. Hescot, A. Seck, M. Guerin, F. Cockenpot, T. Huby, S. Broutin, J. Young, A. Paci, E. Baudin, M. Lombès, *J. Clinical Endocrinol. Metabol.* **2015**, *100*, 2890.
[36] V. Maher, P. Trainer, A. Scoppola, J. Anderson, G. Thompson, G. Besser, *Q. J. Med* **1992**, *84*, 671.
[37] N. Nishiyama, K. Kataoka, *Pharmacol. Ther.* **2006**, *112*, 630.
[38] K. Kataoka, A. Harada, Y. Nagasaki, *Adv. Drug Delivery Rev.* **2012**, *64*, 37.
[39] H. Cabral, N. Nishiyama, K. Kataoka, *J. Controlled Release* **2007**, *121*, 146.
[40] J. Logie, A. N. Ganesh, A. M. Aman, R. S. Al awar, M. S. Shoichet, *Biomaterials* **2017**, *123*, 39.
[41] H. Cabral, K. Kataoka, *J. Controlled Release* **2014**, *190*, 465.
[42] E. Vlassi, A. Papagiannopoulos, S. Pispas, *Eur. Polym. J.* **2017**, *88*, 516.
[43] R. Hoogenboom, *Eur. Polym. J.* **2017**, *88*, 448.
[44] T. Lorson, M. M. Lübtow, E. Wegener, M. S. Haider, S. Borova, D. Nahm, R. Jordan, M. Sokolski-Papkov, A. V. Kabanov, R. Luxenhofer, *Biomaterials* **2018**, *178*, 204.
[45] Y. Han, Z. He, A. Schulz, T. K. Bronich, R. Jordan, R. Luxenhofer, A. V. Kabanov, *Mol. Pharmaceutics* **2012**, *9*, 2302.
[46] R. Luxenhofer, G. Sahay, A. Schulz, D. Alakhova, T. K. Bronich, R. Jordan, A. V. Kabanov, *J. Controlled Release* **2011**, *153*, 73.
[47] H. Witte, W. Seeliger, *Justus Liebigs Annalen der Chemie* **1974**, *1974*, 996.
[48] M. M. Lübtow, L. Hahn, M. S. Haider, R. Luxenhofer, *J. Am. Chem. Soc.* **2017**, *139*, 10980.
[49] M. M. Lübtow, L. Keßler, A. Appelt Menzel, T. Lorson, N. Gangloff, M. Kirsch, S. Dahms, R. Luxenhofer, *Macromol. Biosci.* **2018**, *18*, 1800155.
[50] L. Hahn, M. M. Lübtow, T. Lorson, F. Schmitt, A. Appelt-Menzel, R. Schobert, R. Luxenhofer, *Biomacromolecules* **2018**, *19*, 3119.
[51] K. Letchford, R. Liggins, H. Burt, *J. Pharm. Sci.* **2008**, *97*, 1179.
[52] R. F. Fedors, *Polym. Eng. Sci.* **1974**, *14*, 147.
[53] A. F. Gazdar, H. K. Oie, C. H. Shackleton, T. Chen, T. J. Triche, C. E. Myers, G. P. Chrousos, M. F. Brennan, C. Stein, R. V. La Rocca, *Cancer Res.* **1990**, *50*, 5488.
[54] R. Luxenhofer, M. Bezen, R. Jordan, *Macromol. Rapid Commun.* **2008**, *29*, 1509.
[55] N. Zhang, S. Huber, A. Schulz, R. Luxenhofer, R. Jordan, *Macromolecules* **2009**, *42*, 2215.
[56] B. Guillerm, S. Monge, V. Lapinte, J. J. Robin, *Macromol. Rapid Commun.* **2012**, *33*, 1600.
[57] N. Zhang, R. Luxenhofer, R. Jordan, *Macromol. Chem. Phys.* **2012**, *213*, 973.
[58] R. Luxenhofer, A. Schulz, C. Roques, S. Li, T. K. Bronich, E. V. Batrakova, R. Jordan, A. V. Kabanov, *Biomaterials* **2010**, *31*, 4972.
[59] R. Luxenhofer, *Nanomedicine* **2015**, *10*, 3109.
[60] Z. He, A. Schulz, X. Wan, J. Seitz, H. Bludau, D. Y. Alakhova, D. B. Darr, C. M. Perou, R. Jordan, I. Ojima, *J. Controlled Release* **2015**, *208*, 67.
[61] Y. Milonaki, E. Kaditi, S. Pispas, C. Demetzos, *J. Polym. Sci., Part A: Polym. Chem.* **2012**, *50*, 1226.
[62] X. Wan, Y. Min, H. Bludau, A. Keith, S. S. Sheiko, R. Jordan, A. Z. Wang, M. Sokolsky Papkov, A. V. Kabanov, *ACS Nano* **2018**, *12*, 2426.
[63] S. Lv, Y. Wu, K. Cai, H. He, Y. Li, M. Lan, X. Chen, J. Cheng, L. Yin, *J. Am. Chem. Soc.* **2018**, *140*, 1235.
[64] S. Wieczorek, D. Remmler, T. Masini, Z. Kochovski, A. K. Hirsch, H. G. Börner, *Bioconjugate Chem.* **2017**, *28*, 760.
[65] J. Ding, L. Chen, C. Xiao, L. Chen, X. Zhuang, X. Chen, *ChemComm* **2014**, *50*, 11274.
[66] Y. Shi, M. J. van Steenbergen, E. A. Teunissen, L. Novo, S. Gradmann, M. Baldus, C. F. van Nostrum, W. E. Hennink, *Biomacromolecules* **2013**, *14*, 1826.

[67] P. Severino, E. B. Souto, S. C. Pinho, M. H. Santana, *Pharm. Dev. Technol.* **2013**, *18*, 577.
[68] A. Schulz, S. Jaksch, R. Schubel, E. Wegener, Z. Di, Y. Han, A. Meister, J. r. Kressler, A. V. Kabanov, R. Luxenhofer, *ACS Nano* **2014**, *8*, 2686.
[69] Y. Seo, A. Schulz, Y. Han, Z. He, H. Bludau, X. Wan, J. Tong, T. K. Bronich, M. Sokolsky, R. Luxenhofer, *Polym. Adv. Technol.* **2015**, *26*, 837.
[70] J. Wiest, M. Saedtler, B. Böttcher, M. Grüne, M. Reggane, B. Galli, U. Holzgrabe, L. Meinel, *Mol. Pharmaceutics* **2018**, *15*, 4470.
[71] A. C. Pöppler, M. M. Lübtow, J. Schlauersbach, J. Wiest, L. Meinel, R. Luxenhofer, *ChemRxiv* **2019**, https://doi.org/10.26434/chemrxiv.8943251.v1.
[72] M. M. Lübtow, L. C. Nelke, J. Seifert, J. Kühnemundt, G. Sahay, G. Dandekar, S. L. Nietzer, R. Luxenhofer, *J. Controlled Release* **2019**, *303*, 162.
[73] M. M. Lübtow, M. S. Haider, M. Kirsch, S. Klisch, R. Luxenhofer, *Biomacromolecules* **2019**, *20*, 3041.
[74] C. Cao, J. Zhao, F. Chen, M. Lu, Y. Y. Khine, A. Macmillan, C. J. Garvey, M. H. Stenzel, *Chem. Mater.* **2018**, *30*, 5227.
[75] C. Cao, J. Zhao, M. Lu, C. J. Garvey, M. H. Stenzel, *Biomacromolecules* **2019**, *20*, 1545.
[76] M. Callari, P. L. De Souza, A. Rawal, M. H. Stenzel, *Angew. Chem.* **2017**, *129*, 8561.
[77] Z. Li, T. I. Lenk, L. J. Yao, F. S. Bates, T. P. Lodge, *Macromolecules* **2018**, *51*, 540.
[78] J. Liu, Y. Xiao, C. Allen, *J. Pharm. Sci.* **2004**, *93*, 132.
[79] C. Wu, J. W. McGinity, *Int. J. Pharm.* **1999**, *177*, 15.
[80] R. Nair, N. Nyamweya, S. Gönen, L. M. Miranda, S. Hoag, *Int. J. Pharm.* **2001**, *225*, 83.
[81] S. Y. Lin, C. J. Lee, Y. Y. Lin, *J. Controlled Release* **1995**, *33*, 375.
[82] B. Hossin, K. Rizi, S. Murdan, *Eur. J. Pharm. Biopharm.* **2016**, *102*, 32.
[83] C. M. Hansen, *Hansen Solubility Parameters: a User's Handbook*, CRC press, Boca Raton **2007**.
[84] A. F. Barton, *CRC Handbook of Solubility Parameters and other Cohesion Parameters*, Routledge, New York **2017**.
[85] Z. He, X. Wan, A. Schulz, H. Bludau, M. A. Dobrovolskaia, S. T. Stern, S. A. Montgomery, H. Yuan, Z. Li, D. Alakhova, *Biomaterials* **2016**, *101*, 296.
[86] M. Terzolo, A. Angeli, M. Fassnacht, F. Daffara, L. Tauchmanova, P. A. Conton, R. Rossetto, L. Buci, P. Sperone, E. Grossrubatscher, *N. Engl. J. Med.* **2007**, *356*, 2372.
[87] E. Silveira, I. P. Cavalcante, J. L. Kremer, P. O. R. de Mendonça, C. F. P. Lotfi, *Cancer Cell Int.* **2018**, *18*, 29.
[88] J. Friedrich, C. Seidel, R. Ebner, L. A. K. Schughart, *Nat. Protoc.* **2009**, *4*, 309.
[89] L. B. Weiswald, D. Bellet, V. Dangles Marie, *Neoplasia* **2015**, *17*, 1.

4.6.2 BT44 formulation

Summary: While exploring the therapeutic potential of POx/POzi based micelles, we came across another small molecule i.e. BT44 with poor aqueous solubility. It is a lead compound, being investigated for its potential for neurodegenerative disorders. Neuronal damage may lead to variety of neurodegenerative disorders like Alzheimer's disease, retinal degeneration, amyotrophic lateral sclerosis and neuropathic pain. Like many other small molecules, the poor aqueous solubility of BT44 also pose significant hurdles at various levels for its pre-clinical development and further translation. In this study, we tested the solubilizing capacity of three pure POx based amphiphiles with the increasing side chain length in hydrophobic blocks i.e. poly(2-proyl-2-oxazoline) (pPrOx), poly(2-butyl-2-oxazoline) (pBuOx), poly(2-pentyl-2-oxazoline) (pPentOx). The pPentOx based triblock copolymer gave the highest loading capacity of 47 wt.%. The BT44 formulation was further characterized by ^{1}H-NMR spectroscopy, differential scanning calorimetry (DSC), powder X-ray diffraction (XRD), dynamic light scattering (DLS) and cryo-tranmission/scanning electron microscopy (cryo-TEM/SEM). This novel BT44 formulation has also been tested in vivo and have shown promising results.

Biological activity *In vitro*, absorption, BBB penetration and toxicity of nanoformulation of BT44: RET agonist with disease-modifying potential for the treatment of neurodegeneration

Malik Salman Haider[1,6,‡,*], Arun Kumar Mahato[2,‡], Anastasiia Kotliarova[2], Stefan Forster[1], Bettina Böttcher[3], Philipp Stahlhut[4], Yulia Sidorova[2,*‡], Robert Luxenhofer[1,5‡]

[1]*Functional Polymer Materials, Chair for Advanced Materials Synthesis, Institute for Functional Materials and Biofabrication, Department of Chemistry and Pharmacy, Julius-Maximilians-University Würzburg, Röntgenring 11, 97070 Würzburg, Germany*

[2]*Laboratory of Molecular Neuroscience, Institute of Biotechnology, HiLIFE, University of Helsinki, 00014, Helsinki, Finland*

[3]*Biocenter and Rudolf Virchow Centre, Julius-Maximilians-University Würzburg, Haus D15, Josef-Schneider-Str. 2, 97080 Würzburg, Germany*

[4]*Department of Functional Materials in Medicine and Dentistry, Institute of Functional Materials and Biofabrication and Bavarian Polymer Institute, Julius-Maximilians-University Würzburg, Pleicherwall 2, 97070 Würzburg, Germany*

[5]*Soft Matter Chemistry, Department of Chemistry, and Helsinki Institute of Sustainability Science, Faculty of Science, University of Helsinki, PB 55, 00014 Helsinki, Finland*

[6]*University Hospital of Würzburg, Department of Ophthalmology, Josef-Schneider-Street 11, D-97080 Würzburg, Germany*

Keywords: Receptor tyrosine kinase RET, RET agonist, glial cell line-derived neurotrophic factor (GDNF), neurodegeneration, blood brain barrier, solubility enhancement, drug delivery, amphiphilic block copolymer, poly(2-oxazoline), nanomedicine

‡ contributed equally

*Correspondence to: haider_m@ukw.de and yulia.sidorova@helsinki.fi

Abstract

BT44 is a novel, second generation glial cell line-derived neurotropic factor (GDNF) mimetic, with improved biological activity and a lead compound for the treatment of neurodegenerative disorders. Like many other small molecules, it suffers from intrinsic poor aqueous solubility, posing significant hurdles at various levels for its preclinical development and clinical translation. Herein, we report a poly(2-oxazoline)s (POx) based BT44 micellar nanoformulation with ultra-high drug loading capacity of 47 wt.%. The BT44 nanoformulation was comprehensively characterized by ^{1}H-NMR spectroscopy, differential scanning calorimetry (DSC), powder X-ray diffraction (XRD), dynamic light scattering (DLS) and cryo-transmission/scanning electron microscopy (cryo-TEM/SEM). The DSC, XRD and redispersion studies collectively confirmed that the BT44 formulation can be stored as a lyophilized powder and can be redispersed upon need. The DLS suggested that the redispersed formulation is suitable for parenteral administration (D_h ≈ 70 nm). The cryo-TEM analysis revealed the presence of worm like structures both in plain polymer and BT44 formulation. The BT44 formulation retained biological activity in immortalized cells and in cultured dopamine neurons. The micellar nanoformulation of BT44 exhibited improved absorption (after subcutaneous injection) and blood-brain barrier (BBB) penetration and no acute toxic effects in mice were observed. In conclusion, herein, we have developed an ultra-high BT44 loaded aqueous injectable nanoformulation, which can be used to pave way for its preclinical and clinical development for the management of neurodegenerative disorders.

Introduction

In the past decades, drug discovery has seen significant advancements in technological innovation resulting in development of large number of potential candidates as drug molecules. However, according to some estimate, 90% of the drugs in the development pipeline and 40% of the drugs in the market are highly hydrophobic (poor aqueous solubility) [1]. Unfortunately, poor intrinsic aqueous solubility is a common factor in both synthetic and naturally occurring pharmacophores [2], posing a significant risk for varied oral absorption and require special vehicles for injectable applications. The aqueous solubility plays a pivotal role in the overall product design to attain higher bioavailability and optimum therapeutic concentration at the site of interest.

The aging population brings new challenges and demands to the society in the context of drug development. Elderly people often suffer from co-morbidities that require diverse pharmacological management. In particular, currently incurable neurodegenerative disorders such as Parkinson's disease (PD), retinal degeneration, amyotrophic lateral sclerosis and neuropathic pain affect ever increasing number of patients in the modern society. These disorders are caused by the death of various neuronal populations in the body and are currently incurable [3-5]. The potential disease-modifying treatments can be developed on the basis of neurotrophic factors and secreted proteins which function as the survival and maintenance factors for both developing and mature neurons [6].

Glial cell line-derived neurotrophic factor (GDNF) is the most promising protein for the treatment of PD. GDNF first binds to glycosylphosphatidylinositol-anchored co-receptor GDNF family receptor α and then form a complex with Rearranged during transfection (RET) receptor tyrosine kinase resulting in activation of RET. This leads to RET downstream signalling cascades necessary for the cellular processes like migration, proliferation, differentiation and metabolism [6]. However, GDNF lacks drug-like properties making its clinical translation more challenging. Previously, we have designed and developed series of RET agonists that can bind and activate RET receptor similar to GDNF [7, 8]. Among them, BT44 is a second generation compound that alleviated neuropathic pain in both surgery-based and diabetes-induced models of neuropathic pain in rat models [9]. Further, BT44 also protected

cultured dopamine neurons from neurotoxic damage. It also alleviated motor symptoms and protected dopaminergic fibers in the striatum of 6-hydroxydopamine (6-OHDA) model of PD [10]. Therefore, it is a promising lead compound for the treatment of neurodegenerative disorders and neuropathic pain [9, 10]. However, like many other hydrophobic drugs, BT44 also suffers from intrinsic poor aqueous solubility, posing significant hurdles at various levels for its preclinical development and further clinical translation.

Various methods such as the preparation of salts forms, drug complexes, use of co-solvents [11], drug emulsification, micro-/nanonization, crystal engineering, solid dispersion [12, 13] and nanotechnological approaches are used to enhance the (apparent) aqueous solubility of such molecules. Among all, the nanocarrier approach is a rapidly emerging tool to address such issues [14, 15]. A plethora of studies showed the utilization of nanoparticles, nanospheres, nanocapsules, nanosuspension/-emulsion and micelles for drug delivery applications mainly in the context of solubility enhancement [16, 17].

Besides others, over the last thirty years, polymer micelles (PMs) evolved as promising hydrophobic drug solubilisation and/or delivery vehicle [18-20]. They are self-assembled colloidal particles made up of block copolymers comprising hydrophilic and hydrophobic domains [21]. It is commonly believed that the hydrophobic core is responsible for drug encapsulation and the hydrophilic shell interacts with solvent molecules (representing core-shell morphology) providing colloidal stability [22, 23]. However, depending upon the nature of the hydrophilic domain, cargo and employed (cargo) load, it is becoming more evident that at certain threshold cargo concentration, the hydrophilic domain also starts to interact [24-31] with the cargo, indicative of much more complex morphologies [32-34]. To date, many polymeric micellar formulations underwent preclinical and clinical trials presenting improved pharmacological activity with lower systemic toxicity but successful translation into clinics were few [20, 35-37]. Like other excipients used for formulation development, amphiphilic block copolymers used as vehicles used for such formulations, must also be pharmacologically inert and clinically safe [38].

In the past decades, polymers of cyclic imino ethers [39], particularly poly(2-oxazoline)s (POx) and poly(2-oxazines)s (POzi) have gained significant attention because of their potential in tissue engineering [40-42], drug delivery [37, 43-50] and 3D (bio) printing [42, 51-53]. Based on a highly variable molecular toolbox, fine tuning of the amphiphilic character in AB diblock, ABA triblock or more complex architectures [54] is readily achieved (where A and B are hydrophilic and hydrophobic domains, respectively) [55-58]. In particular, ABA triblock copolymers featuring poly(2-methyl-2-oxazoline) (pMeOx) as hydrophilic A block and moderately hydrophobic poly(2-*n*-butyl-2-oxazoline) (pBuOx), poly(2-*n*-butyl-2-oxazine) (pBuOzi) or poly(2-*n*-propyl-2-oxazoline) (pPrOx) showed interesting properties such as ultra-high drug loading, excellent cytocompatibility and appeared to be well tolerated upon *in vivo* administration [44, 51, 59, 60]. More importantly, they allow significant therapeutic improvements as already demonstrated for several drugs and drug combinations [37, 61-63]. Accordingly, here we report on a micelles based nanoformulation of BT44, a compound which has poor intrinsic aqueous solubility, using POx based ABA triblock copolymers. To the best of our knowledge, this represents the first example of any micellar BT44 nanoformulation with a detailed physicochemical characterization which retains biological activity, demonstrates improved absorption and better blood-brain barrier (BBB) penetration compared to the non-formulated drug upon *in vivo* administration.

Materials and Methods

All substances for the synthesis of polymers were purchased from *Sigma-Aldrich* (Steinheim, Germany) or *Acros* (Geel, Belgium) and were used as received unless otherwise stated. The monomers used in this study are 2-*n*-propyl-2-oxazoline (PrOx), 2-*n*-butyl-2-oxazoline (BuOx) and 2-*n*-pentyl-2-oxazoline (PentOx). The monomer PentOx was particularly synthesized for this study, following a modified procedure of Witte and Seeliger [64] as reported recently [55, 65]. All the other substances used for polymerization i.e. methyl trifluoromethylsulfonate (MeOTf), 2-methyl-2-oxazoline (MeOx) and solvents for polymer synthesis were refluxed over calcium hydride, while benzonitrile (PhCN) was refluxed over P_2O_5 and distilled under argon. Deuterated solvents for NMR analysis were purchased from *Deutero GmbH* (Kastellaun, Germany).

Monomer synthesis

1 equiv. of hexanenitrile, 1.2 equiv. of ethanolamine and 0.025 equiv. of zinc acetate dihydrate were added to a nitrogen flushed flask and heated to 130 °C (SI; synthesis 1). The reaction was kept under reflux (for 4 days) until the reaction mixture turned dark brown. The reaction progress was controlled by ^{1}H-NMR-spectroscopy. The raw product was dissolved in chloroform (30 mL) and washed with deionized (DI) water (60 mL, 3 times). The organic phase was collected and dried with sodium sulfate, filtered and concentrated under vacuum. The residue was mixed with calcium hydride and distilled under vacuum. If necessary, distillation was repeated and the product was stored under argon atmosphere.

Polymer synthesis

The polymerizations and work-up procedures for A-pPrOx-A and A-pBuOx-A triblock copolymers are previously reported [55, 65-67]. The synthesis of A-pPentOx-A triblock copolymer was performed as follows (for details, SI; synthesis 2): the initiator, MeOTf was added to a dried and argon flushed flask followed by PhCN addition. Further, the monomer for the first hydrophilic block (A) i.e. MeOx was added, the reaction mixture was heated to 110°C and incubated under continuous stirring for approximately 4 hours. The reaction progress was controlled by ^{1}H-NMR-spectroscopy. After

complete polymerization of MeOx, the mixture was cooled to room temperature and the monomer for the second block i.e. PentOx was added. The reaction mixture was heated to 110°C and kept on stirring overnight. The procedure was repeated for the third block (MeOx) and after confirmation of full monomer consumption, termination was carried out by addition of 5 eq. of 1 M sodium hydroxide aqueous solution and the mixture was stirred at 50°C for 4 hours. The PhCN was removed under reduced pressure. The highly viscous polymeric residues were dissolved in DI water, transferred into a dialysis bag and dialyzed against DI water for 24 h. The solution was recovered from the bag and lyophilized. The product was obtained as white powder (Yield = 92%).

Lead compound; BT44

BT stands for Baltic Technology, a company, which was originally involved into the discovery of this scaffold. The chemical name for the BT44 is ((4-5-((3,4-dihydroisoquinolin-2(1H)-yl) sulfonyl)-2-methoxyphenyl) piperazin-1-yl (4-fluoro-2 (trifluoromethyl)phenyl) methanone, with the molecular weight of 577.59. The compound was synthesized by EvoBlocks (Hungary, Cat# EBR-10719615). The chemical structure of BT44 was verified by ^{1}H-NMR spectroscopy. The experiments were performed on a Bruker Avance III HD NMR spectrometer operated at 1H frequency of 850.4 MHz equipped with a cryogenic probe head by NMR facility at the Institute of Biotechnology, University of Helsinki, Finland. The purity was further determined by HPLC (97.3%).

Methods

Nuclear Magnetic Resonance Spectroscopy (NMR)

The NMR spectra of monomers, polymers and nanoformulations were recorded on a Fourier 300 (300.12 MHz), *Bruker Biospin* (Rheinstetten, Germany) at 298 K. The spectra were calibrated to the signal of residual protonated solvent ($CDCl_3$ at 7.26 ppm, or D_2O at 4.79 ppm) and analyzed using MestReNova software (version 6.0.2-5475).

Dialysis

The synthesized polymer was dialysed using Spectra/Por membranes with a MWCO of 1 kDa (material: cellulose acetate) obtained from *neoLab* (Heidelberg, Germany). The DI water was renewed after 1, 4,

12 and 24 h and the resulting polymer solution was lyophilized for 48 hours. After lyophilization the polymer was obtained as white flakes.

Gel Permeation Chromatography (GPC)

Gel permeation chromatography (GPC) was performed on SECurity GPC Agilent 1260 Infinity System (*Polymer Standard Service* (Mainz, Germany) with HFIP containing 3 g/L potassium trifluoroacetate; precolumn: 50 x 8 mm PSS PFG linear M; 2 columns: 300 x 8 mm PSS PFG linear M (particle size 7 µm; pore size 0.1 – 1,000 kDa). The columns were kept at 40°C and flow rate was 0.7 ml/min. Prior to each measurement, samples were filtered through 0.2 µm Teflon (PTFE) filters, *Roth* (Karlsruhe, Germany). Conventional calibration was performed using poly(ethylene glycol) standards (0.1 – 1,000 kg/mol) and data was processed with Win-GPC software and further plotted in OriginPro 2015 Sr2 (version b9.2.272) software.

Thermogravimetric analysis (TGA)

Thermogravimetric analysis was performed on TG 209 F1 IRIS, *NETZSCH* (Selb, Germany). The powdered polymer sample (10-15 mg) were placed in aluminium oxide crucibles (*NETZSCH* Selb, Germany) and heated under synthetic air from 30°C to 900°C with the heating rate of 10 K/min while detecting the mass loss.

Polymer-drug compatibility by solubility parameters

The extent of compatibility between BT44 and the hydrophobic block of the A-B-A triblock copolymers was estimated by using the Hildebrand-Scatchard equation [68].

$$\chi_{drug-polymer} = (\delta_{drug} - \delta_{polymer})^2 \frac{V}{RT} \quad (1)$$

Where $\chi_{drug\text{-}polymer}$ (χ_{dp}) represents the Flory-Huggins interaction parameter, δ_{drug} and $\delta_{polymer}$ are the solubility parameters for the drug (BT44) and polymer, respectively. The V is the molar volume of BT44 calculated by Fedor's method [69], R is the gas constant and T is the temperature in K. The δ_{drug} and $\delta_{polymer}$ were calculated by following equations:

$$\delta^2_{drug} = \delta^2_d + \delta^2_p + \delta^2_h \quad (2)$$

$$\delta^2_{polymer} = \delta^2_d + \delta^2_p + \delta^2_h \quad (3)$$

The δ_{drug} and $\delta_{polymer}$ are representing the total solubility parameters (δ_{total}) for drug and polymer, respectively. The δ_{total} is the sum of dispersion (δ_d), polar (δ_p) and hydrogen bonding contributions

(δ_h). The δ_d, δ_p and δ_h were further calculated by Hoftyzer and Van Krevelen's additive group contribution method by using the following equations:

$$\delta_d = \frac{\sum Fdi}{V} \qquad \delta_p = \frac{(\Sigma F_{pi}^2)^{1/2}}{V} \qquad \delta_h = (\Sigma \frac{E_{hi}}{V})^{1/2} \qquad (4, 5, 6)$$

Where F_{di}, F_{pi} and E_{hi} are the molar dispersion, polar attraction constant and hydrogen bonding energy, respectively. Each structural group in the molecule contribute towards the F_{di}, F_{pi} and E_{hi}, the subsequent values were obtained from literature [70].

Drug formulation

The BT44 loaded polymer micelles were prepared using the thin film hydration method. Initially, the polymer (10 or 100 g/L) and the BT44 (15 g/L) stock solutions in ethanol (EtOH) were mixed in desired ratios. After complete removal of the EtOH at 50°C under a mild stream of argon, the films were further dried *in vacuo* (≤ 0.2 mbar) for at least 30 minutes, to remove the traces of ethanol (if any). Subsequently, preheated (37°C) DI water was added to obtain the desired final polymer (10 or 100 g/L) and BT44 concentrations. To ensure complete solubilisation, the formulations were shaken at 55°C for 15 to 30 min at 1250 rpm with a Thermomixer comfort (*Eppendorf AG,* Hamburg, Germany). Non-solubilized BT44 was removed by centrifugation (for 5 min at 10,000 rpm) with a 3-Speed micro centrifuge, (*neoLab,* Heidelberg, Germany). The solubilisation experiments were performed in 3 individually prepared samples and results are presented as mean ± standard deviation (SD).

High performance liquid chromatography (HPLC)

The quantification of BT44 was performed by HPLC. The HPLC analysis was carried out on a LC-20A Prominence HPLC (*Shimadzu,* Duisburg, Germany) equipped with a system controller CBM-20A, a solvent delivery unit LC-20 AT (double plunger), an on-line degassing unit DGU-20A, an auto-sampler SIL-20AC, a photo diode array detector SPD-M20A. As stationary phase, a ZORBAX Eclipse Plus (*Agilent,* Santa Clara, CA, USA) C18 column (4.6 x 100 mm; 3.5 µm) was used. Each HPLC measurement took 18 minutes with flow rate of 1 mL/min. The quantification was performed with a stepwise gradient using acetonitrile (ACN) and water with 0.05% TFA. Within the first 10 min, the ratio of H_2O/ACN was gradually changed from 60/40 (v/v) to 40/60 (v/v). Within next 10 seconds, the solvent was abruptly

changed to 20/80 (v/v) and kept constant for 2 min, followed by sudden change back to 60/40 (v/v). This ratio was kept constant for next 8 min followed by the start of second run. The detection was performed at 230 nm and the retention time of BT44 was found to be 12.6 min.

Loading capacity and loading efficiency (LC & LE)

The following equations were used to calculate the loading capacity (LC) and loading efficiency (LE) of the BT44 formulations:

$$LC = \frac{m_{drug}}{m_{drug} + m_{excipient}} * 100\%$$

$$LE = \frac{m_{drug}}{m_{drug,added}} * 100\%$$

where m_{drug} and $m_{excipient}$ are the weight amounts of the solubilized drug and polymer excipient in solution and $m_{drug,added}$ is the weight amount of the drug initially added to the dispersion. No loss of polymer during micelles preparation was assumed.

Stability studies

For stability studies, all the freshly prepared BT44 formulations were stored at ambient conditions (≈ 25°C) under the exclusion of light. Before the determination of the drug loading by HPLC, all samples were centrifuged for 5 min at 10.000 rpm with a 3-Speed micro centrifuge (*neoLab,* Heidelberg, Germany) to sediment any aggregates or agglomerates. The samples from the supernatant were collected at day 0, 1, 5, and 15 and quantified by HPLC (as described in HPLC section). All the formulations and stability experiments were performed with 3 individually prepared samples and results are presented as means ± SD.

Redispersion studies

The freshly prepared BT44 formulations were frozen in liquid nitrogen and subjected to 24 h lyophilization to get the BT44 formulation as dried powder for redispersion studies. The lyophilized formulations were redispersed in normal saline (0.9% NaCl) and cell culture media (Dulbecco's modified eagle medium, DMEM). After the addition of solvent of interest, the formulations were

shaken at 1250 rpm with a Thermomixer comfort (*Eppendorf AG,* Hamburg, Germany) at room temperature for 5 minutes followed by HPLC analysis as stated in HPLC section.

Differential scanning calorimetry (DSC)

DSC was performed on DSC 204 F1 Phoenix equipped with a CC200 F1 Controller, (*NETZSCH,* Selb, Germany). The dynamic scans were recorded in nitrogen atmosphere with a heating rate of 10K/min (0°C – 200°C). For DSC studies samples were placed into flat-bottom aluminum pans with pierced lids. Prior to DSC measurements, the aqueous BT44 formulations were lyophilized to obtain the dry powdered. The DSC of plain polymer and pristine BT44 were also performed. The data was further analysed in thermoanalysis software and plotted in OriginPro 2015 Sr2 (version b9.2.272) software.

X-Ray diffraction (XRD)

Powder XRD of the lyophilized BT44 formulation was performed on X-ray diffractometer D8 Davinci Design (Bruker AXS). The setup is equipped with radiation source of Cu-Kα and the detector is linear position sensitive detector (PSD). Measurement were done at 0.02° steps each step lasting 1s in transmission mode at 40 kV voltage and 40 mA current and 2Θ angle ranging from 5° to 40° were used. The XRD of plain polymer and pristine BT44 were also performed under same set of conditions. The data was further analysed and plotted in OriginPro 2015 Sr2 (version b9.2.272) software.

Dynamic light scattering (DLS)

The DLS was performed using a Zetasizer Nano ZSP from Malvern (at single angle of 173°), (Malvern Instruments, Worcestershire, UK) in disposable cuvettes (UV cuvettes semi micro, BRAND GmbH, Wertheim, Germany) at ambient temperature (≈ 25 °C). The plain polymer and various BT44 formulations were measured after filtration through 0.45 µm PVDF syringe filter (*Rotilabo*, Karlsruhe). The measurements were recorded as average of three test runs (each with 12 sub-measurements) for one individually prepared sample. Data was analysed by using zetasizer software 7.11 and plotted in OriginPro 2015 Sr2 (version b9.2.272) software.

Cryogenic transmission electron microscopy (cryo-TEM)

The freshly prepared plain polymer solutions with concentration of 10 and 25 g/L (as free flowing liquid solution) and redispersed polymer/BT44 formulation at 10/2 g/L feed (n=1) were subjected to cryo-TEM visualisation. For sample preparation, copper grids coated with holey carbon support film (quantifoil, 400 mesh, R1/2) were glow-discharged in air for 1.5 min in a plasma cleaner (Harrick PDC-002). Afterwards, 5 µl of each sample solution was applied on the grids and plunge-frozen in liquid ethane with a Vitrobot IV (FEI Company, Hilsboro, USA). The humidity in the chamber was set to 100% and the temperature was kept at 25 °C. The following settings were further employed i.e. wait time 0 sec, drain time 0 sec, blot time 5 sec and blot force -5. The samples were imaged on a FEI Tecnai T12 Spirit transmission electron microscope (FEI Company, Hilsboro, USA) equipped with a LaB6 emitter at an acceleration voltage of 120 kV and a temperature of -180 °C. The images were recorded with an Eagle CCD camera (FEI Company, Hilsboro, USA) in low-dose mode with a total dose of 30 e/Å2 and a nominal under focus of -3 µm with serial EM [71]. The images were further processed in ImageJ software (1.46 r, revised edition).

Cryogenic scanning electron microscopy (cryo-SEM)

In comparison to cryo-TEM, relatively much higher plain polymer concentrations i.e. 50 and 100 g/L (as free flowing liquid solution) were visualized with cryo-SEM. The samples were rapidly frozen in slushed nitrogen at −210 °C after placing them between aluminum plates (d = 3 mm) with a 2 mm notch for sample fixation. All the following transfer steps were performed at −140 °C with an EM VCT100 cryo-shuttle (Leica Microsystems). To generate a freshly fractured polymer surface, one of the aluminum plates was knocked off and freeze etched for 15 min at −85 °C under high vacuum ($<1 \times 10^{-3}$ mbar) in a Sputter Coater machine (ACE 400, Leica Microsystems). Afterward, samples were sputtered with 3 nm platinum and transferred to the SEM chamber (Crossbeam 340, Zeiss). The images of the polymer surface morphology were taken at −140 °C using an acceleration voltage of 8 kV. The images were further processed in ImageJ software (1.46 r, revised edition).

***In vitro* Studies**

Cytocompatibility study of the polymer excipient

The cytocompatibility study of the plain polymer was carried out on MG87 RET cell lines. The cell viability was examined using Alamar blue assay as described previously [72]. The MG87 RET cells were cultured overnight in 96 well plate (OptiPlate 96 F HB, Wallac). Various concentrations of polymer i.e. 1, 5, 10, and 50 g/L, dissolved in DMEM and 15 mM HEPES were applied to the cultured cells. At 72 hour post-treatment, Alamar blue was dissolved in the cell culture media in the ratio 1:10 and applied to the cultured cells. After 2 hour of incubation with Alamar blue reagent, the fluorescence was measured using Victor plate reader at an excitation and emission wave length of 540 and 590 nm, respectively. The experiments were repeated 3 times independently.

RET phosphorylation assay

RET phosphorylation assay in response to BT44 was carried out in MG87 RET cells transfected with hGFRα1 and green fluorescent protein (GFP)-expressing plasmids as described previously [8]. In short, MG87 RET cells were cultured in 6 well plates in DMEM, 10% FBS. One day prior to the experiment, 100 µg/ml normocin was added into each well. Subsequently, the cells were transfected with 4 µg/well of GFRα1- and GFP-expressing plasmid using Lipofectamine 2000 (Invitrogen) as described by the manufacturer. The cells were starved (starvation media: serum-free DMEM, 15 mM HEPES, pH 7.2) for 4 h and stimulated for 15 minutes with 0.64 mg/ml (similar to 79 µM) of plain polymer, 100 µM of BT44 nanoformulation, 100 µM of pristine BT44 and 6.6 nM GDNF (PeproTech, Ltd) dissolved in starvation media. After 15 minutes, the cells were washed once with ice-cold PBS containing 1 mM Na_3VO_4 and lysed with RIPA-modified buffer (50 mM Tris-HCl, pH 7.4, 150 mM NaCl, 1 mM EDTA, 1% NP-40, 1% TX-100, 10% glycerol, EDTA-free protease inhibitor cocktail (Roche, Switzerland), 1 mM Na_3VO_4, 6 mM sodium deoxycholate, 1 mM PMSF) on ice followed by centrifugation. The supernatant obtained was used to immunoprecipitate RET with RET antibody (2 µg/ml, R&D, Cat# AF1485) bound to magnetic beads coated with protein G (Dynabeads Protein G, Life Technologies, USA). The precipitated immunocomplexes were resolved on SDS–PAGE, transferred to nitrocellulose membranes and probed with anti-phosphotyrosine antibodies (1:1500, clone 4G10, Merck Millipore, Germany, Cat# 05-321). The stained bands were visualized with enhanced chemiluminescence (ECL)

reagent (Pierce) using LAS3000 imaging software. To ensure equal loading, membranes were stripped and re-stained with anti-RET C-20 antibody (1:500, R&D, Cat# AF1485).

Cell-based ^{125}I-GDNF-displacement assay

The cell-based ^{125}I-GDNF-displacement assay was carried in HEK293 cells. The cells were cultured in DMEM, 10% FBS and 100 µg/ml normocin overnight and then transfected with GFRα1 or GFRα1 and RET using Lipofectamine 2000 (Invitrogen), as described by the manufacturer. Next day, the cells were incubated for 1 hour on ice in the presence of BT44 formulation in concentrations ranging from 0 to 50 pM. Afterwards 50 pM of iodinated GDNF was added and the cells were incubated for 1 hour on ice with ^{125}I-GDNF and nanoformulated-BT44. Subsequently, cells were washed with PBS for four times and lysed with 1 M NaOH, lysates were collected into the scintillation vials and counted using Perkin Elmer Wallac Wizard 1470-020 Gamma Counter. The data for GFRα1-transfected cells were collected in 2 independent experiments and for GFRα1/RET-transfected cells in 4 independent experiments. The binding data were analyzed by nonlinear regression analysis using GraphPad Prism 8.4.2 software to determine the IC_{50} values. Experiments with non-formulated BT44 were not conducted because of insufficient solubility of the compound in assay media.

Binding assay using microscale thermophoresis

The molecular interaction between nanoformulated BT44 and the receptors was studied using microscale thermophoresis (MST). Non-formulated BT44 was not studied in this assays due to insufficient solubility. All the experiments were performed using Monolith NT.115 instrument (NanoTemper Technologies GmbH, Germany). Recombinant human GFRα1 or RET extracellular domain were labelled through His-tag using Monolith His-Tag Labeling Kit RED-tris-NTA (NanoTemper Technologies GmbH; MO-L008). The His-labelled GFRα1 or RET was used at 20 nM concentration. The starting concentration of nanoformulated BT44 (ligand) was 10 µM which was chosen based on the result obtained from cell based experiment. All the measurements were performed using premium coated capillaries (NanoTemper Technologies GmbH; MO-K025) in a buffer containing 20 mM of HEPES, 150 mM NaCl, 186 µM $CaCl_2$ and 0.05% Tween-20. The measurements of the interaction

between formulation and the receptors were carried using red LED source, power set at 100% and medium MST power at 25 °C. The data were obtained from three independent experiments and were analyzed using MO. The affinity analysis software v2.3 was used for analysis and dissociation constant (Kd) was further calculated.

Neuroprotective effect of nanoformulated BT44 in primary dopamine neurons culture

The neuroprotective effect of the plain polymer, nanoformulated BT44 and pristine BT44 dissolved in Dimethyl sulfoxide (DMSO) was studied in 1-methyl-4-phenylpyridinium (MPP+)-challenged dopamine neurons as described previously [7, 10, 72]. The mid brain dopamine neurons were isolated from E13.5 embryos of NMRI mice and cultured for 5 days in dopamine neuron culture medium [(Dulbecco's MEM/Nut mix F12 (Invitrogen/Gibco, Cat# 21331-020), 1xN_2 serum supplement (Invitrogen/Gibco, Cat# 17502-048), 33 mM D-glucose (Sigma-Aldrich, Germany, Cat# G-8769), 0.5 mM L-glutamine (Invitrogen/Gibco, Cat# 25030-032), and 100 µg/ml Primocin (InvivoGen, USA, Cat# ant-pm-2)]. On the day 6, plain polymer (i.e 0.0064 mg/ml similar to 790 nM), nanoformulated BT44 (100 nM) or DMSO BT44 (100 nM) and GDNF (3.3 nM) were added to the cultured cells for the period of 48 hours. Afterwards, the media was removed and cells were fixed with 4% paraformaldehyde (PFA) for 20 minutes, washed with PBS and permeabilized with 0.2 % TritonX-100 in PBS. Further, the cells were blocked with 5% horse serum for one hour and then incubated with mouse anti-TH antibody (1:2000, Merck Millipore, Cat# MAB318) overnight at 4 °C. Subsequently, cells were washed and incubated with Alexa Fluor™ 647 conjugated donkey anti-mouse secondary antibody (1:500, Thermo Fisher Scientific, USA, Cat# A-31571) and 0.2 µg/ml DAPI (4', 6-diamidino-2-phenylindole) for 1 hour at room temperature. Finally, cells were imaged by ImageXpress Nano Automated Imaging System (Molecular Devices) at 10× magnification. The images were analyzed using CellProfiler image analysis software to calculate the number of tyrosine hydroxylase (TH) positive cells. Resulting data were subjected to statistical analysis in GraphPad Prism software.

***In vivo* studies**

Experimental animals

The test animals i.e. mice used in the experiments were housed under 12 hours light–dark cycle with food and water available ad libitum. The experiments were carried out in accordance with 3R principle, European Community guidelines for the use of experimental animals and approved by the National Animal Experiment Board of Finland (license numbers ESAVI/7551/04.10.07/2013 and ESAVI/198/04.10.07/2014) for experiments with living animals. Animals for acute toxicity studies were leftover animals from breeding experiments (Mouse line: C57BL/6JRccHsd and B6C3-Tg (HD82Gln) 81Gschi/J). Both males and females mice (age = 4-5 months) were used for the experiments. The use of animal for primary neuronal culture was approved by Laboratory Animal Centre of the University of Helsinki (license number KEK15-022). The primary dopamine culture was prepared from E13.5 embryos of NMR1 mice.

***In vivo* assessment of acute toxicity of BT44 in propylene glycol or as aqueous POx formulation**

The BT44 acute toxicity in mice was studied in experiment with cross-over design. The mice (n = 24) were randomly divided into 8 groups (3 mice in each group). In the first period of experiment, mice from group 1 to 8 were subcutaneously injected with normal saline, propylene glycol (PG), plain polymer (355 and 586 mg/kg), nanoformulated BT44 at 25 and 50 mg/kg, and BT44 dissolved in PG (25 and 50 mg/kg), respectively. The subcutaneous injection volume was 10 ml/kg. The amount of polymer in the nanoformulated BT44 is same as that of plain polymer used in the *in vivo* experiment. After 7 days washout period, study agents were reshuffled between the groups so that the each group receive different study agent after each wash out period. One hour after injection, mice were placed in the corner of Open-field chamber (30 × 30 cm, Med Associates) and the locomotor activity was monitored for 15 minutes. The health condition of the mice was monitored by experienced personnel on daily basis during the entire time span of experiment. After the second treatment period, animals were terminated, blood and brain were collected for absorption and BBB penetration analysis.

Determination of BT44 concentration in blood and brain

Both blood and brain concentration of BT44 was determined 1 h after single subcutaneous injection of 50 mg/kg of nanoformulated BT44 or BT44 dissolved in PG in mice (n = 4-6 mice per group). One-

hour post subcutaneous injection, mice were anaesthetized using terminal phenobarbital injection (50 mg/kg) and blood samples (0.3–0.8 ml) were collected by cardiac puncture with surgical heart exposure (open method) followed by storage in EDTA tubes (Microvette 100K3E, Sarstedt). The plasma fraction was separated by centrifugation (3000 rpm, 5 min, 4 °C), placed on dry ice followed by storage at −72°C until analysis. For the measurement of brain concentration of BT44, mice were transcardially perfused with an ice cold normal saline and the brain tissues were collected and snap frozen in the liquid nitrogen. The concentration of BT44 in both the plasma and the brain was measured by UPLC coupled with time-of-flight mass spectrometry. The measurements were performed by Pharmidex Pharmaceutical Services Ltd (UK, https://www.pharmidex.com/).

Statistical analysis

The statistical analysis was done using Student's t-test or one-way ANOVA with a Dunnett's or Tukey HSD *post hoc* tests in GraphPad Prism 8 (GraphPad Software Inc., USA). The differences with P values below 0.5 were considered statistically significant.

Results and discussions

Polymer synthesis and characterization

POx based ABA triblock copolymers have shown great potential to deal with difficult to solubilize drugs [37, 45, 47, 73]. In the majority of cases, the hydrophilic block A is pMeOx while hydrophobic block B can be from a series of linear [74, 75], branched (aliphatic POx with varying side chain lengths; C4-C9) [55, 67] or aromatic ring side chains [46, 66]. For POx based amphiphiles, it has been established repeatedly, that a minimal contrast in hydrophilic/lipophilic domains is beneficial [67], for high drug loading [45, 46, 62, 65, 66, 76]. Amongst many POx based triblock copolymers [55], the most repeatedly explored amphiphile is A-pBuOx-A [46, 47, 58] allowing, *inter alia*, ultra-high drug loading for paclitaxel (PTX) (≈ 50 wt.%).

Taking this into account, we selected three POx based copolymers (including the thoroughly investigated pBuOx based amphiphile) [37, 44, 46, 47, 62] comprising a moderately hydrophobic block B i.e. poly(2-*n*-propyl-2-oxazoline) (pPrOx), pBuOx and poly(2-*n*-pentyl-2-oxazoline) (pPentOx) (Figure 1a) and hydrophilic pMeOx A blocks. All polymer amphiphiles in this study were synthesized by living cationic ring opening polymerization (LCROP) as previously described [65]. The BT44 (Figure 1b) loaded POx based micellar formulation were prepared using the thin-film hydration method (Figure 1c).

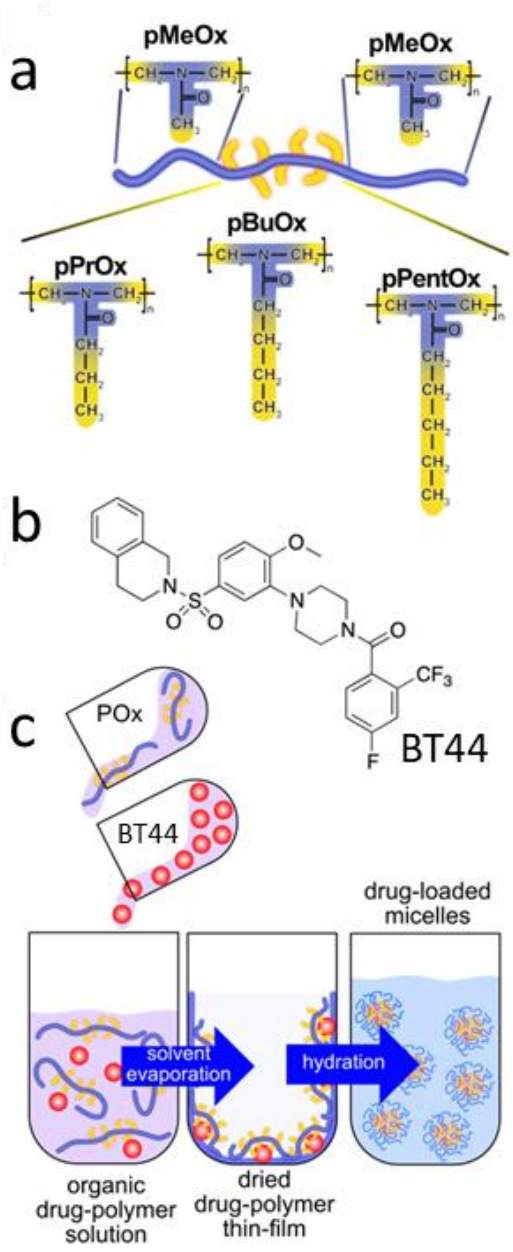

Figure 1l a) Schematic representation of the triblock copolymers used in this study representing hydrophilic and hydrophobic domains. b) Chemical structure of the BT44. c) Schematic illustration of the thin-film hydration method used for the formulation development.

As all ABA triblock copolymers are comprised of pMeOx as A, they are represented according to the hydrophobic block i.e. A-pPrOx-A, A-pBuOx-A and A-pPentOx-A in the following. The targeted block length for each block in the triblock copolymer is A_{35}-B_{20}-A_{35}. The former two polymers were previously investigated for drug formulation [55, 65, 74] while the A-pPentOx-A triblock copolymer was specifically synthesized for this contribution. Initially, we synthesized PentOx monomer followed by characterization with ^{1}H-NMR spectroscopy (see supporting information; synthesis 1). All the signals

were unambiguously assigned. The signals of two methylene groups (signal 1 and 2) originating from 2-oxazoline (at 4.2 and 3.8 ppm) confirmed the successful ring formation (Figure 2a). After purification by distillation, the PentOx monomer was polymerized with MeOx (A) to obtain the desired A-pPentOx-A (see supporting information: synthesis 2). The polymerization was terminated with aqueous sodium hydroxide solution. Previously, we had observed relatively little effect of the polymer termini in POx/POzi based A-B-A triblock copolymers, but this should be assessed on a case-by-case basis [74, 77]. The resulting A-pPentOx-A triblock copolymer was characterized by ^{1}H-NMR, GPC, DSC and TGA. The ^{1}H-NMR spectroscopy showed good synthetic control and agreement to the targeted length for individual block (Figure 2b). During synthesis, after full monomer consumption for individual block, small volume of the reaction mixture was collected and analysed by GPC. With the polymerization of each individual block, a distinct shift to higher molar mass was observed and the elugrams for the intermediates and final polymer appeared essentially monomodal with reasonably low dispersity (Đ < 1.20) (Figure 2c). For the synthesis and characterization of A-pPrOx-A and A-pBuOx-A triblock copolymers, the readers are referred to previous reports [55, 65]. To understand the thermal characteristics of the novel polymer, differential scanning calorimetry (DSC) measurements were performed. Corroborating results from previously reported POx based triblock copolymers [55], all the three triblock copolymer amphiphiles exhibited a single glass transition (T_g) suggesting an amorphous sample and absence of (micro)phase separation in solid state. As expected, a slight decrease in T_g was observed with the increasing side chain length in hydrophobic block i.e. 65, 63 and 58°C for A-pPrOx-A, A-pBuOx-A and A-pPentOx-A, respectively (Figure 2d and Figure S1). The thermogravimetric analysis revealed that A-pPentOx-A remained stable and onset of the first major loss was observed at approximately 330°C (Figure 2e). This high thermal stability, well known for POx and POzi, could be very beneficial for melt processing, e.g. preparation of hot melt extrudates of A-pPentOx-A and drugs of interest.

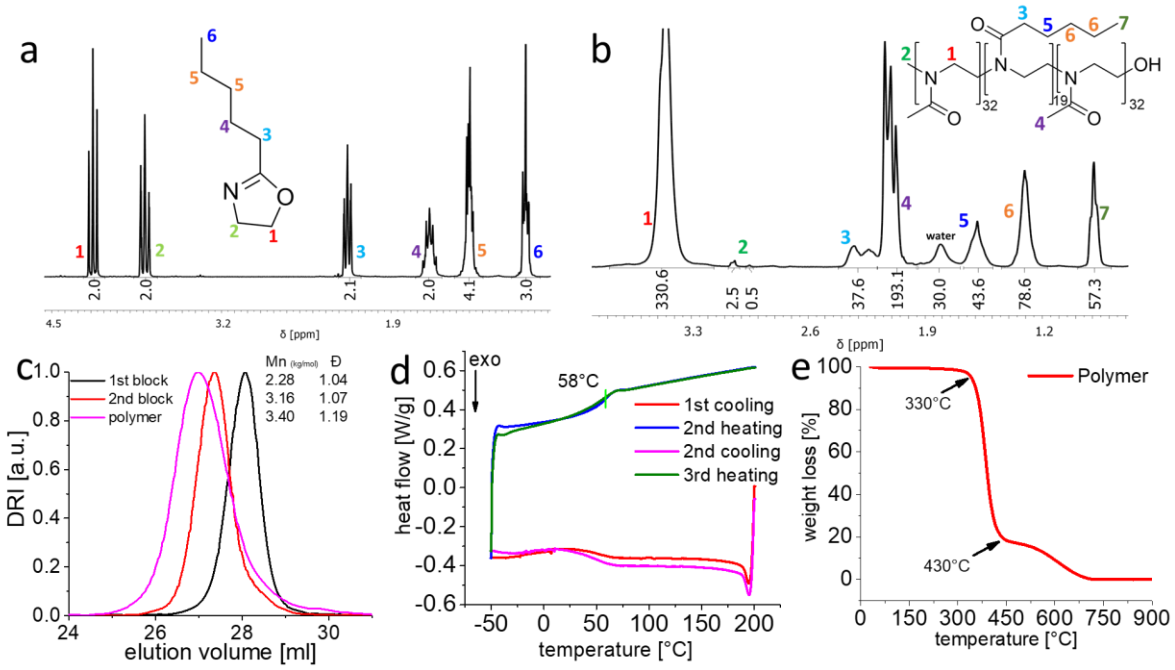

Figure 2| ^{1}H-NMR spectra ($CDCl_3$; 300 MHz; 298 K) and chemical structure of a) 2-*n*-pentyl-2-oxazoline monomer and b) pMeOx-b-pPentOx-b-pMeOx triblock copolymer with signal assignment of all major peaks. c) GPC elugrams (solvent; HFIP, system calibrated with PEG standards) after each polymerized block and purified A-pPentOx-A polymer. d) DSC thermogram of plain A-pPentOx-A triblock with heat flow occurring during the various heating and cooling cycle (10 K/min), green vertical line indicates the glass transition point at 58°C. e) Weight loss occurring during thermogravimetric analysis of A-pPentOx-A. Samples were heated from 30 to 900°C at the heating rate of 10 K/min.

Solubility parameters

The physicochemical compatibility between drug and polymer plays obviously a pivotal role in the ideal characteristics of the formulations. The chemical structure of the drug and the polymer (backbone or side-chain) can significantly impact the drug loading and stability of the formulation [65]. Despite some attempts to "predict" drug loading [50, 55, 78, 79], drug formulations are mostly still developed by trial and error. Considering the magnitude of the problems of hydrophobic drugs in pharmaceutical technology, finding of a universal carrier/solubilizer seems impossible [78]. There are a variety of techniques available to estimate or assess the polymer-drug compatibilities [68, 80-83] in time and cost-effective manner. Here, we estimated the compatibility between BT44 and the hydrophobic block in the ABA triblock copolymers theoretically by calculating Hansen solubility parameters (HSPs) [78, 84, 85]. The HSPs values i.e. dispersion (δ_d), polar (δ_p) and hydrogen bonding

(δ_h) forces were calculated using the group contribution method and the molar volume was calculated by Fedor's method (Figure 3a and Table S1) [69]. Based on the principle of "like dissolves like" the distance between two materials in the 3 dimensional (3D) space is supposed to give an estimate of compatibility between two substances therefore the obtained HSPs values are depicted in 3D space (Figure 3b). Based on δ_d, δ_p, δ_h, δ_{total} values, the Flory-Huggin's interaction parameters (χ_{dp}) can be calculated, which is another measure of compatibility between polymer and drug wherein a lower value of χ_{dp} (ideally = 0) suggests a higher polymer-drug compatibility. Based on the calculated χ_{dp}, BT44 compatibility with the three different hydrophobic blocks should be in the order pPrOx > pBuOx > pPentOx indicating an inverse relationship of side chain length and polymer-drug compatibility. Specifically, pPrOx is suggested to be highly compatible ($\chi_{dp} \approx 0.002$) and therefore could be assumed to be the best solubilizer for BT44, while pBuOx and pPentOx gave χ_{dp} values of 0.66 and 1.50, respectively, indicative of relatively lower compatibility. The χ_{dp} value for highly hydrophilic pMeOx was ≈ 4.26 indicating that plain pMeOx homopolymer is thermodynamically a poor solubilizer for BT44. However, this theoretical prediction represents an oversimplification of the system and the experimental solubilization of BT44 using these three amphiphiles for BT44 must be tested.

a

Solubility Parameters

polymer/drug	[a]δD	[a]δP	[a]δH	[b]δT	[c]molar volume cm³/mol	[d]Flory Huggins parameter
pPrOx	20.1	12.3	8.8	25.1	90.2	0.002
pBuOx	19.6	10.4	8.1	23.6	106.3	0.66
pPentOx	19.2	9.1	7.6	22.5	122.4	1.50
pMeOx	21.9	19.1	11.0	31.1	58.0	4.26
BT44	23.1	7.7	8.4	27.3	367.1	-

[a]Calculated by Hoftyzer and Van Krevelen's method, equation no. 4, 5 & 6, [b]calculated by equation no. 2 & 3, [c]calculated by Fedor's method, [d]calculated by equation no.1.

b

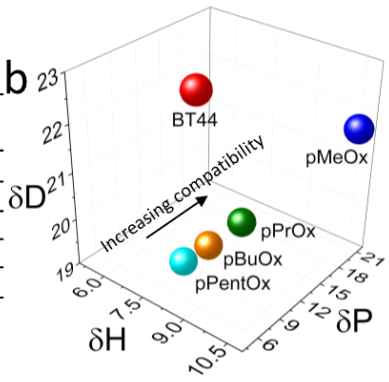

Figure 3| a) Hansen solubility parameters, molar volume and Flory Huggins parameters of BT44 and various blocks of the ABA triblock copolymers. b) Distribution of solubility parameters for BT44 and various blocks of ABA triblock copolymer in three dimensional Hansen space.

Formulation Studies

Previously, we had observed that a minor change such as shifting of one methylene unit from the side chain to the polymer backbone (with in hydrophobic block) and differences in the side chain have significant impact on the loading capacity for hydrophobic drugs indicative of strong polymer/drug specificities [55, 65]. Here, only a few hydrophobic blocks with the increasing side chain length i.e. C3, C4 and C5 were selected and compared for drug loading capacities.

Accordingly, the solubilisation of BT44 was tested with the three triblock copolymers with minimal to moderate amphiphilic contrast (difference of hydrophobicity in hydrophilic and hydrophobic block of the triblock copolymer). Briefly, the polymer and BT44 ethanolic solutions were mixed in desired ratios (in all cases, the target polymer concentration was kept constant at 10 g/L, while BT44 concentration was increased from 2 to 10 g/L, unless otherwise stated) followed by ethanol removal and subsequent hydration of resultant thin-film by deionized (DI) water. The (dissolved) BT44 in the micellar formulation was quantified by HPLC (Figure S2), after removal of (if any) non-solubilized drug particles by centrifugation.

Instead of A-pPrOx-A as predicted by solubility parameters or A-pBuOx-A, proven to be the best solubilizer for many drugs [37, 47, 58, 62], unexpectedly, A-pPentOx-A gave the highest LC for BT44 (LC ≈ 47 wt.%). Increasing the BT44 feed from 2 to 10 g/L, raised the LC from 14 to 47 wt.% (1.7 to 9.0 g/L) (Figure 4a, blue bars). At the highest LC of 47 wt.%, BT44 formulation appeared as clear solution with low viscosity (Figure S3a). The LE at all the tested ratios of BT44 ranged between 80 to 90 % (Figure 4a, blue squares). For *in vitro* biological activity (or cytotoxicity) studies relatively low drug concentrations are required (typically nano- to micromolar range) but when it comes to *in vivo* studies, typically a high dose is required due to the incomplete absorption and (often) large volume of distribution (e.g. volume of distribution of BT44 is 4.6 L/kg [10]). In addition, ultra-high drug loaded formulations are favorable, particularly for injectable administration, because of limitation of injectable volume, in particular in mouse models. However, one cannot *a priori* assume a high LC also benefits therapeutic outcomes and some *in vitro* work by Stenzel *et al.* suggest lower endocytosis of highly loaded polymer micelles [30, 31], albeit in certain cases *in vivo* experiments clearly suggest a

benefit for highly loaded polymer micelles [61]. Previously, Lübtow et al. observed that increasing the polymer feed from 10 to 50 g/L aided to increase the aqueous solubility of curcumin (CUR) from 11 to 55 g/L, respectively [45]. Following this, an additional formulation with higher A-pPentOx-A/BT44 feed i.e. 100/20 g/L was prepared. This formulation provided a BT44 aqueous solubility of around 19.3 g/L. However, because of the high polymer feed, the resulting LC was only 16 wt.%, albeit with a high LE of 96% (Figure 4b).

In the case of A-pBuOx-A triblock (at 10 g/L polymer feed) the highest LC achieved was 19 wt.% (≈ 2.4 g/L at 10/8 g/L feed) (Figure 4a, red bars). Increasing the BT44 feed did not significantly improve the LC i.e. falling in the range of 4 to 19 wt.% at all the tested ratios. As a consequence, LE kept on decreasing with the increasing BT44 feed i.e. 35 to 15 % (Figure 4a, red squares). The A-pPrOx-A triblock appeared to be a poor solubilizer for BT44 (LC ≈ 0.5 wt.%), at all the tested ratios (Figure 4a, black bars), the flakes of undissolved A-pPrOx-A/BT44 films were clearly visible with the naked eye (Figure S3b) during formulation experiments. In summary, formulation results showed a clear decrease in LC in order of A-pPentOx-A > A-pBuOx-A > A-pPrOx-A with loading capacities of 47wt.%, 19wt.%, 0.5wt.%, respectively (Figure 4a).

Comparing the experimental formulation results (i.e. LC for A-pPentOx-A > A-pBuOx-A > A-pPrOx) with the theoretical polymer-drug compatibility results (i.e. pPrOx > pBuOx > pPentOx) obtained by solubility parameters, it is clear that the HSPs gave unsatisfactory results, in fact predictions completely opposite to obtained results. The predictive power of solubility parameters (δ_d, δ_p, δ_h, and δ_{total}) is based on relatively straight forward mathematical calculations [69, 84], limiting the precise prediction of the overall polarity and hydrogen-bonding ability of molecules. In addition, the interplay between hydrophilic/lipophilic domains and cargo in a solution is much more complex which can lead to differing deviations from predicted interactions [24-27, 86] in turn compromising the predictive power of solubility parameters [55]. We are aware that in the past, several authors have claimed that HSPs are well suited for the prediction of polymer-drug compatibilities [78, 87], including in POx-based block copoylmers [88], but our results presented here and before [46, 55] clearly show that one has

to be very careful not to overgeneralize. While it is obvious that HSPs obtained by group contribution methods are unsuitable for compatibility prediction in the present systems, it would be interesting to investigate other approaches such as molecular dynamics or active learning [79].

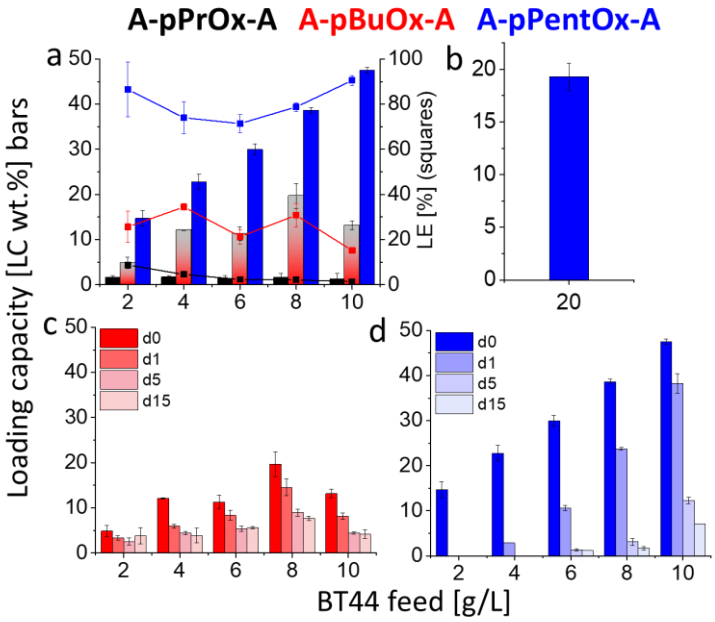

Figure 4| Maximum loading capacity (LC, bars) and loading efficiency (LE, squares) obtained with a) A-pPrOx-A (black), A-pBuOx-A (red) and A-pPentOx-A (blue) at constant polymer feed of 10 g/L, with increasing BT44 feed from 2 to 10 g/L and b) with A-pPentOx-A/BT44 feed of 100/20 g/L. Stability study of the c) A-pBuOx-A and d) A-pPentOx-A based BT44 formulation stored at ambient conditions (day 0 to 15) with constant polymer feed of 10 g/L. Data is given as means ± SD (n=3).

Stability studies

For pharmaceutical development and commercialization, the stability of the formulation is one of the basic requirements. To investigate the shelf life of BT44 formulations, the freshly prepared formulations were stored at room temperature with the initial precipitate (if any) and samples were collected at day 0, 1, 5 and 15. Previously, we had observed that the A-pBuOx-A/PTX formulation exhibited an excellent stability for several months [44, 74] however, in few cases the formulation with similar amphiphiles were found to be much less stable [48, 76]. The A-pPrOx-A/BT44 formulation was not included in stability study because of the poor drug loading (LC ≈ 0.5 wt.%). Unlike stable A-pBuOx-A/PTX formulation, BT44 formulation with A-pBuOx-A was found to be less stable and in the course of time a gradual decrease in LC was observed in all the tested ratios e.g. the highest LC obtained with

A-pBuOx-A/BT44 feed of 10/8 g/L decreased from 19 (at day 0) to 7 wt.% (at day 15) (Figure 4c, red bars).

Interestingly, in the case of A-pPentOx-A, a direct relationship between LC and formulation stability was observed i.e. formulation with high LC were found to be relatively more stable (Figure 4d). The formulations with 2 g/L BT44 feed precipitated completely within 24 h, while the formulations with 4 to 6 and 8 to 10 g/L BT44 feed precipitated completely by day 5 and 15, respectively. The present findings are opposite to our previous results, where mitotane (MT) based formulation with A-pBuOx-A polymer (for adrenocortical carcinoma) was found to be more stable at lower MT feed (2 and 4 g/L). However, at a certain threshold MT feed (≥ 6 g/L), a rapid crystallization of MT was observed corroborated by clear melting peak in DSC thermogram of the precipitate [46]. To investigate the reasons for BT44/A-pPentOx-A/ formulation instability i.e. whether BT44 crystallizes or the formulation is colloidally unstable, the formulations were further characterized by various techniques.

Physico-chemical characterization of BT44/POx formulation

As previously explained, the interactions between drugs and the hydrophilic corona of polymers micelles are becoming more evident, which can either lead to high drug loading [27, 86] or colloidal instability of the formulations [67], but may also affect endocytosis [30, 31, 89]. The limited colloidal stability is evidenced by the fact that the resultant precipitate not only contains the drug but also the otherwise highly water soluble polymer [25, 45]. To evaluate this for the present formulations, the A-pPentOx-A/BT44 (100/20 g/L) formulation was prepared. After centrifugation, the supernatant and the sediment were collected separately and lyophilized. For better comparison, the ^{1}H-NMR spectra of the pristine BT44, plain A-pPentOx-A polymer and the (lyophilized) precipitate in chloroform-D ($CDCl_3$) as non-selective solvent (no micelles formation) were obtained (Figure S4). The ^{1}H-NMR spectra of plain polymer clearly presented all the signals suggesting that polymer existed as unimers in non-aggregated form (Figure S4 green spectra) and it was also evident that the precipitate contained not only the drug but also the hydrophilic polymer (Figure S4 red spectra), corroborating

our previous findings [26, 45, 73]. However, the precipitate was significantly enriched in BT44 compared to the polymer (4/1 drug/polymer ratio).

To gain more insights into the BT44 formulations, ^{1}H-NMR experiments were further performed using deuterium oxide (D_2O) as selective solvent (micelles formation). Initially the ^{1}H-NMR spectra of all the three plain triblock copolymers used in this study were obtained (at concentration of 10 g/L) (Figure S5). The A-pPrOx-A copolymer exhibited all the signals from hydrophilic as well as the hydrophobic block (Figure S5 blue spectra, signals 1 to 6). This shows that polymer existed as unimers in D_2O because of very low amphiphilic contrast, unable to self-assemble into micelles. This could be expected, as the pyrene assay previously also indicted no formation of micelles at 10 g/L concentration for A-pPrOx-A triblock copolymer [55]. Lübtow et al. also observed the similar behaviour for poly(2-*n*-propyl-2-oxazine) based triblock copolymer (A-pPrOzi-A) and the micellization was only induced in the presence of a hydrophobic molecule i.e. CUR. Additionally, at ultra high CUR loading (LC > 50 wt.%), the signals from the hydrophobic block were still visible, albeit with lower intensities (in D_2O), while the CUR signals were completely attenuated [45].The ^{1}H-NMR spectroscopy also revealed a similar pattern for PTX [86] and atorvastatin (ATV) [73] loaded A-pBuOx-A and A-pBuOzi-A ((poly(2-*n*-butyl-2-oxazine)) micellar formulations, respectively. However, in the absence of drug, small angle neutron scattering (SANS) revealed that the plain A-pBuOzi-A polymer existed as spherical self-assemblies without a well-defined core-shell architecture. In contrast, the plain A-pBuOx-A displayed core-shell morphology [27]. The ^{1}H-NMR spectra of A-pBuOx-A [55] also exhibited all the respective signals including the hydrophobic block (Figure S5 green spectra, signals 1 to 7). Herein, the ^{1}H-NMR spectra of the plain A-pPentOx-A (Figure S6 green spectra) and the lyophilized BT44 formulations (Figure S6 red spectra) were also obtained in D_2O. In both spectra, the signals corresponding to the hydrophobic block were completely absent (Figure S5, red spectra, signals 3, 5, 6 and 7) and no signals from the BT44 were visible in the formulation. In contrast, Hiller et al. observed all the representative signals (^{1}H-NMR) from their plain diblock copolymer i.e. $pMeOx_{17}$-$pPentOx_3$ including the signals from hydrophobic pPentOx in D_2O [90]. However, in comparison to present A-pPentOx-A triblock

copolymer, Hiller et al. investigated a very short hydrophobic block (3 repeat units), resulting in very low amphiphilic contrast. While, the complete disappearance of signals from hydrophobic block in plain A-pPentOx-A triblock, presented herein, indicates short transverse relaxation time (T_2) and suggests micelles with a rigid (solid-like) core both in the presence and absence of BT44. The direct comparison of A-pBuOx-A and A-pPentOx-A micellar formulations utilizing the analytical tools like solid state NMR [25, 86] and SANS could give us much deeper understanding of polymer drug interactions resulting in the different micellar structures and dynamics, however such analysis is beyond the scope of current contribution. In order to investigate the reasons for the poor stability of A-pPentOx-A/BT44 formulation, DSC analysis was performed to evaluate, whether the precipitation is associated with BT44 crystallization similar to previously reported MT-formulation [46] or because of colloidal instability, and resulting agglomeration and sedimentation. Initially the DSC thermogram of the pristine BT44 was obtained to determine the melting point (Figure S7a). The sharp endothermic peak at 146°C in the first heating cycle indicated the crystalline nature of BT44 (Figure S7a black curve) while the DSC traces in the second and third heating cycle did not show any melting peak, as BT44 remained in its amorphous form with a T_g of 75°C (Figure S7a, green vertical line). In this regard, only the first heating cycle in the DSC thermograms of pure BT44 and the resultant precipitate in formulation (i.e. A-pPentOx-A/BT44 at 10/4 g/L feed) at day 5 were compared (after lyophilization). Unlike pristine BT44, no melting peak was observed in the precipitate at day 5, suggesting an amorphous nature of BT44 (Figure S7b red curve) corroborating our previous findings [32, 42] that the poor stability can be correlated to micellar agglomeration and sedimentation.

In the pharmaceutical product design, the formulation instability is a serious risk factor which can limit their wide spread use. Lyophilization is generally a primary strategy to improve the shelf life of a drug product. Therefore the A-pPentOx-A/BT44 100/20 g/L formulation was prepared (Figure 4b) and lyophilized. During storage, the physico-chemical stability of the lyophilized formulation is also one of the quality attributes that should be evaluated. Such formulations have the tendency to crystalize during handling, storage or transportation. In order to investigate this, the DSC thermograms of the

plain polymer, pristine BT44 and the lyophilized formulation after 15 days of storage at room temperature were compared (Figure 5a). The absence of a melting peak (at 146°C) in the first heating cycle indicated again that the BT44 remained as amorphous form in lyophilized formulation (Figure 5a blue curve). In the second and third heating cycle, unlike pristine BT44 (T_g at 75°C, Figure S7a) a single T_g was observed at 58°C (Figure S8) which corresponds to the T_g of plain A-pPentOx-A polymer indicative of complete miscibility of the drug and polymer.

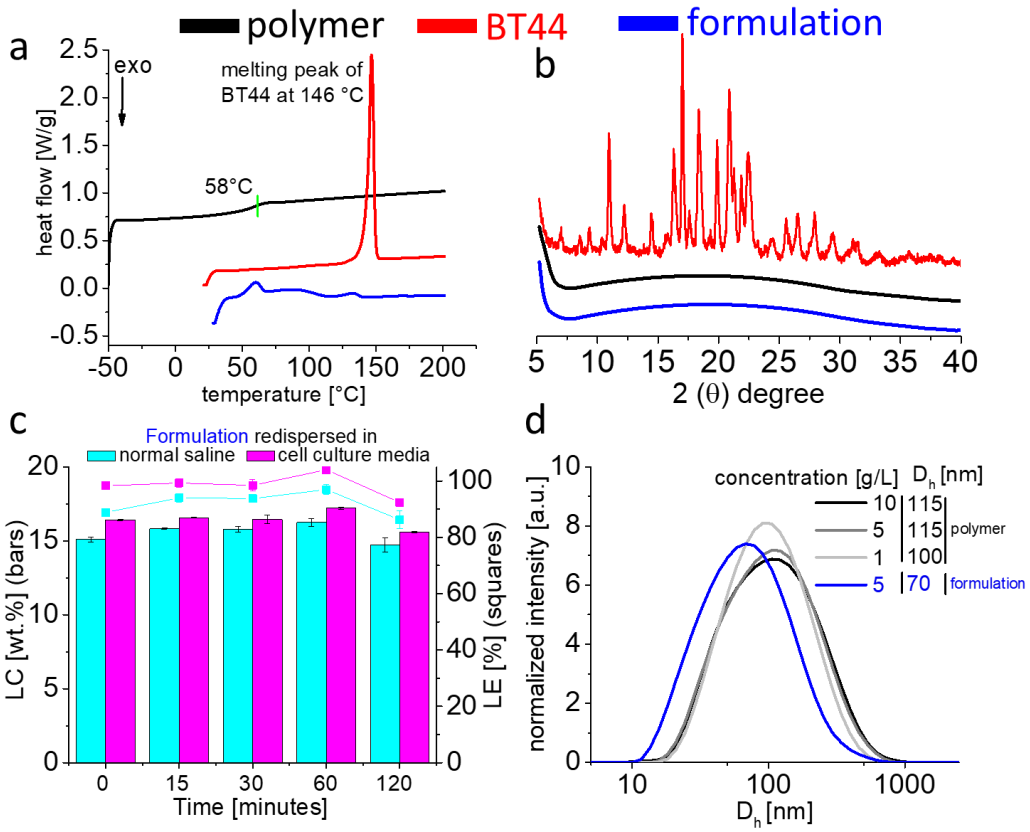

Figure 5| a) DSC thermograms (at heating rate of 10 K/min) of pristine BT44 (red, first heating cycle, sharp melting peak at 146°C), plain polymer (black, second heating cycle, T_g at 58°C) and lyophilized formulation (blue, first heating cycle, absence of melting peak for BT44), respectively after 15 days of storage at room temperature. b) Powder-XRD spectra of pristine BT44 (red), plain polymer (black) and lyophilized formulation (blue) after one month of storage at room temperature. c) Redispersion of lyophilized formulation (polymer/BT44 100/20 g/L) after 30 days of storage at room temperature in normal saline (blue) and cell culture media (magenta) for short term stability studies from time 0 to 120 minutes. Data is given as means ± SD (n=3). d) The size distribution by intensity (measured at 173° scattering vector) of plain polymer (10, 5 and 1g/L) and BT44 formulation (5 g/L) redispersed in normal saline (filtered through 0.45 µm PVDF filter).

For further analysis, the pristine BT44, plain polymer and lyophilized formulation were analysed by powder-XRD after 30 days of storage at room temperature (Figure 5b). The diffractograms of the pristine BT44 showed multiple peaks in the 2Θ range of 10 to 35° showing the crystalline nature of BT44 (Figure 5b, red curve). In contrast, the broad halos without any traces of peaks in the plain polymer and lyophilized formulation indicate their amorphous nature (Figure 5b black and blue curve, respectively). This preliminary stability study using DSC and powder XRD analysis suggests that such formulations can be stored reasonably well, as lyophilized powder without a high risk of recrystallization. However, more detailed studies at different temperature and relative humidities will be needed to complete the picture. In addition, the analysis of traces of crystallinity via multimodal non-linear imaging would also be of interest [91].

For lyophilized formulations, the complete redispersion or aqueous reconstitution is also a very important step for parenteral administration. In addition, the evaluation of short-term stability of the redispersed formulation is relevant in practical settings. The final redispersed formulation should remain stable for desired period of time to conveniently allow for parenteral administration (injection or infusion). Previously, lyophilized POx based PTX, CUR, ATV and MT formulations (without any additional cryo-/lyoprotectants) displayed excellent redispersibility before use [45, 46, 73]. In this regard, A-pPentOx-A/BT44 100/20 g/L lyophilized formulations (after storage at room temperature for 30 days) were redispersed in normal saline and cell culture media (without serum) and quantified at time 0, 15, 30, 60 and 120 minutes by HPLC to determine the short-term storage. Upon redispersion (at t = 0 min) with normal saline, initially a minor decrease in LC (i.e. 16 to 15 wt.%) was observed while with cell culture media, 100 % redispersibility was noticed (LC ≈ 16 wt.%). In the time course of 120 minutes, the LC of normal saline and cell culture media based formulations decreased slightly to 14 and 15 wt.%, respectively, and accordingly, a minor precipitation was noted. From the redispersion results, it can be concluded that A-pPentOx-A/BT44 formulations can be stored as lyophilized powder but need to be used immediately after redispersion.

To estimate the size of self-assemblies, redispersed formulations (in normal saline) were characterized by dynamic light scattering (at 173°) at room temperature. Initially, the self-assemblies of plain A-pPentOx-A polymer at different concentrations (10, 5 and 1 g/L) were measured and the size (hydrodynamic diameter, D_h) fell into the range of 100-115 nm. However, upon incorporation of BT44 (5 g/L), the D_h decreased to approximately 70 nm indicative of BT44 induced reorganization and compaction of the self-assemblies. However, it should be clear that the size of these self-assemblies are beyond the size to be expected for simple, spherical polymer micelles, as the theoretical extended chain length of the polymers is well below 40 nm.

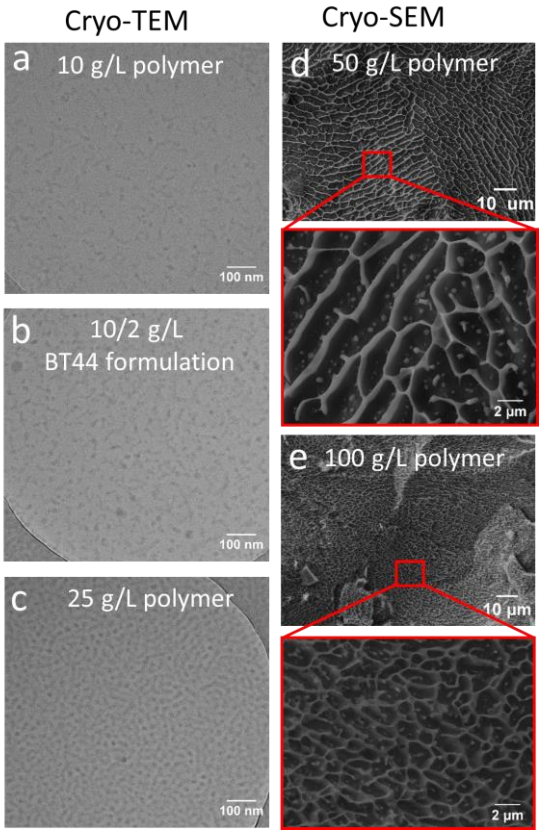

Figure 6| The cryo-transmission electron microscopy analysis (cryo-TEM) of a) 10 g/L plain A-pPentOx-A polymer, b) 10/2 g/L A-pPentOx-A/BT44 formulation, c) 25 g/L plain A-pPentOx-A polymer. The cryo-scanning electron microscopy (cryo-SEM) analysis of d) 50 and e) 100 g/L plain A-pPentOx-A polymer (acceleration voltage ETH: 8kV).

To gain more insights into the size and morphology of the assemblies, initially, we visualized the plain polymer solution (at concentration of 10 and 25 g/L) and polymer/BT44 (10/2 g/L) formulation by cryo-TEM. The results revealed the presence of few short worm-like assemblies (Figure 6a). This can

explain the higher D_h observed by DLS i.e. 100-115 nm (at 10 g/L plain polymer solution). No notable differences were observed in morphology, when plain polymer was compared to the BT44 formulation (at polymer/BT44 10/2 g/L) (Figure 6b). When the polymer concentration increased from 10 to 25 g/L, the overall population of the worms also increased and the whole grid seemed to be saturated with these assemblies (Figure 6c). The alignment, range of intermediate structures and further branching between the worms is indicative of a dense network formation. Generally, the transition to higher-order assemblies often correlates with an increase in viscosity. For example, by cryo-TEM, Hahn et al. observed the morphological transition from spherical micelles to worm like network causing the macroscopic gelation for poly(2-phenyl-2-oxazine) based A-B-A (A-pPheOzi$_{15}$-A) triblock copolymer (at 200 g/L concentration) [92]. Here, both the A-pPentOx-A/BT44 formulation and the plain polymer solution, appeared as free flowing liquids at all the tested concentrations. To obtain further insights into the morphology of A-pPentOx-A plain polymer solutions at 50 and 100 g/L (at which TEM is not feasible), the visualization was performed by cryo-SEM. Similar to the previously reported case of A-pPheOzi$_5$-A [92], the 50 g/L A-pPentOx-A polymer solution also exhibited lamellae like structures (Figure 6d) which were further condensed by increasing the polymer concentration to 100 g/L (Figure 6e). This further condensation lead to structural transition to a honeycomb-like structure. To the best of our knowledge this is the first study presenting the worm like morphological details of any pPentOx based triblock copolymer and its drug formulations. However, previously the worm like structures have been reported for A-pPrOzi-A/CUR [45] and A-pBuOx-A/cisplatin/etoposide formulations [62] while in the presence of PTX, A-pBuOx-A exhibited spherical/raspberry like micelles [33]. The plain A-pPrOzi-A existed as unimers [45] while plain A-pBuOx-A polymer solution exhibited spherical micelles along with the presence of few worm like assemblies [33]. Recently, depending upon the drug feed, Lim et al. observed the transition of freshly prepared A-pBuOx-A/Olaparib spherical micelles ($D_h \approx$ 10-30 nm) to worm like structures ($D_h \approx$ 200 nm) in the time span of 72 hours [93]. The authors further suggested that the spherical micelles can be therapeutically more efficient for systemic delivery of anticancer drugs when compared to worm like assemblies. However, this should be verified on case-

by-case basis, because the nature of hydrophobic block, overall hydrophilic lipophilic balance, chemical nature of drug and the drug feed are the major driving forces for such kind of transitions, which might result in loosely or densely packed micellar architectures, resulting in rapid or slow release of drugs.

***In vitro* and *In vivo* studies**

Assessment of polymer cytocompatibility by Alamar blue assay.

To be suitable for preclinical development and clinical translation the excipients used for formulation development must be non-toxic. We, therefore, evaluated cytocompatibility of the polymer *in vitro* using Alamar blue assay. However, the POx based amphiphiles have been repeatedly established cytocompatible *in vitro* and *in vivo* [33, 45-47]. In this regard, we have also performed the cytocompatibility studies of the A-pPentOx-A based triblock copolymer in MG87 RET cells. The cells were exposed to 1-50 g/L of polymer for 72 hours. We observed a polymer concentration dependent decrease in cell viability with respect to untreated cells (Figure 7a). At 1 g/L polymer, no significant reduction in cell viability was observed, while a minor reduction was observed in the cells treated with 10 g/L of polymer ($p=0.0001$, ANOVA with Dunnett's posthoc). In contrast, at 50 g/L of polymer, cell viability dropped well below 50 % of control ($p<0.00001$, ANOVA with Dunnett's posthoc). Previously, we have seen no considerable cytotoxicity for a variety of POx based AB and ABA triblock copolymers even at such high concentration [45, 46, 73]. However, it should be kept in mind that this is expected to be dependent on the cell type and the used concentrations are relatively high, exceeding commonly investigated concentration ranges by 1-2 orders of magnitude. In addition, some discrepancies in the cytotoxicity assessment might also be related to the differences in experimental methods (MTT/WST vs Alamar Blue assay).

Biological activity of BT44 formulation in immortalized cells

The GDNF family ligands signal through the GFRα/RET complex [94]. Previously, it has been shown that RET agonists BT13 and BT44 stimulate RET phosphorylation and RET-dependent downstream intracellular signaling [6, 7, 9, 94]. Therefore, in the present study we evaluated the ability of

nanoformulated BT44 to activate RET and RET-dependent downstream signaling in MG87 RET fibroblasts transfected with GFRα1 by Western blot and using a reporter gene-based assay.

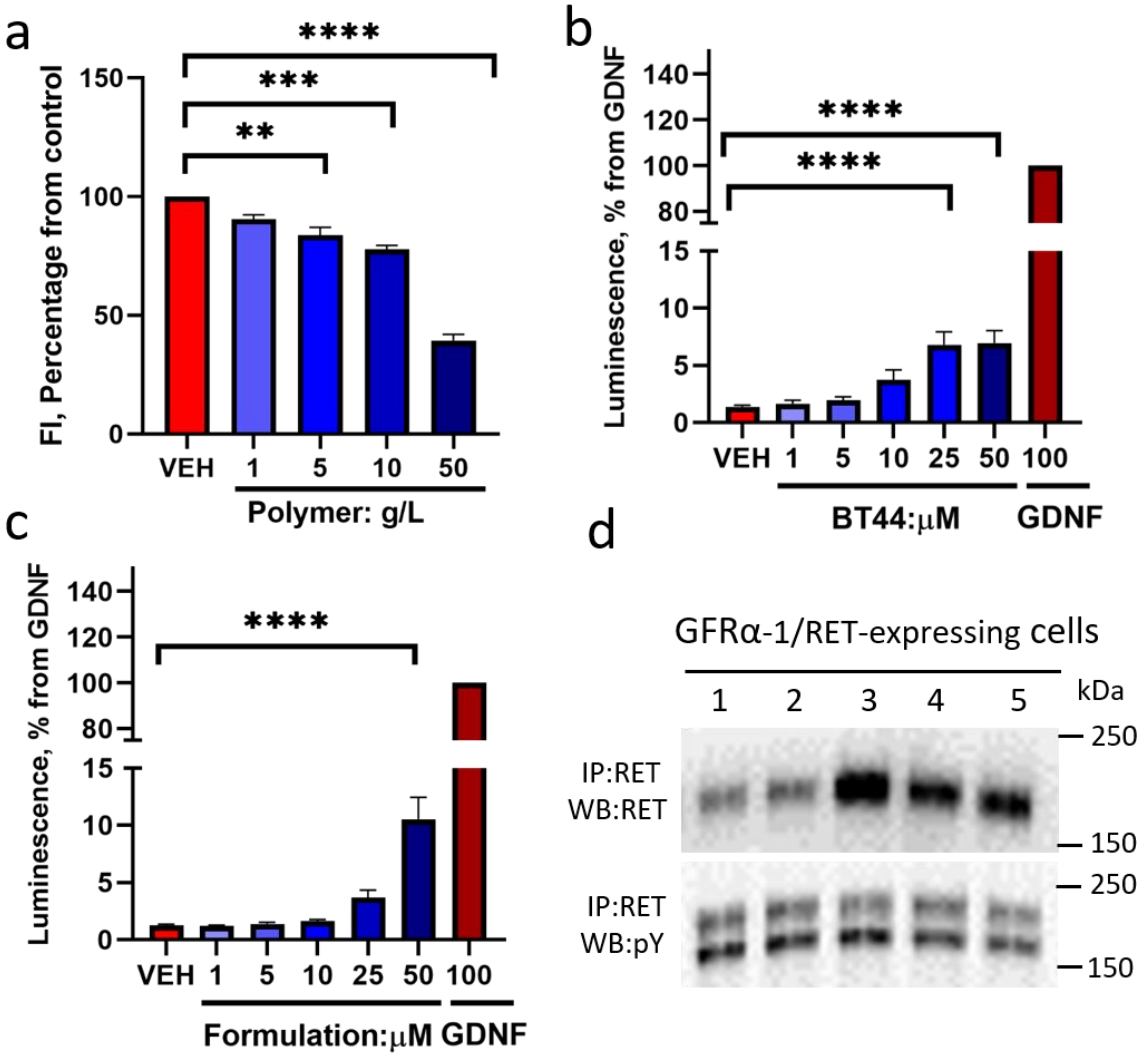

Figure 7l a) Cytotoxicity study of the plain polymer (A-pPentOx-A) at various concentrations, studied by Alamar blue assay after 72 hour of incubation with MG87 RET cells. The quantitative data are presented as mean ± SEM. (VEH; vehicle, cell culture media, FI; Fluorescence Intensity, ANOVA with Dunnett's post-hoc test compared to vehicle, n = 4; ** P < 0.01, *** p < 0.001, **** p < 0.0001). b) BT44 (in 1% DMSO) and c) nanoformulated BT44 (at various concentrations) induced luciferase activity in reporter gene-based assay. d) Assessment of RET phosphorylation by Western blotting in GFRα1-transfected MG87 RET cells. Lanes 1, 2, 3, 4 and 5 are VEH (1% DMSO in DMEM), plain polymer (0.64 mg/mL, similar to 79 μM), BT44 nanoformulation (100 μM), pristine BT44 dissolved in 1% DMSO (100 μM) and GDNF (6.6 nM) respectively. The quantitative data are presented as mean ± SEM. Concentrations provided are in ng/ml for GDNF and μM for polymer, nanoformulation and BT44. (IP; immunoprecipitation, WB; Western blotting. **** p < 0.0001 one-way ANOVA with Dunnett's *post hoc* test, Number of experiment (n=3–4).

The BT44 nanoformulation increased the luciferase activity by 8.4 fold ($p<0.0001$, ANOVA with Dunnett's posthoc) at 50 µM concentration (Figure 7c) in the reporter cell line. In line with previously published results, non-formulated BT44 (Figure 7b) increased the luciferase activity both at 25 and 50 µM concentration by 8.9 fold ($p<0.0001$, ANOVA with Dunnett's posthoc). The GDNF was used as positive control and data was normalized to the signal elicited by GDNF. In line with reporter gene-based assay results, nanoformulated BT44 increased the level of phosphorylated RET in GFRα1 transfected MG87 RET cells compared to both vehicle and plain polymer (Figure 7d). These data indicate that POx based BT44 nanoformulation retained the ability to activate RET.

Neuroprotective properties of BT44 formulation in dopamine neurons

Both BT13 and BT44 were previously shown to promote the survival of cultured dopamine neurons and also protect these neurons from dopamine neurotoxin induced cell death [7, 10]. Therefore, we also tested the ability of nanoformulated BT44 to protect dopamine neurons against N-methyl-4-phenylpyridine (MMP+) induced cell death. MMP+ is a neurotoxin that inhibit the complex I of the mitochondria leading to the depletion of adenosine triphosphate (ATP) and causing eventually cell death. At 100 nM, nanoformulated BT44 increased the number of TH-positive neurons by 1.9 fold ($p= 0.0103$) which is comparable to the effect produced by BT44 dissolved in 1% DMSO (2.2 fold increase, $p=0.0050$) and GDNF (2.2 fold increase, $p=0.0040$) ($p= 0.0013$, ANOVA with Dunnett's post hoc test for all comparisons) (Figure 8a). Thus, the POx based BT44 nanoformulation did not negatively affect the neuroprotective properties of BT44.

Interaction of BT44 formulation with GDNF receptors

Further, we studied the binding of nanoformulated BT44 with GFRα1 and GFRα1/RET using MST and cell-based iodinated GDNF displacement assay. The binding of neurotrophic factors GDNF to GFRα1 and activation of RET receptors has been investigated in various laboratories [95-97]. The GDNF binds to the soluble form of GFRα1 with K_d of 630 pM as shown by surface plasmon resonance binding studies [98]. Using MST assay, we observed a somewhat lower binding affinity of GDNF to GFRα1 (K_d = 260 nM, data not shown), thus validating the assay. The POx based BT44 formulation also bound to

GFRα1, although with much lower affinity (K_d = 3.6 ± 2.2 µM) (Figure 8b). The GDNF is a rather big protein molecule which forms multiple contacts with GFRα1, while compounds belonging to the BT family make only a few hydrogen bonds and other contacts with amino acid residues of GFRa1 [99]. Therefore, higher K_d of BT44 compared to that of GDNF in GFRa1 binding assay is to be expected. Importantly, binding of BT44 formulation to GFRα1 in the presence of RET was not observed, rather aberrant MST traces were seen due to protein aggregation. Here we speculate that aggregates observed in this assay might be due to the complex formation between GFRα1, the nanoformulation and RET. Further studies are needed to verify this hypothesis.

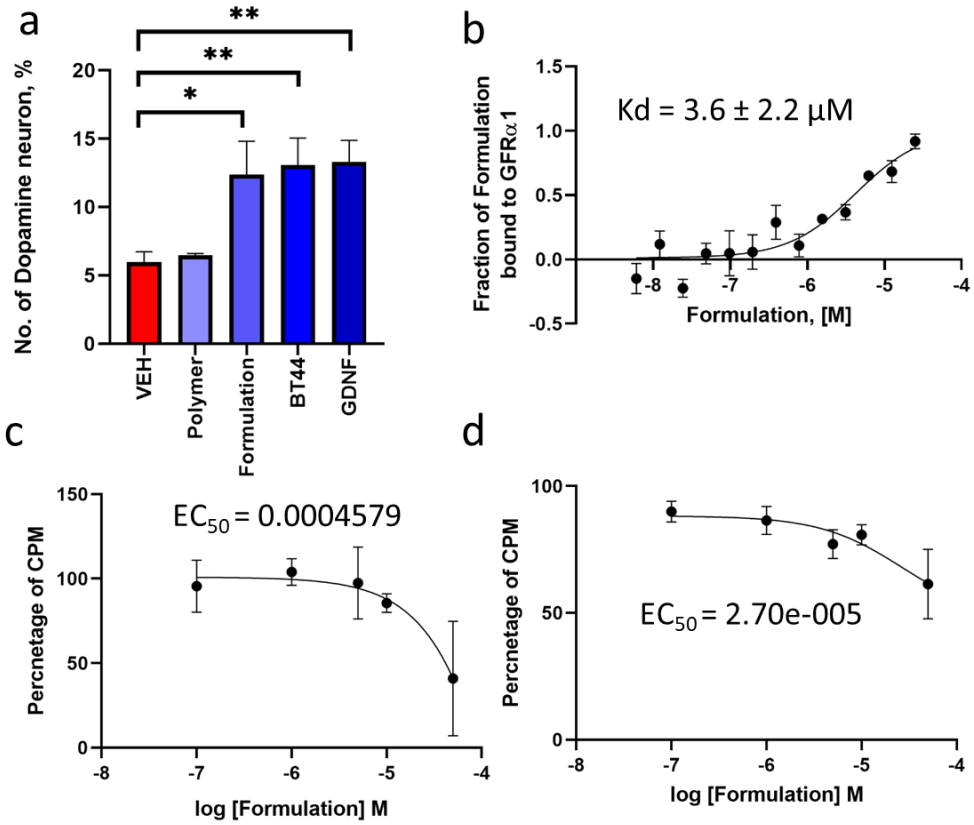

Figure 8l a) The BT44 nanoformulation protected cultured dopamine neurons from MMP+ neurotoxin induced cell death. The number of TH-positive cells in the wild-type midbrain cultures exposed with MPP+, after 6 days *in vitro* culture, were exposed to vehicle, plain polymer (0.0064 mg/ml similar to 790 nM), nanoformulated BT44 (100 nM), pristine BT44 (100 nM in 1% DMSO) or GDNF (3.3 nM), respectively, for 48 hours. The results are normalized to the total number of cells in the culture and presented as percentage of vehicle (1% DMSO in DMEM F12 media)-treated samples (average from 4 independent experiments). The quantitative data are presented as mean ± SEM (VEH; Vehicle, 1% DMSO in DMEM F12 media. * $p < 0.05$, ** $p < 0.01$, one-way ANOVA with Dunnett's *posthoc* test). b) The binding of nanoformulated BT44 (0–10 µM) to GFRα1 (20 nM) monitored by MST. c) & d)

Displacement of 50 pM ^{125}I-GDNF from GFR α1 (c) GFR α1/RET complex (d) by nanoformulated BT44. Each data points represents mean ± SEM of 2-4 independent repeats. The binding isotherms were fitted using nonlinear regression.

We also performed competition-binding studies with formulated BT44 in cells expressing GFRα1 or GFRα1/RET. In this assay, nanoformulated BT44 displaced radiolabeled GDNF with IC_{50} value of 460 × 10^{-6} Min GFRα1 transfected cells (Figure 8c) and 27 × 10^{-6} M (Figure 8d) in GFRα1/RET transfected cells. When GFRα1 was co-expressed with RET at a DNA ratio of 1:1, the potency of the nanoformulated BT44 in ^{125}I-GDNF assay was higher compared to that observed in the cells expressing only GFRα1. A similar trend was also observed for GDNF in GFRα1-expressing cells, wherein unlabeled GDNF displaced ^{125}I-GDNF with an IC_{50} value of 1.9 ± 0.2 × 10^{-9} M, while in GFRα1/RET transfected cells (1:1 DNA ratio) an IC_{50} of 10.6 ± 2.1 × 10^{-12} M for the high affinity site and 2.3 ± 1.1 × 10^{-9} M for the low affinity site [98] was found. Overall, our *in vitro* studies suggest that nanoformulated BT44 has similar effects to that of free BT44 and GDNF.

***In vivo* evaluation of absorption, BBB penetration and acute toxicity of BT44 formulation**

In previous *in vivo* studies, propylene glycole (PG) was used as a vehicle for the BT44 administration, due to poor aqueous solubility of BT44 [9, 10]. In rats, PG did not show any significant toxicity after both subcutaneous and intracranial administration. However, the absorption of BT44 into the blood stream after subcutaneous injection of the BT44 dissolved in PG was found to be rather low [9]. After intravenous administration, a portion of BT44 (approx. 18%) also penetrated through the BBB [10]. Herein, we investigated whether a higher absorption and potentially even better BBB penetration can be achieved with the nanoformulated BT44 after subcutaneous administration.

The plasma and brain concentrations of BT44 were measured one hour post injection and found significantly higher in the case of nanoformulated BT44, compared to PG based solution, i.e 6.6 fold, p=0.0001 and 13 fold, p=0.0094, respectively (Figure 9a and 9b). Apparently, nanoformulated BT44 did not only increase absorption of BT44 into blood stream, but also enhanced BBB penetration of the compound, as the relative increase of BT44 concentration was two times higher in brain than in

plasma. Very recently, Hwang et al. also observed the similar effect by using A-pBuOx-A/vismodegib (VSM) based nanoformulation, as VSM concentration was found to be much higher in medulloblastoma and forebrain of the mice compared to the free drug. The authors hypothesized that the encapsulation of VSM in nanocarriers reduced its interaction with plasma proteins, hence increasing the availability of free VSM leading to relatively higher transport across BBB [37]. Another possibility could be interference with drug efflux pumps which are prevalent in the BBB, and its role in restricting brain entry of multiple drugs is widely accepted [100-102]. However, further studies are needed to support or reject this hypothesis. Alternatively, higher transport across the BBB has also been described for nanoformulated domperidone, which normally does not cross the BBB [103-105]. In any case, the observed increase in BBB penetration is highly beneficial for CNS targeted drugs.

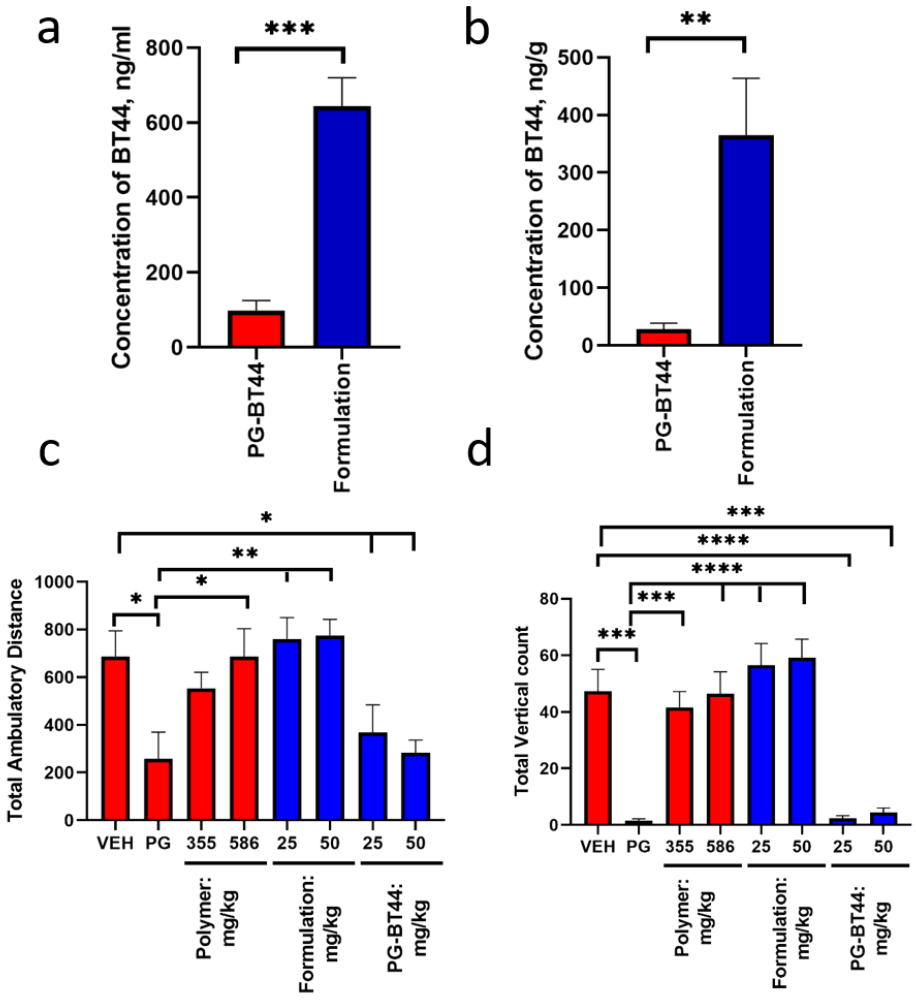

Figure 9| The plasma and brain concentrations of BT44 formulation and toxicity studies in mouse after subcutaneous administration. The plasma (a) and brain (b) concentration of BT44 after one hour propylene glycole (PG) solubilized BT44 and nanoformulation injection. Toxicity of formulation was monitored using behavioural parameters such as total ambulatory distance travelled (c) and total vertical count (d) in Open Field behavioural test. Each data points represents mean ± SEM of 4-5 mice per group. * P < 0.05, ** P < 0.01, *** P < 0.001, **** P < 0.0001 one-way ANOVA with Dunnett's *posthoc* test.

Finally, the toxicity of nanoformulated BT44 in mice was also evaluated. In this regard, the locomotor and exploratory activity were assessed by the open field behavioral test. Additionally, the general conditions of the animals were visually monitored. To our surprise, and in contrast to previous experimental observations in rats, the vehicle i.e. PG negatively impacted the behavior of experimental animals in mice. The statistically significant differences were observed in motor function (both total ambulatory distance travelled and total vertical counts) between the treatment groups (p= <0.0001, one-way ANOVA) one hour post-administration of tested substances. The total ambulatory distance travelled by mice treated with PG (p= 0.0393) alone and PG-BT44 both at 25 (p= 0.0422) at 50 mg/kg (p= 0.0381) was significantly reduced compared to this characteristic for mice treated with saline (Figure 9c). Further, vertical counts were also affected by PG alone (p=0.0001) or in combination with 25 mg/kg (p<0.0001) or 50 mg/kg (p=0.0001) of BT44 (Figure 9d). The reduction in motor activity was also visually very clear in home cages. The mice receiving PG (either alone or in combination with BT44) remained immobile and practically non-reactive to handling. The effect was temporary and within few hours of post injection (2-6 h) the mobility of animals gradually restored. All animals that remained immobile during $\geq$ 2 h received intraperitoneal injection of 1 ml of saline to prevent dehydration. All animals were visually normal at 24 h post treatment. Notably, reported no-observed-effect level (NOEL) and maximum tolerated dose (MTD) for PG in mice when injected intraveneously are 1.036 g/kg and 1.554 g/kg respectively [106]. Toxicity manifestations such as hind limb ataxia, hind limb muscle contraction and hemolysis, were observed when the dose of PG exceeded MTD. According to the information from PubChem database, lethal dose 50 (LD_{50}) of PG in mice and rats (after subcutaneous injection) is equal to 17.4 and 28.8 g/kg, respectively. In the current study, the dose of PG administered subcutaneously constituted 10.3 g/kg. This is much below LD_{50}, but seems to

be sufficient to produce notable adverse effects in mice, even though in a previous studies, no such effects were observed in rats [8]. Thus, there are interspecies differences in sensitivity to PG, which is in line with published data (PubChem). Noteworthy, there are several reports indicating PG toxicity in humans [107, 108]. Further, PG was found to cause neuroapoptosis in the developing mouse central nervous system [109].

In comparison, the nanoformulated BT44 (at 25 and 50 mg/kg) and plain polymer (at corresponding doses of 355 and 586 mg/kg) produced no significant changes in evaluated behavioral parameters (total ambulatory distance and vertical counts) after subcutaneous injection (Figure 11 c and d). The animals receiving plain polymer or BT44 loaded POx formulation freely moved in home cages and were responsive to investigator's manipulations. These data suggest that the plain polymer excipient and nanoformulated BT44 is safe *in vivo* and could be used for future preclinical development.

Conclusion

Herein, we present the first micellar nanoformulation of BT44 with an ultra-high drug loading. The extent and pattern of compatibility between polymer and drug when considering Hansen solubility parameters between BT44 and three amphiphiles were not in accordance with the formulation results. As has been described before for other drugs, Hansen solubility parameters are not the appropriate choice for estimating compatibility in POx based system, especially considering the fact that depending upon nature and overall load of guest molecules, the hydrophilic pMeOx may play an important role in solubility as well as stability of the entire system [25, 27, 86]. The POx based triblock copolymer i.e. A-pPentOx-A gave ultra-high drug loading of around 47 wt.%. The developed formulations underwent detailed physicochemical characterization. The formulation can be stored as lyophilized powder ready for redispersion. The formulated BT44 bind to its cellular receptor, retained its biological activity in immortalized cells and its neuroprotective properties in dopamine neurons. Furthermore, the absorption of formulated BT44 into the blood stream and its blood-brain barrier penetration properties were significantly improved compared to conventional preparation of BT44 in PG. We did not observe acute toxicity of either POx polymer or BT44/POx formulation in mice. Similar

to previously reported POx based triblock copolymers formulations [37, 47, 61, 62], we anticipate that A-pPentOx-A/BT44 micellar formulation will allow the parenteral administration and help to alleviate the use of toxic excipients not only at its preclinical development phase but also potentially for future clinical use.

Associated Content:

Corresponding authors:

E.mail: haider_m@ukw.de

ORCID: Malik Salman Haider: 0000-0003-4248-8828

E-mail: yulia.sidorova@helsinki.fi

ORCID: Yulia Sidorova: 0000-0001-8230-0530

Notes: R.L. is listed as co-inventor on a patent pertinent to some materials in the present work and is co-founder of DelAqua Pharmaceutical Inc. intending commercial development of poly(2-oxazoline)s based drug delivery system. YS is a minor shareholder of GeneCode Ltd, a company holding patent for BT compounds.

Acknowledgement

Malik Salman Haider is grateful to higher education commission of Pakistan and German academic exchange services (HEC-DAAD Pakistan) for the award of PhD scholarship. We also thank Jan Weichhold for providing technical support during XRD measurements. We are grateful to Paula Collin for her excellent technical assistance with cell-based assays and to Pharmidex Pharmaceutical services Ltd (UK) for measuring of plasma and brain concentration of BT44. We further thank NMR core facility supported by University of Helsinki, Biocenter Finland and Helsinki Institute of Life Science (HiLIFE) for verification of the structure of BT44.

References

1. Ali, S. and K. Kolter, *Challenges and opportunities in oral formulation development.* American Pharmacuetical Review, 2012. **15**(7): p. 1.
2. Williams, H.D., et al., *Strategies to address low drug solubility in discovery and development.* Pharmacological Reviews, 2013. **65**(1): p. 315-499.
3. Durães, F., M. Pinto, and E. Sousa, *Old drugs as new treatments for neurodegenerative diseases.* Pharmaceuticals, 2018. **11**(2): p. 44.
4. Enciu, A.M., et al., *Neuroregeneration in neurodegenerative disorders.* BMC neurology, 2011. **11**(1): p. 1-7.
5. Bondarenko, O. and M. Saarma, *Neurotrophic Factors in Parkinson's Disease: Clinical Trials, Open Challenges and Nanoparticle-Mediated Delivery to the Brain.* Frontiers in Cellular Neuroscience, 2021. **15**.
6. Mahato, A.K. and Y.A. Sidorova, *RET Receptor Tyrosine Kinase: Role in Neurodegeneration, Obesity, and Cancer.* International Journal of Molecular Sciences, 2020. **21**(19): p. 7108.
7. Mahato, A.K., et al., *Glial cell line–derived neurotrophic factor receptor rearranged during transfection agonist supports dopamine neurons in vitro and enhances dopamine release in vivo.* Movement Disorders, 2020. **35**(2): p. 245-255.
8. Sidorova, Y.A., et al., *A novel small molecule GDNF receptor RET agonist, BT13, promotes neurite growth from sensory neurons in vitro and attenuates experimental neuropathy in the rat.* Frontiers in Pharmacology, 2017. **8**: p. 365.
9. Viisanen, H., et al., *Novel RET agonist for the treatment of experimental neuropathies.* Molecular Pain, 2020. **16**: p. 1-19.
10. Renko, J.-M., et al., *Neuroprotective Potential of a Small Molecule RET Agonist in Cultured Dopamine Neurons and Hemiparkinsonian Rats.* Journal of Parkinson's Disease, 2021(Preprint): p. 1-24.
11. Bahr, M.N., et al., *Rapid screening approaches for solubility enhancement, precipitation inhibition and dissociation of a cocrystal drug substance using high throughput experimentation.* Journal of Drug Delivery Science and Technology, 2021. **61**: p. 102196.
12. Fernandes, G.J., et al., *A review on solubility enhancement of carvedilol—a BCS class II drug.* Journal of Pharmaceutical Innovation, 2018. **13**(3): p. 197-212.
13. Singh, D., N. Bedi, and A.K. Tiwary, *Enhancing solubility of poorly aqueous soluble drugs: Critical appraisal of techniques.* Journal of Pharmaceutical Investigation, 2018. **48**(5): p. 509-526.
14. Kumar, S., et al., *Nanotechnology as emerging tool for enhancing solubility of poorly water-soluble drugs.* Bionanoscience, 2012. **2**(4): p. 227-250.
15. Chi Lip Kwok, P. and H.-K. Chan, *Nanotechnology versus other techniques in improving drug dissolution.* Current Pharmaceutical Design, 2014. **20**(3): p. 474-482.
16. Shetab Boushehri, M.A., D. Dietrich, and A. Lamprecht, *Nanotechnology as a Platform for the Development of Injectable Parenteral Formulations: A Comprehensive Review of the Know-Hows and State of the Art.* Pharmaceutics, 2020. **12**(6): p. 510.
17. Saka, R. and N. Chella, *Nanotechnology for delivery of natural therapeutic substances: a review.* Environmental Chemistry Letters, 2021. **19**: p. 1097–1106.
18. Cabral, H., et al., *Block copolymer micelles in nanomedicine applications.* Chemical Reviews, 2018. **118**(14): p. 6844-6892.
19. Ghosh, B. and S. Biswas, *Polymeric micelles in cancer therapy: State of the art.* Journal of Controlled Release, 2021. **332**: p. 127-147.

20. Hwang, D., J.D. Ramsey, and A.V. Kabanov, *Polymeric micelles for the delivery of poorly soluble drugs: from nanoformulation to clinical approval.* Advanced Drug Delivery Reviews, 2020. **156**: p. 80-118.
21. Hussein, Y.H. and M. Youssry, *Polymeric micelles of biodegradable diblock copolymers: enhanced encapsulation of hydrophobic drugs.* Materials, 2018. **11**(5): p. 688.
22. Noolandi, J. and K.M. Hong, *Theory of block copolymer micelles in solution.* Macromolecules, 1983. **16**(9): p. 1443-1448.
23. Cammas, S., et al., *Thermo-responsive polymer nanoparticles with a core-shell micelle structure as site-specific drug carriers.* Journal of Controlled Release, 1997. **48**(2-3): p. 157-164.
24. Lübtow, M.M., et al., *Ultra-high to ultra-low drug loaded micelles: Probing host-guest interactions by fluorescence spectroscopy.* Chemistry-A European Journal, 2019. **25**(54): p. 12601-12610.
25. Pöppler, A.C., et al., *Loading-Dependent Structural Model of Polymeric Micelles Encapsulating Curcumin by Solid-State NMR Spectroscopy.* Angewandte Chemie International Edition, 2019. **58**(51): p. 18540-18546.
26. Haider, M.S., et al., *Think beyond the core: The impact of the hydrophilic corona on the drug solubilization using polymer micelles.* ACS Applied Materials & Interfaces, 2020. **12**(22): p. 24531–24543.
27. Sochor, B., et al., *Probing the Complex Loading Dependent Structural Changes in Ultra-High Drug Loaded Polymer Micelles by Small-Angle Neutron Scattering.* Langmuir, 2020. **36**: p. 3494-3503.
28. Slor, G., et al., *Judging Enzyme-Responsive Micelles by Their Covers: Direct Comparison of Dendritic Amphiphiles with Different Hydrophilic Blocks.* Biomacromolecules, 2021. **22**(3): p. 1197–1210.
29. Cao, C., et al., *Drug-Induced Morphology Transition of Self-Assembled Glycopolymers: Insight into the Drug–Polymer Interaction.* Chemistry of Materials, 2018. **30**(15): p. 5227-5236.
30. Chang, T., et al., *Size effects of self-assembled block copolymer spherical micelles and vesicles on cellular uptake in human colon carcinoma cells.* Journal of Materials Chemistry B, 2014. **2**(19): p. 2883-2891.
31. Dag, A., et al., *Modulating the cellular uptake of platinum drugs with glycopolymers.* Polymer Chemistry, 2016. **7**(5): p. 1031-1036.
32. Holder, S.J. and N.A. Sommerdijk, *New micellar morphologies from amphiphilic block copolymers: disks, toroids and bicontinuous micelles.* Polymer Chemistry, 2011. **2**(5): p. 1018-1028.
33. Schulz, A., et al., *Drug-induced morphology switch in drug delivery systems based on poly(2-oxazoline)s.* ACS Nano, 2014. **8**(3): p. 2686-2696.
34. Lim, C., et al., *Drug-dependent morphological transitions in spherical and worm-like polymeric micelles define stability and pharmacological performance of micellar drugs.* bioRxiv, 2021.
35. Nishiyama, N. and K. Kataoka, *Current state, achievements, and future prospects of polymeric micelles as nanocarriers for drug and gene delivery.* Pharmacology & Therapeutics, 2006. **112**(3): p. 630-648.
36. Cabral, H. and K. Kataoka, *Progress of drug-loaded polymeric micelles into clinical studies.* Journal of Controlled Release, 2014. **190**: p. 465-476.
37. Hwang, D., et al., *Poly(2-oxazoline) nanoparticle delivery enhances the therapeutic potential of vismodegib for medulloblastoma by improving CNS pharmacokinetics and reducing systemic toxicity.* Nanomedicine: Nanotechnology, Biology and Medicine, 2021. **32**: p. 102345.
38. Batrakova, E.V. and A.V. Kabanov, *Pluronic block copolymers: evolution of drug delivery concept from inert nanocarriers to biological response modifiers.* Journal of Controlled Release, 2008. **130**(2): p. 98-106.

39. Bloksma, M.M., U.S. Schubert, and R. Hoogenboom, *Poly(cyclic imino ether)s Beyond 2-Substituted-2-oxazolines.* Macromolecular Rapid Communications, 2011. **32**(18): p. 1419-1441.
40. Trachsel, L., M. Zenobi-Wong, and E.M. Benetti, *The role of poly(2-alkyl-2-oxazoline)s in hydrogels and biofabrication.* Biomaterials Science, 2021. **9**(8): p. 2874-2886.
41. You, Y., et al., *Engineered cell-degradable poly (2-alkyl-2-oxazoline) hydrogel for epicardial placement of mesenchymal stem cells for myocardial repair.* Biomaterials, 2021. **269**: p. 120356.
42. Trachsel, L., et al., *Double-network hydrogels including enzymatically crosslinked poly-(2-alkyl-2-oxazoline) s for 3D bioprinting of cartilage-engineering constructs.* Biomacromolecules, 2019. **20**(12): p. 4502-4511.
43. Luxenhofer, R., et al., *Poly(2-oxazoline)s as Polymer Therapeutics.* Macromolecular Rapid Communications, 2012. **33**(19): p. 1613-1631.
44. He, Z., et al., *Poly(2-oxazoline) based micelles with high capacity for 3rd generation taxoids: Preparation, in vitro and in vivo evaluation.* Journal of Controlled Release, 2015. **208**: p. 67-75.
45. Lübtow, M.M., et al., *Drug induced micellization into ultra-high capacity and stable curcumin nanoformulations: Physico-chemical characterization and evaluation in 2D and 3D in vitro models.* Journal of Controlled Release, 2019. **303**: p. 162-180.
46. Haider, M.S., et al., *A Micellar Mitotane Formulation with High Drug-Loading and Solubility: Physico-Chemical Characterization and Cytotoxicity Studies in 2D and 3D In Vitro Tumor Models.* Macromolecular Bioscience, 2020. **20**(1): p. 1900178.
47. Vinod, N., et al., *High-capacity poly(2-oxazoline) formulation of TLR 7/8 agonist extends survival in a chemo-insensitive, metastatic model of lung adenocarcinoma.* Science Advances, 2020. **6**(25): p. 5542.
48. Hwang, D., et al., *Novel poly(2-oxazoline) block copolymer with aromatic heterocyclic side chains as a drug delivery platform.* Journal of Controlled Release, 2019. **307**: p. 261-271.
49. Park, J.-R., et al., *Influence of side-chain length on long-term release kinetics from poly(2-oxazoline)-drug conjugate networks.* European Polymer Journal, 2019. **120**: p. 109217.
50. Raveendran, R., et al., *Poly(2-oxazoline) block copolymer nanoparticles for curcumin loading and delivery to cancer cells.* European Polymer Journal, 2017. **93**: p. 682-694.
51. Lorson, T., et al., *Poly(2-oxazoline)s based biomaterials: A comprehensive and critical update.* Biomaterials, 2018. **178**: p. 204-280.
52. Hu, C., et al., *A Thermogelling Organic-Inorganic Hybrid Hydrogel with Excellent Printability, Shape Fidelity and Cytocompatibility for 3D Bioprinting.* Biofabrication, 2021.
53. Haider, M.S., et al., *Tuning the Thermogelation and Rheology of Poly (2-Oxazoline)/Poly (2-Oxazine) s Based Thermosensitive Hydrogels for 3D Bioprinting.* Gels, 2021. **7**(3): p. 78.
54. Zhang, N., et al., *Cylindrical molecular brushes of poly (2-oxazoline) s from 2-isopropenyl-2-oxazoline.* Macromolecules, 2009. **42**(6): p. 2215-2221.
55. Lübtow, M.M., et al., *Like Dissolves Like? A Comprehensive Evaluation of Partial Solubility Parameters to Predict Polymer-Drug Compatibility in Ultra-High Drug Loaded Polymer Micelles.* Biomacromolecules, 2019. **20**(8): p. 3041-3056.
56. Sahn, M., C. Weber, and U.S. Schubert, *Poly(2-oxazoline)-Containing Triblock Copolymers: Synthesis and Applications.* Polymer Reviews, 2019. **59**(2): p. 240-279.
57. Zahoranová, A., et al., *ABA and BAB Triblock Copolymers Based on 2-Methyl-2-oxazoline and 2-n-Propyl-2-oxazoline: Synthesis and Thermoresponsive Behavior in Water.* Macromolecular Chemistry and Physics, 2017. **218**(13): p. 1700031.
58. Zahoranová, A. and R. Luxenhofer, *Poly(2-oxazoline)- and Poly(2-oxazine)-Based Self-Assemblies, Polyplexes, and Drug Nanoformulations-An Update.* Advanced Healthcare Materials, 2021. **10**(6): p. 2001382.

59. Sedlacek, O. and R. Hoogenboom, *Drug Delivery Systems Based on Poly(2-Oxazoline)s and Poly(2-Oxazine)s.* Advanced Therapeutics, 2020. **3**(1): p. 1900168.
60. Hwang, D., et al., *Bioequivalence assessment of high-capacity polymeric micelle nanoformulation of paclitaxel and Abraxane® in rodent and non-human primate models using a stable isotope tracer assay.* Biomaterials, 2021. **278**: p. 121140.
61. He, Z., et al., *A high capacity polymeric micelle of paclitaxel: Implication of high dose drug therapy to safety and in vivo anti-cancer activity.* Biomaterials, 2016. **101**: p. 296-309.
62. Wan, X., et al., *Drug Combination Synergy in worm-like Polymeric Micelles Improves Treatment Outcome for Small Cell and Non-Small Cell Lung Cancer.* ACS Nano, 2018. **12**(3): p. 2426-2439.
63. Wan, X., et al., *Co-delivery of paclitaxel and cisplatin in poly (2-oxazoline) polymeric micelles: Implications for drug loading, release, pharmacokinetics and outcome of ovarian and breast cancer treatments.* Biomaterials, 2019. **192**: p. 1-14.
64. Witte, H. and W. Seeliger, *Cyclische imidsäureester aus nitrilen und aminoalkoholen.* Leibigs Ann., 1974. **1974**: p. 996-1009.
65. Lübtow, M.M., et al., *Drug specificity, synergy and antagonism in ultrahigh capacity poly(2-oxazoline)/poly(2-oxazine) based formulations.* Journal of the American Chemical Society, 2017. **139**(32): p. 10980-10983.
66. Hahn, L., et al., *Investigating the Influence of Aromatic Moieties on the Formulation of Hydrophobic Natural Products and Drugs in Poly(2-oxazoline)-Based Amphiphiles.* Biomacromolecules, 2018. **19**(7): p. 3119.
67. Lübtow, M.M., et al., *More Is Sometimes Less: Curcumin and Paclitaxel Formulations Using Poly(2-oxazoline) and Poly(2-oxazine)-Based Amphiphiles Bearing Linear and Branched C9 Side Chains.* Macromolecular Bioscience, 2018. **18**(11): p. 1800155-1800172.
68. Letchford, K., R. Liggins, and H. Burt, *Solubilization of hydrophobic drugs by methoxy poly(ethylene glycol)-block-polycaprolactone diblock copolymer micelles: Theoretical and experimental data and correlations.* Journal of Pharmaceutical Sciences, 2008. **97**(3): p. 1179-1190.
69. Fedors, R.F., *A method for estimating both the solubility parameters and molar volumes of liquids.* Polymer Engineering & Science, 1974. **14**(2): p. 147-154.
70. Van Krevelen, D.W. and K. Te Nijenhuis, *Properties of polymers: their correlation with chemical structure; their numerical estimation and prediction from additive group contributions*. 2009: Elsevier.
71. Mastronarde, D.N., *Automated electron microscope tomography using robust prediction of specimen movements.* Journal of Structural Biology, 2005. **152**(1): p. 36-51.
72. Ardashov, O.V., et al., *A novel small molecule supports the survival of cultured dopamine neurons and may restore the dopaminergic innervation of the brain in the MPTP mouse model of Parkinson's disease.* ACS Chemical Neuroscience, 2019. **10**(10): p. 4337-4349.
73. Lübtow, M.M., et al., *In Vitro Blood–Brain Barrier Permeability and Cytotoxicity of an Atorvastatin-Loaded Nanoformulation Against Glioblastoma in 2D and 3D Models.* Molecular Pharmaceutics, 2020. **17**(6): p. 1835-1847.
74. Luxenhofer, R., et al., *Doubly amphiphilic poly(2-oxazoline)s as high-capacity delivery systems for hydrophobic drugs.* Biomaterials, 2010. **31**: p. 4972-4979.
75. Han, Y., et al., *Synergistic combinations of multiple chemotherapeutic agents in high capacity poly(2-oxazoline) micelles.* Molecular Pharmaceutics, 2012. **9**(8): p. 2302-2313.
76. Seo, Y., et al., *Poly(2-oxazoline) block copolymer based formulations of taxanes: effect of copolymer and drug structure, concentration, and environmental factors.* Polymers for Advanced Technologies, 2015. **26**(7): p. 837-850.
77. Luxenhofer, R., et al., *Structure-property relationship in cytotoxicity and cell uptake of poly(2-oxazoline) amphiphiles.* Journal of Controlled Release, 2011. **153**(1): p. 73-82.

78. Liu, J., Y. Xiao, and C. Allen, *Polymer–drug compatibility: a guide to the development of delivery systems for the anticancer agent, ellipticine.* Journal of Pharmaceutical Sciences, 2004. **93**(1): p. 132-143.
79. Pyrhönen, J., et al., *Molecular Dynamics Prediction Verified by Experimental Evaluation of the Solubility of Different Drugs in Poly (decalactone) for the Fabrication of Polymeric Nanoemulsions.* Advanced NanoBiomed Research, 2022. **2**(1): p. 2100072.
80. Lin, S.-Y., C.-J. Lee, and Y.-Y. Lin, *Drug-polymer interaction affecting the mechanical properties, adhesion strength and release kinetics of piroxicam-loaded Eudragit E films plasticized with different plasticizers.* Journal of Controlled Release, 1995. **33**(3): p. 375-381.
81. Wu, C. and J.W. McGinity, *Non-traditional plasticization of polymeric films.* International Journal of Pharmaceutics, 1999. **177**(1): p. 15-27.
82. Nair, R., et al., *Influence of various drugs on the glass transition temperature of poly (vinylpyrrolidone): a thermodynamic and spectroscopic investigation.* International Journal of Pharmaceutics, 2001. **225**(1-2): p. 83-96.
83. Hossin, B., K. Rizi, and S. Murdan, *Application of Hansen Solubility Parameters to predict drug–nail interactions, which can assist the design of nail medicines.* European Journal of Pharmaceutics and Biopharmaceutics, 2016. **102**: p. 32-40.
84. Hansen, C.M., *Hansen solubility parameters: a user's handbook*. 2007: CRC press.
85. Barton, A.F., *CRC handbook of solubility parameters and other cohesion parameters*. 2017: Routledge.
86. Grüne, M., et al., *14 N–1 H HMQC solid-state NMR as a powerful tool to study amorphous formulations–an exemplary study of paclitaxel loaded polymer micelles.* Journal of Materials Chemistry B, 2020. **8**(31): p. 6827-6836.
87. Tian, Y., et al., *Designing micellar nanocarriers with improved drug loading and stability based on solubility parameter.* Molecular Pharmaceutics, 2015. **12**(3): p. 816-825.
88. Raveendran, R., et al., *Poly (2-oxazoline) block copolymer nanoparticles for curcumin loading and delivery to cancer cells.* European Polymer Journal, 2017. **93**: p. 682-694.
89. Kim, Y., et al., *Effect of shell-crosslinking of micelles on endocytosis and exocytosis: acceleration of exocytosis by crosslinking.* Biomaterials Science, 2013. **1**(3): p. 265-275.
90. Hiller, W., et al., *Micellization and mobility of amphiphilic poly (2-oxazoline) based block copolymers characterized by 1H NMR spectroscopy.* Macromolecules, 2015. **48**(12): p. 4032-4045.
91. Novakovic, D., et al., *Understanding dissolution and crystallization with imaging: A surface point of view.* Molecular Pharmaceutics, 2018. **15**(11): p. 5361-5373.
92. Hahn, L., et al., *Inverse thermogelation of aqueous triblock copolymer solutions into macroporous shear-thinning 3D printable inks.* ACS Applied Materials & Interfaces, 2020. **12**(11): p. 12445-12456.
93. Lim, C., et al., *Drug-Dependent Morphological Transitions in Spherical and Worm-Like Polymeric Micelles Define Stability and Pharmacological Performance of Micellar Drugs.* Small, 2021. **2**(1): p. 2103552.
94. Airaksinen, M.S. and M. Saarma, *The GDNF family: signalling, biological functions and therapeutic value.* Nature Reviews Neuroscience, 2002. **3**(5): p. 383-394.
95. Jing, S., et al., *GDNF–induced activation of the ret protein tyrosine kinase is mediated by GDNFR-α, a novel receptor for GDNF.* Cell, 1996. **85**(7): p. 1113-1124.
96. Treanor, J.J., et al., *Characterization of a multicomponent receptor for GDNF.* Nature, 1996. **382**(6586): p. 80-83.
97. Committee, G.N., *Nomenclature of GPI-linked receptors for the GDNF ligand family.* Neuron, 1997. **19**(3): p. 485.
98. Cik, M., et al., *Binding of GDNF and Neurturin to Human GDNF Family Receptor α 1 and 2: INFLUENCE OF cRET AND COOPERATIVE INTERACTIONS.* Journal of Biological Chemistry, 2000. **275**(36): p. 27505-27512.

99. Théry, C., et al., *Minimal information for studies of extracellular vesicles 2018 (MISEV2018): a position statement of the International Society for Extracellular Vesicles and update of the MISEV2014 guidelines.* Journal of Extracellular Vesicles, 2018. **7**(1): p. 1535750.
100. Löscher, W. and H. Potschka, *Blood-brain barrier active efflux transporters: ATP-binding cassette gene family.* NeuroRx, 2005. **2**(1): p. 86-98.
101. Löscher, W., et al., *Drug resistance in epilepsy: clinical impact, potential mechanisms, and new innovative treatment options.* Pharmacological Reviews, 2020. **72**(3): p. 606-638.
102. Neuwelt, E.A., et al., *Engaging neuroscience to advance translational research in brain barrier biology.* Nature Reviews Neuroscience, 2011. **12**(3): p. 169-182.
103. Hemmelmann, M., et al., *HPMA based amphiphilic copolymers mediate central nervous effects of domperidone.* Macromolecular Rapid Communications, 2011. **32**(9-10): p. 712-717.
104. Hemmelmann, M., et al., *Amphiphilic HPMA–LMA copolymers increase the transport of Rhodamine 123 across a BBB model without harming its barrier integrity.* Journal of Controlled Release, 2012. **163**(2): p. 170-177.
105. Clemens-Hemmelmann, M., et al., *Amphiphilic copolymers shuttle drugs across the blood–brain barrier.* Macromolecular Bioscience, 2016. **16**(5): p. 655-665.
106. Thackaberry, E.A., et al., *Solvent-based formulations for intravenous mouse pharmacokinetic studies: tolerability and recommended solvent dose limits.* Xenobiotica, 2014. **44**(3): p. 235-241.
107. Demey, H., et al., *Propylene glycol-induced side effects during intravenous nitroglycerin therapy.* Intensive Care Medicine, 1988. **14**(3): p. 221-226.
108. Yaucher, N.E., et al., *Propylene glycol-associated renal toxicity from lorazepam infusion.* Pharmacotherapy: The Journal of Human Pharmacology and Drug Therapy, 2003. **23**(9): p. 1094-1099.
109. Lau, K., et al., *Propylene glycol produces excessive apoptosis in the developing mouse brain, alone and in combination with phenobarbital.* Pediatric Research, 2012. **71**(1): p. 54-62.

4.6.3 Atorvastatin formulation

Summary: The therapeutic potential of Atorvastatin (ATV) loaded POx/POzi based micelles were further evaluated as potential treatment for glioblastoma. In general, the statins are widely used for the treatment of hypercholesterolemia; recent research efforts have shown increasing evidence on antitumor efficacy including activity against glioblastoma. Interestingly, ATV (a hydrophobic statins), showed permeability through the blood-brain-barrier (BBB) in vitro and in vivo models. The poor aqueous solubility of ATV prevents e.g. IV administration necessary to reach sufficiently high blood concentrations. In general, the ATV aqueous solubility was strongly increased by solubilization with POx/POzi based amphiphiles. However, POzi based amphiphilie i.e. A-pBuOzi-A was found to be highly efficient ATV solubilizer. When the aqueous solubility of ATV formulation was greater than 3 g/L (at 10 g/L polymer feed), large aggregates were observed with hydrodynamic diameters > 600 nm. Nevertheless, at lower drug loading i.e. 1 g/L ATV formulation solubility, the nanosized micelles (D_h = 26 nm) were observed, which exhibited pronounced cytotoxicity against various mouse and human glioblastoma cells in 2D cell culture. This was also true for 3D spheroid models of highly aggressive and rapidly proliferating mouse brain tumor initiating bRiTS-G2 cells. Compared to ATV, dissolved in DMSO, the permeability of the A-pBuOzi-A/ATV formulation through an artificial BBB derived from human induced pluripotent stem cells was not enhanced. However, co-administration of agents, enhancing the (temporarily) permeability could assist to increase ATV transport across the BBB.

molecular pharmaceutics

pubs.acs.org/molecularpharmaceutics Article

In Vitro Blood–Brain Barrier Permeability and Cytotoxicity of an Atorvastatin-Loaded Nanoformulation Against Glioblastoma in 2D and 3D Models

Michael M. Lübtow, Sabrina Oerter, Sabina Quader, Elisabeth Jeanclos, Alevtina Cubukova, Marion Krafft, Malik Salman Haider, Clemens Schulte, Laura Meier, Maximilian Rist, Oltea Sampetrean, Hiroaki Kinoh, Antje Gohla, Kazunori Kataoka, Antje Appelt-Menzel, and Robert Luxenhofer*

Abstract

Inhibitors of 3-hydroxy-3-methylglutaryl-coenzyme A (HMG-CoA) reductase of the family of statins have been suggested as therapeutic options in various tumors. Atorvastatin is a statin with the potential to cross the blood−brain barrier; however, the concentrations necessary for a cytotoxic effect against cancer cells exceed the concentrations achievable via oral administration, which made the development of a novel atorvastatin formulation necessary. We characterized the drug loading and basic physicochemical characteristics of micellar atorvastatin formulations and tested their cytotoxicity against a panel of different glioblastoma cell lines. In addition, activity against tumor spheroids formed from mouse glioma and mouse cancer stem cells, respectively, was evaluated. Our results show good activity of atorvastatin against all tested cell lines. Interestingly, in the three dimensional (3D) models, growth inhibition was more pronounced for the micellar formulation compared to free atorvastatin. Finally, atorvastatin penetration across a blood−brain barrier model obtained from human induced-pluripotent stem cells was evaluated. Our results suggest that the presented micelles may enable much higher serum concentrations than possible by oral administration; however, if transport across the blood−brain barrier is sufficient to reach the therapeutic atorvastatin concentration for the treatment of glioblastoma via intravenous administration remains unclear.

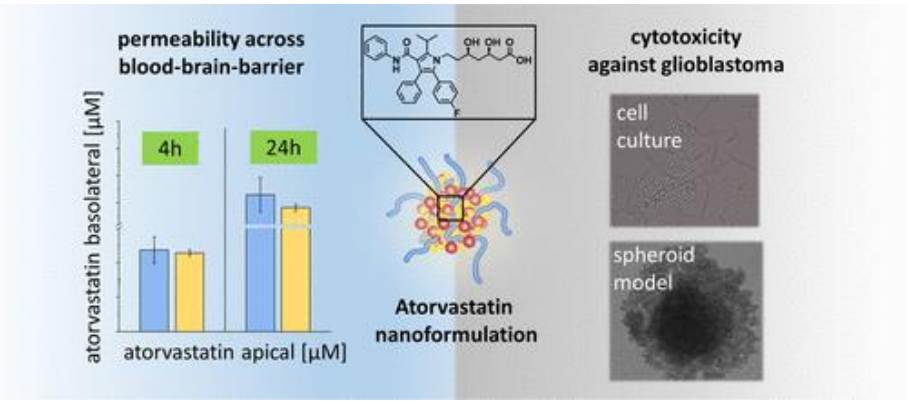

4.7 Poly(2-oxazoline)s and Poly(2-oxazine)s based Hydrogels for Tissue Engineering Applications

As discussed previously, because of rapidly growing interests in precision medicine, emergence of gene/immune therapies and advancements in 3D (bio) printing, there is an increasing demand for smart biomaterials. In this regard, in the year 2017, Thomas Lorson from our group, for the first time, successfully synthesized the first of its kind, POx/POzi based AB di-block copolymer (A = pMeOx, B = pPrOzi), exhibiting lower critical solution type (LCST) behaviour. This polymer is under investigation in various lab after its modification to be used for tissue engineering applications, as fugitive support material or for drug delivery applications.

4.7.1 POx/POzi based Hydrogels as Fugitive Support Material

Summary: The 3D (bio) printing is the most promising technique for the development of cell-laden constructs for the tissue engineering applications. In this regard, the developed constructs must have highly controlled microstructures and should be closer to natural tissues and organs, which can facilitate the cell behaviours including growth, adhesion, proliferation etc. However, there are various challenges, e.g. the current bioprinted equivalent are too small in size or even many biomaterials have very poor printability. Considering these issue, we tend to utilize our polymer platform (AB diblock copolymer, pMeOx-pPrOzi, respectively) as fugitive support/sacrificial material to improve the printability of such biomaterials. Many researchers are using alginate (ALG) for bioprinting process. However, ALG hydrogels for tissue engineering applications suffer from brittleness, low mechanical strength and poor printability because of their limiting rheological properties. So in this study, we aimed at improving the printability of ALG by utilizing our POx based (pMeOx-pPrOzi) diblock copolymer. The thermogelling and shear thinning properties of pMeOx-pPrOzi based diblock copolymer facilitated the cell laden extrusion based bioprinitng process with the good printability, high stackability and shape fidelity. The printed scaffolds were followed by ionic crosslinking which provided them mechanical stability, flexibility and structural integrity. The pMeOx-pPrOzi based diblock copolymer (as physically crosslinked network) was extracted by extensive washing leaving behind the highly porous stable ALG scaffold. This is basically a proof of concept study, which shows that POx based thermoresponsive polymer have the great potential to be used as fugitive support material to improve the pritibility of various poorly printable polymers like collagen, hyaluronic acid, Gelatin meth-acryloyl (GelMa) etc.

Biofabrication

PAPER

A thermogelling organic-inorganic hybrid hydrogel with excellent printability, shape fidelity and cytocompatibility for 3D bioprinting

Chen Hu[1], Taufiq Ahmad[2], Malik Salman Haider[1], Lukas Hahn[1], Philipp Stahlhut[2], Jürgen Groll[2] and Robert Luxenhofer[4,1,3]

Published 24 January 2022 • © 2022 IOP Publishing Ltd

Biofabrication, Volume 14, Number 2

Citation Chen Hu *et al* 2022 *Biofabrication* **14** 025005

Abstract: The development of 3D bioprinting technology highly depends upon the availability of suitable bioinks and biomaterial inks. In this study, an advanced hybrid hydrogel ink was developed, based on a poly(2-oxazoline)s/poly(2-oxazine)s diblock copolymer, alginate and clay i.e. Laponite XLG. The reversible thermogelling and shear thinning properties of the poly(2-oxazoline)-based diblock copolymer, acting as a fugitive material, facilitated the cell-laden extrusion based bioprinting process with high printability, shape fidelity and cell viability. Various three-dimensional constructs, including suspended filaments, were printed successfully with high shape fidelity and excellent stackability. Subsequent ionic crosslinking of alginate, fixates the printed scaffolds which exhibit good mechanical stability, flexibility and structural integrity after extracting the fugitive print-support from the hydrogels by exhaustive washing. Finally, cell-laden printing and culture over 5 days demonstrated the cytocompatibility and feasibility of the novel hybrid hydrogels for 3D bioprinting. We believe that the developed material could be interesting for a wide range of bioprinting applications including tissue engineering and drug delivery, potentially enabling also other biological bioinks such as collagen, hyaluronic acid, decellularized extracellular matrix or cellulose based bioinks.

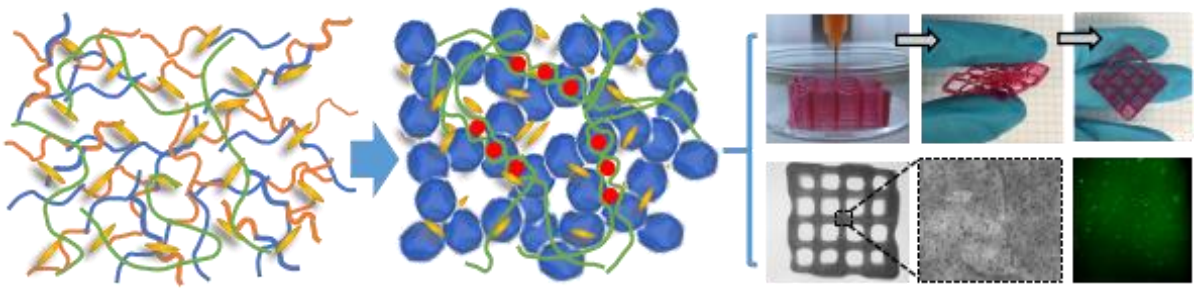

4.7.2 POx/POzi based Highly Stretchable and 3D Printable Hydrogel

Summary: In this work, a 3D printable and highly stretchable ternary hydrogel was developed which was composed of POx based diblock copolymer i.e. pMeOx-pPrOzi, poly(N, N-dimethylacrylamide) (PDMAA) and laponite XLG (clay). While exploring the applicability of POx based diblock copolymer in different domain of pharmaceutical and biomedical applications, the major aim of the study was also to improve the printability of PDMAA. The POx based diblock copolymer with its thermoresponsive and highly shear thinning character, helped in printing of constructs, while the added laponite improved both printability and mechanical properties. Prior to crosslinking of PDMAA by free radical polymerization, the POx based diblock copolymer maintained its thermoresponisve behaviour, once crosslinked, the resultant constructs showed excellent mechanical properties with high stretch ability. In contrast to ALG based hydrogel scaffold, the results confirmed that after extensive extraction and washing, the considerable amount of POx based diblock copolymer retained inside the cross-linked constructs. The possible reasons for this retention need further investigations as POx based diblock copolymer is physically crosslinked netework and generally should be extracted out during washing or extraction process (as we have observed I the case of ALG hydrogels). Such hydrogels are interesting for wide range of applications in tissue engineering, drug delivery and additive manufacturing etc.

Journal of Materials Chemistry B

ROYAL SOCIETY OF CHEMISTRY

PAPER

View Article Online
View Journal | View Issue

Check for updates

Cite this: J. Mater. Chem. B, 2021, 9, 4535

Development of a 3D printable and highly stretchable ternary organic–inorganic nanocomposite hydrogel†

Chen Hu,[a] Malik Salman Haider,[a] Lukas Hahn,[a] Mengshi Yang[a] and Robert Luxenhofer *[ab]

Abstract:

Hydrogels that can be processed with additive manufacturing techniques and concomitantly possess favorable mechanical properties are interesting for many advanced applications. However, the development of novel ink materials with high intrinsic 3D printing performance has been proven to be a major challenge. Herein, a novel 3D printable organic–inorganic hybrid hydrogel is developed from three components, and characterized in detail in terms of rheological properties, swelling behavior and composition. The nanocomposite hydrogel combines a thermoresponsive hydrogel with clay LAPONITEs XLG and in situ polymerized poly(N,N-dimethylacrylamide). Before in situ polymerization, the thermogelling and shear thinning properties of the thermoresponsive hydrogel provides a system well-suited for extrusion-based 3D printing. After chemical curing of the 3D-printed constructs by free radical polymerization, the resulting interpenetrating polymer network hydrogel shows excellent mechanical strength with a high stretchability to a tensile strain at break exceeding 550%. Integrating with the advanced 3D-printing technique, the introduced material could be interesting for a wide range of applications including tissue engineering, drug delivery, soft robotics and additive manufacturing in general.

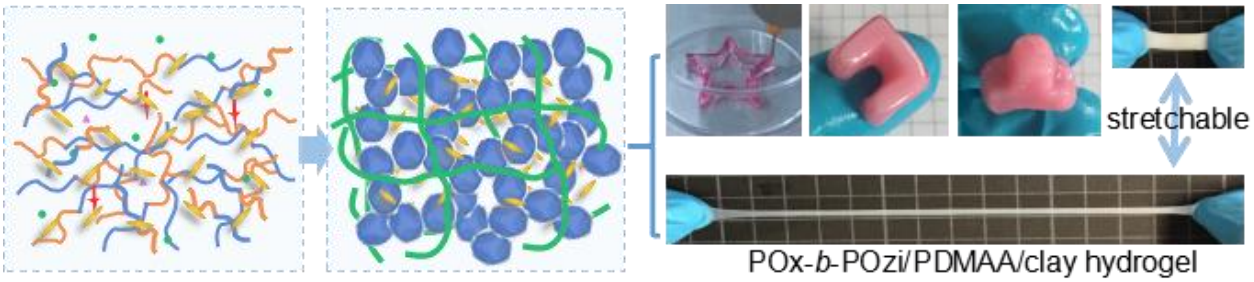

4.7.3 POx/POzi based Novel thermoresponsive Hydrogels and Structure Property Relationship

Summary: After exploring the few possible applications of pMeOx-pPrOzi based diblock copolymer and after unraveling the fact that hydrophilic block play a very important role in self-assembly and drug loading of the micelles, we further extended our investigations (related to hydrophilic block) in the field of hydrogels as well. As discussed previously, we already have a well established POx/POzi based hydrogel (pMeOx-pPrOzi) platform which has been extensively investigated. In order to investigate the impact of hydrophilic block in this hydrogel, we synthesized a novel thermo-sensitive AB diblock copolymer in which hydrophilic pMeOx was replaced with another hydrophilic POx i.e. pEtOx. The resultant polymer was capable to form optically transparent hydrogel at room temperature while in ice bath, transforms to low viscosity liquid. The novel hydrogel was thoroughly characterized for rheology (gelation temperature, yield stress, shear-thinning and structure recovery etc.) as this can directly impact the extrusion based 3D (bio) printing. The hydrogels were further visualized with SEM and cryo-SEM. Various 2D and 3D scaffolds were printed with good shape fidelity and high stackability. The sharp filament corners and intersections in the grid were all well resolved. Various biological experiments were also performed with human adipose derived stem cells laden hydrogels. This hydrogel can potentially be used as hydrogel-bioink, injectable hydrogels or fugitive support material. In the later section, we will learn how changing the hydrophilic block from pMeOx to pEtOx affected the rheology and printability of the resultant diblock copolymer.

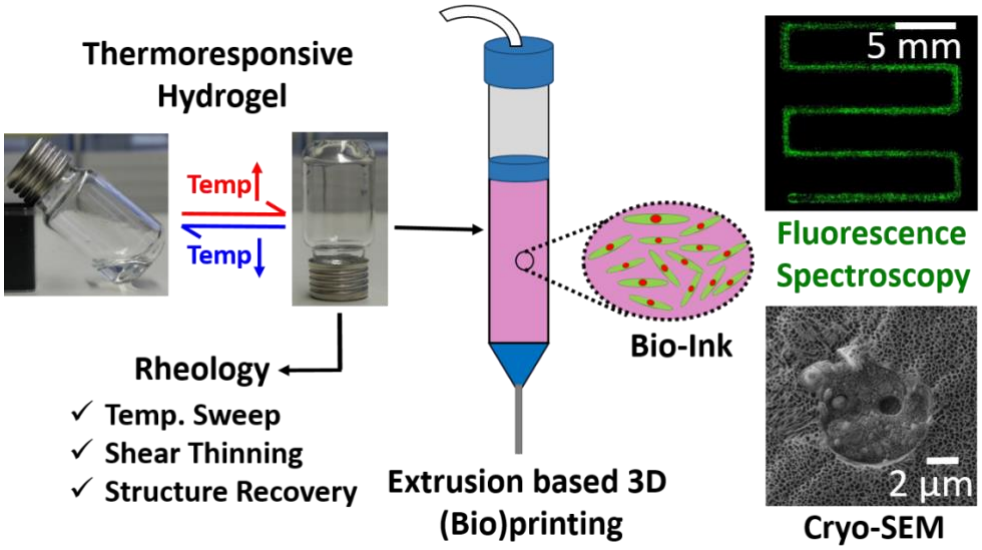

gels

MDPI

Article

Tuning the Thermogelation and Rheology of Poly(2-Oxazoline)/Poly(2-Oxazine)s Based Thermosensitive Hydrogels for 3D Bioprinting

Malik Salman Haider [1,*], Taufiq Ahmad [2], Mengshi Yang [1], Chen Hu [1], Lukas Hahn [1], Philipp Stahlhut [2], Jürgen Groll [2] and Robert Luxenhofer [1,3,*]

[1] Functional Polymer Materials, Chair for Advanced Materials Synthesis, Institute for Functional Materials and Biofabrication, Department of Chemistry and Pharmacy, Julius-Maximilians-University Würzburg, Röntgenring 11, 97070 Würzburg, Germany; mengshi.yang@uni-wuerzburg.de (M.Y.); chen.hu@uni-wuerzburg.de (C.H.); lukas.hahn@uni-wuerzburg.de (L.H.)

[2] Department of Functional Materials in Medicine and Dentistry, Institute for Functional Materials and Biofabrication and Bavarian Polymer Institute, Julius-Maximilians-University Würzburg, Pleicherwall 2, 97070 Würzburg, Germany; taufiq.ahmad@fmz.uni-wuerzburg.de (T.A.); philipp.stahlhut@fmz.uni-wuerzburg.de (P.S.); juergen.groll@fmz.uni-wuerzburg.de (J.G.)

[3] Soft Matter Chemistry, Department of Chemistry and Helsinki Institute of Sustainability Science, Faculty of Science, University of Helsinki, PB 55, 00014 Helsinki, Finland

* Correspondence: malik.haider@uni-wuerzburg.de (M.S.H.); robert.luxenhofer@helsinki.fi (R.L.)

Abstract: As one kind of "smart" material, thermogelling polymers find applications in biofabrication, drug delivery and regenerative medicine. In this work, we report a thermosensitive poly(2-oxazoline)/poly(2-oxazine) based diblock copolymer comprising thermosensitive/moderately hydrophobic poly(2-*N*-propyl-2-oxazine) (pPrOzi) and thermosensitive/moderately hydrophilic poly(2-ethyl-2-oxazoline) (pEtOx). Hydrogels were only formed when block length exceeded certain length (≈100 repeat units). The tube inversion and rheological tests showed that the material has then a reversible sol-gel transition above 25 wt.% concentration. Rheological tests further revealed a gel strength around 3 kPa, high shear thinning property and rapid shear recovery after stress, which are highly desirable properties for extrusion based three-dimensional (3D) (bio) printing. Attributed to the rheology profile, well resolved printability and high stackability (with added laponite) was also possible. (Cryo) scanning electron microscopy exhibited a highly porous, interconnected, 3D network. The sol-state at lower temperatures (in ice bath) facilitated the homogeneous distribution of (fluorescently labelled) human adipose derived stem cells (hADSCs) in the hydrogel matrix. Post-printing live/dead assays revealed that the hADSCs encapsulated within the hydrogel remained viable (≈97%). This thermoreversible and (bio) printable hydrogel demonstrated promising properties for use in tissue engineering applications.

Keywords: poly(2-ethyl-2-oxazoline); shear thinning; shape fidelity; cyto-compatibility; bio-printability

Citation: Haider, M.S.; Ahmad, T.; Yang, M.; Hu, C.; Hahn, L.; Stahlhut, P.; Groll, J.; Luxenhofer, R. Tuning the Thermogelation and Rheology of Poly(2-Oxazoline)/Poly(2-Oxazine)s Based Thermosensitive Hydrogels for 3D Bioprinting. *Gels* **2021**, *7*, 78. https://doi.org/10.3390/gels7030078

Academic Editor: Michael T. Cook

Received: 26 April 2021
Accepted: 15 June 2021
Published: 24 June 2021

1. Introduction

Recent innovations in biomaterials have had a huge impact on all aspects of tissue engineering, regenerative medicine and drug delivery, resulting in development of "smart" biomaterials (responsive to external stimuli, e.g., temperature, pH, light etc.) [1,2]. Because of rapidly growing interests in precision medicine, emergence of gene/immune therapies and advancements in three-dimensional (3D) (bio) printing, there is an increasing demand for smart biomaterials.

A thermogel is a stimuli-responsive "smart" material which responds to change in temperature, above or below the critical temperature by a (typically reversible) sol-gel transition. The gelation process is typically due to the development of supramolecular structures yielding 3D, physically crosslinked networks because of hydrogen bonding,

coulomb or hydrophobic interactions often in combination with simple entanglement [3]. In the majority of cases, the transition takes place upon increase in temperature [4] but inverse gelation has also been observed [5–7]. These are highly versatile materials and repetitively proposed for multiple applications in biomedical, pharmaceutical and food industry. Apart from thermogelling natural polymers [8], few synthetic polymers also exhibit this behaviour [9]. In this context, poly(*N*-isopropylacrylamide) [10,11] and few members of Pluronics® family (also known as poloxamers) (ABA triblock copolymer where A is hydrophilic poly(ethylene glycol) (PEG) and B is thermoresponsive/hydrophobic poly(propylene glycol) (PPG)) [12] are most frequently discussed. Several studies have presented PEG as highly cytocompatible [13]. Furthermore, few members of the PEG family have been approved by US Food and Drug Administration as sealants [14,15]. However, the limited biodegradability [16–18] and more recently emerging, PEG immunogenicity [19] has remained the associated issues. A very interesting multiblock terpolymer from PEG, PPG and poly(ε-caprolactone) has been recently investigated for its utilization as a vitreous substitute [20].

Polymers of cyclic imino ethers, particularly poly(2-oxazoline)s (POx) and poly(2-oxazine)s (POzi) [21] with a thermoresponsive profile [22,23] have attained significant attention in the past decade [23,24]. POx has shown huge potential in tissue engineering [25–29], drug delivery [30–35] and 3D (bio) printing [24,36]. They are structural isomers of polypeptides, are synthetically relatively easily accessed and are highly tunable in their physico-chemical characteristics [37]. POx with fewer than four carbons in their side chain are water soluble. Regardless of temperature, poly(2-methyl-2-oxazoline) (pMeOx) is soluble in water while poly(2-ethyl-2-oxazoline) (pEtOx), poly(2-propyl-2-oxazoline) (pPrOx), poly(2-isopropyl-2-oxazoline) (p*i*PrOx) and poly(2-cyclopropyl-2-oxazoline) (p*c*PrOx) exhibit lower critical solution temperature (LCST) type behaviour and temperature dependent aqueous solubility [38,39]. Among these, pMeOx and pEtOx have been studied thoroughly as highly hydrophilic polymers which is discussed as one potential alternative to PEG, because of non-toxic and non-immunogenic nature, low unspecific organ uptake and rapid clearance (at right size) [25,40–42]. Utilizing the light scattering technique, Grube et al. explored the solution properties of POx in comparison to PEG, and reported that both pMeOx and pEtOx with same molar mass (as PEG) were less solvated and more compact in shape. These results further suggested that on basis of absolute physico-chemical properties, POx are an interesting alternative to PEG [43]. In various attempts to control the protein adsorption and cell adhesion on the biomaterials, the POx particularly pMeOx, pEtOx and pMeOzi (poly(2-methyl-2-oxazine)) showed better performance than PEG [44–46].

A plethora of studies show the utilization of pMeOx and pEtOx as hydrophilic polymer for the development of hydrogels [28,47–49], electrospun fibres [50], polymer brushes [51], nanoparticles [52], micelles for drug delivery [53–57] and for melt electrowriting [58,59]. Bloksma et al. also investigated the thermoresponsive behaviour of few POzi based homopolymers [22]. Interestingly though, there are few reports that solely address the thermogelation of pure POx/POzi based systems. Inspired by the Pluronics family, Zahoranova et al. studied various ABA and BAB triblock copolymers based on pMeOx (A) and pPrOx (B) but no thermogelation could be observed up-to 30 wt.% concentration at the investigated temperature range of 10 to 50 °C [60]. More recently, Lübtow et al. reported on the development of ABA triblock copolymer comprised of pMeOx (A) and poly(2-iso-butyl-2-oxazoline) (p*i*BuOx) (B) which form thermogels at 20 wt.% but its rheological characteristics, in particular its low yield stress were not conducive for extrusion-based 3D printing [48]. In addition, Hahn et al. reported on several ABA POx/POzi-based triblock copolymers exhibiting inverse gelation [6,61].

While both pMeOx and pEtOx (and more recently pMeOzi) are routinely considered as potential alternative to PEG or other hydrophilic polymers, these two polymers have shown distinct physico-chemical solution properties. Recently, we have observed that by replacing pMeOx with pEtOx as hydrophilic block (A) can dramatically reduce the drug loading efficiency of ABA type POx/POzi based triblock copolymer micelles [55]. Previ-

ously, we synthesized POx/POzi based thermogelling bio-ink composed of pMeOx (no LCST) as A and thermoresponsive poly(2-propyl-2-oxazine) (pPrOzi) (LCST ≈ 12 °C) [59] as B (pPrOzi-*b*-pMeOx). The aqueous solution of pPrOzi-*b*-pMeOx hydrogel exhibited reversible thermogelation above 20 wt.% concentration. This hydrogel proved to be cytocompatible and (bio) printable [47,62]. Here, we replaced pMeOx with pEtOx in this type of block copolymer and investigated how the rheological and thermogelling properties of the resultant diblock copolymer (pPrOzi-*b*-pEtOx) are affected. The morphology, cytocompatibility and (bio) printability of the hydrogel were further evaluated.

2. Results and Discussion

2.1. Synthesis, Characterization and Rheology

To date, few reports investigated the thermogelation of pure POx or POx/POzi based systems [6,47,48,60,63]. Very recently, Monnery and Hoogenboom reported a POx based BAB triblock copolymer with the degree of polymerization (DP) ranging from 50–100 and up to 1000 repeats units for pPrOx and pEtOx (B and A, respectively), with reversible thermal gelation. Hydrogel formation (above 20 wt.%) was only observed when the pEtOx had extremely high DP (i.e., $pPrOx_{100}$-*b*-$pEtOx_{700}$-*b*-$pPrOx_{100}$) [63], in contrast for pPrOzi-*b*-pMeOx diblock, the gelation was observed at much lower DP (i.e., $pPrOzi_{50}$-*b*-$pMeOx_{50}$) [47]. It was further confirmed that the fine tuning of cloud point temperature (T_{cp}) with respect to the block length is necessary for the development of thermoresponsive hydrogels [63]. Investigating the impact of polymer concentration on T_{cp} of various AB diblock copolymers, A being EtOx while switching the B to poly(2-heptyl-2-oxazoline) (HepOx), poly(2-butyl-2-oxazoline) (BuOx) or *i*PrOx, Hijazi et al. suggested that the copolymer with lower differences in their hydrophobicity might be best suited for development of thermoswitchable hydrogels [64,65].

In this regard, we have synthesized a thermoresponsive diblock copolymer which is based on thermosensitive pEtOx as hydrophilic (A) and pPrOzi more hydrophobic, yet still thermoresponsive block (B), respectively. It should be noted, as both pMeOx and pEtOx are highly water-soluble and well-known stealth-polymers, we were interested in investigating how the thermogelling/rheological properties and printibility of AB diblock copolymer would be affected when exchanging pMeOx with pEtOx.

Initially, we synthesized pPrOzi-*b*-pEtOx diblock copolymer with the DP = 50 for each block (i.e., $pPrOzi_{50}$-*b*-$pEtOx_{50}$). The polymer was analysed by ^{1}H-NMR, GPC and DSC. The ^{1}H-NMR spectra were in good agreement with targeted block lengths for individual blocks (Figure 1a) with a dispersity Đ ≈ 1.3. DSC thermogram showed a single distinct glass transition (T_g) at 23 °C suggesting that no (micro)phase separation (Figure 1b) occurred in the solid. Previously, we had observed the similar behaviour for the POx/POzi based ABA triblock copolymers [66]. Tube inversion test is the simplest test to see if a self-supporting hydrogel is formed or not. This was performed with 25 and 30 wt.% $pPrOzi_{50}$-*b*-$pEtOx_{50}$ solution by keeping at room temperature and 37 °C (to simulate the body temperature) (Figure 1c). Both polymer solutions appeared as highly viscous liquids and no macroscopic gel was observed in vials as the material flowed under its own weight.

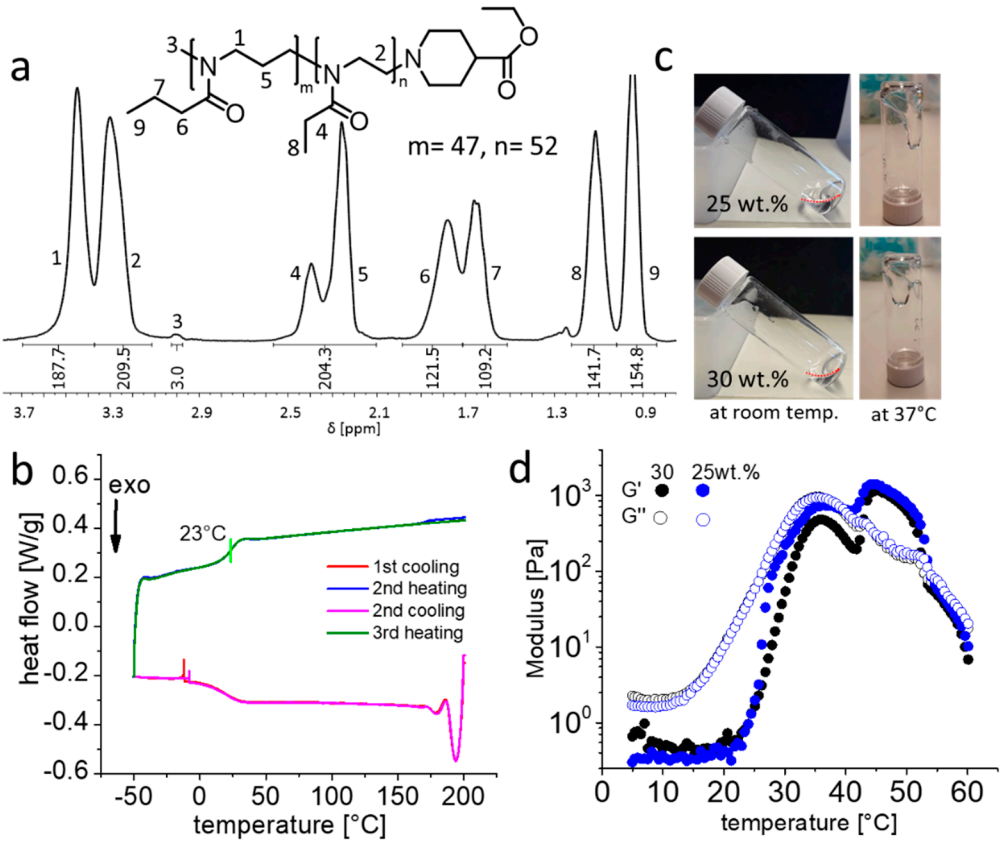

Figure 1. (**a**) Chemical structure and ^{1}H-NMR spectra ($CDCl_3$, 300 MHz, 298K) of $pPrOzi_{50}$-*b*-$pEtOx_{50}$ with the signal assignment of all major peaks. (**b**) Heat flow during several heating and cooling cycles (10 K/min) of differential scanning calorimetry, green vertical line indicating the glass transition point. (**c**) Visual appearance of the 25 and 30 wt.% polymer solution at room temperature and 37 °C, the red dotted lines are showing the liquid meniscus. (**d**) Temperature dependent rheology from 5 to 60 °C (at heating rate of 0.05 °C/s) of the 25 and 30 wt.% block copolymer solution with storage modulus (G′) and loss modulus (G″).

Whether the gel is formed or not was further studied by temperature dependent rheological measurements of 25 and 30 wt.% $pPrOzi_{50}$-*b*-$pEtOx_{50}$ polymer solution. Initially, dynamic oscillation temperature sweeps from 5 °C to 60 °C were carried out (Figure 1d). The gel point is usually defined as the crossover point of storage modulus (G′) and loss modulus (G″) and corresponding temperature as gel temperature (T_{gel}). No gelation was observed in the temperature range of 5 °C to 37 °C. However, for both concentrations rapid increase in G′ and G″ was observed at 23 °C and 12 °C, respectively. The increase in G″ at 12 °C can be correlated to the T_{cp} of the pPrOzi block [22]. Additionally, at slightly higher temperatures, a T_{gel} was eventually observed at 39 °C and 42 °C for 25 and 30 wt.% polymer solution, respectively. However, the resulting gel was not very stable as G′ and G″ start to decrease and the gel liquefied again at around 52 °C. In comparison, a 20 wt.% solution of $pPrOzi_{50}$-*b*-$pMeOx_{50}$ exhibited a sharp sol-gel transition and a G′ value of 4 kPa (at 27 °C) indicating the formation of relatively stiffer gel [47].

As previously discussed, the length of each block in block copolymers can significantly impact the gelation behaviour [63–65]. Accordingly, we synthesized a new diblock copolymer with chain length of hundred repeat units for each block, i.e., $pPrOzi_{100}$-*b*-$pEtOx_{100}$. The ^{1}H-NMR spectra showed the desired block length (≈100) (Figure 2a) with dispersity Đ ≈ 1.4.

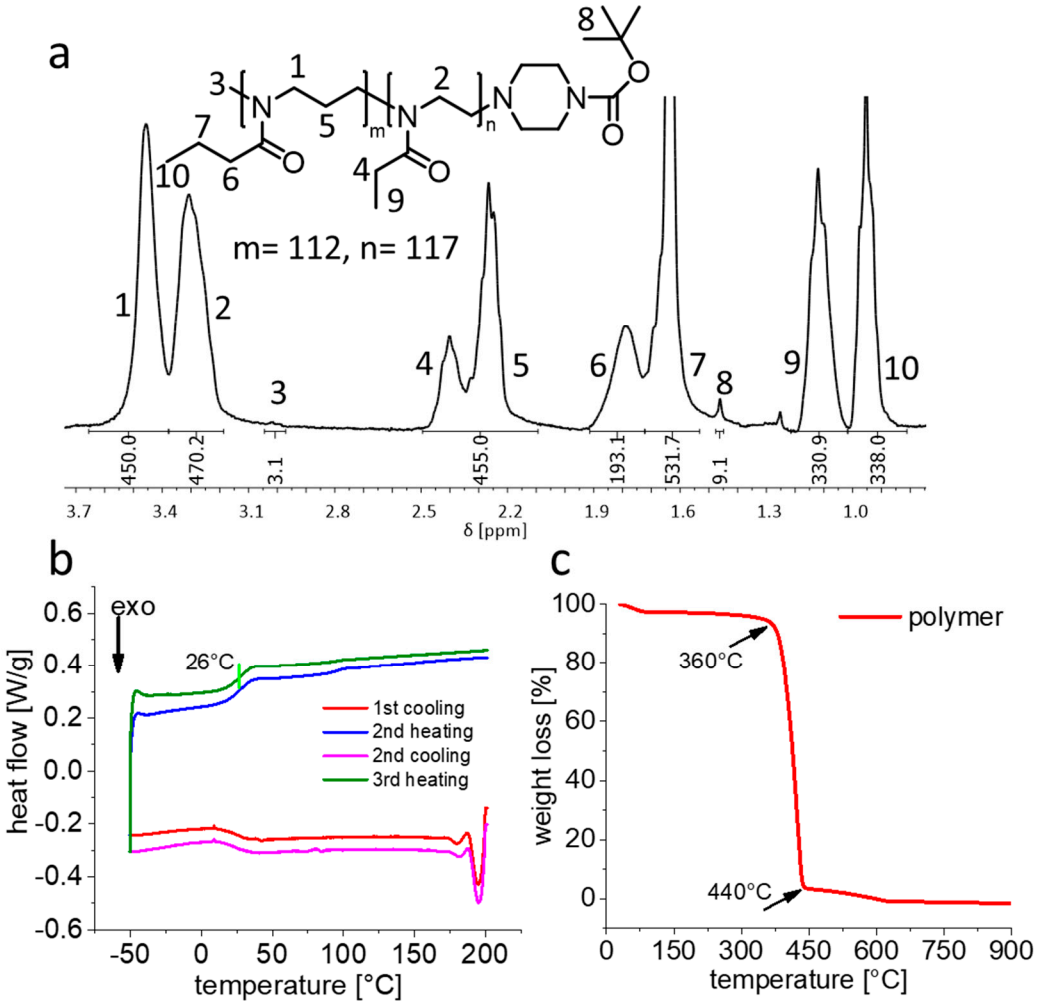

Figure 2. (**a**) Chemical structure and ^{1}H-NMR spectra ($CDCl_3$, 300 MHz, 298 K) of pPrOzi$_{100}$-*b*-pEtOx$_{100}$ with the signal assignment of all major peaks. (**b**) Heat flow occurring during the several consecutive heating and cooling cycle (10 K/min) of differential scanning calorimetry, green vertical line indicating the glass transition point. (**c**) Weight loss occurring during thermogravimetric analysis of pPrOzi$_{100}$-*b*-pEtOx$_{100}$. Samples were heated from 30 to 900 °C at the heating rate of 10 K/min.

Previously, for the diblock copolymer pPrOzi$_{100}$-*b*-pMeOx$_{100}$, we had observed two T_g values, corresponding to the T_g values of the two homopolymers (pPrOzi ≈ 10 °C and pMeOx ≈ 77 °C) suggesting immiscibility and microphase separation of two individual blocks (Figure S1) [47,67]. In contrast, the DSC thermogram of pPrOzi$_{100}$-*b*-pEtOx$_{100}$ showed only a single T_g at ≈ 26 °C (slightly higher in comparison to pPrOzi$_{50}$-*b*-pEtOx$_{50}$ T_g ≈ 23 °C) suggesting that again no microphase separation (Figure 2b) occurred in the solid. This finding is particularly interesting as Hoogenboom recently reported that pEtOx and pPrOx homopolymers show immiscibility when the molar mass exceeded 10 kg/mol (i.e., DP ≈ 100) [68]. One might have expected that pEtOx and pPrOzi would be less miscible than pEtOx and pPrOx, but in the present case we have block copolymers at hand, while Hoogenboom and co-workers studied homopolymer blends, which can be expected to phase separate more readily. Thermogravimetric analysis (TGA) showed the commonly known good thermal stability of POx and POzi with major losses occurring ≥360 °C (Figure 2c).

After successful synthesis and characterization, the visual appearance of the aqueous solutions of pPrOzi$_{100}$-*b*-pEtOx$_{100}$ at various concentrations (1, 10, 15, 20, 25 and 30 wt.%) was noted. Up to 15 wt.%, all solutions were turbid at room temperature indicating the presence of mesoglobules or larger self-assemblies responsible for light scattering

(Figure 3a; 1st row). For the homologue pPrOzi$_{100}$-*b*-pMeOx$_{100}$ diblock, dynamic and static light scattering suggested the formation of polymersomes [69] while, for pPrOzi$_{100}$-*b*-pEtOx$_{100}$ diblock, at this point, we can only speculate the presence of similar assemblies. In contrast, in ice cold water, all the samples were optically transparent. This can be attributed to the T_{cp} of pPrOzi block (13 °C as homopolymer) [22]. Similar observations were made for pPrOzi-*b*-pMeOx based diblock copolymer (turbid below 10 wt.%) [47]. Above 15 wt.% all the tested concentrations were optically clear, at 20 wt.% the solution appeared as highly viscous yet flowable liquid. Self supporting, optically clear hydrogels were observed at 25 and 30 wt.% polymer solution at room temperature (Figure 3a; 2nd row).

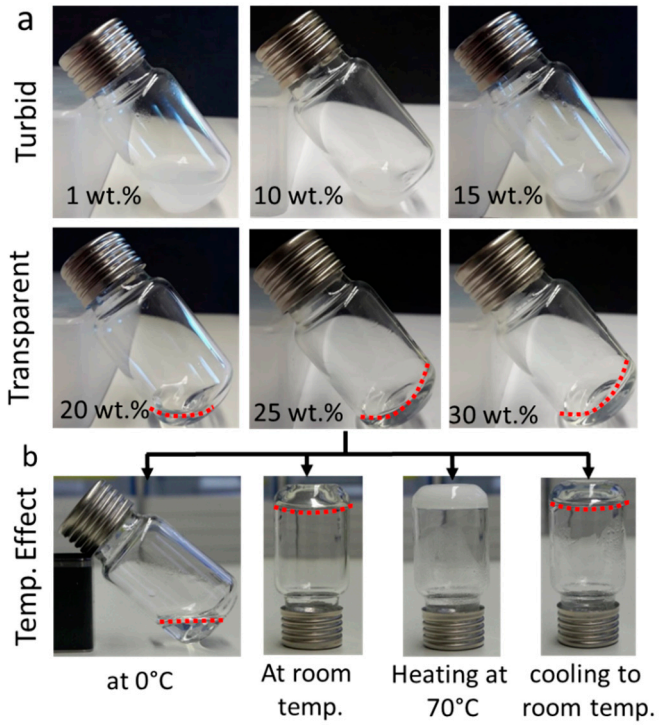

Figure 3. (**a**) Visual appearance of aqueous pPrOzi$_{100}$-*b*-pEtOx$_{100}$ diblock polymer solutions (1 to 30 wt.%) at room temperature. (**b**) Visual appearance of 25 wt.% polymer solution at different temperatures. Dotted red lines are added for better visibility of colourless liquid or hydrogel meniscus.

In contrast to pMeOx, pEtOx also exhibits thermoresponsive solubility behavior in water. Lin and colleagues reported T_{cp} values in water ranging between 61–69 °C, which were highly dependent on molar mass and concentration [70]. According to Hoogenboom, Schubert and colleagues, pEtOx homopolymers with degree of polymerization less than hundred do not exhibit T_{cp} (below 100 °C) but a chain length dependent decrease in T_{cp} (94 to 66 °C) was observed when chain length is greater than hundred [37,71]. Accordingly, upon heating the (25 wt.%) pPrOzi$_{100}$-*b*-pEtOx$_{100}$ hydrogel to 70 °C, it immediately turned opaque which was reversed upon cooling (Figure 3b). Throughout heating and cooling, the gel character was maintained, i.e., no syneresis was observed. This opacity can be correlated to the T_{cp} and dehydration of pEtOx at this temperature. It can be expected that the T_{cp} of pEtOx is lower in the block copolymer compared to the homopolymer [72].

Rheological properties of solutions of 15 wt.% to 30 wt.% were investigated in dependence of temperature (5 to 60 °C). After gelation, G' reached a plateau at values of 3 (at 30 °C) and 1.5 kPa (at 25 °C) for 30 and 25 wt.% polymer solution, respectively (Figure 4a). While many other thermogelling polymers solutions from literature are weaker ($G' < 1$ kPa) [73,74], the homologue 20 wt.% pPrOzi$_{50}$-*b*-pMeOx$_{50}$ based hydrogel is in fact somewhat stronger ($G' \approx 4$ kPa) [47]. The loss factor ($\tan \delta = G''/G'$) informs on the ratio

of elastic vs. viscous property of the material (tan δ < 1, more elastic and tan δ > 1, more viscous). At both concentrations (30 and 25 wt.%), rather low tan δ values of ≈ 0.07 and 0.16, respectively, were obtained. Accordingly, once formed, the pEtOx based hydrogels show a slightly higher elastic character compared to those bearing a pMeOx hydrophilic block (tan δ ≈ 0.2) [47].

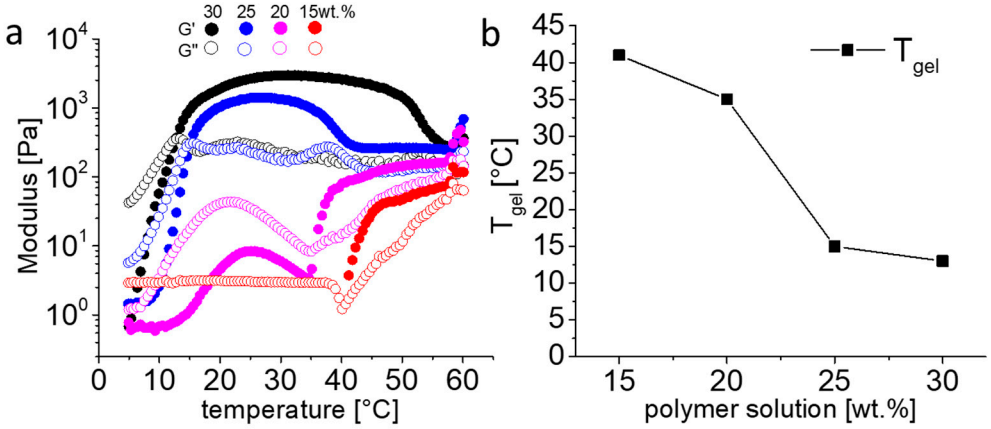

Figure 4. (**a**) Temperature dependent rheology from 5 to 60 °C of the 15, 20, 25 and 30 wt.% diblock copolymer solution with storage modulus (G′) and loss modulus (G″). (**b**) Graphical representation of the reduction in gelation temperature (T_{gel}) with the increasing polymer concentration (in wt.%). Lines between data points are guide for the eyes only.

The crossover point for G′ and G″ was also observed for 20 and 15 wt.% polymer solution at 35 and 41 °C, respectively. However, the resultant gel at such concentration was very weak (G′ < 0.2 kPa). The G′ value of the 15 wt.% polymer solution registered as zero until 40 °C but increased rapidly above this temperature. Overall, the temperature sweep (5 to 60 °C) showed an inverse relationship between T_{gel} and polymer concentration, i.e., for 30, 25, 20 and 15 wt.% polymer solutions, the obtained T_{gel} was 13, 15, 35 and 41 °C (Figure 4b). In case of pPrOzi-*b*-pEtOx, increasing DP from 50 to 100 resulted in a stable hydrogel, while in case of pPrOzi-*b*-pMeOx based hydrogels, without a significant change in G′ values, the T_{gel} was decreased from 27 to 17 °C, respectively [47].

To assess the linear viscoelastic (LVE) region (stable values for G′ and G″), an amplitude sweep was conducted with constant angular frequency of 10 rad/s and increasing amplitude of 0.01 to 500% (Figure 5a). Within the LVE range, this test confirmed the occurrence of only elastic rather than plastic deformations (which can lead to damage of sample). With G′ > G″ for 30 and 25 wt.% polymer samples, the viscoelastic solid character of the material is confirmed. The sharp drop in G′ indicate a brittle fracturing behaviour. Before this occurs, the G″ increases before reaching a peak maximum, after which the curve again dropped. The common interpretation of the rise in G″ in zone 1 (exemplified with 30 wt.% polymer solution, black dashed lines) is the occurrence of micro-cracks while the overall structural integrity is maintained as G′ remains constant and dominant over G″ (Figure 5a) [75,76]. However, for the present materials, one might rather assume that small domains start to liquefy under the increasing stress, increasing the loss modulus but retaining the storage modulus until further breakdown of the network. With further increasing amplitude (zone 2) individual domains grew further and connect, resulting in the flow of entire material (G″ > G′: fluid state). The 20 wt.% solution showed minor differences in G′ and G″ values but at very low amplitude sweep, a crossover point was observed which is indicative of fluid state, while G″> G′, in case of 15 wt.% confirmed the free-flowing liquid (Figure S2a). The yield stress (or linearity limit) is defined as the value of shear stress at the limit of LVE region, while flow point is represented as the value of shear stress at the crossover point of G′ and G″ (where, G′ = G″) [77]. In the region between yield stress and flow point where G′ is still greater than G″, the material has already lost the initial structural strength but still displays the properties of solid material. Further

increase in shear stress (above flow point) eventually leads to a flow of material (G″ > G′). In (bio) printing, these are crucial factors which are usually correlated to the collapse and shape fidelity of structures being printed [78,79]. The yield stress and flow point values of 30 and 25 wt.% pPrOzi$_{100}$-*b*-pEtOx$_{100}$ hydrogels were extracted from amplitude sweep measurements (Figure 5b). Increasing the polymer concentration from 25 to 30 wt.% led to an increase in yield stress (from 110 to 310 Pa) and flow point values (from 160 to 520 Pa), respectively. A frequency sweep revealed little frequency dependency in the investigated range (0.1–100 rad/s) within the LVE range and 0.1% strain. Only at lowest frequencies and 25 wt.%, the tan δ approached unity (Figure 5c).

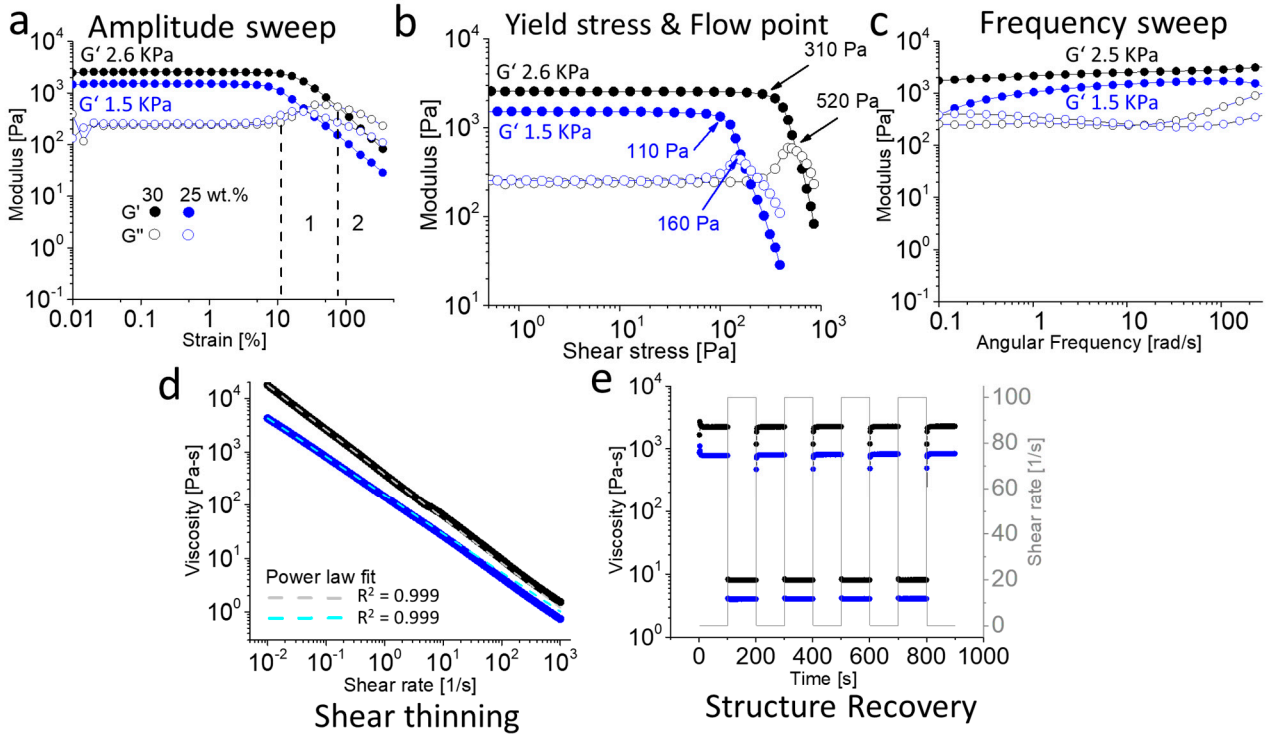

Figure 5. (**a**) Amplitude sweep at an angular frequency of 10 rad/s, zone 1 and 2 (exemplified only for 30 wt.%) indicating the hydrogel's gradual transition from solid to liquid state under applied strain. (**b**) Yield and flow point values obtained from amplitude sweep (**c**) Frequency sweep at an applied strain of 0.1%. (**d**) Viscosity depending on the applied shear rate at 25 °C representing the shear thinning behaviour including power law fit (dashed lines). (**e**) Structure recovery property under alternative applied shear rate of 0.1 and 100/s. All of the experiments were performed for 25 (blue) and 30 wt.% (black) pPrOzi$_{100}$-*b*-pEtOx$_{100}$ diblock polymer hydrogels.

When extrusion-based applications such as 3D (bio) printing and injectable drug depots are desired, shear thinning, and fast structure recovery are important factors to assess. For pPrOzi$_{100}$-*b*-pEtOx$_{100}$ hydrogels the viscosity decreased profoundly as shear rate increased (0.01 to 1000, 1/s) at both 30 and 25 wt.% (Figure 5d). The flow index *n* in the power-law expression described by Ostwald-de Waele ($n < 1$ indicate shear thinning) and consistency index K characterize the gels [80]. The presently studied materials can be clearly modeled using the power-law expression using very low flow and rather high consistency indices ($n \approx 0.16$ and 0.27, K ≈ 380 and 152, for 30 and 25 wt.% hydrogel, respectively) (Figure 5d; dashed lines). The structure recovery was investigated using a rotational approach with an angular frequency of 10 rad/s and temperature of 25 °C (Figure 5e). At first, a low amplitude strain regime of 0.1/s was applied for 100 s followed by higher amplitude strain of 100/s for 100 s (5 cycles). At both tested concentrations, a sharp decrease in viscosity at high shear rate was recovered instantly upon cessation of shear rate. Together, pronounced shear thinning and rapid recovery facilitate extrusion

through fine nozzles with shape fidelity after leaving the nozzle, which is relevant for 3D printing of bio-ink or for drug delivery applications.

2.2. SEM and Cryo-SEM Analysis

For tissue engineering applications, the printed scaffolds should provide a 3D environment with sufficient porosity to ensure nutrient and oxygen supply to the encapsulated cells. To obtain insights into the morphology and microarchitecture of hydrogels, initially, the images of the 30 wt.% pPrOzi$_{100}$-*b*-pEtOx$_{100}$ lyophilized gel were obtained by SEM. The lyophilized gel exhibited a highly porous, rather heterogeneously distributed network of capillary channel (Figure 6a) and the top view showed randomly distributed micropores, probably produced because of water sublimation (Figure S3). As currently discussed in scientific community, factors such as pore formation by water evaporation during lyophilization and/or ice crystal formation during slow freezing can strongly influence appearance of a freeze-dried hydrogels and might cause artifacts [81]. To elude such possibilities, the cryogenic SEM (cryo-SEM) was also conducted. During the sample preparation for cryo-SEM, the slush nitrogen provided the sufficient cooling rates resulting in faster cooling and reduction of crystallization artifacts. The cryo-SEM revealed that the intrinsic hydrogel morphology was preserved and pPrOzi$_{100}$-*b*-pEtOx$_{100}$ hydrogel exhibited highly homogenous, honeycomb-like porous structure in the sub-micrometer range (Figure 6b). Generally, the high porosity is significant for drug delivery and biomedical applications due to its capacity to facilitate drug loading and release, also offering void space for oxygen and nutrient transport for cell proliferation.

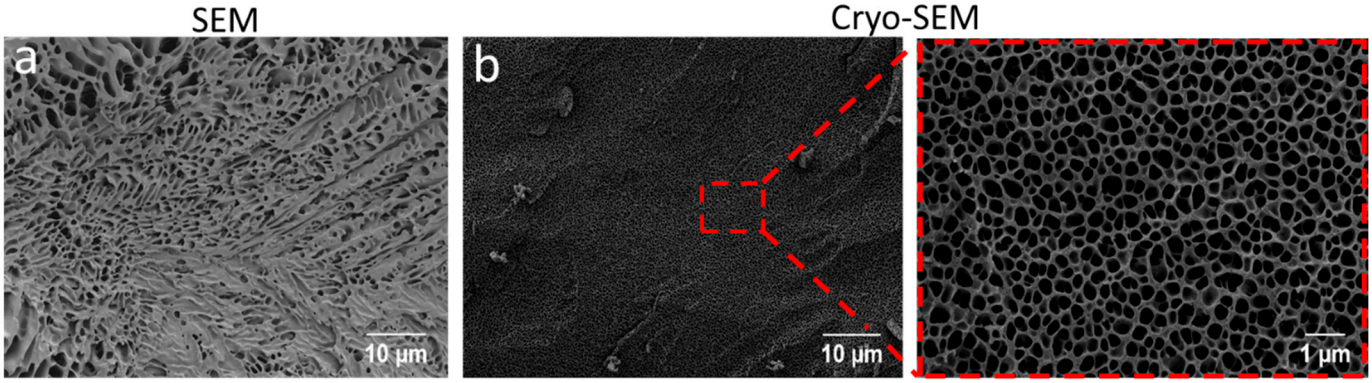

Figure 6. Visualization of the (**a**) morphology of 30 wt.% lyophilized hydrogel by scanning electron microscopy (SEM) and (**b**) freshly prepared hydrogel by cryo-SEM (acceleration voltage ETH: 2 kV).

2.3. 3D-Printing of Hydrogels

The printability of pPrOzi$_{100}$-*b*-pEtOx$_{100}$ based hydrogel was assessed using extrusion-based 3D printing. As this polymer formed hydrogel at/above 25 wt.%, the printing experiments were performed at 25 and 30 wt.% polymer concentrations. The filament fusion test was accomplished to assess the shape fidelity or print accuracy, strand fusion and undesired spreading of the printed construct. The shape fidelity or print accuracy can generally be defined as the degree of dimensional faithfulness of the printed object in comparison to computer aided design [82] and in the case of pPrOzi$_{100}$-*b*-pEtOx$_{100}$ based hydrogels, the assessment was accomplished only qualitatively, by visual inspection. A 2D pattern of one meandering filament with stepwise increasing strand distances from 0.5 to 0.75, 1, 1.25 and 1.5 mm was printed (Figure 7a). Even at the lowest distance (0.5 mm), the printed filament did fuse only at a few points but mainly remained separated, above this distance, the filaments were fully separated. To assess filament stability and sagging under its own weight when suspended, a filament collapse test was performed on a serrated mold with stepwise increasing gaps of 1, 2, 4, 8 and 16 mm. At 30 wt.% concentration, the suspended hydrogel filament strand did show some sagging but remained continuous

even at the longest distance of 16 mm (Figure 7b), while at 25 wt.% the filament collapsed in the case of the 16 mm gap.

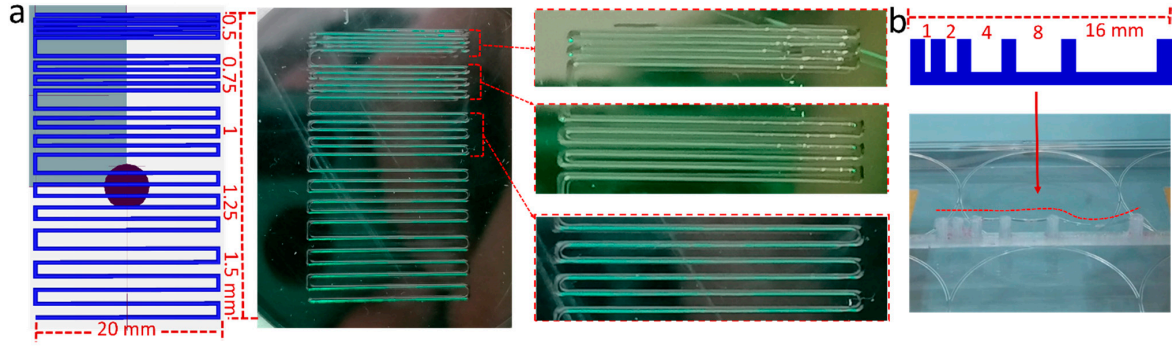

Figure 7. 3D-printibility assessment of $pPrOzi_{100}$-*b*-$pEtOx_{100}$ based hydrogel by (**a**) film fusion test (25 wt.%) by printing a stepwise increasing strand to strand distance of 0.5, 0.75, 1.0, 1.25, 1.5 mm (pressure; 80 kPa, speed; 2 mm/s) and (**b**) filament collapse test (30 wt.%) by using a serrated mold of increasing gap (pressure; 120 kPa, speed; 6 mm/s), red dashed line is added for eye guidance. The screen shots of the designed structures were directly taken from Repetier software during G-Code writing.

The printability and shape fidelity were further assured by printing various shapes such as a serpentine line pattern, five-pointed star and a 2-layered 5 × 5 strand grid (Figure 8a). The sharp filament corners (in serpentine such as line and star) and intersections in the grid were all well resolved. In the case of pPrOzi-*b*-pMeOx based diblock copolymer, Hu et al. showed that such kind of printability and shape fidelity was achieved by the addition of clay (Laponite XLG 1.2–2 wt.%) while the polymer alone exhibited a lower quality printing, albeit at 20 wt.% diblock concentration [67].

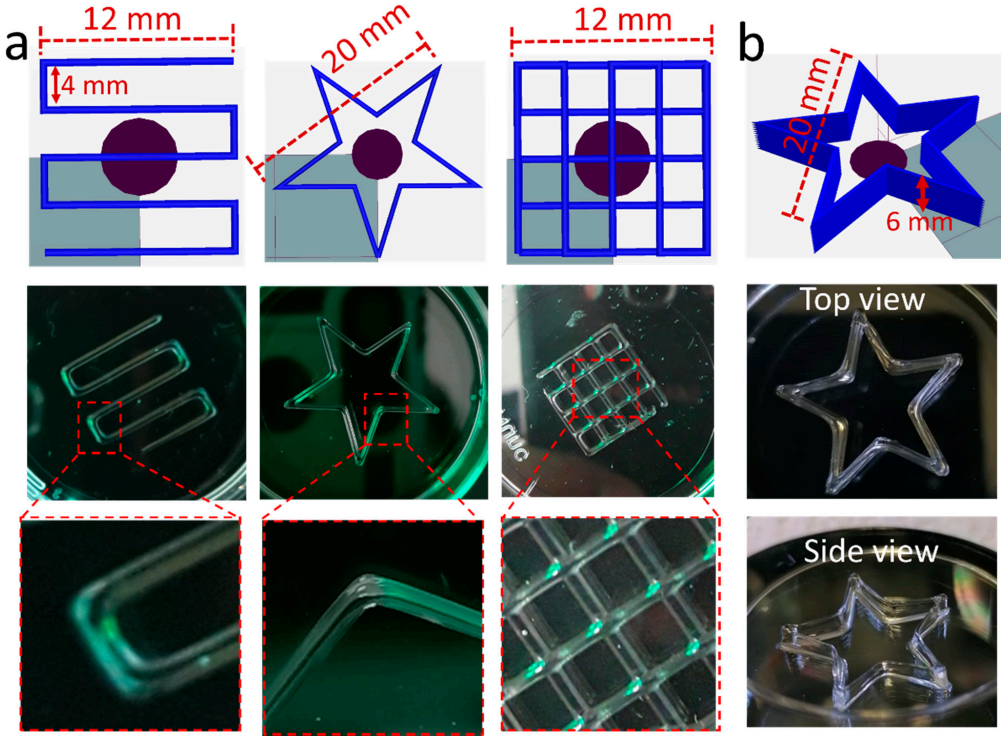

Figure 8. (**a**) 3D printability of 25 wt.% $pPrOzi_{100}$-*b*-$pEtOx_{100}$ based hydrogel with various forms such as serpentine line, a star and a double layer grid (pressure; 90 kPa, speed 2 mm/s) (left to right). (**b**) 3D printability of 25 wt.% $pPrOzi_{100}$-*b*-$pEtOx_{100}$ based hydrogel with 1 wt.% laponite XLG (12 layered star) (pressure; 120 kPa, speed 1 mm/s). The screen shots of the designed structures were directly taken from Repetier software during G-code writing.

2.4. Printability and Rheology of POx-Laponite Hybrid Hydrogels

In fact, laponite is routinely applied as rheology modifier [83,84] and has shown potential in biomedical applications [85]. Laponite comprises disc-like silicate particles. It is non-toxic and capable to enhance the biological activities such as cell adhesion and proliferation [86,87]. As a cyto-compatible additive, it can not only improve mechanical strength and printability [88] of the bio-ink but also biological effects [89]. The development of multilayered successive alternating structure (high stackability) is one of the most desirable characteristics for (bio) printing of the constructs for tissue engineering applications [90]. In order to observe the stackability, the pristine hydrogel (25 wt.% pPrOzi$_{100}$-*b*-pEtOx$_{100}$) and a hybrid hydrogel (with 1 wt.% additional laponite XLG) were printed. For the plain hydrogel, printing more then 3 layers greater lead to slight flattening of the scaffold (Figure S4a) while with only 1 wt.% laponite XLG a 12 layered star was easily printed with good shape fidelity and no collapse of the high single filament stacks (Figure 8b). Cryo-SEM of the hybrid hydrogel revealed the uniform microporous structure and pore size of the hydrogel (Figure S4b) is apparently not affected by the presence of the added laponite.

Rheology of a material give generally a good indication for printability [91]. Similar to many other polymers [67,85,88,92], in this particular case, the laponite also improved the printability (in terms of stackability) of pEtOx based hydrogel. To correlate the rheology with printability, the rheological profile of hybrid hydrogel (under same set of conditions as previously explained) was obtained and compared to plain hydrogel. No significant difference was observed in T_{gel}, while the storage modulus increased from 1.5 kPa for plain hydrogel to 3 kPa for hybrid (at 25 °C), indicating a stiffer gel, which may be attributed to the physical interaction between polymer and laponite (Figure S5a). The loss factor tan δ decreased from 0.16 (plain) to 0.05 (hybrid) indicating a higher elastic character. No significant differences were observed in overall LVE range of both plain and hybrid hydrogel. However, the yield point values for hybrid hydrogel (190 Pa) was found to be higher than plain hydrogel (110 Pa) (Figure S5b,c) which is likely to be one important factor responsible for improved stackability. The dynamic frequency sweep experiment revealed that G′ value of hybrid hydrogel remained stable and higher than G″ value throughout the investigated frequency range indicative of typical gel phase (Figure S5d) while the plain hydrogel appeared to be in transition phase of gelation at low shear frequency. In comparison to the plain hydrogel, the steady state flow test revealed more pronounced shear thinning behaviour for hybrid hydrogel (Figure S5e) which is particularly interesting and beneficial for (bio) printing, as cells are more prone to mechanical disruption caused by extrusion pressure from the printing cartridge. Shear thinning is beneficial to reduce shear stress (if the yield points are sufficiently low). A structure recovery test was also performed to investigate the effect of clay on reversible sol-gel transition under episodes of high and low strain values (Figure S5f). Cyclic strain sweeps revealed that at high and low strains, the hybrid hydrogel was capable of transitioning from predominantly elastic to viscous material.

In summary, the addition of small amount of clay significantly improved the rheological properties of pPrOzi$_{100}$-*b*-pEtOx$_{100}$ hydrogels (and in turn printability) without compromising the innate thermogelling behaviour. In most cases, the interaction of clay with polymers is indirectly explored rather than directly investigating the interactions at molecular levels. Very recently, Le Coeur et al. studied the interactions of clay with pMeOx and PEG by NMR spectroscopy and small angle neutron scattering [92]. The results revealed that pMeOx had stronger interaction with clay than PEG. At this point, we have only investigated a single combination of hybrid hydrogel, which showed promising results. By further tuning the polymer and clay ratio, it may be possible for further tailoring the rheological properties. Additionally, it will be very interesting to study in depth the effects of addition of laponite to pPrOzi-b-pMeOx and pPrOzi-b-pEtOx based hydrogels, as the potentially different interactions between the polymers and the clay nanoparticles may affect the rheological properties quantitatively different. Very recently we have observed that pPrOzi-b-pMeOx/clay combination has proved to be highly efficient

fugitive support material [93] for poorly printable sodium alginate [94]. We anticipate that pPrOzi-b-pEtOx/clay combination also holds similar potential and can be explored as fugitive support material for variety of polymers. However, such detailed investigation of polymer/clay interactions and application of pPrOzi-b-pEtOx as fugitive material are separate studies at their own and are beyond the scope of current contribution.

2.5. Biological Studies

In addition to the seeded cells, the scaffold providing a 3D micro-environment to the cells is an essential element in tissue engineering. An appropriate scaffold should provide a room for homogeneous distribution of cells, should be cyto-compatible, non-toxic and promote the cell's proliferation and differentiation. The generally excellent cyto-compatibility of POx-based polymers has been repeatedly shown while POzi-based polymers were studied to a lesser extent [24,36,66,95]. The cyto-compatibility of a certain polymer class must be assessed based on a defined set of experiments, cell-type and should never be generalized but rather verified on case-by-case basis.

Herein, we investigated the cell distribution and the impact of printing process on the cell survival in this new material. The 30 wt.% $pPrOzi_{100}$-*b*-$pEtOx_{100}$ hydrogels used for biological studies were prepared in cell culture medium. Initially, the rheological properties of the hydrogels prepared in media were investigated to screen for additional effect of media. Generally, the cell culture media did not significantly impact the rheological properties (Figure S6), except a slight decrease in gel strength was observed (i.e., from 3 kPa to 2 kPa) when compared to water-based hydrogels, albeit the same handling and printing conditions were used. This highlights to benefit of using a non-ionic bio-ink, as it is less prone to be affected by physiologically relevant proteins, salt concentrations and pH values.

Here, we used human adipose derived stem cells (hADSCs), which have gained wide attention in bioprinting, not only to show the cyto-compatibility of developed material for a somewhat more sensitive cell line, but also to pave way to future tissue engineering applications, where stem cells will likely be preferably used. The fluorescently labelled hADSCs were mixed in the hydrogels (for details, see Section 4) followed by printing and imaging. Important to note, the printability was not influenced by the presence of cells and shape fidelity was entirely preserved.

The homogenous cell distribution was observed throughout the printed construct (Figure 9a). The low viscosity of thermoresponsive hydrogel facilitated the cell distribution just by gently mixing at low temperature. The cell laden bio-ink was further visualized with cryo-SEM to observe the lodging of hADSCs in the hydrogel and to observe (if any) change in overall morphology of hydrogel itself because of cell culture media. Cryo-SEM of the cell laden bio-ink revealed a random distribution of the cells within hydrogel matrix showing cell interior with various organelles (Figure 9b) and no apparent change in porous structure of the hydrogel was observed. The images also make very clear that the pores of the hydrogel are much smaller than the cell diameter.

The cytocompatibility of POx based amphiphiles have been established several times [42,47,95]. In addition to the homogenous distribution of cells in the hydrogels, the measurement of cell viability in the printed scaffolds is more relevant. There are multiple factors such as printing pressure, nozzle inner diameter and shear profile of hydrogel etc. that can directly affect the cells viability and proliferation. The cell mechanical disruption is the direct consequence of pressure gradient/shear stress produced during bioink extrusion from the nozzle. In this regard, post printing live and dead assay was performed to evaluate the proportion of living (green) and dead (red) cells. Two constructs (serpentine line and a star) were printed and immediately visualized under fluorescence microscope (Figure 10a,b). A high extent of viable cells (97 and 98% in serpentine line and a star shape, respectively) confirmed that the printing parameters did not affect the cell viability. For better visibility, the few dead cells (red) in each individual region are highlighted in Figure S7.

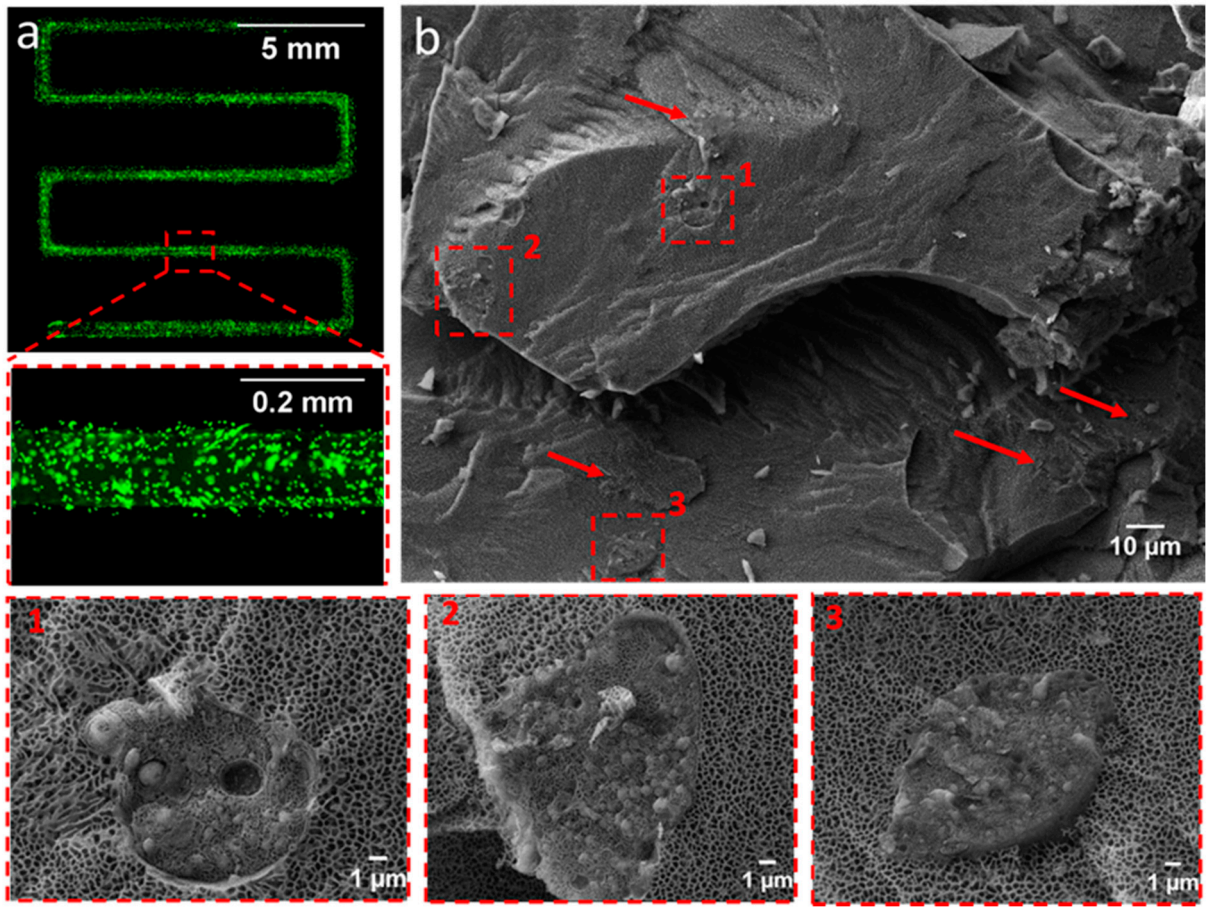

Figure 9. (**a**) Stitched fluorescence microscopic image of the cells distribution in single printed serpentine-like line, hADSCs were labelled with fluorescent dye (**b**) Cryo-SEM image of the cells laden 30 wt.% bio-ink with representative images (1, 2, 3) showing individual cells (arrows are also indicating the presence of cells) (acceleration voltage ETH: 8 kV).

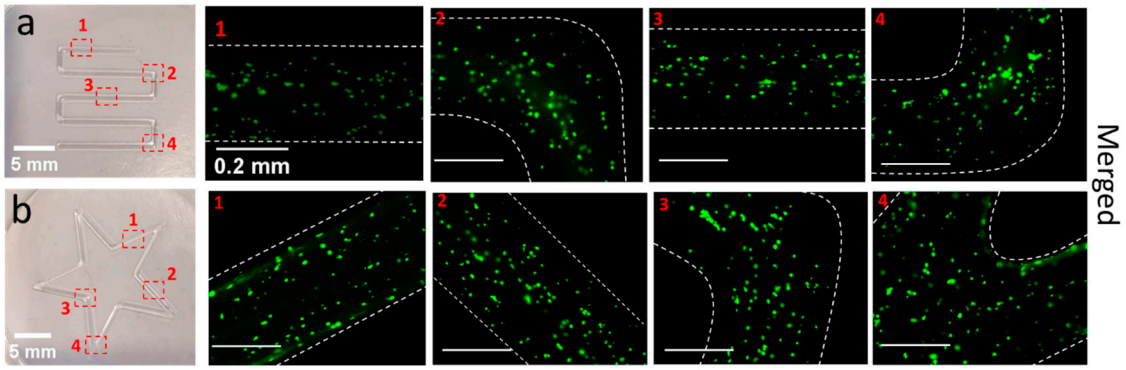

Figure 10. Live (green) and dead (red) viability assay of post-printing cell laden 30 wt.% bio-ink (**a**) serpentine line and (**b**) a star. Number of the live and dead cells were counted from cellular fluorescence images at four different places in individual construct by imageJ software. The images are presented as merged for live and dead cells. Dashed white lines are added for eye guidance (scale bar in fluorescence images is 0.2 mm).

3. Conclusions

In summary, thermosensitive pPrOzi$_{100}$-*b*-pEtOx$_{100}$ based diblock copolymer was successfully synthesized by living cationic ring opening polymerization and was further characterized by ^{1}H-NMR spectroscopy, GPC, DSC and TGA. The pPrOzi$_{100}$-*b*-pEtOx$_{100}$ aqueous solution (i.e., 30 wt.%) underwent reversible sol-gel transition at T_{gel} around

13 °C. Stable and optically clear hydrogels with microporous structure and relatively high mechanical strength of $G' \approx 3$ kPa (at 30 wt.%), were obtained. At the same time this material is highly shear thinning with good structure recovery properties. Additionally, with extrusion-based 3D printing technique, various 2D and 3D patterns with high resolution and shape fidelity could be printed. The hADSC stem cells could be efficiently encapsulated into the hydrogels and this material appeared to be cyto-compatible in post-printing cell experiments.

The newly synthesized diblock pPrOzi-*b*-pEtOx as a structural variant to a previously reported pPrOzi-*b*-pMeOx polymer has potential for further exploration. However, pMeOx and pEtOx are routinely addressed as alternative and similar material [39,40,83] when compared to PEG but it will be interesting to see more of direct comparison of both polymers at molecular level. Advanced applications in biofabrication still may benefit from new smart materials which should be tunable with respect to physicochemical and rheological properties, (bio) printability and cyto-compatibility. With this diblock copolymer, an alternative platform which satisfies most demands needed in the context of biofabrication is introduced. We anticipate that the highly tunable character of POx with respect to rich chemistry would enable us to add crosslinking and/or bio (functionalization), albeit that the range of applications will be affected by the relatively high necessary concentrations. Considering this, the present materials could be of particular interest as a fugitive additive to be combined with other bioinks, to improve their printability or as a drug delivery platform.

4. Material and Methods

4.1. Materials

All substances for the preparation of the polymers were purchased from Sigma-Aldrich (Steinheim, Germany) or Acros (Geel, Belgium) and were used as received unless otherwise stated. The monomers 2-*N*-propyl-2-oxazine (PrOzi) and 2-ethyl-2-oxazoline (EtOx) were prepared following the procedure by Witte and Seeliger [96]. All substances used for polymerization, specifically methyl trifluoromethylsulfonate (MeOTf), EtOx, PrOzi and benzonitrile (PhCN), were refluxed over calcium hydride or phosphorus pentoxide and distilled and stored under argon. Laponite XLG was purchased from BYK-chemical GmbH (Wesel, Germany). Human adipose-dervived stem cells (hADSCs) were purchased from Lonza (Basel, Switzerland). Dulbecco's modified eagle medium (DMEM) + GlutaMAX and Fetal bovine serum (FBS) were obtained from Gibco (Darmstadt, Germany) and Penicillin and streptomycin (P/s) solution were purchased from Biochrom AG (Berlin, Germany).

4.2. Methods

4.2.1. Diblock Copolymer Synthesis

The polymerization and workup procedures were carried out as described previously [47,96]. As a general synthetic procedure, the initiator MeOTf was added to a dried and argon flushed flask and dissolved in the respective amount of solvent (PhCN). The monomer PrOzi was added to the reaction mixture and heated to 120 °C for approximately 12 h. Reaction progress was controlled by ^{1}H-NMR-spectroscopy. After complete consumption of PrOzi monomer, the mixture was cooled to room temperature and the monomer for the second block, i.e., EtOx was added. The reaction mixture was heated to 110 °C for 4–6 h. After complete monomer consumption was confirmed, termination was carried out by the addition of 1-Boc-piperazine (PipBoc) at 50 °C and kept on stirring for 6 h. Subsequently, potassium carbonate was added and the mixture was stirred at 50 °C for further 4 h. The solvent was removed at reduced pressure under schlenk line. The dried polymer mass was dissolved in deionized (DI) water in ice, followed by process of rotary evaporation resulting in concentrated polymer solution. The polymer solution was transferred to a dialysis bag (MWCO 10 kDa, cellulose acetate) and dialyzed against DI water for 48 h. The polymer solution was recovered from the dialysis bag and lyophilized, finally obtained as white powder.

4.2.2. Nuclear Magnetic Resonance

Deuterated solvents for NMR analysis were obtained from Deutero GmbH (Kastellaun, Germany). NMR spectra were recorded on a Fourier 300 (300.12 MHz), Bruker Biospin (Rheinstetten, Germany) at 298 K. The spectra were calibrated to the signal of residual protonated solvent ($CDCl_3$ at 7.26 ppm). All the data were analysed by using the MNova software.

4.2.3. Gel Permeation Chromatography (GPC)

GPC was performed on an Agilent 1260 Infinity System, Polymer Standard Service (Mainz, Germany) with Hexafluoro isopropanol (HFIP) containing 3 g/L potassium trifluoroacetate; having precolumn: PSS PFG 7μm, 5 cm length, 0.8 cm diameter followed by one AppliChrom ABOA HFIP-P-350 30 cm length, 0.8 cm diameter main column. The columns were kept at 40 °C and flow rate was 0.3 mL/min (HFIP). Prior to each measurement, samples were dissolved in HFIP and filtered through 0.2 μm PTFE filters, Roth (Karlsruhe, Germany). Conventional calibration was performed with PEG standards (0.1–1000 kg/mol) and data was processed with Win-GPC software.

4.2.4. Dialysis

The synthesized polymer was dialysed by using Spectra/Por membranes with a molecular weight cut-off (MWCO) of 10 kDa (material: cellulose acetate) obtained from neoLab (Heidelberg, Germany). Deionized water (DI) water was renewed after 1 h, 4 h and every 12 h subsequently, until end of dialysis (48 h).

4.2.5. Differential Scanning Calorimetry (DSC)

DSC was performed on DSC 204 F1 Phoenix equipped with a CC200 F1 Controller, (NETZSCH, Selb, Germany). The dynamic scans were recorded in nitrogen atmosphere with a heating rate of 10 K/min (25–200 °C) and subsequently cooled to −50 °C (10 K/min). The samples were heated and cooled two additional times from −50 °C to 200 °C (10 K/min) (three heating and 2 cooling cycles). For DSC studies, samples (8 to 10 mg) were placed into flat-bottom aluminum pans with crimped-on lids (pierced on the top).

4.2.6. Thermogravimetric Analysis (TGA)

Thermogravimetric analysis was performed on TG 209 F1 IRIS, NETZSCH (Selb, Germany). The powdered polymer samples (10–15 mg) were placed in aluminium oxide crucibles (NETZSCH Selb, Germany) and heated under synthetic air from 30 °C to 900 °C with the heating rate of 10 K/min while detecting the mass loss.

4.2.7. Rheology Measurements

Rheological measurements were performed using the MCR 301 rheometer from Anton Paar (Ostfildern, Germany) using a 25 mm diameter parallel-plate geometry and a Peltier system for temperature control. First, under a constant angular frequency and strain of 10 rad/s and 0.5%, respectively, the temperature sweeps from 5 to 60 °C were carried out at a heating rate of 0.05 °C/s to study the thermogelling behavior. Second, amplitude sweeps in the oscillation strain range of 0.01–500% was performed at a constant angular frequency of 10 rad/s, from which the linear viscoelastic (LVE) range was determined. Third, the frequency sweep was performed in an angular frequency range of 0.1–500 rad/s at a certain strain of 0.5% (within the LVE range obtained from the amplitude sweep). Finally, the steady-state shear flow from 0.01 to 1000/s of shear rate were performed to characterize the shear thinning behavior. The structure recovery properties were investigated utilizing the rotational approach with alternating (5 cycles) low (0.1/s) and high (100/s) amplitude strain (100 s each). Except for the temperature sweep, all tests were performed at 25 °C. A solvent trap was utilized in all experiments to prevent drying.

4.2.8. Scanning Electron Microscopy

The 30 wt.% pPrOzi$_{100}$-*b*-pEtOx$_{100}$ hydrogel was frozen with liquid nitrogen and lyophilized afterwards. The lyophilized hydrogel was mounted on aluminum sample holders with conductive carbon tape and sputtered with a 4 nm layer of platinum in a sputter coater (Leica Microsystems ACE 400, Wetzlar, Germany). The morphology of the samples was subsequently analyzed using a Crossbeam 340 field emission scanning electron microscope (Carl Zeiss Microscopy, Oberkochen, Germany) by setting the acceleration voltage ETH to 2 kV, and detection of secondary electrons (SE) was performed with an Everhart-Thornley detector. The obtained images were further processed in imageJ software (1.46 r, revised edition).

4.2.9. Cryo-Scanning Electron Microscopy

The 30 wt.% pPrOzi$_{100}$- *b*-pEtOx$_{100}$ hydrogel was also visualized with cryo-SEM. Samples were rapidly frozen in slushed nitrogen at −210 °C after placing them between aluminum plates (d = 3 mm) with a 2 mm notch for sample fixation. All the following transfer steps were performed at −140 °C with a EM VCT100 cryo-shuttle (Leica Microsystems). To generate a freshly fractured hydrogel surface, one of the aluminum plates was knocked off and freeze etched for 15 min at −85 °C under high vacuum (<1 × 103 mbar) in a Sputter Coater machine (ACE 400, Leica Microsystems). Afterward, samples were sputtered with 3 nm platinum and transferred to the SEM chamber (Crossbeam 340, Zeiss). Images of the hydrogel surface morphology were taken at −140 °C using an acceleration voltage of 2–8 kV. The images were further processed in ImageJ software (1.46 r, revised edition). The same process was also applied for cell-laden hydrogels.

4.2.10. D-Printing of Hydrogel

Hydrogel printing experiments were performed using the extrusion-based 3D bioprinter BIO X from CELLINK (Gothenburg, Sweden) equipped with pneumatic driven print head and a 0.25 mm inner diameter precision needle (25 G). The extrusion pressure and printing speed was controlled and varied according to different user-defined printing structures, which were programmed by G-code. The ice-cold pPrOzi$_{100}$-*b*-pEtOx$_{100}$ solution was loaded as the ink into a printing cartridge and kept in 4 °C fridge before printing to eliminate air bubbles. The pPrOzi$_{100}$-*b*-pEtOx$_{100}$ filled printing cartridge was mounted in the 3D printer and driven pneumatically through the nozzle to print the hydrogel on a petri dish placed on 37 °C print-bed.

4.2.11. Biological Studies

a. Cell Culture

For biological evaluation, human adipose derived stems cells (hADSCs) were cultured in DMEM + GlutaMAX supplemented with 10% FBS and 5% P/S under standard culture conditions (37 °C and 5% CO_2). At 80 to 90% confluence, the cells were rinsed with phosphate buffer saline (PBS pH 7.4) and passaged using trypsin as detachment agent. The cell suspension was centrifuged for 5 min and the cell pellet was resuspended in culture media. The exact number of cells were obtained by manual cell counting.

b. Polymer Sterilization and Bio-Ink Preparation

Prior to each cell experiment, the weighed amount of polymer was sterilized under UV light (254 nm) for 1 h followed by addition of cell culture media. The polymer dispersion was kept in fridge at 4 °C until a clear solution was obtained. The cell suspension was added to the liquefied hydrogel kept in ice bath followed by 10 min of continuous slow manual rotation for homogenous distribution of cells (avoid using vortex mixer, it can damage the cells). The cell count was kept at 0.5 million cells/mL of 30 wt.% hydrogel for all experiments unless otherwise stated. The cell laden bio-ink was transferred to the printing cartridge and used accordingly.

c. Cell Distribution

To observe the cell distribution in hydrogel, the human adipose derived stem cells (hADSCs) were initially labelled with green fluorescent dye (cell tracker Green CMFDA from Invitrogen). In brief, the harvested cell pellet (1 million cells/mL) was resuspended with fluorescent reagent and incubated for 30 min in serum free media according to the manufacturer's instructions. After centrifugation, the labelling solution was removed followed by addition of fresh pre-warmed media and cells were incubated for additional 30 min. The labelled hADSCs cells were dispersed in the prepared hydrogel as explained earlier. The serpentine line-like construct was printed, visualized and photographed under fluorescent microscope (Zeiss Axioimager Z1 microscope) at λ_{Ex} and λ_{Em} wavelength of 492 and 517 nm, respectively.

d. Post-Printing Live and Dead Assay

The Live/Dead viability assay was used to assess cell viability in the printed scaffolds according to the manufacturer's instructions. Initially the harvested hADSCs pellet was dispersed in live/dead reagent solution prepared in cell culture media (calcein-AM (1:1000) and ethidium bromide (1:500), respectively). After 5 min of incubation, the cell suspension was added to the ice-cold liquid hydrogel and mixed (as explained earlier). In brief, 2 constructs with cell laden bio-ink were printed and samples were immediately examined and photographed by a fluorescent microscope (Zeiss Axioimager Z1 microscope). The live and dead cells appeared as green and red at excitation/emission wave length of 492/517 and 528/617 nm, respectively. The cell viability was reported as the ratio of the number of live cells to the total number of cells in each image counted with ImageJ software (1.46 r, revised edition). We estimate that from first mixing of the bio-ink to the live/dead analysis, the cells were exposed roughly one hour to the bio-ink. From each scaffold (n = 1), live cells with green fluorescence in cytosol or dead cells with red fluorescence in nuclei were counted at 4 different locations with in each construct.

Supplementary Materials: The following are available online at https://www.mdpi.com/article/10.3390/gels7030078/s1. Synthesis of pPrOzi-*b*-pEtOx 50 and 100 repeat units. Figure S1. Heat flow occurring during the various heating and cooling cycle (10 K/min) of differential scanning calorimetry of pPrOzi$_{100}$-*b*-pMeOx$_{100}$, green vertical line indicating the glass transition point. Figure S2. (a) Amplitude and (b) frequency sweep of pPrOzi$_{100}$-*b*-pEtOx$_{100}$ diblock copolymer at 20 and 15 wt.% concentration at constant temperature of 25 °C. Figure S3. SEM image of 30 wt.% pPrOzi$_{100}$-*b*-pEtOx$_{100}$ diblock copolymer lyophilized hydrogel (Top view). Figure S4. (a) 3D printability of 25 wt.% pPrOzi$_{100}$-*b*-pEtOx$_{100}$ based hydrogel, a 5 layered star (pressure; 90 kPa, speed 2 mm/s). (b) cryo-SEM image of the 25 wt.% pPrOzi$_{100}$-*b*-pEtOx$_{100}$ diblock copolymer with 1 wt.% laponite XLG. Figure S5. Comparison of rheological properties of pristine (25 wt.%) and hybrid hydrogel (25 + 1 wt.% clay) prepared in water including (a) temperature dependent sweep (from 5 to 60 °C), (b) amplitude sweep, (c) yield stress and flow point, (d) frequency sweep, (e) shear thinning and (f) structure recovery properties (at 25 °C). Figure S6. Visual appearance of 30 wt.% pPrOzi$_{100}$-*b*-pEtOx$_{100}$ diblock copolymer hydrogel in water (blue) and cell culture media (magenta). Comparison of rheological properties of hydrogel prepared in water and media including temperature dependent sweep (from 5 to 60 °C), frequency sweep, angular sweep, shear thinning and structure recovery properties (at 25 °C). Figure S7. Live/dead viability assay of post-printing cell laden bio-ink (a) serpentine line and (b) a star showing the dead cells (red). Arrows indicating the dead cells and dashed lines are added for eye guidance.

Author Contributions: Conceptualization; M.S.H. and R.L., study design; M.S.H., synthesis and characterization; M.S.H., T.A., M.Y. and P.S., writing original draft; M.S.H., reviewing-editing-polishing; M.S.H., C.H., L.H., J.G. and R.L. All authors have read and agreed to the published version of the manuscript.

Funding: This research was funded by Deutsche Forschungsgemeinschaft (DFG) under project number 398461692-TRR 225, subproject A03 (awarded to R.L.) and the crossbeam scanning electron microscope Zeiss CB 340 (INST 105022/58-1 FUGG) within the DFG State Major Instrumentation Programme.

Institutional Review Board Statement: Not Applicable.

Informed Consent Statement: Not applicable.

Data Availability Statement: The data presented in this study are available on request from the corresponding authors.

Acknowledgments: M.S.H. is grateful to higher education commission of Pakistan and German academic exchange services (HEC-DAAD Pakistan) for the award of PhD scholarship. C.H. and M.Y. thank China Scholarship Council (CSC) for the financial support for doctoral studies.

Conflicts of Interest: R.L. is listed as inventor on a patent pertinent to some materials in the present work. The authors declare no other competing financial interest.

References

1. Kowalski, P.S.; Bhattacharya, C.; Afewerki, S.; Langer, R. Smart biomaterials: Recent advances and future directions. *ACS Biomater. Sci. Eng.* **2018**, *4*, 3809–3817. [CrossRef]
2. Loh, X.J.; Chee, P.L.; Owh, C. Biodegradable thermogelling polymers. *Small Methods* **2019**, *3*, 1800313. [CrossRef]
3. Karoyo, A.H.; Wilson, L.D. Physicochemical properties and the gelation process of supramolecular hydrogels: A review. *Gels* **2017**, *3*, 1. [CrossRef]
4. Al Khateb, K.; Ozhmukhametova, E.K.; Mussin, M.N.; Seilkhanov, S.K.; Rakhypbekov, T.K.; Lau, W.M.; Khutoryanskiy, V.V. In situ gelling systems based on Pluronic F127/Pluronic F68 formulations for ocular drug delivery. *Int. J. Pharm.* **2016**, *502*, 70–79. [CrossRef]
5. Ye, H.; Owh, C.; Loh, X.J. A thixotropic polyglycerol sebacate-based supramolecular hydrogel showing UCST behavior. *RSC Adv.* **2015**, *5*, 48720–48728. [CrossRef]
6. Hahn, L.; Maier, M.; Stahlhut, P.; Beudert, M.; Flegler, V.; Forster, S.; Altmann, A.; Töppke, F.; Fischer, K.; Seiffert, S.; et al. Inverse thermogelation of aqueous triblock copolymer solutions into macroporous shear-thinning 3D printable inks. *ACS Appl. Mater. Interfaces* **2020**, *12*, 12445–12456. [CrossRef]
7. Wellinghoff, S.; Shaw, J.; Baer, E. Polymeric materials from the gel state: The development of fringed micelle structure in a glass. *Macromolecules* **1979**, *12*, 932–939. [CrossRef]
8. Chatterjee, S.; Hui, P.C.-l.; Kan, C.-W. Thermoresponsive hydrogels and their biomedical applications: Special insight into their applications in textile based transdermal therapy. *Polymers* **2018**, *10*, 480. [CrossRef] [PubMed]
9. Hogan, K.J.; Mikos, A.G. Biodegradable thermoresponsive polymers: Applications in drug delivery and tissue engineering. *Polymer* **2020**, *211*, 123063. [CrossRef]
10. Schild, H.G. Poly(N-isopropylacrylamide): Experiment, theory and application. *Prog. Polym. Sci.* **1992**, *17*, 163–249. [CrossRef]
11. Stile, R.A.; Burghardt, W.R.; Healy, K.E. Synthesis and characterization of injectable poly (N-isopropylacrylamide)-based hydrogels that support tissue formation in vitro. *Macromolecules* **1999**, *32*, 7370–7379. [CrossRef]
12. Alexandridis, P.; Hatton, T.A. Poly(ethylene oxide)-poly(propylene oxide)-poly(ethylene oxide) block copolymer surfactants in aqueous solutions and at interfaces: Thermodynamics, structure, dynamics, and modeling. *Colloids Surf. A Physicochem. Eng. Asp.* **1995**, *96*, 1–46. [CrossRef]
13. Li, X.; Katsanevakis, E.; Liu, X.; Zhang, N.; Wen, X. Engineering neural stem cell fates with hydrogel design for central nervous system regeneration. *Prog. Polym. Sci.* **2012**, *37*, 1105–1129. [CrossRef]
14. Burkett, C.J.; Patel, S.; Tabor, M.H.; Padhya, T.; Vale, F.L. Polyethylene glycol (PEG) hydrogel dural sealant and collagen dural graft matrix in transsphenoidal pituitary surgery for prevention of postoperative cerebrospinal fluid leaks. *J. Clin. Neurosci.* **2011**, *18*, 1513–1517. [CrossRef]
15. Spotnitz, W.D.; Burks, S. Hemostats, sealants, and adhesives III: A new update as well as cost and regulatory considerations for components of the surgical toolbox. *Transfusion* **2012**, *52*, 2243–2255. [CrossRef]
16. Cui, Z.; Lee, B.H.; Pauken, C.; Vernon, B.L. Degradation, cytotoxicity, and biocompatibility of NIPAAm-based thermosensitive, injectable, and bioresorbable polymer hydrogels. *J. Biomed. Mater. Res. A* **2011**, *98*, 159–166. [CrossRef] [PubMed]
17. Galperin, A.; Long, T.J.; Garty, S.; Ratner, B.D. Synthesis and fabrication of a degradable poly(N-isopropyl acrylamide) scaffold for tissue engineering applications. *J. Biomed. Mater. Res. A* **2013**, *101*, 775–786. [CrossRef]
18. Watson, B.M.; Kasper, F.K.; Engel, P.S.; Mikos, A.G. Synthesis and characterization of injectable, biodegradable, phosphate-containing, chemically cross-linkable, thermoresponsive macromers for bone tissue engineering. *Biomacromolecules* **2014**, *15*, 1788–1796. [CrossRef] [PubMed]
19. Hoang Thi, T.T.; Pilkington, E.H.; Nguyen, D.H.; Lee, J.S.; Park, K.D.; Truong, N.P. The importance of poly (ethylene glycol) alternatives for overcoming PEG immunogenicity in drug delivery and bioconjugation. *Polymers* **2020**, *12*, 298. [CrossRef]
20. Liu, Z.; Liow, S.S.; Lai, S.L.; Alli-Shaik, A.; Holder, G.E.; Parikh, B.H.; Krishnakumar, S.; Li, Z.; Tan, M.J.; Gunaratne, J. Retinal-detachment repair and vitreous-like-body reformation via a thermogelling polymer endotamponade. *Nat. Biomed. Eng.* **2019**, *3*, 598–610. [CrossRef]
21. Bloksma, M.M.; Schubert, U.S.; Hoogenboom, R. Poly(cyclic imino ether)s Beyond 2-Substituted-2-oxazolines. *Macromol. Rapid Commun.* **2011**, *32*, 1419–1441. [CrossRef] [PubMed]

22. Bloksma, M.M.; Paulus, R.M.; van Kuringen, H.P.C.; van der Woerdt, F.; Lambermont-Thijs, H.M.; Schubert, U.S.; Hoogenboom, R. Thermoresponsive Poly(2-oxazine)s. *Macromol. Rapid Commun.* **2012**, *33*, 92–96. [CrossRef] [PubMed]
23. Weber, C.; Hoogenboom, R.; Schubert, U.S. Temperature responsive bio-compatible polymers based on poly (ethylene oxide) and poly(2-oxazoline)s. *Prog. Polym. Sci.* **2012**, *37*, 686–714. [CrossRef]
24. Lorson, T.; Lübtow, M.M.; Wegener, E.; Haider, M.S.; Borova, S.; Nahm, D.; Jordan, R.; Sokolski-Papkov, M.; Kabanov, A.V.; Luxenhofer, R. Poly(2-oxazoline)s based biomaterials: A comprehensive and critical update. *Biomaterials* **2018**, *178*, 204–280. [CrossRef] [PubMed]
25. Sedlacek, O.; Monnery, B.D.; Filippov, S.K.; Hoogenboom, R.; Hruby, M. Poly(2-Oxazoline)s—Are They More Advantageous for Biomedical Applications Than Other Polymers? *Macromol. Rapid Commun.* **2012**, *33*, 1648–1662. [CrossRef]
26. Victor, R. Poly(2-oxazoline)s as materials for biomedical applications. *J. Mater. Sci. Mater. Med.* **2014**, *25*, 1211–1225.
27. Trachsel, L.; Johnbosco, C.; Lang, T.; Benetti, E.M.; Zenobi-Wong, M. Double-network hydrogels including enzymatically crosslinked poly-(2-alkyl-2-oxazoline)s for 3D bioprinting of cartilage-engineering constructs. *Biomacromolecules* **2019**, *20*, 4502–4511. [CrossRef]
28. You, Y.; Kobayashi, K.; Colak, B.; Luo, P.; Cozen, E.; Fields, L.; Suzuki, K.; Gautrot, J. Engineered cell-degradable poly(2-alkyl-2-oxazoline) hydrogel for epicardial placement of mesenchymal stem cells for myocardial repair. *Biomaterials* **2021**, *269*, 120356. [CrossRef] [PubMed]
29. Kim, D.; Thangavelu, M.; Baek, J.S.; Kim, H.S.; Choi, M.J.; Cho, H.H.; Song, J.E.; Khang, G. Fabrication of POX/PLGA Scaffold for the Potential Application of Tissue Engineering and Cell Transplantation. *Macromol. Res.* **2020**, *28*, 196–202. [CrossRef]
30. He, Z.; Schulz, A.; Wan, X.; Seitz, J.; Bludau, H.; Alakhova, D.Y.; Darr, D.B.; Perou, C.M.; Jordan, R.; Ojima, I.; et al. Poly(2-oxazoline) based micelles with high capacity for 3rd generation taxoids: Preparation, in vitro and in vivo evaluation. *J. Control. Release* **2015**, *208*, 67–75. [CrossRef]
31. Simon, L.; Vincent, M.; Le Saux, S.; Lapinte, V.; Marcotte, N.; Morille, M.; Dorandeu, C.; Devoisselle, J.; Bégu, S. Polyoxazolines based mixed micelles as PEG free formulations for an effective quercetin antioxidant topical delivery. *Int. J. Pharm.* **2019**, *570*, 118516. [CrossRef] [PubMed]
32. Wan, X.; Beaudoin, J.J.; Vinod, N.; Min, Y.; Makita, N.; Bludau, H.; Jordan, R.; Wang, A.; Sokolsky, M.; Kabanov, A.V. Co-delivery of paclitaxel and cisplatin in poly(2-oxazoline) polymeric micelles: Implications for drug loading, release, pharmacokinetics and outcome of ovarian and breast cancer treatments. *Biomaterials* **2019**, *192*, 1–14. [CrossRef] [PubMed]
33. Haider, M.S.; Schreiner, J.; Kendl, S.; Kroiss, M.; Luxenhofer, R. A Micellar Mitotane Formulation with High Drug-Loading and Solubility: Physico-Chemical Characterization and Cytotoxicity Studies in 2D and 3D In Vitro Tumor Models. *Macromol. Biosci.* **2020**, *20*, 1900178–1900191. [CrossRef] [PubMed]
34. Simon, L.; Marcotte, N.; Devoisselle, J.; Begu, S.; Lapinte, V. Recent advances and prospects in nano drug delivery systems using lipopolyoxazolines. *Int. J. Pharm.* **2020**, *585*, 119536. [CrossRef]
35. Abilova, G.K.; Kaldybekov, D.B.; Ozhmukhametova, E.K.; Saimova, A.Z.; Kazybayeva, D.S.; Irmukhametova, G.S.; Khutoryanskiy, V.V. Chitosan/poly (2-ethyl-2-oxazoline) films for ocular drug delivery: Formulation, miscibility, in vitro and in vivo studies. *Eur. Polym. J.* **2019**, *116*, 311–320. [CrossRef]
36. Zahoranová, A.; Luxenhofer, R. Poly(2-oxazoline) and Poly(2-oxazine) Based Self-Assemblies, Polyplexes, and Drug Nanoformulations-An Update. *Adv. Healthc. Mater.* **2021**, *10*, 2001382. [CrossRef]
37. Hoogenboom, R.; Schlaad, H. Thermoresponsive poly(2-oxazoline)s, polypeptoids, and polypeptides. *Polym. Chem.* **2017**, *8*, 24–41. [CrossRef]
38. Delecourt, G.; Plet, L.; Bennevault, V.; Guegan, P. Synthesis of double hydrophilic block copolymers poly(2-oxazoline-b-ethylenimine) in a two-step procedure. *ACS Appl. Polym. Mater.* **2020**, *2*, 2696–2705. [CrossRef]
39. Oleszko-Torbus, N.; Utrata-Wesołek, A.; Bochenek, M.; Lipowska-Kur, D.; Dworak, A.; Wałach, W. Thermal and crystalline properties of poly(2-oxazoline)s. *Polym. Chem.* **2020**, *11*, 15–33. [CrossRef]
40. Gaertner, F.C.; Luxenhofer, R.; Blechert, B.; Jordan, R.; Essler, M. Synthesis, biodistribution and excretion of radiolabeled poly(2-alkyl-2-oxazoline)s. *J. Control. Release* **2007**, *119*, 291–300. [CrossRef]
41. Barz, M.; Luxenhofer, R.; Zentel, R.; Vicent, M.J. Overcoming the PEG-addiction: Well-defined alternatives to PEG, from structure–property relationships to better defined therapeutics. *Polym. Chem.* **2011**, *2*, 1900–1918. [CrossRef]
42. Sedlacek, O.; Monnery, B.D.; Mattova, J.; Kucka, J.; Panek, J.; Janouskova, O.; Hocherl, A.; Verbraeken, B.; Vergaelen, M.; Zadinova, M.; et al. Poly(2-ethyl-2-oxazoline) conjugates with doxorubicin for cancer therapy: In vitro and in vivo evaluation and direct comparison to poly [N-(2-hydroxypropyl) methacrylamide] analogues. *Biomaterials* **2017**, *146*, 1–12. [CrossRef] [PubMed]
43. Grube, M.; Leiske, M.N.; Schubert, U.S.; Nischang, I. POx as an alternative to PEG? A hydrodynamic and light scattering study. *Macromolecules* **2018**, *51*, 1905–1916. [CrossRef]
44. Konradi, R.; Pidhatika, B.; Mühlebach, A.; Textor, M. Poly-2-methyl-2-oxazoline: A peptide-like polymer for protein-repellent surfaces. *Langmuir* **2008**, *24*, 613–616. [CrossRef] [PubMed]
45. Zhang, N.; Pompe, T.; Luxenhofer, R.; Werner, C.; Jordan, R. Poly (2-oxazoline) bottle-rush brushes for the control of protein adsorption and cell adhesion. *Polymer Prepr.* **2012**, *53*, 301.
46. Morgese, G.; Verbraeken, B.; Ramakrishna, S.N.; Gombert, Y.; Cavalli, E.; Rosenboom, J.G.; Zenobi-Wong, M.; Spencer, N.D.; Hoogenboom, R.; Benetti, E.M. Chemical Design of Non-Ionic Polymer Brushes as Biointerfaces: Poly(2-oxazine)s Outperform Both Poly(2-oxazoline)s and PEG. *Angew. Chem.* **2018**, *57*, 11667–11672. [CrossRef]

47. Lorson, T.; Jaksch, S.; Lübtow, M.M.; Jüngst, T.; Groll, J.; Lühmann, T.; Luxenhofer, R. A thermogelling supramolecular hydrogel with sponge-like morphology as a cytocompatible bioink. *Biomacromolecules* **2017**, *18*, 2161–2171. [CrossRef]
48. Lübtow, M.M.; Mrlik, M.; Hahn, L.; Altmann, A.; Beudert, M.; Lühmann, T.; Luxenhofer, R. Temperature-Dependent Rheological and Viscoelastic Investigation of a Poly(2-methyl-2-oxazoline)-b-poly(2-iso-butyl-2-oxazoline)-b-poly(2-methyl-2-oxazoline)-Based Thermogelling Hydrogel. *J. Funct. Biomater.* **2019**, *10*, 36. [CrossRef]
49. Wloka, T.; Czich, S.; Kleinsteuber, M.; Moek, E.; Weber, C.; Gottschaldt, M.; Liefeith, K.; Schubert, U.S. Microfabrication of 3D-hydrogels via two-photon polymerization of poly(2-ethyl-2-oxazoline) diacrylates. *Eur. Polym. J.* **2020**, *122*, 109295. [CrossRef]
50. Kalaoglu-Altan, O.I.; Li, Y.; McMaster, R.; Shaw, A.; Hou, Z.; Vergaelen, M.; Hoogenboom, R.; Dargaville, T.R.; De Clerck, K. Crosslinking of electrospun and bioextruded partially hydrolyzed poly(2-ethyl-2-oxazoline) using glutaraldehyde vapour. *Eur. Polym. J.* **2019**, *120*, 109218. [CrossRef]
51. Kang, J.-J.; Shehu, K.; Sachse, C.; Jung, F.A.; Ko, C.-H.; Barnsley, L.C.; Jordan, R.; Papadakis, C.M. A molecular brush with thermoresponsive poly(2-ethyl-2-oxazoline) side chains: A structural investigation. *Colloid Polym. Sci.* **2020**, *299*, 193–203. [CrossRef]
52. Dirauf, M.; Grune, C.; Weber, C.; Schubert, U.S.; Fischer, D. Poly(ethylene glycol) or poly(2-ethyl-2-oxazoline)–A systematic comparison of PLGA nanoparticles from the bottom up. *Eur. Polym. J.* **2020**, *134*, 109801. [CrossRef]
53. Han, Y.; He, Z.; Schulz, A.; Bronich, T.K.; Jordan, R.; Luxenhofer, R.; Kabanov, A.V. Synergistic combinations of multiple chemotherapeutic agents in high capacity poly(2-oxazoline) micelles. *Mol. Pharm.* **2012**, *9*, 2302–2313. [CrossRef]
54. Lübtow, M.M.; Hahn, L.; Haider, M.S.; Luxenhofer, R. Drug specificity, synergy and antagonism in ultrahigh capacity poly(2-oxazoline)/poly(2-oxazine) based formulations. *J. Am. Chem. Soc.* **2017**, *139*, 10980–10983. [CrossRef]
55. Haider, M.S.; Lübtow, M.M.; Endres, S.; Forster, S.; Flegler, V.J.; Böttcher, B.; Aseyev, V.O.; Pöppler, A.-C.; Luxenhofer, R. Think beyond the core: The impact of the hydrophilic corona on the drug solubilization using polymer micelles. *ACS Appl. Mater. Interfaces* **2020**, *12*, 24531–24543. [CrossRef]
56. Leiske, M.N.; Lai, M.; Amarasena, T.; Davis, T.P.; Thurecht, K.J.; Kent, S.J.; Kempe, K. Interactions of core cross-linked poly (2-oxazoline) and poly (2-oxazine) micelles with immune cells in human blood. *Biomaterials* **2021**, *274*, 120843. [CrossRef] [PubMed]
57. Xu, M.; Yao, C.; Zhang, W.; Gao, S.; Zou, H.; Gao, J. Anti-Cancer Activity Based on the High Docetaxel Loaded Poly (2-Oxazoline) s Micelles. *Int. J. Nanomed.* **2021**, *16*, 2735. [CrossRef] [PubMed]
58. Hochleitner, G.; Hümmer, J.F.; Luxenhofer, R.; Groll, J. High definition fibrous poly(2-ethyl-2-oxazoline) scaffolds through melt electrospinning writing. *Polymer* **2014**, *55*, 5017–5023. [CrossRef]
59. Li, Y.; Vergaelen, M.; Schoolaert, E.; Hoogenboom, R.; De Clerck, K. Effect of crosslinking stage on photocrosslinking of benzophenone functionalized poly (2-ethyl-2-oxazoline) nanofibers obtained by aqueous electrospinning. *Eur. Polym. J.* **2019**, *112*, 24–30. [CrossRef]
60. Zahoranová, A.; Mrlík, M.; Tomanová, K.; Kronek, J.; Luxenhofer, R. ABA and BAB Triblock Copolymers Based on 2-Methyl-2-oxazoline and 2-n-Propyl-2-oxazoline: Synthesis and Thermoresponsive Behavior in Water. *Macromol. Chem. Phys.* **2017**, *218*, 1700031. [CrossRef]
61. Hahn, L.; Karakaya, E.; Zorn, T.; Sochor, B.; Maier, M.; Stahlhut, P.; Forster, S.; Fischer, K.; Seiffert, S.; Pöppler, A.-C.; et al. An Inverse Thermogelling Bioink Based on an ABA Type Poly(2-Oxazoline) Amphiphile. *ChemRxiv* **2021**. [CrossRef]
62. Hahn, L.; Beudert, M.; Gutmann, M.; Keßler, L.; Stahlhut, P.; Fischer, L.; Lorson, T.; Thievessen, I.; Lühmann, T.; Luxenhofer, R. Biomechanical and Biological Performances of Diels-Alder Crosslinked Thermogelling Bioink. *ChemRxiv* **2021**. [CrossRef]
63. Monnery, B.D.; Hoogenboom, R. Thermoresponsive hydrogels formed by poly(2-oxazoline) triblock copolymers. *Polym. Chem.* **2019**, *10*, 3480–3487. [CrossRef]
64. Zhang, Q.; Weber, C.; Schubert, U.S.; Hoogenboom, R. Thermoresponsive polymers with lower critical solution temperature: From fundamental aspects and measuring techniques to recommended turbidimetry conditions. *Mater. Horiz.* **2017**, *4*, 109–116. [CrossRef]
65. Hijazi, M.; Schmidt, M.; Xia, H.; Storkmann, J.; Plothe, R.; Dos Santos, D.; Bednarzick, U.; Krumm, C.; Tiller, J.C. Investigations on the thermoresponsive behavior of copoly(2-oxazoline)s in water. *Polymer* **2019**, *175*, 294–301. [CrossRef]
66. Lübtow, M.M.; Keßler, L.; Appelt-Menzel, A.; Lorson, T.; Gangloff, N.; Kirsch, M.; Dahms, S.; Luxenhofer, R. More Is Sometimes Less: Curcumin and Paclitaxel Formulations Using Poly(2-oxazoline) and Poly(2-oxazine)-Based Amphiphiles Bearing Linear and Branched C9 Side Chains. *Macromol. Biosci.* **2018**, *18*, 1800155–1800172. [CrossRef] [PubMed]
67. Hu, C.; Hahn, L.; Yang, M.; Altmann, A.; Stahlhut, P.; Groll, J.; Luxenhofer, R. Improving Printability of a Thermoresponsive Hydrogel Biomaterial Ink by Nanoclay Addition. *J. Mater. Sci.* **2021**, *56*, 691–705. [CrossRef]
68. Schoolaert, E.; Merckx, R.; Becelaere, J.; Everaerts, M.; Van Guyse, J.F.; Sedlacek, O.; De Geest, B.G.; Van den Mooter, G.; D'hooge, D.R.; De Clerck, K. Immiscibility of chemically alike amorphous polymers: Phase separation of poly (2-ethyl-2-oxazoline) and poly (2-n-propyl-2-oxazoline). *Macromolecules* **2020**, *53*, 7590–7600. [CrossRef]
69. Lorson, T. Novel Poly(2-oxazoline) Based Bioinks. Ph.D. Thesis, Julius-Maximilians-University Würzburg, Würzburg, Germany, 2019. [CrossRef]
70. Lin, P.; Clash, C.; Pearce, E.; Kwei, T.; Aponte, M. Solubility and miscibility of poly(ethyl oxazoline). *J. Polym. Sci. Part B* **1988**, *26*, 603–619. [CrossRef]

71. Hoogenboom, R.; Hanneke, M.T.; Mark, J.H.C.J.; Bart, M.v.L.; Fijten, M.W.M.; Schubert, U.S. Tuning the LCST of poly(2-oxazoline)s by varying composition and molecular weight: Alternatives to poly(N-isopropylacrylamide)? *Chem. Commun.* **2008**, 5758–5760. [CrossRef] [PubMed]
72. Huber, S.; Hutter, N.; Jordan, R. Effect of end group polarity upon the lower critical solution temperature of poly(2-isopropyl-2-oxazoline). *Colloid Polym. Sci.* **2008**, *286*, 1653–1661. [CrossRef]
73. Li, C.; Buurma, N.J.; Haq, I.; Turner, C.; Armes, S.P.; Castelletto, V.; Hamley, I.W.; Lewis, A.L. Synthesis and characterization of biocompatible, thermoresponsive ABC and ABA triblock copolymer gelators. *Langmuir* **2005**, *21*, 11026–11033. [CrossRef]
74. Xuan, S.; Lee, C.-U.; Chen, C.; Doyle, A.B.; Zhang, Y.; Guo, L.; John, V.T.; Hayes, D.; Zhang, D. Thermoreversible and injectable ABC polypeptoid hydrogels: Controlling the hydrogel properties through molecular design. *Chem. Mater.* **2016**, *28*, 727–737. [CrossRef] [PubMed]
75. Sathaye, S.; Mbi, A.; Sonmez, C.; Chen, Y.; Blair, D.L.; Schneider, J.P.; Pochan, D.J. Rheology of peptide-and protein-based physical hydrogels: Are everyday measurements just scratching the surface? *Wiley Interdiscip. Rev. Nanomed. Nanobiotechnol.* **2015**, *7*, 34–68. [CrossRef] [PubMed]
76. Mezger, T. *The Rheology Handbook: For Users of Rotational and Oscillatory Rheometers*; European Coatings: Wilmington, NC, USA, 2020.
77. Balmforth, N.J.; Frigaard, I.A.; Ovarlez, G. Yielding to stress: Recent developments in viscoplastic fluid mechanics. *Annu. Rev. Fluid Mech.* **2014**, *46*, 121–146. [CrossRef]
78. Blaeser, A.; Duarte Campos, D.F.; Puster, U.; Richtering, W.; Stevens, M.M.; Fischer, H. Controlling shear stress in 3D bioprinting is a key factor to balance printing resolution and stem cell integrity. *Adv. Healthc. Mater.* **2016**, *5*, 326–333. [CrossRef] [PubMed]
79. Malkoc, V. Challenges and the future of 3D bioprinting. *J. Biomed. Imaging. Bioeng.* **2018**, *2*, 64–65.
80. Ghica, M.V.; Hîrjău, M.; Lupuleasa, D.; Dinu-Pîrvu, C.-E. Flow and thixotropic parameters for rheological characterization of hydrogels. *Molecules* **2016**, *21*, 786. [CrossRef]
81. Kaberova, Z.; Karpushkin, E.; Nevoralová, M.; Vetrík, M.; Šlouf, M.; Dušková-Smrčková, M. Microscopic structure of swollen hydrogels by scanning electron and light microscopies: Artifacts and reality. *Polymers* **2020**, *12*, 578. [CrossRef]
82. Schwab, A.; Levato, R.; D'Este, M.; Piluso, S.; Eglin, D.; Malda, J. Printability and shape fidelity of bioinks in 3D bioprinting. *Chem. Rev.* **2020**, *120*, 11028–11055. [CrossRef]
83. Dávila, J.L.; d'Ávila, M.A. Laponite as a rheology modifier of alginate solutions: Physical gelation and aging evolution. *Carbohydr. Polym.* **2017**, *157*, 1–8. [CrossRef] [PubMed]
84. Jin, Y.; Shen, Y.; Yin, J.; Qian, J.; Huang, Y. Nanoclay-based self-supporting responsive nanocomposite hydrogels for printing applications. *ACS Appl. Mater. Interfaces* **2018**, *10*, 10461–10470. [CrossRef] [PubMed]
85. Das, S.S.; Hussain, K.; Singh, S.; Hussain, A.; Faruk, A.; Tebyetekerwa, M. Laponite-based nanomaterials for biomedical applications: A review. *Curr. Pharm. Des.* **2019**, *25*, 424–443. [CrossRef] [PubMed]
86. Choi, D.; Heo, J.; Milan, J.A.; Oreffo, R.O.; Dawson, J.I.; Hong, J.; Kim, Y.-H. Structured nanofilms comprising Laponite® and bone extracellular matrix for osteogenic differentiation of skeletal progenitor cells. *Mater. Sci. Eng. C* **2021**, *118*, 111440. [CrossRef]
87. Mignon, A.; Pezzoli, D.; Prouvé, E.; Lévesque, L.; Arslan, A.; Pien, N.; Schaubroeck, D.; Van Hoorick, J.; Mantovani, D.; Van Vlierberghe, S. Combined effect of Laponite and polymer molecular weight on the cell-interactive properties of synthetic PEO-based hydrogels. *React. Funct. Polym.* **2019**, *136*, 95–106. [CrossRef]
88. Dávila, J.L.; d'Ávila, M.A. Rheological evaluation of Laponite/alginate inks for 3D extrusion-based printing. *Int. J. Adv. Manuf. Tech.* **2019**, *101*, 675–686. [CrossRef]
89. Ahlfeld, T.; Cidonio, G.; Kilian, D.; Duin, S.; Akkineni, A.; Dawson, J.; Yang, S.; Lode, A.; Oreffo, R.; Gelinsky, M. Development of a clay based bioink for 3D cell printing for skeletal application. *Biofabrication* **2017**, *9*, 034103. [CrossRef]
90. Zhuang, P.; Ng, W.L.; An, J.; Chua, C.K.; Tan, L.P. Layer-by-layer ultraviolet assisted extrusion-based (UAE) bioprinting of hydrogel constructs with high aspect ratio for soft tissue engineering applications. *PLoS ONE* **2019**, *14*, e0216776. [CrossRef]
91. Corker, A.; Ng, H.C.-H.; Poole, R.J.; García-Tuñón, E. 3D printing with 2D colloids: Designing rheology protocols to predict 'printability'of soft-materials. *Soft Matter* **2019**, *15*, 1444–1456. [CrossRef]
92. Le Coeur, C.; Lorthioir, C.; Feoktystov, A.; Wu, B.; Volet, G.; Amiel, C. Laponite/poly(2-methyl-2-oxazoline) hydrogels: Interplay between local structure and rheological behaviour. *J. Colloid Interface Sci.* **2021**, *582*, 149–158. [CrossRef]
93. Hu, C.; Ahmad, T.; Haider, M.S.; Hahn, L.; Stahlhut, P.; Groll, J.; Luxenhofer, R. A Thermogelling Organic-Inorganic Hybrid Hydrogel with Excellent Printability, Shape Fidelity and Cytocompatibility for 3D Bioprinting. *ChemRxiv* **2021**. [CrossRef]
94. Hazur, J.; Detsch, R.; Karakaya, E.; Kaschta, J.; Teßmar, J.; Schneidereit, D.; Friedrich, O.; Schubert, D.W.; Boccaccini, A.R. Improving alginate printability for biofabrication: Establishment of a universal and homogeneous pre-crosslinking technique. *Biofabrication* **2020**, *12*, 045004. [CrossRef]
95. Kroneková, Z.; Lorson, T.; Kronek, J.; Luxenhofer, R. Cytotoxicity of 2-oxazines and poly(2-oxazine)s in mouse fibroblast. *ChemRxiv* **2018**. [CrossRef]
96. Witte, H.; Seeliger, W. Cyclische imidsäureester aus nitrilen und aminoalkoholen. *Leibigs Ann.* **1974**, *1974*, 996–1009. [CrossRef]

5 Summary and Outlook

In this work, we have explored the pharmaceutical and biomedical applications of POx/POzi based ABA triblock and AB diblock copolymers, respectively with the special emphasis on SPR. The triblock copolymers were used for formulation development of various hydrophobic drugs to improve their aqueous solubility. The poor aqueous solubility can limit the drug administration and subsequent pharmacological response because of varied oral absorption and poor pharmacokinetic profile. After the development of first ultra-high drug loaded POx based PTX formulation, as a scientist we asked ourself a very common but important question, what makes this system ultra-high drug loaded. As in the literature, usually the micelles based systems rarely exceed the drug loading above 20-30 wt.%. The relative low drug loading requires large amounts of excipients (polymer) to achieve the desired dose, which in turn limit the use during clinical translation (because of excipient toxicity) and very high administration volume, which limit the intravenous administration. From this point we started exploring, what makes our system ultra-high drug loaded and whether POx based triblock copolymers can be considered as one solution for all hydrophobic drugs. Based on the general concept i.e. hydrophobic block is responsible for solubilizing the hydrophobic cargo while the hydrophilic block provide the colloidal stability, we initially developed a considerable library of ABA triblock copolymers (18 in total) and tested the solubilizing capacity for five different hydrophobic drugs. In this library, only the hydrophobic block B was changed from linear, branched (aliphatic POx with varying side chain lengths; C4-C9) or an aromatic ringside chains while keeping the hydrophilic block A as pMeOx. The results showed that the hydrophobic blocks with shorter side chain length (or simply minor amphiphilic contrast in the hydrophobic and hydrophilic block) appeared to be the best solubilizer for hydrophobic drugs. Exploring further, from this library, we selected four different amphiphilies with the minor amphiphilic contrast and check their solubilizing capacity for 21 different hydrophobic drugs. In the formulation library, 11 out of 21 drugs exhibited loading capacity greater than 20 wt.% while the rest fell below this limit. However, It is worth mentioning that the drug loading in POx/POzi based triblock copolymers was much higher than many other reported systems in the literature for the same drugs. The development of polymer and formulation libraries is quite laborious task, so in the meantime we were also focusing on the different theoretical approaches to estimate the polymer drug compatibility for the design of cost-effective and efficient drug delivery system. It is usually desirable to predict theoretically the extent of compatibility between polymer and drugs before any experimentation. For many years, solubility parameters are routinely employed for estimation of compatibility between solute and solvent especially in paint/polymer industry. Unfortunately, collectively the polymer-drug compatibilities of 18 different polymer amphiphiles and 5 different

hydrophobic/structurally diverse drugs could not be predicted with widely applied group contribution methods (i.e. HnV and YMB using commercially available software i.e. HSPiP) from Hildebrand or Hansen solubility parameters. Although certain trends regarding good and poor solubilizers could be estimated, the influence of small changes in the chemical structure such as branching or cyclization in the sidechain of hydrophobic block in triblock copolymers, was out of range. This was true for purely calculated as well as empirically determined solubility parameters. In the second study, the results obtained by compatibility estimation between 4 polymers and 21 hydrophobic drugs were not in accordance with the obtained formulation results. There were few exceptions, which can be considered completely coincidental than systematic. The practical weakness of this approach can be correlated to, the limited number of functional groups available in the literature and most importantly the impact of secondary factors like thermodynamics, hydrophilic lipophilic balance, drug structure, drug rigidity, interfacial tension, polymer and drug concentration, the solvent and the method for formulation development, which are usually not taken into consideration in such approaches. Based on obtained results, we can conclusively say that the compatibility estimation by solubility parameters between polymer and drugs in POx/POzi based amphiphiles is not the ideal tool to be used. Therefore, it is extremely essential to build a theoretical method, capable to bring most of the factor discussed above into consideration, for drug-polymer compatibility evaluation to guide the formulation design of polymeric micelles.

Turning back to ultra-high drug loaded POx/POzi based micelles, the theoretical consideration suggested that it is not possible that the amount of drug in one micelle can merely accommodate in hydrophobic block. Based on this idea, we hypothesized that hydrophilic block/corona could have role in drug solubilisation, which has not been systematically studied to date. A library of new ABA triblock copolymers which differ only in their hydrophilic blocks were synthesized (A= pMeOx or pEtOx). The drug loading capacities and various analytical techniques confirmed that besides hydrophobic block, the hydrophilic blocks of the amphiphiles also play very important role in drug solubilisation. These results show for the first time that the hydrophilic corona of polymer micelles may not only be involved in providing colloidal stability, but also that a minor change in the hydrophilic block of a polymer amphiphile can have a significant impact on drug loading. These results shed new light and give clear instructions on how to design and optimize drug delivery system polymeric excipients in general. These finding open a new research avenue to study the system at molecular level and to analyse the characteristics of materials at such scale. This will unravel that clusters of such atoms or molecules often have the properties, which are different from the properties of same matter as single molecule or at bulk scale. Nanoscale science together with material engineering will play an important role to discover, describe, and manipulate these

special properties in order to develop new capabilities with potential applications across all fields of science, engineering, technology, and medicine.

After the development of formulation library of 21 hydrophobic drugs, checking the applicability of solubility parameters and exploring these fundamental questions of high drug loading, we also investigated the therapeutic potential of selected POx/POzi based micellar formulations. Mitotane is the drug of choice for adrenocortical carcinoma, it is commercially available as tablet dosage form. After several months of high daily dosage (4-6 g/d), more than 50% of the patients do not achieve therapeutic plasma concentration (14-20 mg/L). Therefore, the treatment outcomes are limited because of variable pharmacokinetic profile. In this regard, we thrived to understand the underlying cause of this problem, which can be directly correlated to poor aqueous solubility of mitotane. Considering this, we presented for the first time the idea of mitotane intravenous administration. In the meantime, we were also successful in solubilizing mitotane up to 6 -7.5 g/L by two of the POx based triblock copolymers. A detailed physico-chemical characterization of the POx-based mitotane formulations showed excellent stability despite the high loading. Moreover, the formulation can be stored as a lyophilized powder ready for redispersion, as needed. The formulation also exhibited excellent activity in vitro in 2D and 3D adrenocortical cell cultures (NCI-H295R tumor cell line). The obtained IC_{50} values in conventional 2D monolayer cell culture were comparable for mitotane dissolved in ethanol and POx micelles. Currently, no other compounds with anti-secretory and antitumor activity are available for adrenocortical carcinoma, so mitotane is the only drug of choice. Presently, the idea of mitotane injectable formulation is in infancy, and substantiated only from the side of formulation development, characterization and in vitro data. Currently, we are working on a protocol design and its implementation for in vivo studies. We hope that by developing an injectable mitotane formulation, an improved understanding of the pharmacokinetic properties, reduction in dose and adverse events might be possible, which would be important steps towards an improved ACC therapy. Additionally, the alternative administration will provide us with novel insights into the association of mitotane with serum LPs and potential changes in elimination half-life and tissue distribution.

The second formulation, which we have thoroughly investigated, is BT44, a lead compound for the neurodegenerative disorders. The POx based triblock copolymer i.e. A-pPentOx-A gave the ultra-high drug loading of 47 wt.% for BT44. To the best of our knowledge this is the first ever reported any BT44 nanoformulation. Like mitotane formulation, the BT44 formulation was also thoroughly characterized by various analytical techniques. Additionally, it was also subjected to in vitro and in vivo studies. The POx based BT44 formulation retained it biological activity in cell lines. No acute toxicity was observed for plain

polymer even at very high doses of around 500 mg/kg in animal model. After subcutaneous injection in mice, the BT44 formulation exhibited higher absorption into the general circulation and subsequent higher blood brain barrier penetration. We anticipate that this formulation can potentially be used as injectable formulation to pave way for its preclinical and clinical development for the management of neurodegenerative disorders. A number of other developed formulations during this project are also under investigation by other collaboration partners in various labs. The here reported library of formulation strongly encourage the use and further evaluation of these formulation for wide variety of clinical indications.

We further investigated the role of hydrophilic block in POx/POzi based thermogelling diblock copolymers. Similar to pPrOzi-pMeOx based thermoresponsive diblock copolymer, we synthesized a novel thermoresponsive polymer, in which pMeOx was replaced with another hydrophilic POx i.e. pEtOx. This polymer was capable to form optically transparent hydrogel at room temperature. However slightly higher polymer concentration (25 wt.%) was needed to form hydrogel while in the case of pMeOx based diblock the macroscopic geleation was observed at 20 wt.%. The rheology experiments revealed that hydrogel is highly shear thinning with good structure recovery properties, these properties make this hydrogel ideal for extrusion based 3D bioprinting. It also revealed slightly higher elastic character of pEtOx based hydrogel (when compared to pMeOx based hydrogel). Various 2D and 3D scaffolds were printed with good shape fidelity and high stackability. The sharp filament corners and intersections in the grid were all well resolved. While in the case of pMeOx based hydrogels, the printability was not ideal. The biological experiments with human adipose derived stems cells (hADSCs) also revealed that this hydrogel could potentially be used as bioink. The post printing live and dead assay revealed that the hADSCs remained viable through out the printing process. The hydrogel in its present form can be used as fugitive support material e.g. to improve the printability of poorly printable polymer like alginate or GelMA. However, it is very important to mention that the hydrogel in its present form is a physically crosslinked network has no cell adhesive/attractive motif. However, thanks to the chemical versatility of POx/POzi, which make it highly tunable and present us a possibility for its chemical modification. The introducing cross-linking sites, which can be easily done, would allow for longer incubation up to several weeks. The introduction of cell adhesive moieties will make it ideal candidate for further exploration. Again, the manifold possibilities allow an adjustment of the gel according to the needs of the envisioned application. Expanding further, the combination of hydrogel with ABA triblock copolymers with outstanding solubilization properties for hydrophobic drugs would allow for the development of sustained drug delivery system. This novel

POx/POzi based hydrogel hold tremendous potential which might help to further advance the upcoming field of biofabrication.

The pMeOx and pEtOx are routeinly addressed as similar materials, when compared to poly(ethylene glycol) (PEG), but it will be very interesting to see a direct comparison of both polymers at molecular level. Summarily, besides outstanding pharmaceutical and biological applications of ABA and AB tri-/di-block copolymer, respectively, as discussed, the strong structure property relationship was repetitively observed in all of the above-mentioned cases. As discussed, replacing hydrophilic block (A) pMeOx with pEtOx in ABA triblock copolymers had a negative impact on drug loading in micelles, while in the case of AB diblock copolymer, the same replacement improved the printability of resultant hydrogel. Both pMeOx and pEtOx differ from each other by just one methylene unit and have distinct physico-chemical properties, which are already reflected in our experiments. Therefore, we can conclude that the decisive factor is not only the selection of right hydrophilic block but also its ultimate application. In majority cases, PEG is used as hydrophilic segments to provide a long and safe circulation of drugs. PEG based micellar formulations for anticancer therapy are under clinical evaluation e.g Genexol PM, NK105 and Nanoplatin. Considering that the vast majority of drug-delivery systems reported in the literature contain PEG as a hydrophilic polymer, which is very similar to pEtOx in its amphiphilicity, a question can be raised whether the limited drug loading of micelles reported in literature may be strongly correlated with the choice of PEG, which is very similar to pEtOx in its amphiphilicity. Additionally, the occurrence of immunogenic responses against PEG after systemic injection result in hypersensitivity reactions and lack of therapeutic efficacy of drug during clinical protocols. In our opinion, the use of alternative polymers like pMeOx or pEtOx as hydrophilic segment offers the potential to obtain safer, more effective and non-immunogenic stealth nanomedicine/biomaterial. The most noticeable progress in this area has already been observed in context of results obtained from first in-human clinical trails involving the use of POx-Rotigotine conjugate for Parkinson’s disease.

Declaration

The present work was carried out under the supervision of Prof. Dr. Robert Luxenhofer from October 2016 to September 2021 at the Faculty of Chemistry and Pharmacy at the Julius Maximilians University of Würzburg, Germany.

I hereby confirm that I have completed this work without any help or support from third parties or commercial consultants. All sources and/or materials applied are listed and specified in the thesis.

The thesis has not been submitted to another examination authority either in Germany or abroad in the same or a similar form.

Date, Place

_____

Malik Salman Haider

Appendix

Honours/Awards/Courses (during PhD)

1. **Award for best oral presentation** at CRS local chapter meeting, 2020, LMU, Munich, Germany.
2. **Award for outstanding Poster presentation** at 83rd Pargue meeting on macromolecules 2019, Czech Republic.
3. **Award for best poster appetizer presentation** at Gesselschaft Deutscher Chemiker, 2018, JMU Würzburg, Germany.
4. **Animal Handling course (FELASA B)**

Conferences/delegations (during PhD)

1. Attended one day "Agilent Academic Seminar" January 2017, Würzburg.
2. Delegate at "Annual meeting of German Society of Biomaterials" November 2017, Würzburg. **I presented a poster**.
3. Delegate at "Macromolecular Colloquium Freiburg" Freiburg Germany, February 2018. **I gave a 3-minute talk and presented a poster afterwards.**
4. Delegate at international conference "Advanced Functional Polymer Materials" in Montpellier, France May 2018. **I presented a poster.**
5. Delegate at "ACHEMA exhibition" in Frankfurt Germany, June 2018. **I gave 30-minutes oral presentation.**
6. Delegate at retreat of Interdisciplinary Centre for Clinical Research, Kloster banz Germany, June 2018. **I presented a poster.**
7. Attended a one day work shop on "Particle Characterization in Medicine and Biology", Frankfurt, Germany September 2018.
8. Delegate at 2 day "Galenus Workshop" Würzburg, Germany, November 2018. **I presented a poster.**
9. Delegate at one day "Chemie Symposiums der Studierenden Mainfrankens" (ChemSyStM), December 2018, Würzburg and gave 3 minute talk and **got best Poster Appetizer prize** for the presentation**.**
10. Delegate at 2 day "5th Euro BioMAT 2019" Weimar, Germany, May 2019. **I gave 20 minute oral presentation.**
11. Delegate at 5 day international conference "83rd Prague meeting on macromolecules" Prague, Czech Republic, June 2019. **I got a travel grant from the organization committee and I got outstanding poster prize.**
12. Delegate at 2 days "CRS local chapter meeting" Münich, Germany, February 2020, **I gave 10 minutes talk and got award for best oral presentation.**

Author's Contribution

"Think beyond the core: The impact of the hydrophilic corona on the drug solubilization using polymer micelles"

(doi.org/10.1021/acsami.9b22495**)**

Malik Salman Haider (**A1**), Michael M. Lübtow (**A2**), Sebastian Endres (**A3**), Stefan Forster (**A4**), Vanessa J. Flegler (**A5**), Bettina Böttcher (**A6**), Vladimir Aseyev (**A7**), Ann-Christin Pöppler (**A8**), and Robert Luxenhofer*(**A9**)

Role	**A1**	**A2**	**A3**	**A4**	**A5**	**A6**	**A7**	**A8**	**A9**	**Sum in %**
Monomer and polymer synthesis	12	2								14
Drug formulation	13	1								14
Reichardt's dye formulation	3									3
NMR	5	0,5								5,5
Dynamic light scattering	2	1								3
Differential scanning calorimetry	2	0,5								2,5
Thermogravimetric analysis	2	0,5								2,5
Critical micelles concentration	2	0,5								2,5
Micro DSC							3			3
Cryo-TEM				1	1	1				3
Diffusion NMR and Noesy			3					4		7
Publication writing	10	1						3	14	28
Coordination	6	1						1	4	12
Total	57	8	3	1	1	1	3	8	18	100

"A Micellar Mitotane Formulation with High Drug-Loading and Solubility: Physico-Chemical Characterization and Cytotoxicity Studies in 2D and 3D In Vitro Tumor Models"

(doi: 10.1002/mabi.201900178)

Malik Salman Haider (**A1**), Jochen Schreiner (**A2**), Sabine Kendl (**A3**), Matthias Kroiss* (**A4**), Robert Luxenhofer* (**A5**)

Role	A1	A2	A3	A4	A5	Sum in %
Monomer and polymer synthesis	5					5
Mitotane formulation/characterization	8					8
Solubility parameters	3					3
NMR	3					3
Differential scanning calorimetry	3					3
Thermogravimetric analysis	3					3
dynamic light scattering	3					3
Cytocompatibility studies	8	4	2			14
Cytotoxocity studies	8	4	2			14
Publication writing	13	2		4	9	28
Coordination	4	1		3	8	16
Total	61	11	4	7	17	100

"**Tuning the Thermogelation and Rheology of Poly(2-Oxazoline)/Poly(2-Oxazine)s Based Thermosensitive Hydrogels for 3D Bioprinting**"

(doi.org/10.3390/gels7030078**)**

Malik Salman Haider* (**A1**), Taufiq Ahmad (**A2**), Mengshi Yang (**A3**), Chen Hu (**A4**), Lukas Hahn (**A5**), Philipp Stahlhutt (**A6**), Jürgen Groll (**A7**), Robert Luxenhofer* (**A8**)

Role	A1	A2	A3	A4	A5	A6	A7	A8	Sum in %
Monomer and polymer synthesis	**6**		**2**						**8**
Characterization	**6**		**2**						**8**
Rheology	**6**			**2**	**2**				**10**
Printing	**6**			**2**	**2**				**10**
Bioprinting/cell studies	**3**	**6**							**9**
SEM/Cryo-SEM	**2**					**6**			**8**
Publication writing	**19**	**2**					**2**	**7**	**30**
Coordination	**9**	**1**					**2**	**5**	**17**
Total	**57**	**9**	**4**	**4**	**4**	**6**	**4**	**12**	**100**